AD-A142 003 PROCEEDINGS OF THE ANTENNA APPLICATIONS SYMPOSIUM HELD AT MONTICELLO ILLI.. (U) ROME AIR DEVELOPMENT CENTER GRIFFISS AFB NY MAR 84 RADC-TR-84-52-VOL-1 1/3

UNCLASSIFIED F/G 9/5 NL

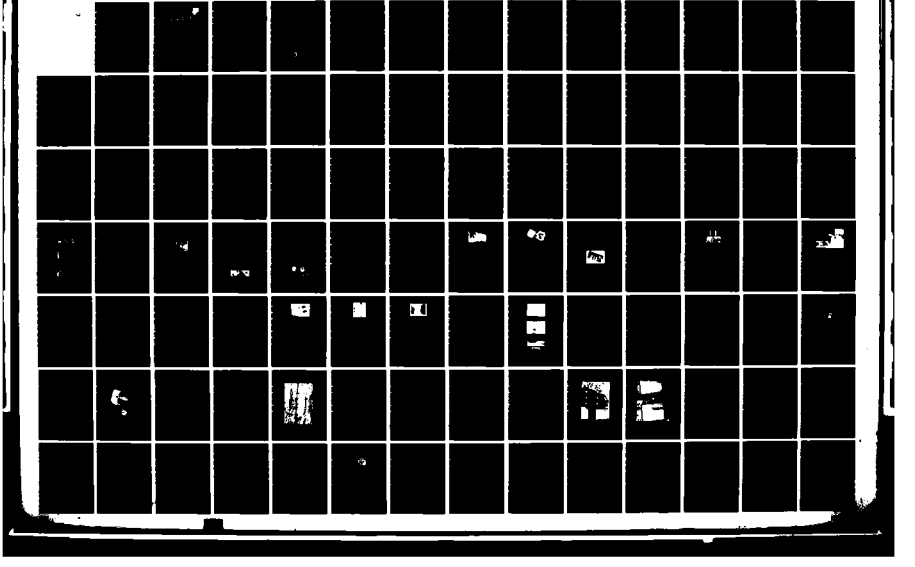

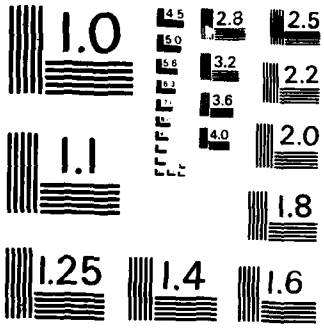

RADC-TR-84-52, Vol I (of two)
In-House Report
March 1984

PROCEEDINGS OF THE 1983 ANTENNA APPLICATIONS SYMPOSIUM

Sponsored by
ELECTROMAGNETIC SCIENCES DIVISION
ROME AIR DEVELOPMENT CENTER
HANSCOM AFB, BEDFORD MASS. 01731
AIR FORCE SYSTEMS COMMAND

APPROVED FOR PUBLIC RELEASE; DISTRIBUTION UNLIMITED

ROME AIR DEVELOPMENT CENTER
Air Force Systems Command
Griffiss Air Force Base, NY 13441

This report has been reviewed by the RADC Public Affairs Office (PA) and is releasable to the National Technical Information Service (NTIS). At NTIS it will be releasable to the general public, including foreign nations.

RADC-TR-84-52, Volume I (of two) has been reviewed and is approved for publication.

APPROVED:

JOHN K. SCHINDLER
Chief, Antennas & RF Components Branch
Electromagnetic Sciences Division

APPROVED:

ALLAN C. SCHELL
Chief, Electromagnetic Sciences Division

FOR THE COMMANDER:

JOHN A. RITZ
Acting Chief, Plans Office

If your address has changed or if you wish to be removed from the RADC mailing list, or if the addressee is no longer employed by your organization, please notify RADC (EEA) Hanscom AFB MA 01731. This will assist us in maintaining a current mailing list.

Do not return copies of this report unless contractual obligations or notices on a specific document requires that it be returned.

COMPONENT PART NOTICE

THIS PAPER IS A COMPONENT PART OF THE FOLLOWING COMPILATION REPORT:

(TITLE): Proceedings of the Antenna Applications Symposium Held at Monticello, Illinois on 21-23 September 1983. Volume 1.

(SOURCE): Rome Air Development Center

Hanscom AFB, Massachusetts 01731

TO ORDER THE COMPLETE COMPILATION REPORT USE AD-A142 003.

THE COMPONENT PART IS PROVIDED HERE TO ALLOW USERS ACCESS TO INDIVIDUALLY AUTHORED SECTIONS OF PROCEEDINGS, ANNALS, SYMPOSIA, ETC. HOWEVER, THE COMPONENT SHOULD BE CONSIDERED WITHIN THE CONTEXT OF THE OVERALL COMPILATION REPORT AND NOT AS A STAND-ALONE TECHNICAL REPORT.

THE FOLLOWING COMPONENT PART NUMBERS COMPRISE THE COMPILATION REPORT:

AD#:	TITLE:
AD-P003 401	Antenna Applications and System Engineering
AD-P003 402	Fundamental Design Issues for Monolithic Phased Arrays
AD-P003 403	Integration of Monolithic Microwave Integrated Circuits Into Phased Array Antenna Systems
AD-P003 404	A Wide Band 44 GHz Printed Circuit Conformal Array
AD-P003 405	Development of Scanning Dipole Array By D. Davis
AD-P003 406	The Design of a Low-Loss, Light-Weight, S-Band, Phase-Shifter
AD-P003 407	A Compact Fully Overlapping Subarray Antenna
AD-P003 408	Geodesic Cone Antenna
AD-P003 409	The Mechanical Design of a High-Power, Dual-Frequency, Millimeter-Wave Antenna Feed System
AD-P003 410	Earth Coverage Corrugated Horns (44.5 GHz and 20.7 GHz)
AD-P003 411	Advances in Spiral Antenna Technology
AD-P003 412	Designing Antennas to Price, or the Economics of Antenna Design
AD-P003 413	Rebuttal to Floating a Satellite on Microwaves

COMPONENT PART NOTICE (CON'T)

AD#: TITLE:

Unclassified

SECURITY CLASSIFICATION OF THIS PAGE

REPORT DOCUMENTATION PAGE

1a. REPORT SECURITY CLASSIFICATION: Unclassified	1b. RESTRICTIVE MARKINGS
2a. SECURITY CLASSIFICATION AUTHORITY	3. DISTRIBUTION/AVAILABILITY OF REPORT: Approved for public release; Distribution unlimited.
2b. DECLASSIFICATION/DOWNGRADING SCHEDULE	
4. PERFORMING ORGANIZATION REPORT NUMBER(S)	5. MONITORING ORGANIZATION REPORT NUMBER(S): RADC-TR-84-52 (Volume I)
6a. NAME OF PERFORMING ORGANIZATION: Rome Air Development Center; 6b. OFFICE SYMBOL (If applicable): EEA	7a. NAME OF MONITORING ORGANIZATION
6c. ADDRESS (City, State and ZIP Code): Hanscom AFB, Massachusetts 01731	7b. ADDRESS (City, State and ZIP Code)
8a. NAME OF FUNDING/SPONSORING ORGANIZATION; 8b. OFFICE SYMBOL (If applicable)	9. PROCUREMENT INSTRUMENT IDENTIFICATION NUMBER
8c. ADDRESS (City, State and ZIP Code)	10. SOURCE OF FUNDING NOS

PROGRAM ELEMENT NO.	PROJECT NO	TASK NO	WORK UNIT NO
62702F	4600	14	01

11. TITLE (Include Security Classification): (U)Proceedings of the 1983 Antenna Applications Symposium (Vol I)

12. PERSONAL AUTHOR(S)

13a. TYPE OF REPORT	13b. TIME COVERED	14. DATE OF REPORT (Yr., Mo., Day)	15. PAGE COUNT
In-House	FROM _____ TO _____	1984 March	266

16. SUPPLEMENTARY NOTATION: Nicholas Kernweis, Contract Monitor (RADC/EEA)

17 COSATI CODES			18. SUBJECT TERMS (Continue on reverse if necessary and identify by block number)
FIELD	GROUP	SUB GR	
09	03		Phased Array Antennas; Microstrip & Conformal Antennas
09	05		Millimeter Wave Antennas; Reflector Antennas; Measurement

19. ABSTRACT (Continue on reverse if necessary and identify by block number)

(U)The Proceedings of the 1983 Antenna Applications Symposium is a collection of the State-of-the-Art papers relating to Phased Array Antennas, Millimeter Wave Antennas, Microstrip and Conformal Antennas and Reflector Antennas.

20. DISTRIBUTION/AVAILABILITY OF ABSTRACT	21. ABSTRACT SECURITY CLASSIFICATION
UNCLASSIFIED/UNLIMITED ☐ SAME AS RPT ☒ DTIC USERS ☐	Unclassified

22a. NAME OF RESPONSIBLE INDIVIDUAL	22b. TELEPHONE NUMBER (Include Area Code)	22c. OFFICE SYMBOL
Nicholas P. Kernweis	(617)861-3191	RADC/EEA

DD FORM 1473, 83 APR EDITION OF 1 JAN 73 IS OBSOLETE

Unclassified

SECURITY CLASSIFICATION OF THIS PAGE

Preface

The Antenna Symposium held at the University of Illinois was co-sponsored by RADC (EEA) Electromagnetic Sciences Division, Hanscom AFB, Bedford, MA and the University of Illinois, Urbana, IL under contract number F19628-83-M-0003.

A-1

Contents

* NOT INCLUDED IN THIS REPORT

SOLID STATE PHASED ARRAY TECHNOLOGY

HAROLD WEBER
AF WRIGHT AERONAUTICAL LABORATORIES
WRIGHT-PATTERSON AFB, OHIO

INTRODUCTION

The solid state (or active) phased array represents a new opportunity in microwave systems. It is a critical new technology for military system applications due to its potential for high reliability and low life cycle costs. For example, a conventional airborne radar antenna, transmitter, and receiver which has a MTBF (mean-time-between-failure) of approximately 200-300 hours could be implemented as a solid state phased array having an MTBF of 2500 hours. The real impact of this reliability is in the savings incurred from elimination of flight line maintenance, thus utilizing depot maintenance only. This permits elimination of several million dollars worth of microwave support equipment at each forward base, and significantly reduces the demand for highly skilled military maintenance personnel at these forward sites. Current skilled military manpower retention problems demand that this technology be evolved quickly into operational systems. The 2500 hours MTBF previously noted will permit the transmit, receive, and antenna functions of an airborne radar implemented as a solid state array to be installed on an aircraft and operated maintenance free for 3-5 years, at which time the array would be replaced and the old unit returned to a US depot for refurbishment. Studies have revealed a significant performance advantage from the solid state array, which accrues from system architecture and from the agility afforded by a phased array.

REQUIREMENTS

The airborne radar system which any array development must support is for multimode air-to-air and air-to-ground missions. The radar must have air-to-air modes for air superiority or self defense, ground imaging capabilities for target classification or navigation update, and terrain following/avoidance modes for survivability. Air-to-air mission requirements consist primarily of detection and tracking of airborne targets, thus furnishing target coordinate and rate information to the threat assessment and/or fire control system. Pulse doppler radar waveforms will interlace low, medium, and high PRF (pulse repetition frequency) modes to generate unambiguous velocity and range data. Mainbeam and sidelobe ground clutter doppler spread can significantly reduce target detectability, particularly in look down attitudes. For this reason, the solid state phased array must possess very low peak and average sidelobe levels, which translates into low phase and amplitude errors throughout the feed manifold, transmit-receive modules, and radiating aperture. The low average sidelobe level also constrains the number of module failures which can be accepted. Summarily, the air-to-air modes are most demanding in terms of module to module amplitude and phase variations and in the number of module failures which can be tolerated. The MTBF requirement for each module is 60-75,000 hours. These parameters are fully attainable through solid state array technology. Air-to-ground requirements are primarily ground imaging synthetic aperture modes for (1) tactical target recognition and classification, or (2) waypoint target recognition/tracking for strategic navigation update. The principal problem associated with SAR (synthetic aperture radar) modes is the broad instantaneous bandwidths required in the RF feed manifold, transmit-receive modules, and radiating aperture. Terrain following/avoidance modes are normally not demanding in terms of sidelobes or power, but do require polarization diversity and precise stabilization of the antenna pattern against aircraft roll, pitch, and yaw.

Ground based radar system applications are also being considered to exploit the solid state array promise for maintenance free reliable operation; some of these applications include remote site unattended operation. In general, these applications do not require large instantaneous but will require wide operating (untuned) bandwidths to prevent intentional and/or local electromagnetic interference. Peak sidelobe requirements will be moderately severe, but average sidelobes will be less demanding than the airborne radar case thus permitting some relaxation in amplitude and phase error performance. Higher module output powers may also be required for these ground based surveillance radars.

Solid state arrays are also being investigated for communication satellite spaceborne terminal down link applications. It is once again the significant potential for reliable operation which is being sought. Instantaneous bandwidth, operating bandwidth, and sidelobe requirements are not normally demanding for these applications. In some cases, linear operation with very low intermodulation distortion is needed when frequency division multiplexing is employed. Moderate phase distortion, i.e. deviation from a linear phase-frequency slope, is frequently necessary to preserve low error rates in the modulation-demodulation process.

BACKGROUND

There have been two previous airborne radar solid state array development efforts. It became obvious during these programs that direct x-band power generation and module interfaces were necessary, both of which are now possible due to significant advances in gallium arsenide (GaAs) field-effect-transistor (FET) technology.

The MERA (Molecular Electronics for Radar Applications) system was the first of the solid-state phased array radars. This program started in 1964, and the program objective was primarily to advance the state-of-the-art in molecular electronics. It resulted in a fixed frequency radar containing 604 transmit and receive elements. Each of these elements had an output of approximately 0.5 watt at 9GHz. The transmitted power was 352 watts (peak). A mixer down-converter and 500 MHz IF amplifier was implemented on each module and resulted in a 12.5 dB system noise figure. Receive beam collimation and steering was achieved through phase control of the local oscillator signal which was manifolded at 2.125 GHz and frequency multiplied to the 8.5 GHz LO signal frequency. The module transmitters accepted excitation input from the transmit manifold at 2.25 GHz, amplified this signal to 2 watts (nominal), and then frequency multiplied to the 9 GHz output frequency. Uniform transmit aperture illumination was used with a gain of 32 dB. Reduced sidelobe amplitude taper was used on receive and produced 30dB gain. Pulse compression techniques were used to enhance sensitivity and improve range resolution (pulse compression ratios of 113.1).

RASSR was a second-generation system leading to the design and development of an all solid-state airborne radar with flexibility and long operating life. The RASSR program was designed to build on the results of MERA. The Reliable Advanced Solid State Radar (RASSR) array was composed of 1648 dual-ridge waveguide antenna elements. Bandwidth of the system was 0.3 GHz, centered at 9.35 GHz. The overall diameter of the array was 36 inches, with the active aperture being approximately 32 inches in diameter. An equilateral triangular element grid was implemented with 824 dual-element modules. Each module contained two transmit/receive elements driven from a common S-band source. The 2.675 GHz (nominal) signal was used for both transmit excitation and receiver local oscillator X-band signal generation. One S-band phase shifter was used for

both transmit and receive modes, with shifting between modes accomplished also at S-band by a T/R switch. In transmit, the signal was amplified and X4 frequency multiplied to X-band with a 1.66 watt (peak) power output per element. In receive, the signal was X4 frequency multiplied. The measured module RMS phase errors from all sources (manifolds, module components, antenna mismatch, temperature gradients, etc.) was 28.5 degrees on transmit and 28.7 degrees on receive. System assembly and preliminary checkout of RASSR was completed in September 1974.

A twenty month RASSR system performance test effort was initiated in January 1975. Extensive antenna pattern range measurement was conducted on the array (equivalent to over 10,000 single plane cuts) to evaluate transient patterns, dynamic pattern, beamshape, sidelobes, polarization purity, quantization (bit simulation roudoff), beam pointing accuracy, noise, and gain characteristics. Array performance tests did not reveal any anomalies. A primary RASSR design goal was demonstration of 500 hours system MTBF and 33,000 hours module MTBF. The measured system MTBF was 199.7 hours based upon 1398 hours of stem operating time accrued during the array evaluation effort. Similarly, e actual module MTBF was 17,374 hours based upon 1,025,061 module operati hours. This program has demonstrated that solid state aperture reliability i n achievable goal within the performance requirements of multi-function radar stems.

PRESENT MODULE TECHNOLOGY

Solid state modules are being fabricated and evaluated for various spaceborne communication satellite and airborne radar applications. The more mature performance (and the greatest number of potential applications) exists at X-band frequencies. Device and circuit technology readily support 1-2 watt CW power levels which appears adequate for a number of applications. One exemplary program has produced about 300 X-band monolithic four stage power amplifiers having a one watt power output (cw) with 30 dB gain and 30 percent power added efficiency. These amplifiers were each fabricated on 0.240 x 0.040 x 0.006-inch gallium arsenide substrate . Another program has fabricated ninety x-band transmit-receive modules with 2 watt RF output, 3.5 dB module receive path noise figure, and five-bit PIN diode phase shifter. All these circuit functions were integrated into a module housing measuring 3.75 x 1.125 x 0.675 inch. Measured bandwidths, amplitude/phase error, power output, and gain performance on these and similar module developments have been adequate to meet respective system specifications.

COST CONSIDERATIONS/CHALLENGES

The objective of Air Force solid state phased array technology application to microwave systems is elimination of flight line maintenance requirements. The potential for 2500 hr MTBF's for transmitter, receiver, and antenna functions will support such maintenance philosophies. The microwave sensor "front end" would be installed on an airframe and operated maintenance free for 3-5 years with only periodic (e.g. biannual) performance checks. Upon determining a loss in system performance, or at the end of prescribed period of time, the array would be removed from the aircraft and returned to a maintenance depot for refurbishment. The array (microwave sensor "front end") would be replaced as a complete unit with no attempt at flight line repair or refurbishment of the replaced unit. The advantages and savings accruing from such maintenance concepts are as follows. The first is elimination of the need for field automatic support equipment (ASE) used by maintenance personnel to diagnose

hardware problems and evaluate repair effectiveness. Such ASE typically will cost several million dollars per set. Flight line spares can be eliminated, along with the need to transport spares and ASE. A significant reduction in need for flight line maintenance personnel will result, and those required can effectively work at a lower skill level with less training. Field shop ASE maintenance and calibration will also be eliminated. Finally, each aircraft will have significantly reduced maintenance down-time and will thus have higher mission readiness, which translates into the capability of doing a given job with fewer aircraft.

Solid state phased array microwave technology feasibility has been demonstrated. There remain some problems in manufacturing technology which relate to large volume module production with acceptable phase and amplitude error performance. There also remain some very significant challenges in reducing the cost of the solid state transmit - receive modules. The Avionics Laboratory has worked extensively at implementing this array technology and at reducing module acquisition costs. A continuing question is that of establishing a reasonable module cost which will permit a 20 percent reduction in the ten year life cycle costs associated with the microwave sensor "front end". Precise accounting procedures and data from which life cycle cost estimates can be derived are not readily available on all microwave systems. A composite of communication and radar system data was used for this study, with considerations and assumptions as shown. Conventional system (i.e. discrete transmitter, receiver, and mechanically scanned antenna) acquisition cost is defined as A_c, and all other system costs derived are normalized to this value. The hybrid system is comprised of a discrete transmitter, receiver, and electronically scanned phased array; the phased array acquisition cost is always higher and the hybrid system cost A_H is assumed to be equal to 1.25 A_c. Ten year maintenance costs (M_{10}) were found to range between 5 and 15 percent of the acquisition cost, depending primarily on system complexity. The M_{10} costs covered only the removal, diagnostics, repair, and re-installation manpower costs. The automatic support equipment (ASE) acquisition cost were found to range from 200 to 1500 percent of the system acquisition cost (A_c), and depended on system complexity as well as maintenance philosophies. It was assumed that one ASE complement would service twenty-five aircraft systems on the average, this number being driven primarily by deployment scenarios. It was also assumed that twenty ASE complements would be required at the depot level to support 1000 aircraft for both maintenance and recurring engineering development. Prorating these total ASE acquisition costs translates into a 12-90 percent of the system acquisition cost A_c assessment for each aircraft. Ten year field support costs (F_{10}) includes ASE transportation, spares transportation, training, personnel, facilities, supply documentation etc. It is a difficult factor to prorate but estimates range from 10 to 95 percent of A_c dependent on system complexity and deployment strategy.

Ten year life cycle cost (LCC_{10}) and the percent of life cycle costs absorbed by support functions were computed for typical airborne multimode radar microwave front-ends (transmitter, receiver, and antenna), based on the previously described assumptions and maintenance philosophies. Results of these computations show that LCC_{10} is equal to 2.85 A_c for a conventional system, and 2.45 A_c for a hybrid system. Stated another way, a $500,000 conventional system would have ten year life cycle costs of $1,425,000. It is noted that LCC_{10} is lower for a hybrid system ($1,225,000) even though the initial acquisition cost is 25 percent higher, due largely to the much improved array reliability. Stated yet another way, maintenance/support costs represent 65 percent of the ten year life cycle cost for a conventional system, and 49 percent for a hybrid system.

The next questions to be addressed were solid state phased array module and system acquisition costs, based upon the above described cost factors. Further assumptions were that the solid state array (1) achieves a 20 percent reduction in ten year life cycle cost, and (2) support costs are 10 percent of acquisition costs. The per element acquisition cost to achieve a 20 percent LCC_{10} savings is \$600, about 80 percent of which (\$480) is for the module. The above cost requirements are for replacement of a conventional system, and each must be reduced by about \$65 if replacing a hybrid system. Restating these cost estimates, one may pay 2.1 times A_c and still achieve a 20 percent savings, or 1.4 times A_H with the same savings. In other words one might pay \$1,050,000 for a solid state array as compared to \$500,000 for a conventional system, and still achieve a 20 percent savings in the ten year life cycle cost. It is noted that current solid state module costs are an order of magnitude higher than the nominal \$500 cost cited above.

Over the years, a number of attempts have been made to incorporate phased arrays into advanced development and operational systems. The conventional (passive) phased array offers significant system benefits which evolve from beam agility, and has demonstrated reliability improvements over the mechanically scanned antenna. Conventional array use has been inhibited by two factors; viz, RF losses and high acquisition costs. These two issues plus the fact that the passive array only partially solves the reliability and support cost problem (transmitter and receiver ASE would be needed) portend a limited future for this configuration. The solid state (active) phased array will offer significant reductions in RF losses (1-2dB versus 6-7dB) by virtue of moving transmit-receive amplification further forward in the aperture. This permits a more efficient utilization of RF power generated at 25-35 percent efficiencies, and also provides lower receive system noise figures. The reliability and life cycle cost saving potential associated with two level maintenance (depot versus flight line) have already been described herein. The solid state array will offer even greater system flexibility through beam agility, beam shape diversity by turning on/off modules, and eventually antenna pattern control through gain/amplitude control at the module level. The one remaining restraint to application is the need for a ten to one reduction in transmit-receive module acquisition cost.

By way of status, it is believed that RF circuit and device technology are available and that prices in these areas are decreasing. It is not clear that hybrid or functional monolithic circuits will either achieve a dominant position in module manufacturing; i.e., both technologies will be needed for the immediate future and the winner will be decided on the basis of cost. Integrated module phase and amplitude error performance are proving to be adequate in terms of antenna performance for most system applications. A number of companies now have the capability for small volume fabrication. There are still some system issues to be addressed, the most challenging being simple (but effective) thermal control. Lesser problems are associated with RF manifolds, logic manifolds, beam steering computer architecture, and power supplies.

Antenna Applications and System Engineering

Fred I. Diamond
Rome Air Development Center

The Rome Air Development Center (RADC) is an appropriate co-sponsor of a symposium on antenna applications. The antenna group of RADC has a distinguished research history dating back to its earlier association with the Air Force Cambridge Research Laboratories. And because RADC is the Air Force's C3 Laboratory, radar and communications have been and will continue to be major areas of research and development. We anticipate continued challenges for the Antenna Community not only in the development of new, advanced antenna systems, which exploit of advances in digital signal processing and new devices such as monolithic microwave integrated circuits.

Currently, RADC is involved in radar and communications developments for spaceborne, airborne and ground platforms. In spaceborne applications, the need for radars with high power-aperture products and communications satellites with large amounts of effective radiated power promote consideration of very large apertures with dimensions in the order of hundreds of wavelengths. Radar requirements of accuracy and resolution and communications needs for very high data rates imply greater bandwidths. The need for broad radar coverage and multiple target tracking and communications needs for diversity, coverage, and multiple accesses give rise to consideration of greater beam agility. Size and weight are important for spaceborne and airborne applications; but mobility requirements for tactical radar and communications make this ar essential consideration for ground-based applications. Concerns over electronics counter measures impose further requirements such as ultra-low sidelobes, adaptive nulling, and wide band signals. Needless to say, low-cost and reliability are important design factors, too.

Some have characterized antenna development as a "mature" technology, perhaps not worthy of the talent required in other areas. Nevertheless, the challenges in antenna development are still imposing. For space applications, the large apertures on the order of hundreds of wavelengths pose problems in pattern control, feed, and test and evaluation. To achieve the needed flexibility in radar performance -- beam agility, combined search and track, power management--phased arrays emerge as leading candidates. Indeed, this capability has been successfully demonstrated in large radar systems currently operational in the Army, Navy, and Air Force. Radars such as these use planar arrays, but for airborne and ground applications, other configurations merit consideration. For example, because of the possibility of increased mobility and aircraft transportability, cylindrical arrays are being designed for tactical ground radar. And for airborne applications, conformal antennas are desired so that aircraft performance is not impaired.

As stated earlier, future radar systems require greater resolution and accuracy and future communications systems will involve increased capacity and higher data rates. This, coupled with the use of spread spectrum techniques for anti-jamming, imply use of very large bandwidths. Thus, design of future cost-effective phase array systems, linear, planar, cylindrical, or possibly spherical, offer greater challenges in pattern control, (especially ultra-low sidelobes or nulling), in beam formation and scanning, in order to handle broad-band signals, and to cope with jamming and other forms of electronic counter-measures. Above all, cost is a major consideration. Large phased array radars in use have, in many cases, been justified on the basis of the cost effectiveness of a single multi-function array radar compared to the alternative of using several non-electronically scanned radars for the same overall function. Therefore, the general use of electronically-scanned phased arrays will be highly dependant upon low-cost design, development and fabrication

techniques.

Multi-function arrays capable of supporting a variety of C3 missions-surveillance, communications, IFF, ELINT and ECCM - from a single array-face represent a major technological challenge. These arrays must be conformally structured for airborne applications and be capable of electronical reconfiguration to transmit and receive the wide variety of waveforms over the extremely wide tunable range of frequencies encountered in these C3 missions. In these arrays, we must exploit the GaAs monolithic circuit revolution which, along with the myriad of analog signal generation, control and processing devices, should provide untold array flexibility. Fiber optic distribution of information, control and synchronization of signals in these large arrays also needs to be considered. Finally, with so much of the vital information generation and processing occurring at the array face, we should have renewed interest in radomes; that is, advanced "radomes" which act as protective shields to provide EMP, lightning, blast and radiation protection, TEMPEST control radar cross section and thermal radiation control.

With advances in electronic technology and signal processing, new challenges and opportunities exist for achieving such desired capabilities. For example, an exciting new technique is digital beamforming, whereby analog information from antenna terminals, both amplitude and phase, is converted into digital form. Conceptually, direct analog-to-digital (A/D) Conversion is possible. Practically speaking, amplification and heterodyning may be required, at least in the near future. With in-phase and quadrature signals from each element, a variety of antenna functions can be formed through appropriate digital processing: multiple beam formation, beam agility, monopulse tracking, sidelobe reduction, null steering, power management, etc. Practical developments may be highly dependent on electronic components including A/D conversion, and on software, but digital beamforming potentially adds a new dimension to the area of adaptive antennas. The term adaptive antennas implies a host of potential benefits--automatic nulling for reduction of jamming, RFI, and clutter; self-focussing; platform motion compensation for improved airborne MTI performance; compensation of propagation effects and antenna element phase and amplitude errors; automatic direction finding. Currently, the greatest emphasis is being placed on null steering, the adaptive formation of nulls in the direction of undesired signal such as jamming, clutter, and multipath. As an anti-jamming technique, it complements, rather than replaces, spread spectrum techniques, thus providing the potential for enhanced anti-jam performance.

Today, null-steering antennas are being investigated for application to radar and communications in virtually every frequency band from VLF through microwave frequencies. Theoretical work has provided an understanding of the principles of operation, several classes of algorithms for adaptive control have been conceived and implemented, and null steering has been successfully demonstrated. However, particularly for large arrays, it is important to address antenna design factors such as element arrangements, mutual coupling, and required tolerances. Unless proper conventional antenna design principles are applied, serious deficiencies such as undesired grating lobes can occur. It is also possible that nulling can cause serious signal distortion. Thus it is necessary that we understand the relationships between null patterns and bandwidth.

Finally, in addressing the implementation of antenna designs, recent progress in device development is an important factor. For example advances in fiber optics and magnetostatics offer new approaches and/or devices for providing time - delay elements required for broad-band, wide-angle scanning arrays. Fiber optics appear to be a natural medium for transmitting information, control and synchronization signals in large arrays employing monolithic circuit amplification at the array face. Fiber optic sources and detectors

may be directly integrated with the monolithic circuits. Another important area of device technology is microstrip antennas, particularly for their potential to achieve thin conformal arrays for aircraft. This concept, combined with advances in monolithic microwave integrated circuits provides the opportunity to produce low-cost, light-weight arrays, even at EHF frequencies. The monolithic integration of radiating elements, power amplifiers, phase shifters, etc. as a subarray on a gallium arsenate substrate is a desirable goal, but achieving the needed bandwidth, accomplishing the physical layout and thermal design, within the space constraints is indeed a challenge. However, alternate physical configurations such as multilayer construction may be suitable, to address these problems. But there is also a need for theoretical studies involving the relationship between array configurations, layout, mutual coupling and pattern control.

Developments and trends that were described above -- broad-band phased arrays, conformal antennas, null-steering, digital beamforming -- are subjects not unfamiliar to antenna engineers. We will be hearing about these at this symposium. But these topics and others -- synthetic apertures and high resolution through spectral estimation techniques such as maximum entropy -- are of interest to other technologists. The point is, this technology is multidisciplinary. For example, in a digital beamforming array, antenna performance is as much dependent on digital processing and the necessary software as it is on the configuration of radiating elements and front end microwave components. Furthermore, overall design and performance of a radar using digital beamforming is not independent of the array, if one desires flexibility in beam formation, beam steering, power management, tracking, null steering, clutter cancellation, etc.

Despite the demonstrated capabilities of null steering, one must consider the interaction of wide-band spread spectrum signals with null-steering processing and possible signal distortion effects. Furthermore, the ability to reduce sidelobe interference is no excuse for ignoring good antenna design. And despite pattern synthesis that can provide deep wide-band nulls at specified angles, such systems cannot perform effectively open-loop. Algorithms, both analog and digital, and their implementation offer challenges in control system theory and signal processing. Furthermore, antenna performance and null steering over many degrees of freedom vs. the relative merits of spread spectrum processing gain for various operational scenarios vs. circuitry limitations is a major consideration.

Clearly, the antenna engineer of the future must be a systems-oriented individual. With the evolution of VLSI and VHSIC, the distinction between devices and circuits is vanishing. And even at higher frequencies, progress in monolithic microwave integrated circuits and the inclusion of radiating elements in the same substrate raise new subsystem and system issues. And with further advances in high speed ital processing and A/D conversion, the prospect of all-digital proces arting at the radiating terminals faces us. Adaptive processing ith signal processing requires a knowledge of modern information l control theory. The digital manipulation of data, the processing of , and the generation of control signals requires skills in inform n sciences.

Probably the concept of digital beamforming is the best example of the total system aspects of new antenna engineering. The overall design requires a system-oriented group; it involves not only antenna systems, but microelectronics, signal processing, computer architecture and software. How we collectively deal with these multidisciplinary issues, how we allocate resources and tasks among specialists and systems-oriented engineers and , how these changes impact on education and training -- this is the real challenge.

FUNDAMENTAL DESIGN ISSUES FOR MONOLITHIC PHASED ARRAYS

R. J. Stockton
Ball Aerospace Systems Division
Boulder, Colorado

ABSTRACT

Basic design issues associated with the monolithic implementation of microwave and millimeter-wave active aperture, conformal, phased array antenna systems are presented. Since the planar surface area is limited and large regions must be set aside as unused exclusion zones to prevent mutual coupling, fitting all of the essential components such as phase shifters, amplifiers and a feed network within the available inter-element area is extremely difficult. Electrical, thermal and mechanical tradeoffs related to monolithic subarray technology are described in detail.

1. INTRODUCTION

In general, conformal phased array antenna systems for communications applications at X-band and below have been implemented in a multi-layer/hybrid approach using laminated Teflon-fiberglass dielectric materials. Planar elements and monolithic circuitry are photoetched on metal clad dielectrics and active components are added to create a hybrid circuit. Above 20 GHz, however, the need for increased photolithographic precision and greatly reduced circuit features make microwave hybrid circuits resemble digital integrated circuits.

Relating this trend to the significant and steady advancements in GaAs devices and monolithic microwave integrated circuits, it is apparent that the concept of a totally monolithic, active aperture antenna is justified. The shorter wavelengths will enable significant portions of the aperture, such as subarrays, to be fabricated by cost effective integrated circuit processes instead of labor intensive monolithic/hybrid procedures. Distributed on-chip low noise amplification for receive and high power amplification for transmit will overcome the effects of increased transmission line losses encountered at these higher frequencies and also provide performance improvements in G/T and EIRP.

Although the foundation technologies have been established, there are many design challenges requiring solutions. This paper examines some of the fundamental design issues associated with active monolithic transmit and receive phased array antenna systems.

Topics requiring detailed tradeoff investigations include substrate selection, area and topology constraints, yield considerations, power and control line distribution and subarray mounting techniques.

2. SUBSTRATE SELECTION

Unlike discrete active components, monolithic antenna systems are a very unique blend of microwave or millimeter wave devices and integrated circuit technology. Typical microwave solid state devices are fabricated in mass, by the wafer, for economy and product uniformity. When processing is completed, the wafer is diced up into individual chips for packaging. As a result, the properties of the bulk material in between or adjacent to device or circuit areas are of little concern. Monolithic antenna systems, on the other hand, are single, functional circuits which utilize the entire wafer area with only a sparse population of active devices. In this application the semi-insulating characteristics of the bulk material are extremely important since a single material must satisfy the requirements of the active device, the planar RF circuitry and the radiating element.

For active devices the substrate must be a semiconductor with high mobility, a large maximum drift velocity and a large breakdown field. When conduction electrons have high mobility and high peak drift velocities, active devices will exhibit lower parasitic resistances, larger transconductance and shorter electron transit times. A high resistivity semi-insulating state of 10^6-10^7 ohm-cm

is necessary to maintain isolation between the active channel region and the bulk material in addition to providing isolation between adjacent devices. A high resistivity state also results in lower gate-bonding pad parasitic capacitances.

A semi-insulating state is also essential for the planar microwave circuits. Hyltin[1] has shown that the dissipation factor, D, for materials having losses solely due to the migration of charge carriers can be computed from the resistivity and dielectric constant according to the equations given below:

$$D = \frac{1}{\omega RC} \tag{1}$$

where $R = \rho(t/A)$ and $C = \varepsilon(A/t)$. Therefore this expression reduces to

$$D = \frac{1}{\omega\rho\varepsilon} \tag{2}$$

From equation (2) is it clear that a high resistivity, ρ, will minimize the material dissipation factor, D. It should be noted, however, that the dielectric loss tangent only has to be reasonable in order to assure low dielectric losses. In high dielectric constant materials, which is a characteristic of all semiconductor elements or compounds, conductor losses dominate in planar transmission line mediums. For a 50Ω microstrip line on .008 inch thick GaAs, the conductor loss is 85% of the total loss per unit length.

In choosing a suitable substrate material the relative dielectric constant, ε_r, is also important. A high dielectric constant is advantageous since it will increase the available inter-element area in a monolithic array by reducing the size of the radiating elements. This will be covered in detail in the next section, 3.

Substrate selection must also include the mechanical and thermal properties of the material. In both the transmit and receive array applications, the distributed amplifiers operate at relatively low efficiencies and produce a substantial heat load which must be removed through the substrate. Therefore, good thermal conductivity is essential. To facilitate heat removal from the substrate by conduction, the thickness of the processed material should be minimized. As a result, the substrate must be mechanically rugged to prevent breakage during handling, test, installation and final use in an array environment.

Practical substrate considerations include cost, size, availability and processing maturity. The substrate material must be available in the quantities and size required at a reasonable cost with the necessary quality. A mature processing technology associated with the material will tend to reduce development risks by focusing attention on the monolithic array problems rather than diluting the effort with process development issues.

At frequencies below X-band, substrate selection for a monolithic amplifier application can be based on compromises between

device and microwave circuit considerations. Tradeoffs are possible due to small performance margins associated with the active devices. Above 10 GHz, however, low noise devices are state-of-the-art and must be pushed to their performance limits in the monolithic receive array application. As a result, the active device requirements will dominate the substrate selection procedure and the RF circuits and radiators must be adapted to the device medium. A summary of the substrate selection criteria and relative importance of each factor is presented in Table 1.

3. AREA CONSTRAINTS

In a monolithic array, components such as phase shifters and amplifiers, and circuit traces for RF feed lines, device control lines and power busses are required to fit within the inter-element area. This is a fundamental feature of a true monolithic antenna array.

The inter-element surface area is a function of the element lattice and spacing with respect to the free space wavelength, λ_o, and the dielectric constant, ε_r, of the substrate material. The available area is simply calculated by referring to Figure 1. For a standard matrix array lattice with half-wave element spacing, the unit cell area within the dashed boundary is derived from the expression given below:

$$A = (0.5\ \lambda_o)^2 - (0.5\ \lambda_d)^2 \qquad (3)$$

where

$$\lambda_o = \sqrt{\varepsilon_r}\ \lambda_d. \qquad (4)$$

Table 1. Ranking of Substrate Selection Criteria

CONSIDERATION	RELATIVE IMPORTANCE	REASON
Device Performance	1	• LNA and HPA operation is state-of-the-art technology
Semi-Insulating State	2	• Device isolation • Low loss tangent desired
High Dielectric Constant	3	• Increases inter-element area • Affects element bandwidth
Thermal Conductivity	4	• Amplifiers require conduction cooling through substrate
Processing Maturity	5	• Impacts ability to implement monolithic designs • Improves yield
Mechanical Ruggedness	6	• Minimize breakage • Improves yield
Size	7	• Small wafer diameters may limit subarray size
Availability	8	• Small quantities required initially • Quality affects performance
Cost	9	• Small quantities required initially

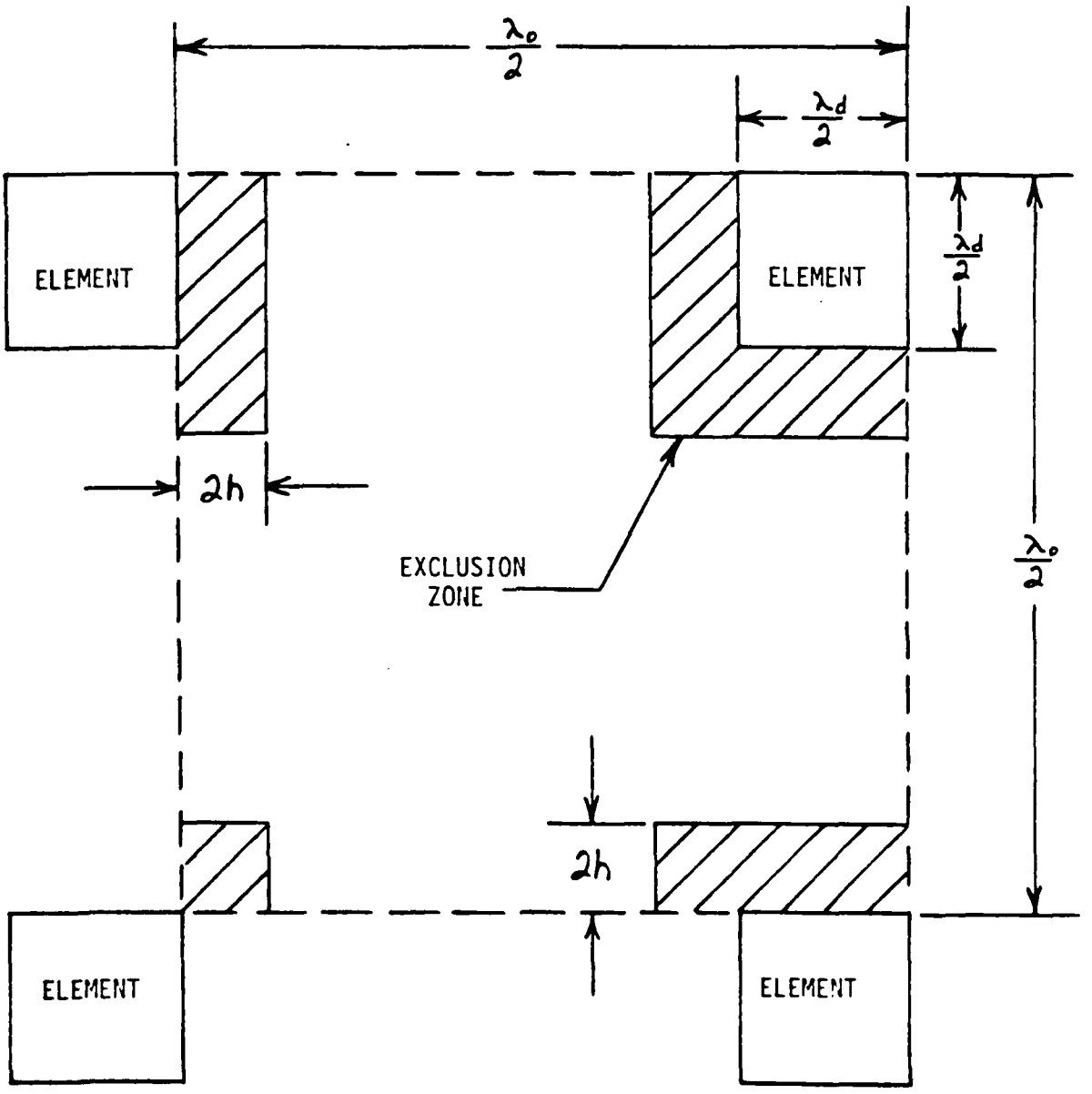

Figure 1. Planar Array Element Layout For Unit Cell Area Calculation

However, in order to retain the integrity of the microstrip radiating element and the array components, an exclusion zone must be included around the radiating element. Excluding circuits and active components from the high field region immediately surrounding the microstrip element is essential to minimize the effects of mutual coupling. The need for this exclusion zone and empirical mutual coupling data for both the E and H planes is documented in reference 2. Although it is desirable to maintain an exclusion zone at least three substrate thicknesses wide on each side of the element, a more practical value of two substrate thicknesses will be used in view of the extraordinary area constraints associated with monolithic phased arrays. Equation (5) below includes the crosshatch exclusion zones shown in Figure 1.

$$A=(0.5\ \lambda_o)^2-(0.5\ \lambda_d)^2-3(2h(0.5\ \lambda_d+2h))-2h(0.5\ \lambda_d)-(2h)^2 \qquad (5)$$

Assuming h = .008 inch, which is a reasonable compromise for microstrip lines on GaAs material, equation (5) can be rewritten as follows for ε_r = 12.9.

$$A = 2.36\ \lambda_d^2 \qquad (6)$$

Equation (6) has more of an impact when it is expressed as .252 inch x .252 inch, which is the total area available for a n-bit phase shifter, a m-stage low noise amplifier and all the attendant bias chokes, control lines, power busses, RF feed network and line separations associated with a single element at 20 GHz. As

mentioned in the previous section, a high ε_r will increase the available area according to the relationships expressed in equations (3) and (4).

The ability to replace large, distributed transmission line inductances and capacitances with lumped element monolithic components in bias choke and impedance matching circuits will greatly reduce the area requirements. Therefore, a key technology contributing to the success of monolithic arrays will be the fabrication of satisfactory lumped element passive components or the use of active components in these applications.

4. TOPOLOGY CONSTRAINTS

As the number of components or functions integrated onto a planar surface increases, topology constraints also increase due to the larger number of control or power busses which must be routed to one of the four edges for access.

Accessibility of these non-microwave lines may limit subarray size as illustrated by the examples shown in Figures 2 and 3. In the 4 x 4 array of Figure 2 only the interior four elements require lines routed to the outside edges. However, in the 8 x 8 array shown in Figure 3, the number of interior elements increases to 16. If we assume that a 4-bit phase shifter is used at each element along with an LNA, the minimum number of non-RF lines is five, four phase shifter control lines plus one power bus shared between the phase shifter and amplifier. DC ground is obtained with either a via hole to the ground plane or an edge wraparound. In the 4 x 4

array the five lines each from elements 1 and 2 can be routed without difficulty through the center of the array to the top edge. Similarly the ten lines from elements 3 and 4 can be routed to the bottom edge with five lines on each side of the RF feed line. In view of the line widths and separation required, this should present little difficulty.

Applying the same rationale to Figure 3, it is apparent that the lines from elements 1-10 must exit between elements 11 and 12 with half the lines on each side of the RF feedline. Assuming typical values of half-wave element spacing, an .008 inch thick GaAs substrate and a 20 GHz operating frequency, the total distance is .213 inch. Subtracting .006 inch for the width of the 50Ω transmission line and applying the two board thickness exclusion zone adjacent to the elements and RF feedline, two corridors each .178 inch wide are available for exiting non-RF lines. Assuming that only a single, common DC power line is required for all 5 elements, each corridor must handle 21 lines. Therefore .0042 inch or 107 micron lines and spaces are required. These dimensions do not present any problems. However, if the array lattice or element size assumptions change, then the routing of control lines and power busses may limit subarray size.

Another topology consideration which complicates the layout within the limited area is the submicron gate length of the active devices. These structures are created by either direct write electron beam techniques or E-beam fabricated masks. Since these

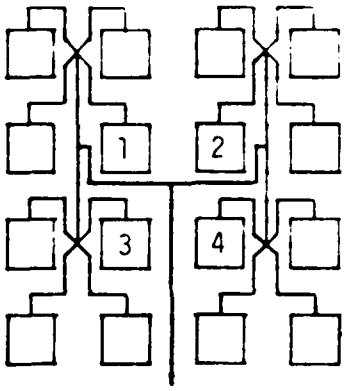

Figure 2. Typical RF Circuitry Layout For a Planar 4 x 4 Array

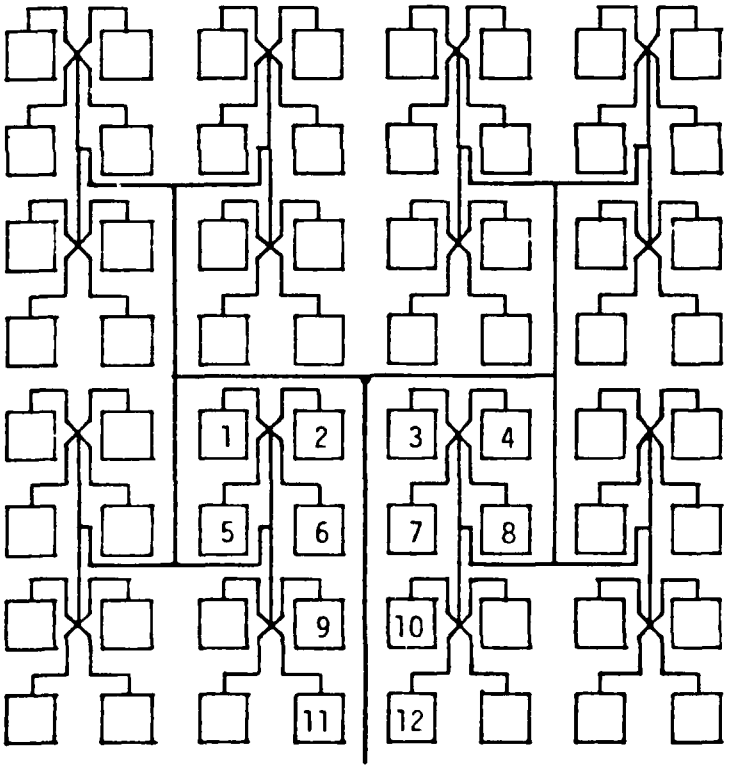

Figure 3 Typical RF Circuitry Layout For a Planar 8 x 8 Array

are typically raster scan systems, all of the gates must be aligned parallel to each other. This is also a consideration in terms of processing uniformity. The impact of parallel gate alignment, however, is a loss of freedom with respect to device orientation. This tends to reduce the effectiveness with which the available area may be utilized.

It should be noted that topology constraints can be made almost negligible by removing the planar feed network from the subarray surface. In order to accomplish this, however, the array feed network must be capable of power division and feeding at the element level which may be impractical for large arrays containing several thousand elements.

5. YIELD CONSIDERATIONS

A key factor in the development of a practical, cost effective monolithic phased array is device yield. Although the number of devices in a 4 x 4 subarray, for example, is modest in terms of large scale integration, the individual wafer size is large. The important factors directly influencing device yield are: photolithographic defects, array and active element topology, material defects and device design geometry.

Photolithographic quality is fixed by mask quality, process selection and process control. For a 20 GHz low noise amplifier application, a sub-half micron feature size is required. A critical mask inspection procedure will be necessary to insure that a reasonable chip yield is possible. A key issue is whether masks of

sufficient quality can be printed with a sub-half micron feature size and a chip area equivalent to state-of-the-art large scale integration.

Another factor related to photolithographic yield is active element topology. Photolithographic processes, in general, produce defect free areas in the central region of a wafer but near the edge exhibit a high density of defects as shown in Figure 4.

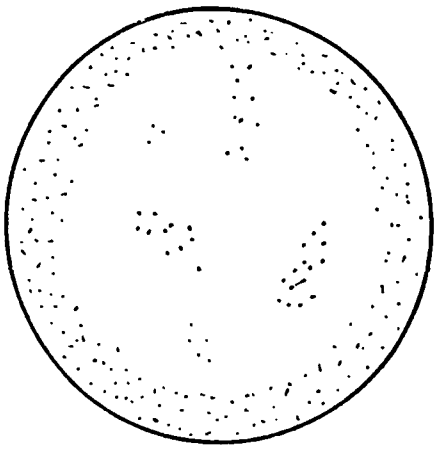

Figure 4. Failure Locations for Submicron Devices on a Typical 2 Inch Diameter Wafer

To optimize yield, the layout configuration should attempt to cluster the active elements and orient them as close to the center of the wafer as possible. This can be accomplished with the unique layout schemes that are possible using electron beam generated masks.

Material defects will be one of the underlying limitations in the successful development of monolithic subarrays. Commercially available GaAs substrates are second only to silicon substrates in terms of overall crystalline semiconductor quality. However, the two major techniques for growing GaAs substrates, Horizontal Bridgman and Liquid Encapsulated Czochralski result in defect densities on the order of $5x10^3/cm^2$ and $5x10^4/cm^2$, respectively. Although the number of active elements per chip are small, the chip is large and all elements must be functional. A correlation study of device yield across large area chips and material defect density is required to set the yield limits defined by the starting material.

Device yields can be optimized by using the largest possible gate length commensurate with the performance objectives.

6. DC POWER DISTRIBUTION

Although the DC power distribution system has non-critical design parameters compared to the RF circuits, its impact on the subarray design cannot be ignored since it also competes for the most precious resource, area. In addition, its physical cross-section is commensurate with the required current carrying capacity. These lines must be routed over the subarray surface without coupling to the RF circuits or radiating elements and without crossovers which increase fabrication complexity.

Considering the 4 x 4 subarray concept illustrated in Figure 2, it is apparent that a DC power bus needs to service a maximum of two amplifiers. Assuming that each amplifier requires 100mA of current,

the physical dimensions of the thin-film gold conductor are easily calculated. Gold is the logical choice since it is the final device contact metallization as well as the second layer metal for all the RF circuits. The limiting current density for a thin gold film is 4×10^5 A/cm^2. Assuming a conductor width of 25μm or .001 inch, and a conductor thickness of 1.1μm (1.1×10^{-4}cm), the current carrying capacity is roughly 110mA. This is satisfactory for a single amplifier drawing 100mA, but is inadequate for two amplifiers operating from a common power bus. Therefore, either the initial conductor width or thickness needs to be doubled. The easiest solution is to increase the trace width which avoids the additional processing steps required to increase the thickness. Initial metal film thicknesses greater than 1.1μm are undesirable since it adversely affects photolithography resolution.

Extending the current carrying analysis to the 8 x 8 subarray illustrated in Figure 3 results in a conductor cross-section which is three times greater than the 4 x 4 example. Six amplifiers (i.e. elements 1, 2, 5, 6, 9 and 11) must be served by a single DC power bus instead of only two. Since the useable exit dimension between element 11 and the input feedline is only .016 inch, a DC bus width of .006 inch consumes valuable area which must be shared with control lines. In this case, the extra process steps necessary to increase the conductor thickness may be required in order to reduce the width to a more practical value.

These examples show that the DC power distribution on a monolithic subarray is a significant design issue. Their large size consumes valuable surface area and routing to the interior subarray elements is complicated by the close proximity of the RF feed network and the necessity to remain decoupled. These problems emphasize the need to design the amplifier stages to operate on a single drain to source voltage thereby, eliminating the need for multiple power busses or thin-film dropping resistors. A separate DC return bus is not required since this function is provided by the microstrip ground plane which covers the entire rear or bottom surface of the subarray. This approach is compatible with a typical common source amplifier configuration which employs a grounded source through a via hole connection to achieve a low inductance path.

From the above examples it is also apparent that the subarrays will contain multiple DC power busses which will exit the monolithic subarray along all four edges. Although topology will accommodate a single, combined bus around the periphery, this configuration is undesirable since control lines will be forced to bridge over this wide conductor.

A summary of the critical DC power bus design issues and their impact on the subarray are presented in Table 2.

7. SUBARRAY ATTACHMENT

The mounting of the individual subarrays into an integrated configuration as shown in Figure 5 requires a design which provides both an electrically conductive and low thermal impedance interface between several materials of different coefficients of thermal expansion.

Table 2. DC Power Distribution Issues and Their Impact on the Subarray Design

DC Power Bus Considerations	Design Impact
Current Carrying Capacity	• Imposes minimum cross-sectional area requirement
Conductor Metal	• Must be compatible with semiconductor substrate, device type and processing technology
Conductor Thickness	• Thicker conductors have poorer photolithography resolution • Thickness build-up requires additional process steps
Conductor Width	• Wider traces consume more area and complicate decoupling from RF feed network
DC Return	• Minimal impact - uses subarray ground plane and via hole feedthroughs

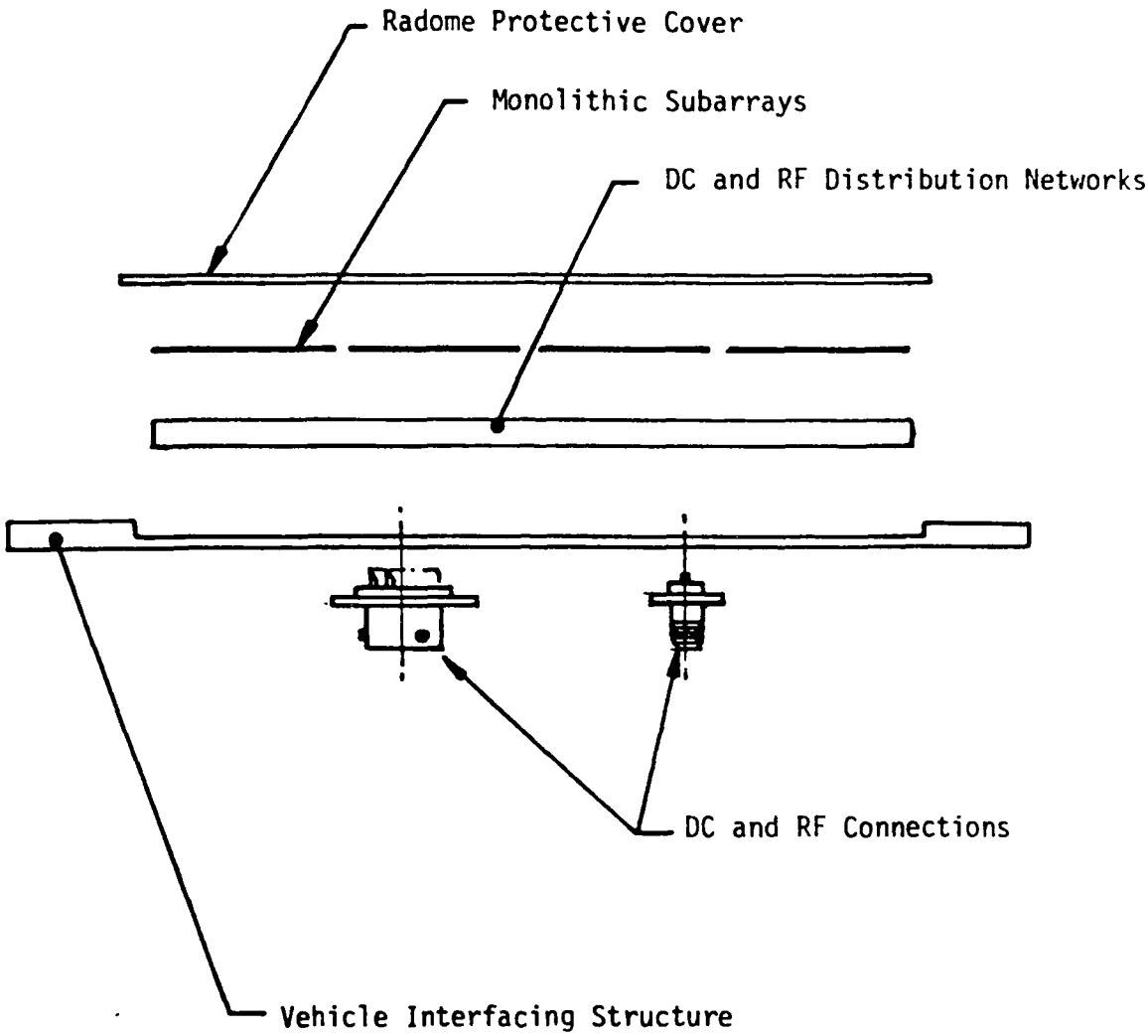

Figure 5. A Multi-Layer Assembly Technique

Since the monolithic subarrays require semiconductor materials which are different than the RF distribution and DC control circuit materials, it is possible to have mismatches in coefficients of thermal expansion approaching 5:1. This factor alone results in problems of warpage and bond-line stresses due to changes in temperature during the manufacturing process and antenna operation. The fragility of thin semiconductors and their RF and DC connections are especially critical and must not be subjected to excessive stress.

When these different materials are integrated into the antenna, the mounting interface must also provide sufficient mechanical integrity to reliably withstand environmentally induced loads. The environmental aspects are numerous and include changes in atmospheric pressure during air-transportation or flight; changes in dynamic loading as the result of handling, shock or nuclear overpressure; heating due to aerodynamics or blast; and vibrations associated with the parent vehicle.

In view of the factors mentioned above, the subarray attachment problems are equally as difficult as the design and fabrication issues. The selection of antenna materials and lamination and bonding techniques must consider critical, interdependent electrical, thermal and mechanical parameters.

8. CONCLUSIONS

Monolithic phased array antennas have the potential of implementing active aperture transmit and receive functions up to

frequencies well above X-band. Although this paper has outlined numerous tradeoffs with respect to electrical, thermal and mechanical design issues, no fundamental limitations have been encountered which would prohibit hardware fabrication.

In a monolithic array, however, traditional planar transmission line tradeoffs, involving efficiency and size, are overshadowed by totally different requirements imposed by the semiconductor device. Since active device performance is uniquely related to the physical properties of the material, the radiator and passive RF components must be adapted to this special medium.

The major design issues for any monolithic subarray are fitting the essential components within the limited aperture surface area, conducting heat out of the subarrays, optimizing device yield and mounting the individual subarrays to create a high gain antenna array.

ACKNOWLEDGMENTS

This work was supported by Ball Aerospace Systems Division, Boulder, Colorado.

REFERENCES

1. Hyltin, T. M. (1965) Microstrip Transmission On Semiconductor Dielectrics, IEEE TRANS. on Microwave Theory and Techniques, Vol. MTT-13, pp. 777-781.

2. Munson, R. E., et al, (1976) Microstrip Communications Antenna, Final Report, Contract F30602-74-C-0295, Ball Brothers Research Corporation.

INTEGRATION OF MONOLITHIC MICROWAVE INTEGRATED CIRCUITS INTO PHASED ARRAY ANTENNA SYSTEMS

BY: Brian J. Edward
Electronics Laboratory
General Electric Company
Syracuse, New York

ABSTRACT

Monolithic Microwave Integrated Circuit (MMIC) technology will have a dramatic impact upon future radar, electronic warfare, and communication systems which utilize phased arrays. Systems in both the commercial and defense industries which require large quantities of densely packed circuitry will become the prime benefactors of MMIC technology. The microwave and antenna engineers responsible for the integration of MMICs into these new systems must develop compatible radiating elements, feed networks, and module configurations as well as techniques for satisfying electrical, mechanical, and thermal interfaces in the array.

This paper discusses techniques that have been developed for interfacing MMIC modules to phased array systems. Radiating elements suitable for integration with monolithic circuitry including some novel implementations of classic radiators are presented. Examples of monolithic circuits as well as mounting and packaging methods for complete transmit/receive modules are given.

1. INTRODUCTION

Numerous papers reporting on the design and performance of Monolithic Microwave Integrated Circuits (MMICs) have appeared recently in the open literature. Only a small number of papers however have been devoted to the packaging and testing of these circuits, and even fewer have addressed the topics of integrating MMICs into transmit/receive modules and assembling these modules into complete arrays.

This paper gives examples of typical monolithic circuits which will find applications in future microwave systems. Methods of mounting and testing MMICs are considered. Examples of functional transmit/receive modules, some with integral controller circuitry are also given. The considerations for assembling modules into arrays, such as possible RF feed networks, the DC power/control signal distribution system, and thermal management methods are discussed. The paper concludes with a survey of possible radiating elements that may be directly integrated with transmit/receive modules.

2. MONOLITHIC CIRCUITS FOR PHASED ARRAY APPLICATIONS

A variety of amplifier circuits including low noise, variable gain, and power amplifiers have been fabricated in monolithic form[1]. Circuits with usable gain up through K-band have been reported on[2]. Figure 1 shows a two-stage low noise GaAs amplifier for receive applications designed at the General Electric Electronics Laboratory. The amplifier is complete in that it includes the input, output, and interstage matching circuitry as well as the DC bias networks. The chip size is only 0.89 by 2.29 mm and has a thickness of 0.10 mm. This extremely small size is made possible by the use of lumped elements in the impedance matching networks. The spiral inductors and interdigitated capacitors of these networks can be seen in the photograph of Figure 1. Two versions of this low noise amplifier circuit have been fabricated, one for S-band and the other for C-band. Both deliver a gain of approximately 18 dB over a 10 percent bandwidth.

Figures 2 and 3 show typical monolithic power amplifiers fabricated on GaAs for transmit applications. Both amplifiers employ distributed element impedance matching circuitry and include on chip DC bias networks. These circuits have been thinned to 0.10 mm thickness to lower the thermal resistance between the MESFETs and the chip carrier. Via or plated through holes are also used to realize low inductance contacts to ground. The three-stage amplifier of Figure 2 has demonstrated 20 dB

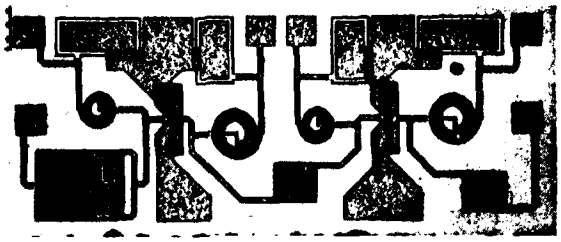

FIGURE 1. TWO-STAGE C-BAND LOW NOISE MONOLITHIC AMPLIFIER.
CHIP SIZE IS 0.89 BY 2.29 mm.

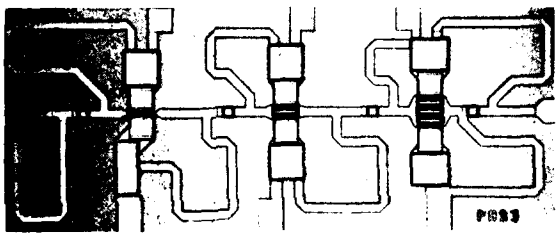

FIGURE 2. THREE-STAGE C-BAND DRIVER AMPLIFIER.
CHIP SIZE IS 1.91 BY 4.70 mm.

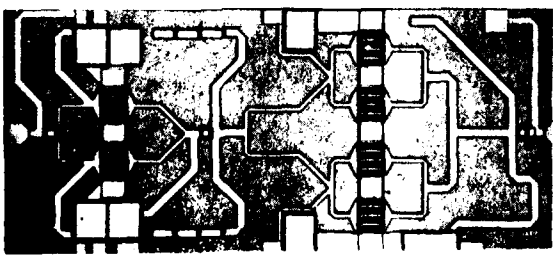

FIGURE 3. TWO-STAGE C-BAND POWER AMPLIFIER.
CHIP SIZE IS 2.16 BY 4.83 mm.

of gain between 5.2 and 6.0 GHz and a power output of 400 mW. The chip size measures 1.91 by 4.70 mm. Similar designs have also been fabricated for S- and X-band operation. The two-stage power amplifier of Figure 3 delivers 1.5 watts of output power at C-Band with a gain of better than 16 dB. The chip size measures 2.16 by 4.83 mm.

Variable gain amplifiers allow for adaptive amplitude weighting in phased array systems. Amplifiers having a gain continuously variable from -15 to +5 dB have been fabricated in monolithic form by using dual gate MESFETs as the gain controlling element[3]. A variable DC bias voltage is applied to one gate while the second gate is terminated in a specific impedance so as to make the amplifier's phase shift relatively unchanged with gain setting.

Phase shifters and transmit/receive switches have been successfully fabricated in monolithic form by utilizing resonated MESFETs as switching elements. Figure 4 shows a complete four-bit GaAs phase shifter with integral T/R switch. The circuit uses series loaded lines for the 22.5 and 45 degree bits, and a switched line configuration for the 90 and 180 degree bits. The relative phase shift over the frequency range of 5.3 to 5.9 GHz is shown in Figure 5 for each of the sixteen phase states. The RMS phase error from ideal over the above band and over all phase states is only 11.1 degrees. The phase shifter has a mean measured insertion loss of 7.5 dB with a deviation of less than $\pm$1.0 dB for any phase state. The complete circuit measures 8.00 by 8.26 mm with a thickness of 0.10 mm.

A monolithic high power transmit/receive switch is shown in the photograph of Figure 6. The single-pole, double-throw switch consists of a series FET in the transmitter branch and a shunt FET located a quarter wavelength away from the output junction in the receiver branch. The application of a sufficient negative gate bias to the FETs switches the transistors "off" and the T/R switch into the receive mode. Removal of the gate bias places the T/R switch into the transmit mode. The high power T/R switch has a measured insertion loss of less than 1.2 dB when in either the transmit or receive mode and provides 22 dB of receiver isolation during transmitting. The switch has been tested at power levels of up to 10 watts with no performance degradation. The circuit is 4.62 by 1.75 mm and is also 0.10 mm in thickness.

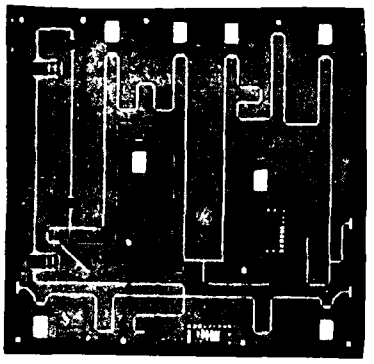

FIGURE 4. FOUR-BIT GaAs PHASE SHIFTER WITH INTEGRAL T/R SWITCH. CHIP SIZE IS 8.00 BY 8.26 mm.

The degree of integration for monolithic microwave circuitry has been limited primarily by yield considerations[4]. Circuits with large areas have a proportionately higher probability of defects. Examples of the most complex circuits that have been successfully fabricated to date with acceptable yields include the four-bit phase shifter with integral low power T/R switch discussed above, and power amplifiers with three and four stages. With the continuing improvements in processing techniques and the maturing of material fabrication, the degree of circuit integration is increasing. More transmit/receive module functions are being combined onto a single chip such as the first stages of of receiver low noise amplification with the high power T/R switch and the inclusion of digital logic with the phase shifter. Ultimately, a complete transmit/receive module will be fabricated on a single monolithic chip.

3. PACKAGING AND TESTING OF MONOLITHIC CIRCUITS

A MMIC package or carrier should provide mechanical support for the fragile circuit as well as affording connecting terminals to the circuit's RF ports and

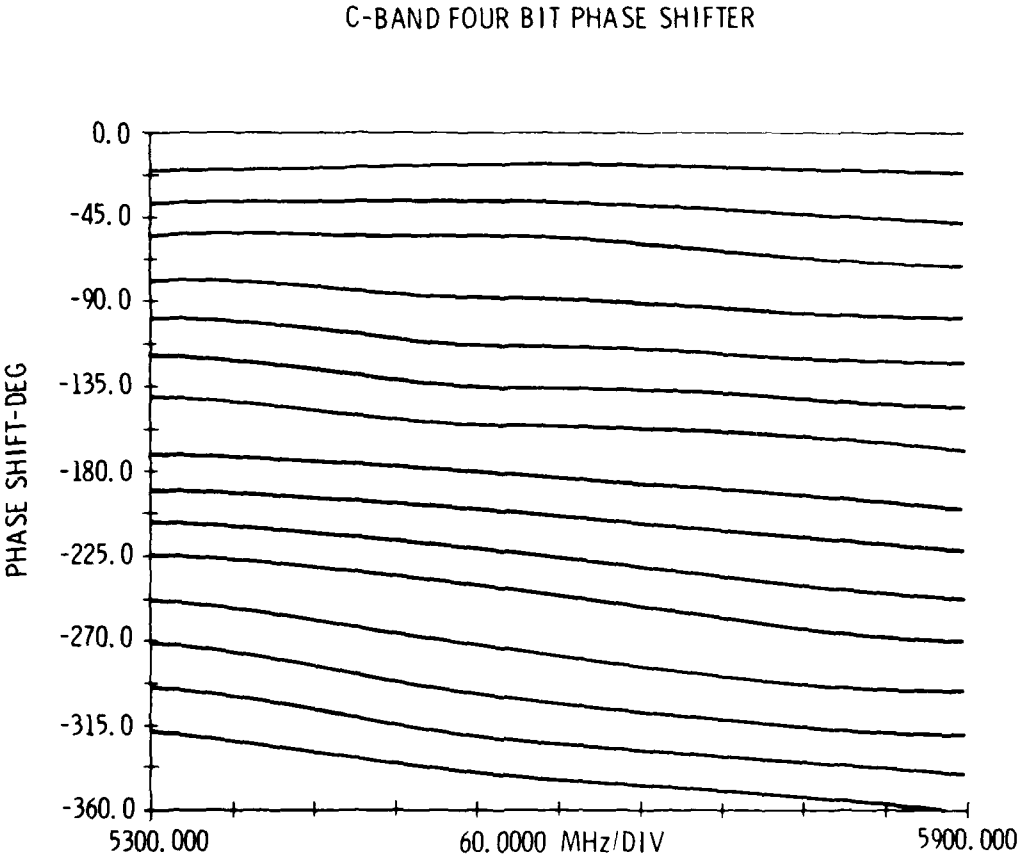

FIGURE 5. RELATIVE PHASE SHIFT AS A FUNCTION OF FREQUENCY FOR THE C-BAND MONOLITHIC PHASE SHIFTER.

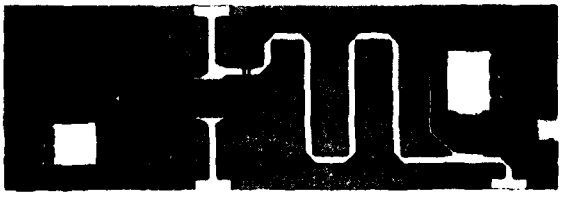

FIGURE 6. HIGH POWER MONOLITHIC TRANSMIT/RECEIVE SWITCH. CHIP SIZE IS 4.62 BY 1.75 mm.

DC/control lines. The carrier design should allow for testing of the MMIC before it is placed into the transmit/receive module, and once in the module housing the carrier should interface to other circuit carriers with minimal parasitics. Additionally, a method of fastening the carrier to the module housing must be provided. It is also desirable that the carrier design be universal in that a single design is amenable to a wide variety of monolithic circuits.

Many of the carriers reported upon for the mounting of MMICs resemble the packages used for power transistors. The circuit is bonded to a flange style base with alumina substrate microstrip lines providing connections for the RF ports and separate pads for the connection of the required DC voltages. The disadvantage of this style of carrier is that the flange mounting scheme results in the overall carrier size being substantially larger than the MMIC. Also the method for DC connections may not be optimum for application of the circuit in a T/R module.

A MMIC carrier in use at General Electric is shown in the photograph of Figure 7. The carrier base is machined from brass and is gold plated. On the top surface of the carrier a slot is machined with length and width corresponding to that of the MMIC chip. The slot depth is selected so as to make the chip top surface coplanar with the carrier and the alumina RF interconnecting boards. This feature facilitates making short wire bond connections from the circuit's RF ports to the interconnecting boards and if required, from the circuit's ground points to the metal carrier.

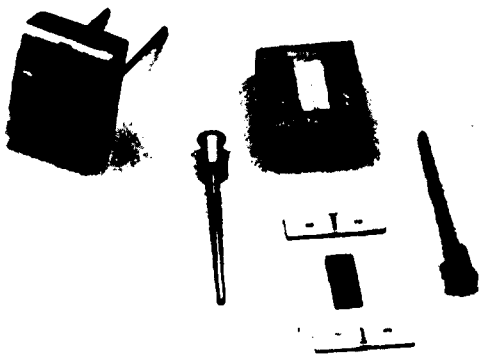

FIGURE 7. MMIC CARRIER FOR MODULE APPLICATIONS.

The alumina RF interconnecting boards have a 50Ω microstrip transmission line with a large bonding pad at the end. The large pad allows for the use of a greater number of wire bonds when interconnecting to other circuit carriers and helps compensate for the discontinuity at the carrier to carrier interface. Both the interconnecting boards and the MMIC chip are fastened to the metal carrier base with silver loaded epoxy. When maximum thermal conductivity between the circuit and the carrier is required, the chip should be soldered in place.

Connection to the circuit's DC power and control points are made via miniature feed-through pins which are soldered into the carrier base. These pins consist of a 0.46 mm diameter gold plated Kovar wire glass fritted into a 1.57 mm diameter gold plated Kovar eyelet. Wire bonds make the connection from the top of the feed-through pins to the MMIC. The circuit carriers are held into module housings by an 0-80 screw. A tapped blind hole is located in the bottom of the carrier for this purpose.

A hermetically sealed refinement of this circuit carrier, which is presently under development, is illustrated in Figure 8. The carrier base is gold plated Kovar which is flat on both the top and bottom surfaces. The Kovar material has a thermal coefficient of expansion which is well matched to that of alumina and GaAs. Feed-through pins for DC power and control line connections are fritted directly into the carrier base thereby eliminating the pin soldering operation. A one piece alumina interconnect board bonded to the carrier base is printed with microstrip lines for the RF interconnects. The size of the cut-out in this interconnect board can be varied so as to accommodate different circuit sizes with a single carrier design. The alumina has a thickness of 0.13 mm which is well matched to that of our GaAs circuits. A ceramic cover seals to all four sides of the interconnect board to complete the hermetic package.

An 0-80 mounting stud welded to the carrier base provides a means of fastening the circuit carrier to the module housing. With this arrangement, the MMIC carrier may be made much thinner than the present design which has a tapped hole for mounting. Therefore, not only is the weight of the carrier reduced, but the carrier to carrier interfaces are improved making the design usable up to higher frequencies.

A number of interesting circuit carriers are presently being developed for high speed digital integrated circuits[5]. Research is being devoted to improved

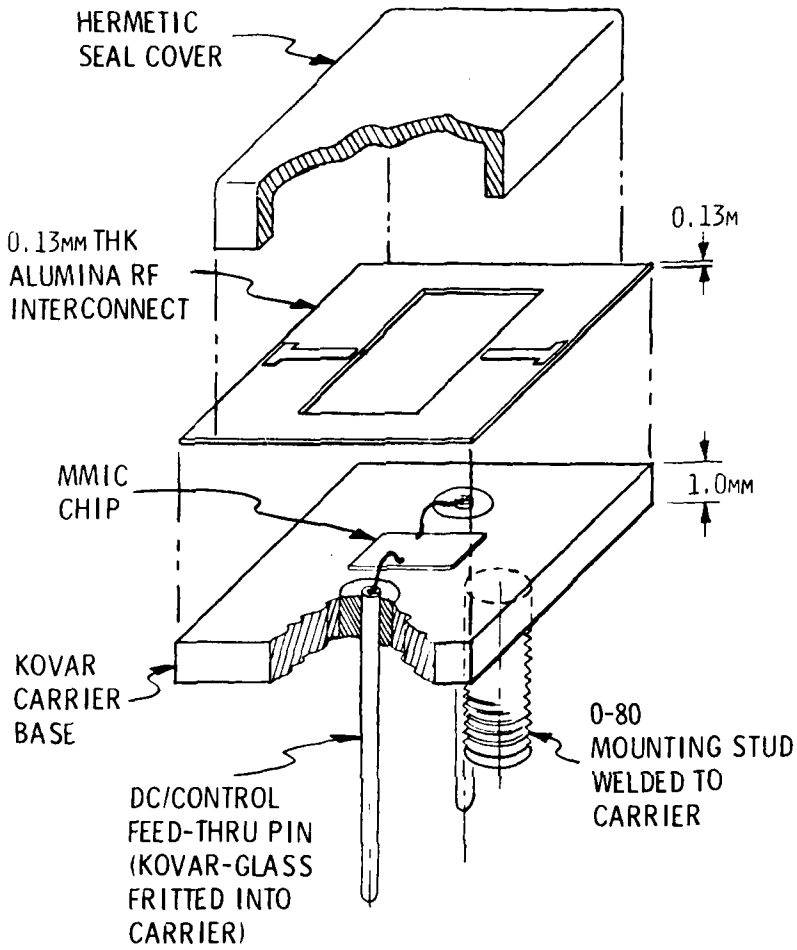

FIGURE 8. HERMETICALLY SEALED MMIC CARRIER.

substrate materials[6], chip bonding methods, and carrier hermetic sealing techniques. A number of the developments will be directly applicable to the packaging of monolithic microwave integrated circuits.

Monolithic circuits are characterized with respect to their RF performance before they are committed to a module. A simple, low cost test fixture for performing this function is shown in Figure 9. The MMIC carrier is held to the test fixture base with a single screw. SMA series connectors are mounted on end plates which attach to the test fixture base. The center pins of the SMA connectors make pressure contact on the RF microstrip lines and DC power is applied from the

FIGURE 9. LOW COST FIXTURE FOR RF TESTING PACKAGED MMICs. USABLE UP THROUGH 16 GHz.

underside via the feed-through pins. The connectors shown have been found to have good performance and yield reproducible data at frequencies up through 16 GHz.

It is often desirable to test MMIC chips for their RF performance before they are mounted onto a carrier. Figure 10 shows a test fixture for this purpose which has been used for the evaluation of silicon-on-sapphire phase shifter bits. The test fixture consists of an upper and lower half. The MMIC to be tested is held into position in the lower half of the fixture by pressure on the chip's edges. The top portion of the fixture aligns with dowel pins to the lower half. Short probes soldered to the fixture's microstrip lines make contact to the MMIC's RF and DC pads. A set of these fixtures has been used to test over 5,000 circuits during a 3 month period.

For large scale production of MMICs it will be necessary to RF probe test circuits at the wafer level, i.e., before the wafer is separated into individual chips[7]. This technique has the advantage that bad circuits may be identified and dismissed before further handling.

4. ASSEMBLING MMICs INTO TRANSMIT/RECEIVE MODULES

The extremely small size of monolithic microwave integrated circuitry makes possible the assembly of transmit/receive modules which may be located at each element of a phased array system. A block diagram of a typical module developed at General Electric for a C-Band Advanced Tactical Radar is shown in Figure 11. Functions within a dotted box represent those contained on a single monolithic chip.

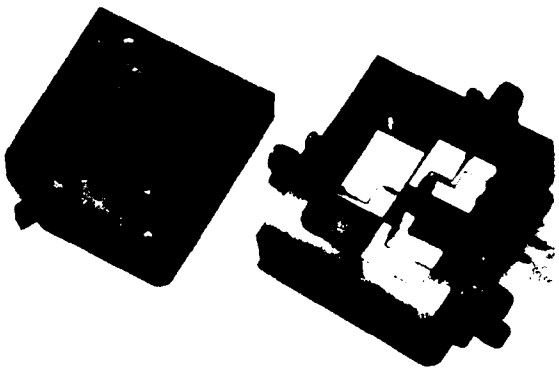

FIGURE 10. FIXTURE FOR RF TESTING UNPACKAGED MMIC CHIPS.

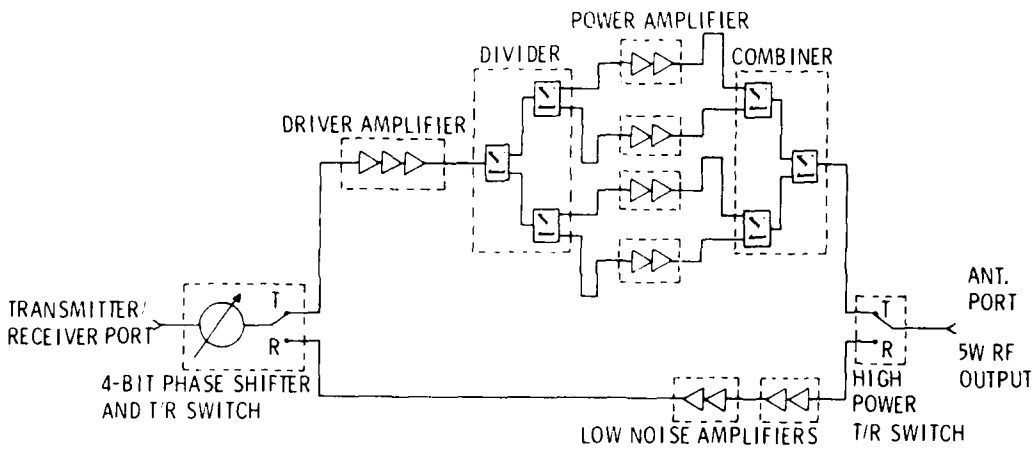

FIGURE 11. TRANSMIT/RECEIVE MODULE FOR AN ADVANCED TACTICAL RADAR.

A four-bit bi-directional phase shifter provides element phase weighting during both transmit and receive modes. Transmit gain is achieved with a 3-stage driver amplifier cascaded with the parallel combination of four 2-stage power amplifiers. Pairs of power amplifiers are driven in quadrature to eliminate even mode reflections from their input and certain intermodulation products at their output. Each power amplifier is designed to deliver 2 watts of power output so that after combination and the insertion losses associated with the module front end, the net RF output power will be a minimum of 5 watts. Receive gain is provided by two cascaded 2-stage low noise amplifiers. The high power T/R switch provides 22 dB

of isolation between the transmitter output and the receiver first low noise amplifier stage. During operation the receive stages are biased "off" when in the transmit mode and the transmit stages are biased "off" when in the receive mode.

The breadboard version of the C-Band module is shown in the photograph of Figure 12. The module assembly consists of the circuit carriers (described in Section 2.) mounted into an aluminum housing. The DC power and control signal feed-through pins plug into a printed wiring board which is located on the underside of the module housing. The power/control lines are routed to a single multi-pin connector located on the housing end. Four-way Wilkinson dividers for transmitter RF power division and combination are evident in the photograph. These circuits are fabricated using a monolithic process on silicon-on-sapphire substrates.

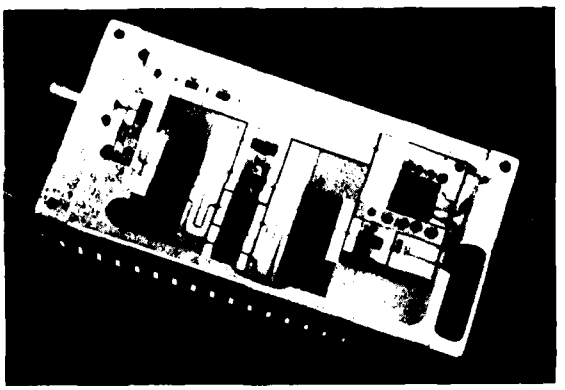

FIGURE 12. C-BAND MMIC TRANSMIT/RECEIVE MODULE.

Circuit carriers are butted directly together with the RF microstrip interconnects being made with multiple wire bonds. The use of multiple wire bonds reduces the equivalent series inductance of the interconnect thereby improving the electrical performance of the carrier to carrier interface[8]. An interconnect made with multiple bond wires will actually have less inductance and be mechanically stronger than one made with an equivalent ribbon.

To prevent low frequency amplifier oscillations, a large parallel plate chip capacitor is bonded to the amplifier carrier's top surface and wired in shunt with

the amplifier's drain bias line. This capacitor is evident in the photograph of Figure 7. For maximum effectiveness the capacitor should be located as close as possible to the amplifier chip. Low frequency oscillations can be particularly detrimental in a T/R module since they may mix with the desired signal rendering in-band spurious signals.

The internal dimensions of the C-Band module housing were carefully selected so as to avoid in-band cavity resonances. For this particular module, the operating band is between the calculated first and second resonant modes. If any in-band resonances do occur, they can usually be eliminated by bonding a magnetically lossy material to the housing cover to suppress surface currents. The overall module size (83 x 41 x 25 mm) was selected so that unit would fit into the phased array element grid pattern. A thermal analysis was performed on the module housing to ensure that there existed adequate heat sinking for the power amplifier circuits.

The C-Band breadboard module has a measured net gain of 27 dB in the receive mode and 20 dB in the transmit mode. A prototype module now under development will integrate more circuit functions per GaAs chip thereby reducing the module part count and size. It will also include provisions for an integral module controller.

A MMIC module for controlling the element phase in a space based phased array lens antenna is shown in Figure 13. The RF monolithic circuitry which is mounted onto one side of an alumina supporting substrate consists of a 4-bit phase shifter and two baluns for transitioning to the lens dipole radiating elements. An 8-bit microprocessor based controller system is located on the opposite side of the alumina substrate. The controller calculates the proper phase shifter state based on the element position, compensating for the spherical phase front incident upon the lens. The beam steering information is encoded in the RF signal sent by the main feed and is decoded by the controller. Plated through holes in the alumina substrate provide interconnection for the controller and RF circuitry. The entire module is only 25 x 25 x 3.6 mm in size.

5. INTEGRATION OF MODULES INTO PHASED ARRAYS

The form in which transmit/receive modules using MMICs are integrated into a phased array will be dictated by the application and performance requirements for the phased array system. Some aspects of the array design that will be impacted by

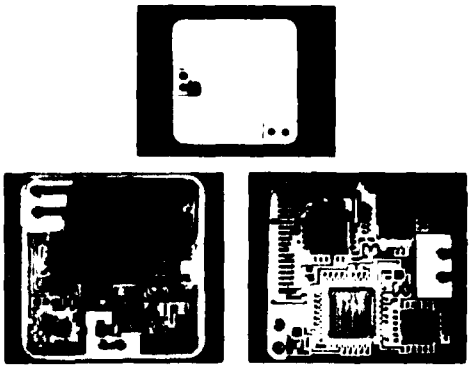

FIGURE 13. PHASE SHIFT MODULE WITH INTEGRAL CONTROLLER FOR A PHASED ARRAY LENS ANTENNA.

the use of MMIC modules and must be considered by the array designer include the type and media for the RF feed network, a technique for the distribution of DC power and control signals, a means by which the modules may be fastened into the array and be accessible for easy replacement, as well as a method for the removal of excess heat generated by the active circuitry.

A concept for the assembly of a 30 GHz active receive array to be used as the primary feed in a dual reflector satellite antenna is shown in Figure 14. Because of the high frequency of operation, the spacing between array elements is extremely limited. By orientating the modules in a longitudinal fashion as shown in the figure, it is possible to locate the active circuitry with each radiating element.

The array concept shown is actually two interleaved independent arrays, one horizontally polarized and the other vertically polarized. Grooved guide posts attached to a structural face plate are arranged in a pattern dictated by the element grid. The active module which consists of a low noise amplifier, variable gain amplifier, and phase shifter integrated with a printed end-fire radiating element is inserted between the guide posts in the appropriate vertical or horizontal orientation. The RF signal connection to the beam combining network is made with a plunge style connector having one part secured to the module and the mating part secured to the structural face plate. The DC power and control signal connections are made via a multi-pin miniature connector secured in the same fashion as the

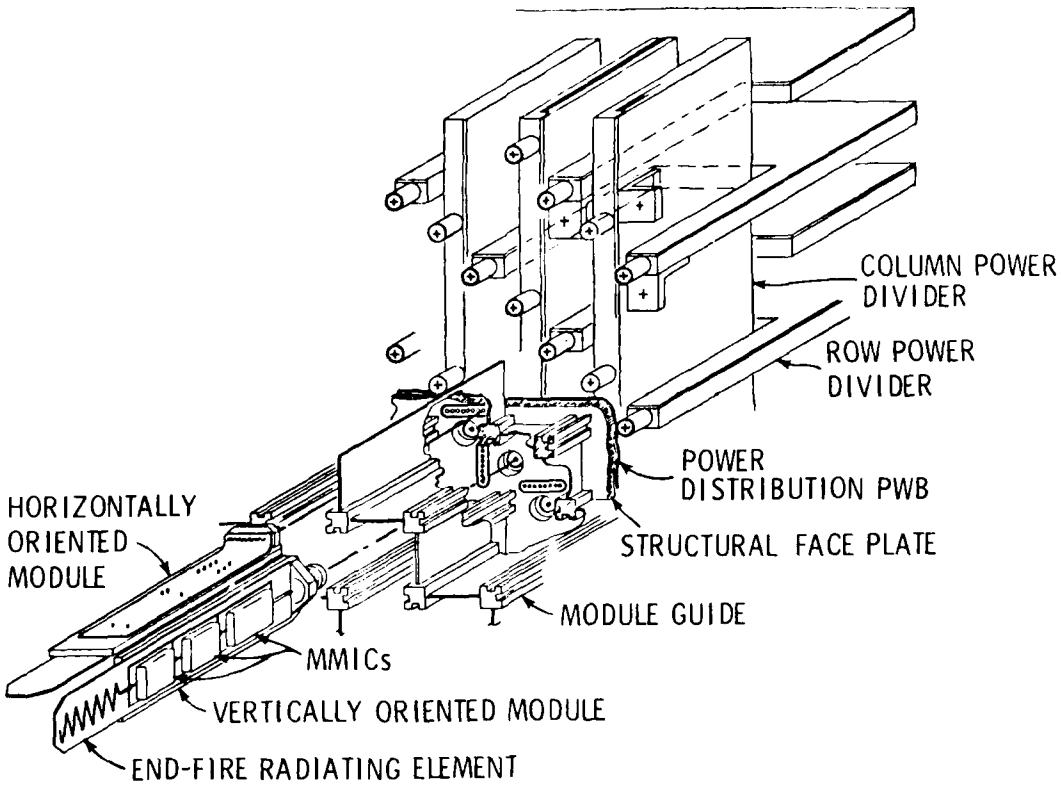

FIGURE 14. DUAL-REFLECTOR FEED ARRAY ASSEMBLY UTILIZING MMIC RECEIVE MODULES.

RF connector. The vertical and horizontal beam combining networks are stripline dividers. Stripline circuitry has been selected because its self-shielding property will minimize the detrimental effects of transmission line radiation and coupling, and because of its wide flexibility with respect to combiner/divider design and line impedances. A printed wiring harness for the DC power and control lines is laminated to the back side of the structural face plate. A one piece protective cover fits over the array face.

Excess heat generated by the active circuitry is transferred by conduction from the module housing to the structural face plate. Heat pipes may be integrated into the face plate to efficiently conduct heat from the array to an external radiator[9].

An ECM phased array also assembled from modules orientated in a longitudinal fashion is shown in Figure 15. The array is comprised of eight row subarrays each

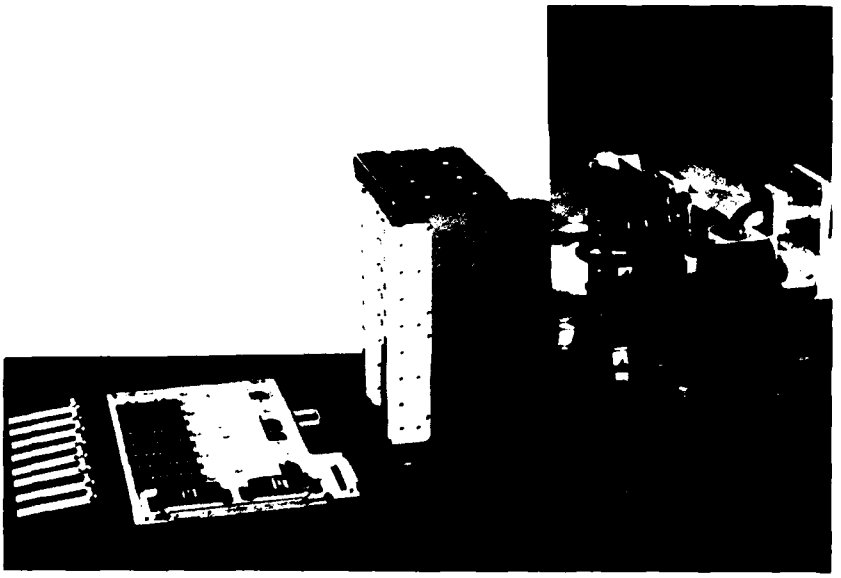

FIGURE 15. WIDEBAND ECM PHASED ARRAY.

consisting of eight elements. A subarray assembly contains two 4-way power dividers, eight wide band 2-bit phase shifters, and two beam steering computers. The beam steering computers are located on the bottom side of the subarray housing and are interconnected to the phase shifters via a multi-layer printed wiring board. A subassembly of eight end-fire radiating elements plugs into the row subarray with plunge style RF connectors. The row boards mate with column power dividers also through plunge connectors. The next iteration in the development of this array will include both a monolithic transmit and receive amplifier for each radiating element.

When a phased array system must be conformal, such as in airborne installations where the array must not alter the aerodynamic contour of the aircraft or intrude significantly into the aircraft structure, it is necessary to configure the transmit/receive circuitry along with the radiating element in a transverse fashion. To minimize the array depth, the radiating element, active RF circuitry, beam combining network, and logic control circuitry may all be located in a single plane or may be subdivided into multiple planes with the electrical interconnections between them. The feasibility of locating all the circuitry in a single plane which will result in the thinnest possible array, is dependent upon the element spacing, the size of

the radiating element and active circuitry, and the type of beam combining network selected.

A 20 GHz conformal receive array presently under development is shown in Figure 16. A circularly polarized radiating element, low noise amplifier, and three-bit phase shifter are fabricated on a single GaAs substrate. This implementation reduces the number of RF wire bond interconnects that would be required with separate chips. Sixteen active elements are bonded to a thin alumina supporting substrate to form a four by four element subarray. This supporting substrate is suspended approximately $\lambda_0/10$ above a ground plane that serves as a reflecting surface for the radiating element. A series coupler beam combining network is located in the space between rows of radiating elements. The couplers' isolated port terminating resistors are implanted into the GaAs substrates and grounded with via holes. Multiple wire bonds interconnect the couplers and GaAs circuitry. DC power and data bus lines are printed onto the bottom side of the alumina supporting substrate. Interconnects to the GaAs circuitry are made via plated through holes.

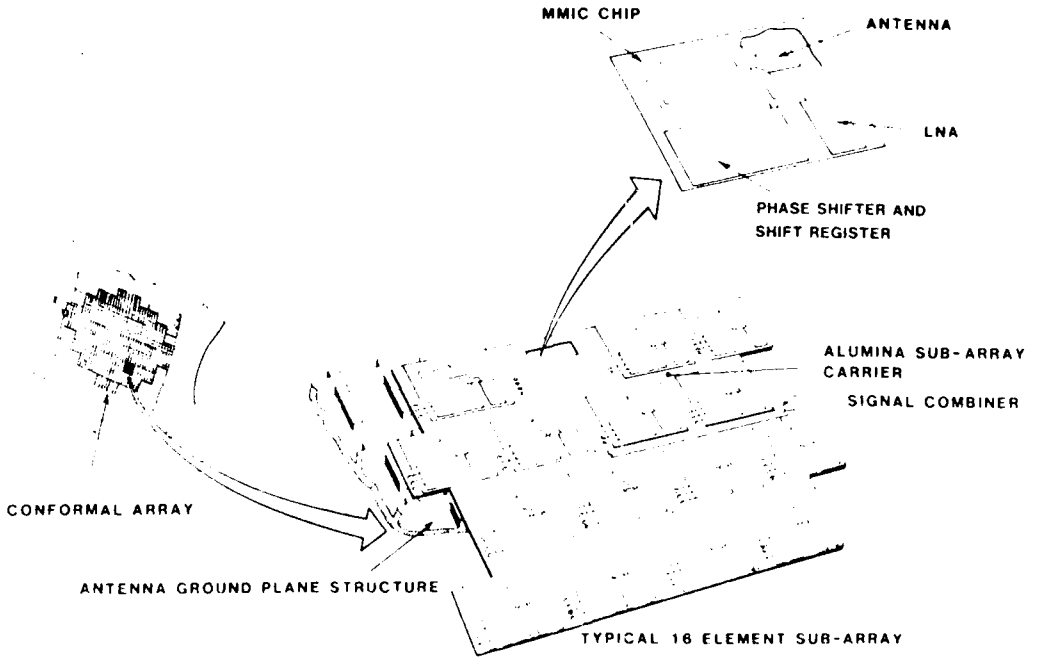

FIGURE 16. CONFORMAL RECEIVE ARRAY USING SERIAL BEAM COMBINING NETWORK.

the radiating element and active circuitry, and the type of beam combining network selected.

A 20 GHz conformal receive array presently under development is shown in Figure 16. A circularly polarized radiating element, low noise amplifier, and three-bit phase shifter are fabricated on a single GaAs substrate. This implementation reduces the number of RF wire bond interconnects that would be required with separate chips. Sixteen active elements are bonded to a thin alumina supporting substrate to form a four by four element subarray. This supporting substrate is suspended approximately $\lambda_0/10$ above a ground plane that serves as a reflecting surface for the radiating element. A series coupler beam combining network is located in the space between rows of radiating elements. The couplers' isolated port terminating resistors are implanted into the GaAs substrates and grounded with via holes. Multiple wire bonds interconnect the couplers and GaAs circuitry. DC power and data bus lines are printed onto the bottom side of the alumina supporting substrate. Interconnects to the GaAs circuitry are made via plated through holes.

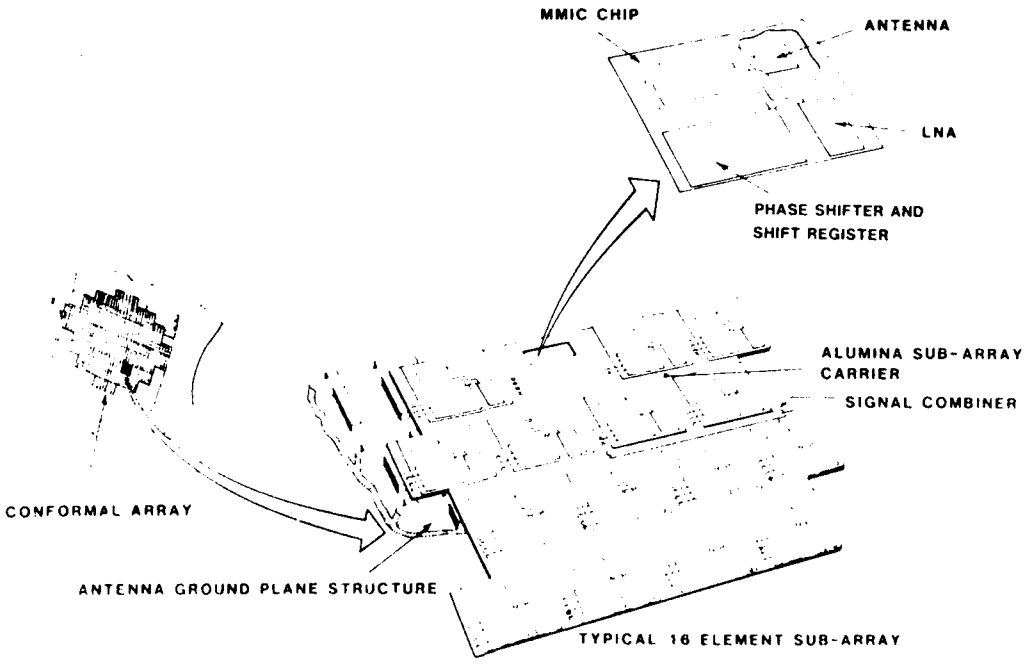

FIGURE 16. CONFORMAL RECEIVE ARRAY USING SERIAL BEAM COMBINING NETWORK.

It is also possible to update current phased array systems with monolithic circuitry for improved performance. Figure 17 shows an example of this concept where the horn elements of a waveguide fed 20 GHz transmit array have been replaced by active modules. Each module consists of a multi-stage 0.5 watt amplifier, a 5-bit phase shifter, and a subarray of circularly polarized patch radiating elements. A microstrip to waveguide transition allows interconnecting the GaAs circuitry with the waveguide feed.

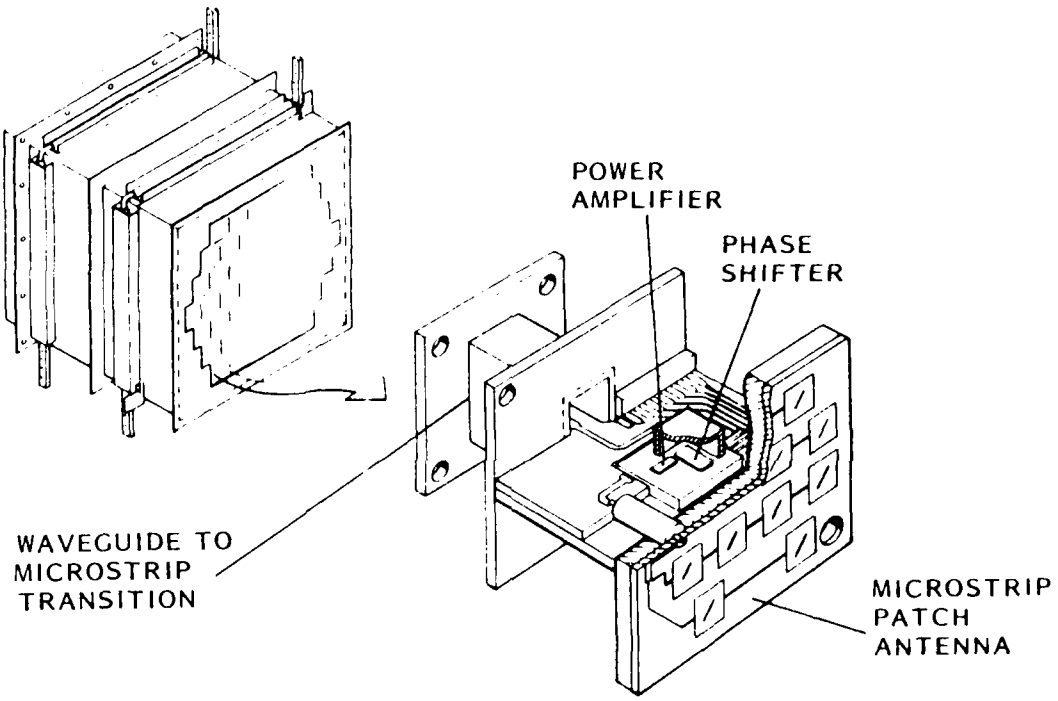

FIGURE 17. WAVEGUIDE PHASED ARRAY UPDATED WITH ACTIVE MMIC MODULES.

RADIATING ELEMENTS FOR INTEGRATION WITH MMICs

A number of radiating elements including some novel implementations of classic radiators have been developed recently which are ideally suited for integration with monolithic transmit/receive modules. One type of element which has received much attention lately, particularly for application in conformal arrays, is the microstrip patch[10].

Patch radiators are printed onto one surface of a dielectric substrate, while the other side is completely metallized to form a ground plane. The patch may

take on various geometric shapes with rectangular and circular being the most common. The radiator may be fed from the backside of the substrate by a coaxial line, by a microstrip line located on the same surface of the substrate as the patch, or excited as a parasitic element by a secondary radiator.

The half-power beamwidth and operating bandwidth of a patch element is a function of the dielectric constant of the substrate onto which the element is printed. For low dielectric constant substrates, the half-power beamwidths are in the neighborhood of 90^{o}. The 2:1 VSWR bandwidth may range between 1 and 10 depending upon the substrate thickness. To increase the half-power beamwidth the physical size of the patch must be decreased by printing it onto a high dielectric constant substrate. This implementaion, however, has an adverse effect on the element's operating bandwidth and efficiency. For patches printed onto a GaAs substrate, the 2:1 VSWR bandwidth ranges from only 0.1 to 0.5 .

Basic patch elements produce a linearly polarized field pattern. Circular polarization may be obtained from a single-feed-point patch element by either slightly altering the shape of the radiator or by including capacitive or inductive elements in the structure so as to excite two orthogonal modes. The disadvantage of this technique is that the excitation of the two modes varies as a function of frequency. Therefore, the ellipticity of the polarization degrades rapidly off the element's center frequency. A 30 GHz single feed circularly polarized patch element fabricated at General Electric is shown in the photograph of Figure 18. This element is printed on a 0.43 mm thick GaAs substrate.

Circular polarization may also be obtained from a patch element by feeding it orthogonally with two lines from an external quadrature divider. If an isolated type of divider is employed, the element's bandwidth with respect to VSWR and pattern ellipticity may be increased. Signals reflected at the element feed points are dissipated in the quadrature divider's isolating load as opposed to being re-radiated at the opposite feed point. As a result, the input VSWR and polarization purity for the dual-feed circularly-polarized patch element can potentially be less frequency dependent than a comparable single-feed circularly polarized patch. The disadvantage of the dual-feed element is the additional area required for the external divider.

FIGURE 18. SINGLE FEED CIRCULARLY POLARIZED PATCH ANTENNA PRINTED ON GaAs.

Dipole elements may also be printed onto a dielectric substrate and interfaced directly with monolithic circuitry. Figure 19 shows a 30 GHz fan or bow-tie type dipole antenna that has been fabricated along with a low noise mixer on a single GaAs substrate. A 100Ω balanced coplanar line interconnects the mixer diode with the feed point of the dipole. Future development efforts include the addition of a low noise amplifier between the dipole and the mixer. These integrated modules will be assembled into an array for a satellite communications uplink.

An interesting printed radiating element which can provide a broad main beam with circular polarization is a folded-dipole within an annular slot[11]. The element, as shown in Figure 20, consists of a rectangular slot radiator in the metallized surface of a dielectric substrate. Located within this slot is a printed folded-dipole radiator. A single microstrip feed line excites both the dipole and the slot. The continuous metallization that surrounds the element provides a ground plane for monolithic microstrip circuitry. The substrate is suspended approximately $\lambda_0/4$ from a second ground plane that serves as a reflector for the radiating element.

The area between the radiating element circuitry substrate and the reflecting ground plane can be either left void or filled with a low-loss, low-dielectric constant material. The low radiation resistance normally associated with a dipole located close to a conducting surface is transformed to a higher value due to its folded nature. The transformation ratio may be tailored to a specific value by altering the relative widths of the radiating sections.

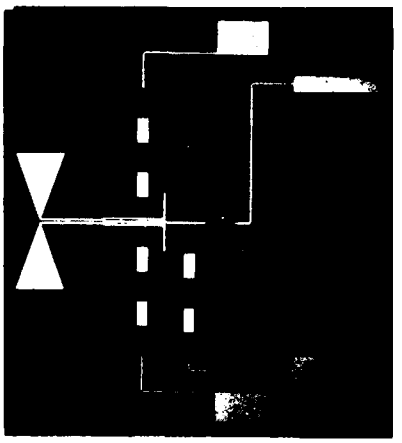

FIGURE 19. BOW-TIE DIPOLE WITH MIXER CIRCUIT FABRICATED ON GaAs.

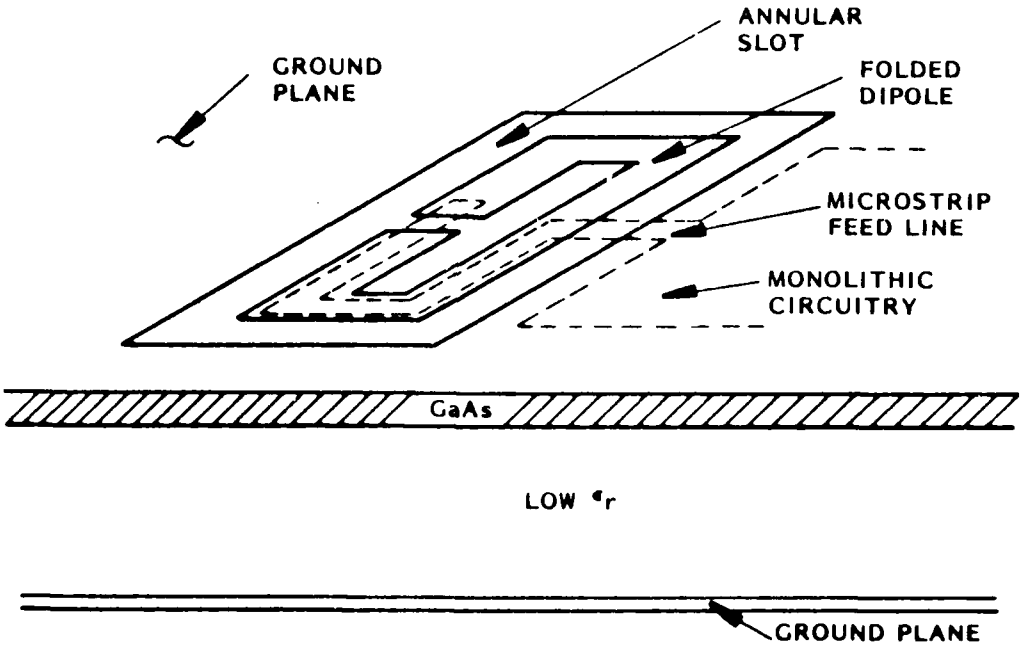

FIGURE 20. PRINTED SLOT-DIPOLE ANTENNA FOR BROADBEAM CIRCULAR POLARIZATION.

A photograph of an S-band slot-dipole developed at General Electric is shown in Figure 21. This element has an input VSWR which remains under 2:1 over a bandwidth of 11% with respect to its center frequency. Figure 22 shows the circularly polarized electric field components for the element operating at 2200 MHz. This cut is the E-plane for the folded dipole and the H-plane for the

FIGURE 21. SLOT-DIPOLE ANTENNA FOR S-BAND.

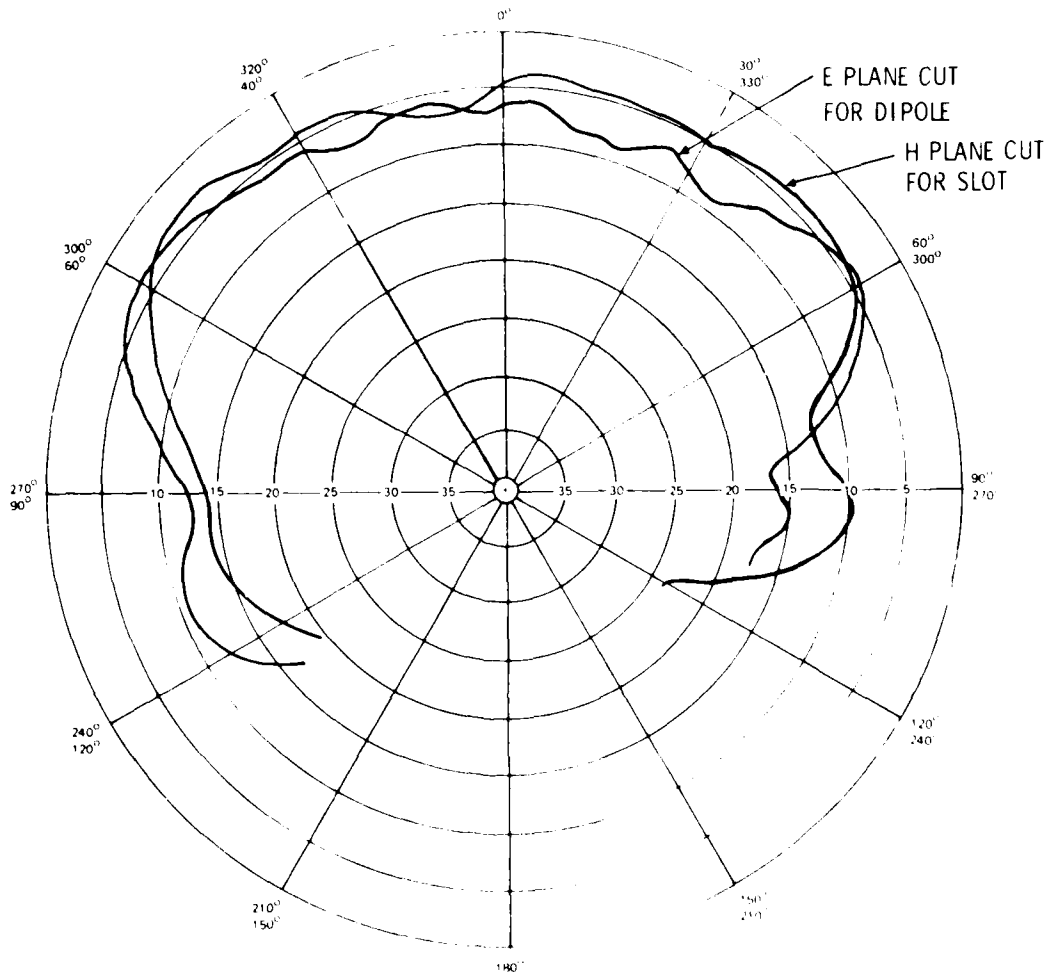

FIGURE 22. ELECTRIC FIELD COMPONENTS FOR THE S-BAND SLOT-DIPOLE ANTENNA OPERATING AT 2200 MHz.

annular slot. The ellipticity ratio is essentially 3 dB or less for the sector of $+80^{0}$ from broadside. This element design is being scaled for operation at higher frequencies.

Two types of elements that will provide linearly polarized end-fire radiation are the zig-zag[12] and the yagi. A zig-zag antenna is the two-dimensional equivalent of a helix. It may be printed onto a supporting substrate and fed directly with a microstrip line. The peak directive gain and operating bandwidth are determined by the element's section lengths, section pitch angles, and the total number of sections. A 30 GHz zig-zag antenna is shown in the photograph of Figure 23. This six-section example is printed onto a low dielectric constant woven teflon-glass supporting substrate. Measurements showed the element to have moderate gain (12 dBi) at its center frequency.

A ten element 30 GHz yagi antenna also printed onto a teflon-glass supporting substrate is shown in Figure 24. The driven element is fed by a coplanar balanced line. A reflector element is located on the backside of the substrate so as to avoid interference with the feed line. The parasitic element spacing and taper schedule were selected so as to achieve a moderate level (approximately 12 dBi) of relatively constant forward gain over a 12% bandwidth. The yagi antenna was found to have a wider gain bandwidth and lower cross-polarization components than the equivalent size zig-zag. Both the zig-zag and yagi designs were developed using method-of-moments modeling techniques.

A printed flared-notch element may be used to obtain end-fire linearly polarized radiation over a bandwidth in excess of 2:1. Figure 25 shows a flared-notch element that has been developed for use over the 8 to 18 GHz band. This microstrip fed element is printed onto a 0.25 mm thick alumina substrate. The shaded region of the photograph is the far side metallization showing through the alumina. The measured input VSWR remained generally under 2:1 over the entire 8 to 18 GHz band. Coupling for nearest neighbors in an array environment, whether colinear, broadside, or orthogonal, generally did not exceed 25 dB. The measured forward gain as a function of frequency for an isolated flared-notch element is given in Figure 26.

FIGURE 23. SIX-SECTION PRINTED ZIG-ZAG ANTENNA FOR 30 GHz.

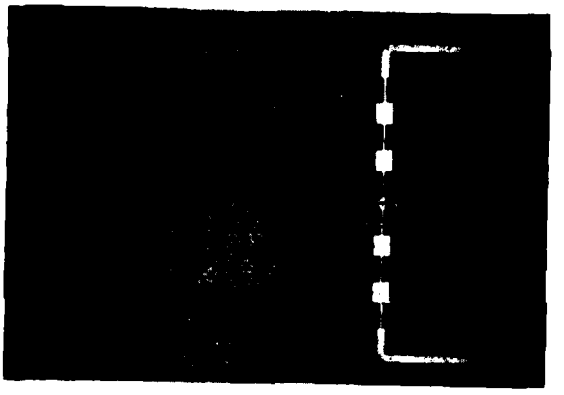

FIGURE 24. TEN-ELEMENT PRINTED YAGI ANTENNA FOR 30 GHz.

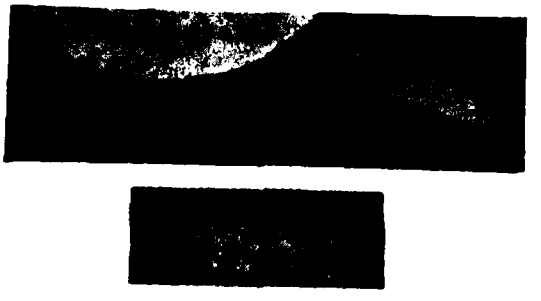

FIGURE 25. 8 TO 18 GHz NOTCH ANTENNA PRINTED ON AN ALUMINA SUBSTRATE.

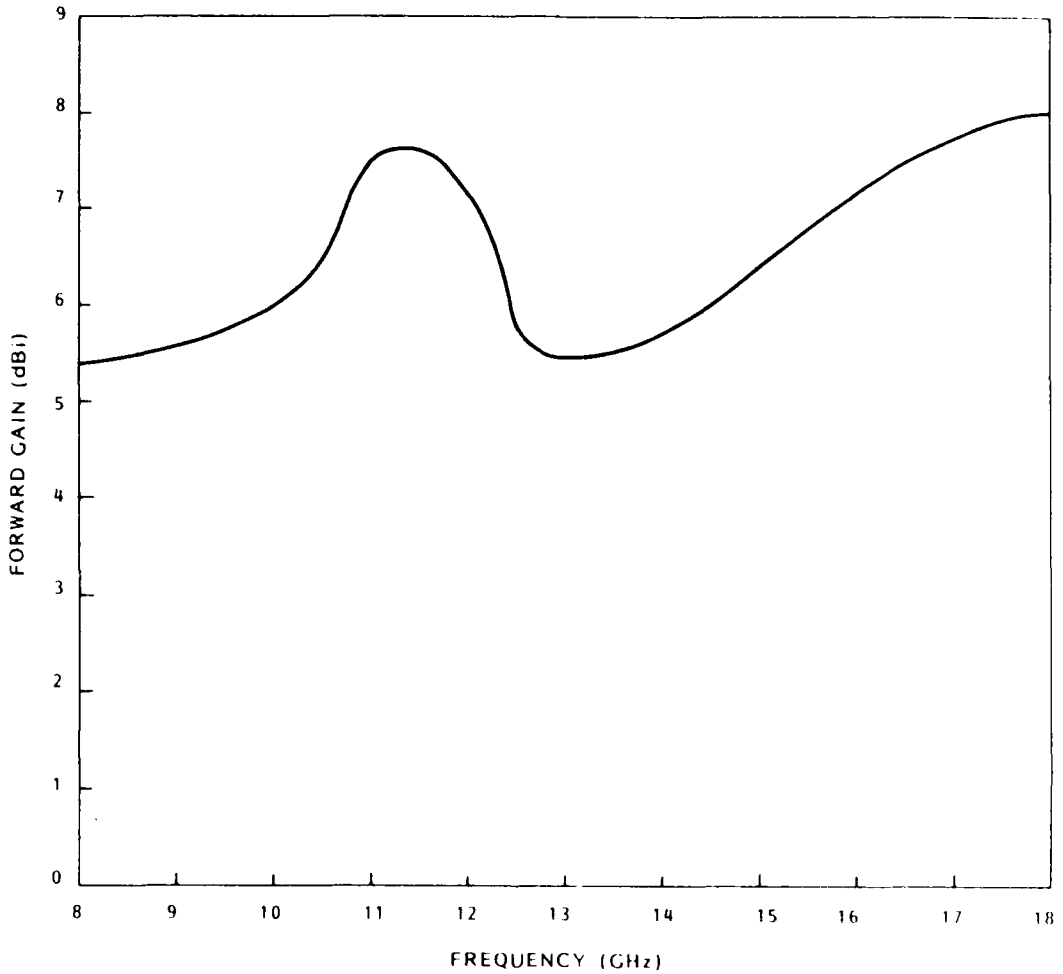

FIGURE 26. MEASURED FORWARD GAIN VS. FREQUENCY FOR PRINTED FLARED-NOTCH ANTENNA.

7. SUMMARY

Examples of monolithic microwave integrated circuits that have been developed for phased array applications, and methods for packaging and RF testing of these MMICs have been given. Examples of functional transmit/receive modules implemented with monolithic circuit technology have also been presented. Concepts for the integration of modules into complete phased array systems including compatible radiating elements have been discussed.

ACKNOWLEDGEMENT

The author wishes to express his appreciation to the members of the General Electric Electronics Laboratory who developed the circuits and concepts described herein, and to those who assisted in the preparation of this paper.

REFERENCES

1. Naster, R.J. (1983) MMIC Technology for Microwave Radar and Communication Systems, Microwave Journal, Vol. 26, No. 2: 109-112.
2. Peterson and Gupta (1983) A Two-Stage Monolithic Buffer Amplifier for 20 GHz Satellite Communication. Paper presented at the IEEE Monolithic Circuits Symposium, Boston, Mass.
3. Vorhaus, Pucel, and Tajima (1982) Monolithic Dual-Gate GaAs FET Digital Phase Shifter, IEEE Transactions on Electron Devices, Vol. ED-29, No. 7: 1078-1088.
4. Gupta, Peterson, and Decker (1982) Yield Considerations in the Design and Fabrication of GaAs MMICs, Microwave Journal, Vol. 25, No. 11: 77-84.
5. Dance, F.J. (1983) Interconnecting Chip Carriers: A Review, Circuits Manufacturing Vol. 23, No. 5: 60-70.
6. Ford, D. (1983) A Near Perfect Hybrid Substrate, Soon? Circuits Manufacturing, Vol. 23, No. 6: 44-48.
7. Gleason, Reeder, and Strid (1983) Precise MMIC Parameters Yielded by 18-GHz Wafer Probe, Microwave System News, Vol. 13, No.5: 55-65.
8. Neuf and Lamagna (1983) "Drop-In" Mixer-Preamp Offers Integrated Limiter Diode Protection, Microwave System News, Vol. 13, No. 2: 158-170.
9. Newberry, D. (1983) Heat Pipes: Plumbing a Hot Issue, Circuits Manufacturing, Vol. 23, No. 6: 54-57.
10. Carver and Mink (1981) Microstrip Antenna Technology, IEEE Transactions on Antennas and Propagation, Vol. 29, No. 1: 2-24.
11. Sidford, M.J. (1973) A Radiating Element Giving Circularly Polarized Radiation Over a Large Solid Angle. Paper presented at the IEE Conference on Satellite Systems for Mobile Communications and Surveillance, Pub. No. 95: 18-23.
12. Cumming, W.A. (1955) A Nonresonant Endfire Array for VHF and UHF, IRE Transactions on Antennas and Propagation, Vol. 3, No. 2: 52-58.

A WIDE BAND 44 GHz PRINTED CIRCUIT CONFORMAL ARRAY*

Darrel F. Sedivec
Brian F. Hubin
SANDERS ASSOCIATES, INC.
Antenna and RF Systems Department
95 Canal Street
Nashua, New Hampshire 03061

ABSTRACT:

A 16-element printed circuit array in four by four configuration was designed, developed, and tested at 44 GHz using stripline techniques. The array incorporated the Sanders wide band Tee-Fed Slot element[1] with integral corporate power divider, and produced a well defined main beam in a broadside direction with sidelobes -16 dB or better from 43 to 45 GHz. The VSWR was measured to be less than 2:1 over the band and the gain measured at 17 dBi.

Extended measurements of VSWR, E & H Plane patterns, and gain from 41 to 48 GHz showed VSWR no greater than 2.5:1 and gain to be no less than 16 dBi, with reasonable radiation patterns.

[1]Patent Number 4197545

This effort was sponsored by the Air Force Systems Command, Rome Air Development Center, contract F19628-82-C-0132.

The development methodology was to design, test, and evaluate all components and the array at 11 GHz and scale by four to 44 GHz taking into account the errors introduced by transmission line surface finish and dielectric properties.

This procedure, together with well controlled fabrication techniques, yielded an array at EHF whose electrical characteristics were nearly identical to those of the SHF array.

1.0 INTRODUCTION

This paper describes the methodology for design and development of a four by four 16 element EHF stripline array. The initial objectives were to design, fabricate and test transitions, and other transmission line components at X Band, then scale to Q Band.

It was verified that when properly desinged at 11 GHz, with all scaling factors accounted for, antenna scaling to 44 GHz would not substantially vary the characteristics of the array except for loss. The end result of the scaling procedure is shown in Figure 1-1.

All specifications and design objective were successfully met or exceeded, verifying scaling procedures in stripline and verifying the feasiblility of using stripline feed networks for stripline slot element array at , Band.

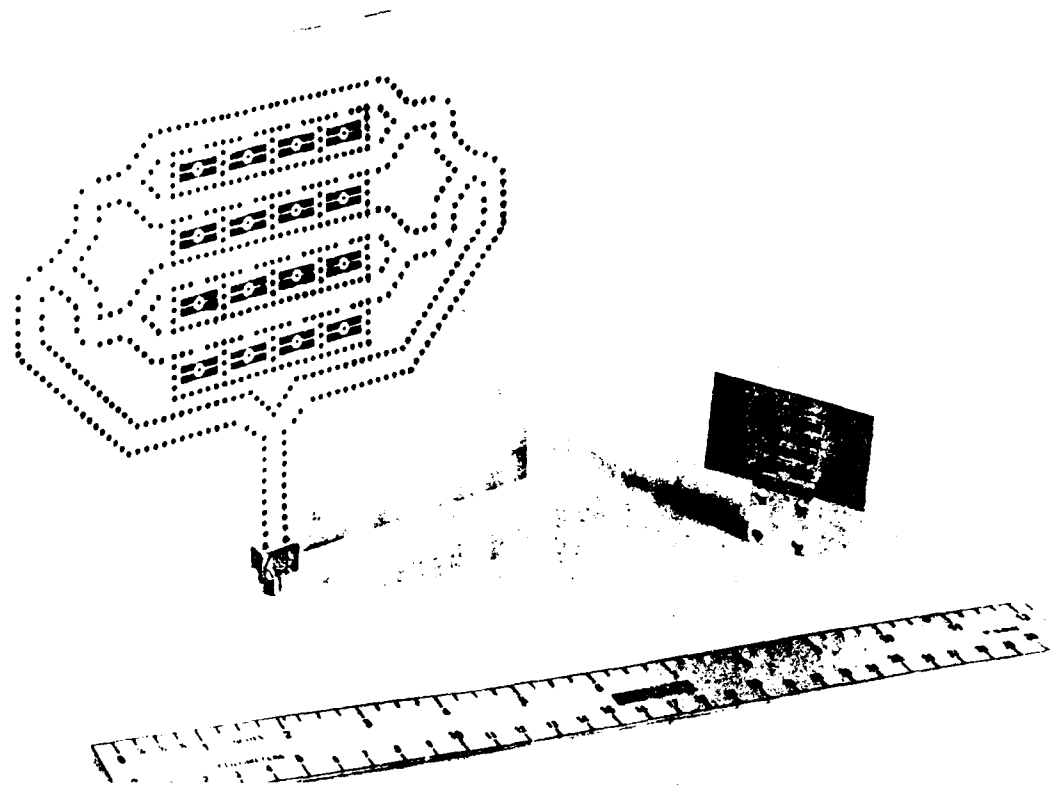

FIGURE 1-1. 16 ELEMENT, 11 AND 44 GHz, ARRAYS

2.0 SCALING METHODOLOGY

Sanders procedure was to evaluate individual components and the complete array at 11 GHz and then scale by a factor of four to 44 GHz. The primary antenna components are:

(A) Transmission Lines

(B) Plated Through Holes

(C) Waveguide-to-Stripline Transition

(D) Antenna Elements

(E) Corporate Power Divider

A summary of Sanders' scaling methodology is shown in Figure 2.0-1 where each of the critical components are configured at X and Q bands. The performance characteristics of these components are individually addressed in the following text.

3.0 TRANSMISSION LINES

Rogers Corporation 5880 substrate material was selected primarily because the loss tangent was low and the substrate was filled with small random oriented fibers as opposed to the layered large fibers of the 3M material which might have effected the velocity of propagation, depending on fiber orientation.

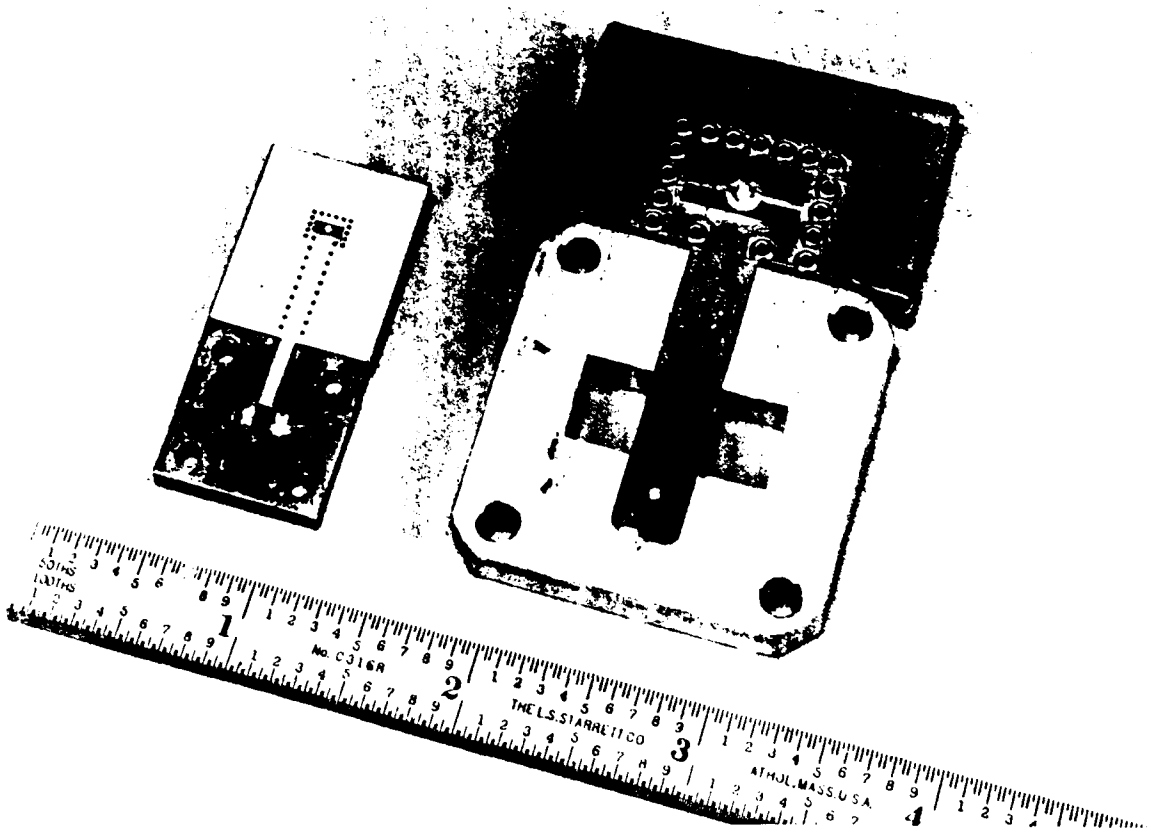

FIGURE 2.0-1. SANDERS SCALING METHODOLOGY SHOWING CRITICAL COMPONENTS AT X AND Q BANDS

Beyond these factors it was necessary to meet three other considerations. First, the material had to be sufficiently thick to permit efficient operation of the cavity backed element. Second, the separation of the ground planes had to be large enough to reduce line losses, but not so large that higher order modes might be excited. Third, commercial materials must be available to meet the scaling requirement from 11 to 44 GHz.

These conditions were all met with .125 inch ground plane spacing at 11 GHz and .031 inch spacing at 44 GHz.

One of the key factors effecting the realization of Q band feed networks is the tolerance level required for fabrication. Consideration of tolerances in PC techniques must be expanded at Q band to include not only dielectric properties, but also the etching process, metal finishes, and the generation of artwork.

3.1 TRANSMISSION LINE LOSSES

To reduce transmission line losses, feed lines should possess a conductor surface finish better than one skin depth or 0.3 μm at 44 GHz. The surface finish of one ounce copper clad 5880 Duroid is on the order of 2 μm, Figure 3.1-1. Table 3.1-2 shows measured data versus the theoretical transmission line loss of a perfect conductor in stripline together with the additional loss imposed by a surface roughness of six times the skin depth which increases the effective copper surface resistivity by a factor of approximately 1.75.

Additional insight into the effects of surface finish on conductor losses is given in an article authored by James D. Woermbke, January 1982 issue of "Microwaves", pages 89-98.

FIGURE 3.1-1. 1 OZ COPPER ON DUROID 980X MAG

FREQUENCY GHz	LOSS IN DECIBELS/ INCH FOR PERFECT CONDUCTOR WITH A SURFACE FINISH OF .3 μm.	LOSS IN DECIBELS/ INCH FOR CONDUCTOR WITH A SURFACE FINISH OF 2 μm. (DUROID 5880)	MEASURED LOSS IN DECIBELS/ INCH (DUROID 5880)
43	.457	.574	.77
44	.465	.584	.78
45	.472	.593	.80

TOTAL CONDUCTOR AND DIELECTRIC LOSS IN 50 OHM TRANSMISSION LINE OF DUROID 5880 MATERIAL

TABLE 3.1-2

3.2 STRIPLINE TRANSMISSION LINE IMPEDANCES

The various impedances as a function of the width of the center conductor used at X and Q bands are given in Table 3.2-1. These impedances are used throughout the corporate feed network of Figure 3.2-1. The ground plane spacing is .125 inches at X band and .031 inches at Q band. One ounce copper was used in both bands.

X BAND		Q BAND	
IMPEDANCE IN OHMS	WIDTH OF CENTER CONDUCTOR IN INCHES	IMPEDANCE IN OHMS	WIDTH OF CENTER CONDUCTOR IN INCHES
50	.0996	50	.0249
51	.0968	51	.0242
60	.0735	60	.0184
67	.0597	67	.0149
71	.0537	71	.0134
78	.0425	78	.0106
95	.0276	95	.0069
100	.0240	100	.0060

TRANSMISSION LINE CHARACTERISTICS

TABLE 3.2-1

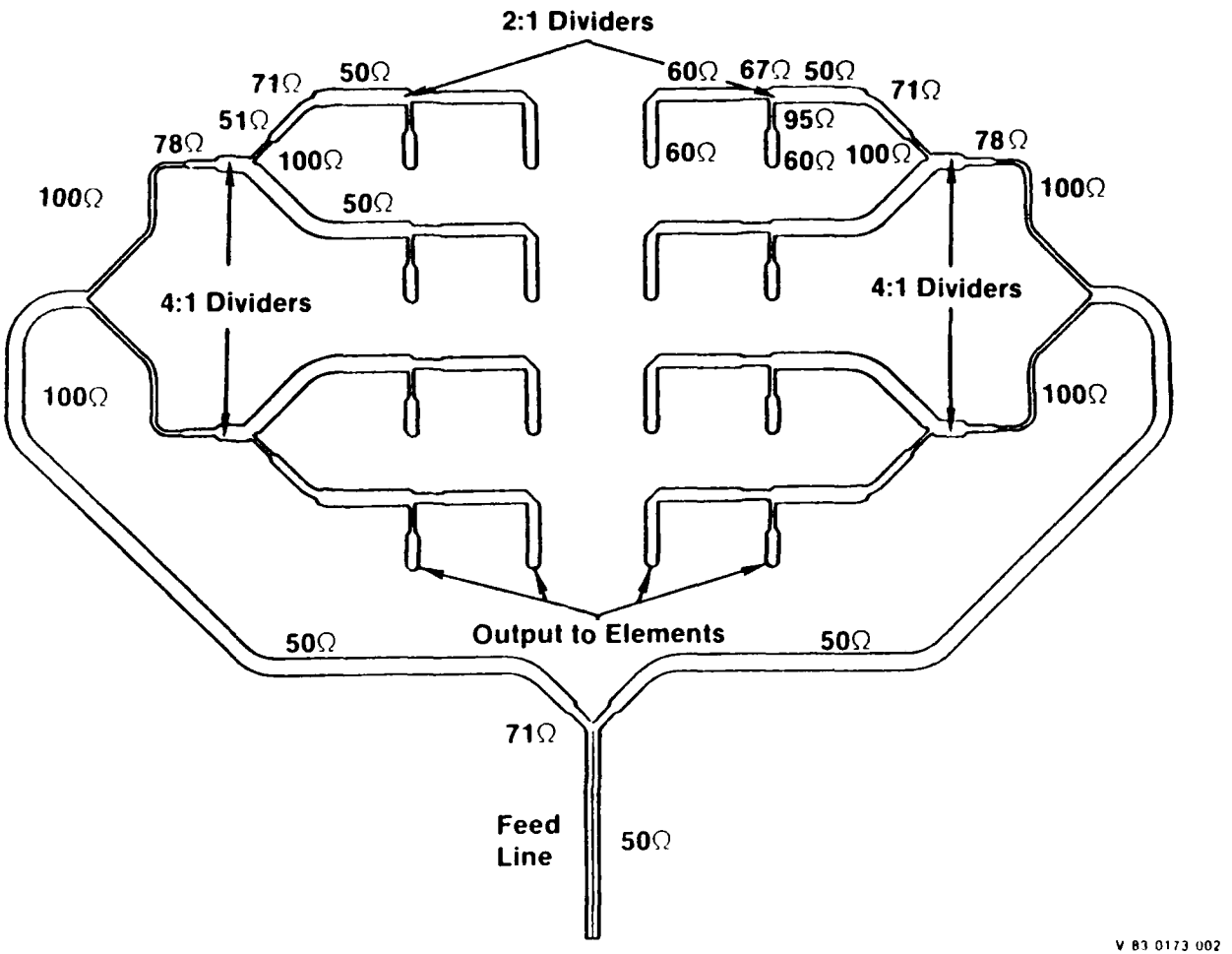

FIGURE 3.2-1. 16 ELEMENT ARRAY FEED STRUCTURE

3.3 FABRICATION

Antenna elements and arrays were fabricated utilizing both film and filmless bonding techniques. There appeared to be no noticeable electrical difference between bonding methods during antenna element tests. However, those arrays fabricated using the film bonding process performed better than those of the filmless process. Arrays using filmless bonding were opened and visually inspected. It is believed that one or more of the following may be the cause of poor performance.

A. Air gaps between substrates.

B. Higher dielectric at the bonding surface resulting from heat and pressure.

C. Change in ground plane spacing.

3.4 PLATED THROUGH HOLES

Eyelets are normally used to conveniently define the antenna element cavities and to isolate transmission lines at X Band, but because of size reduction, it was necessary to incorporate plated through holes at Q Band in accordance with specification MIL-P-55110C. The integrity of those holes is shown in Figures 3.4-1 and 3.4-2 at 33 and 88 times magnificaton respectively.

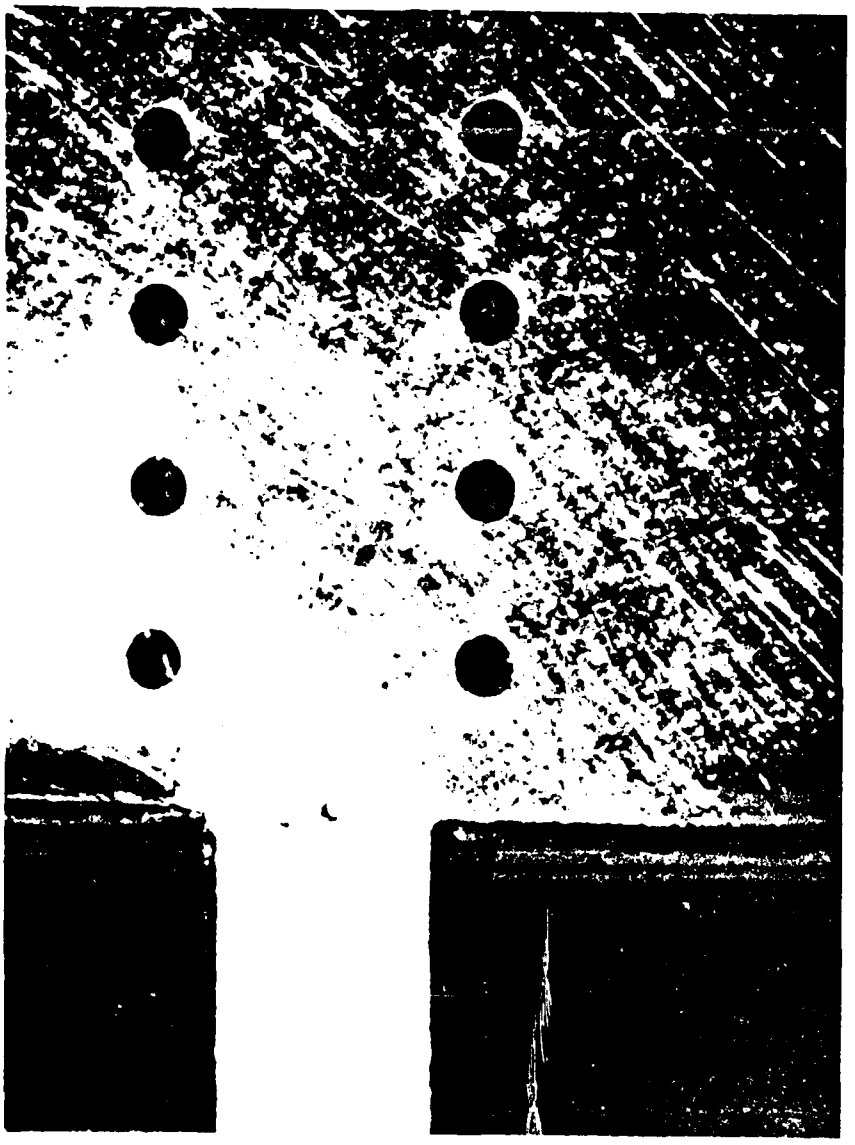

FIGURE 3.4-1. PLATED THROUGH HOLES
AT 33 TIMES MAGNIFICATION

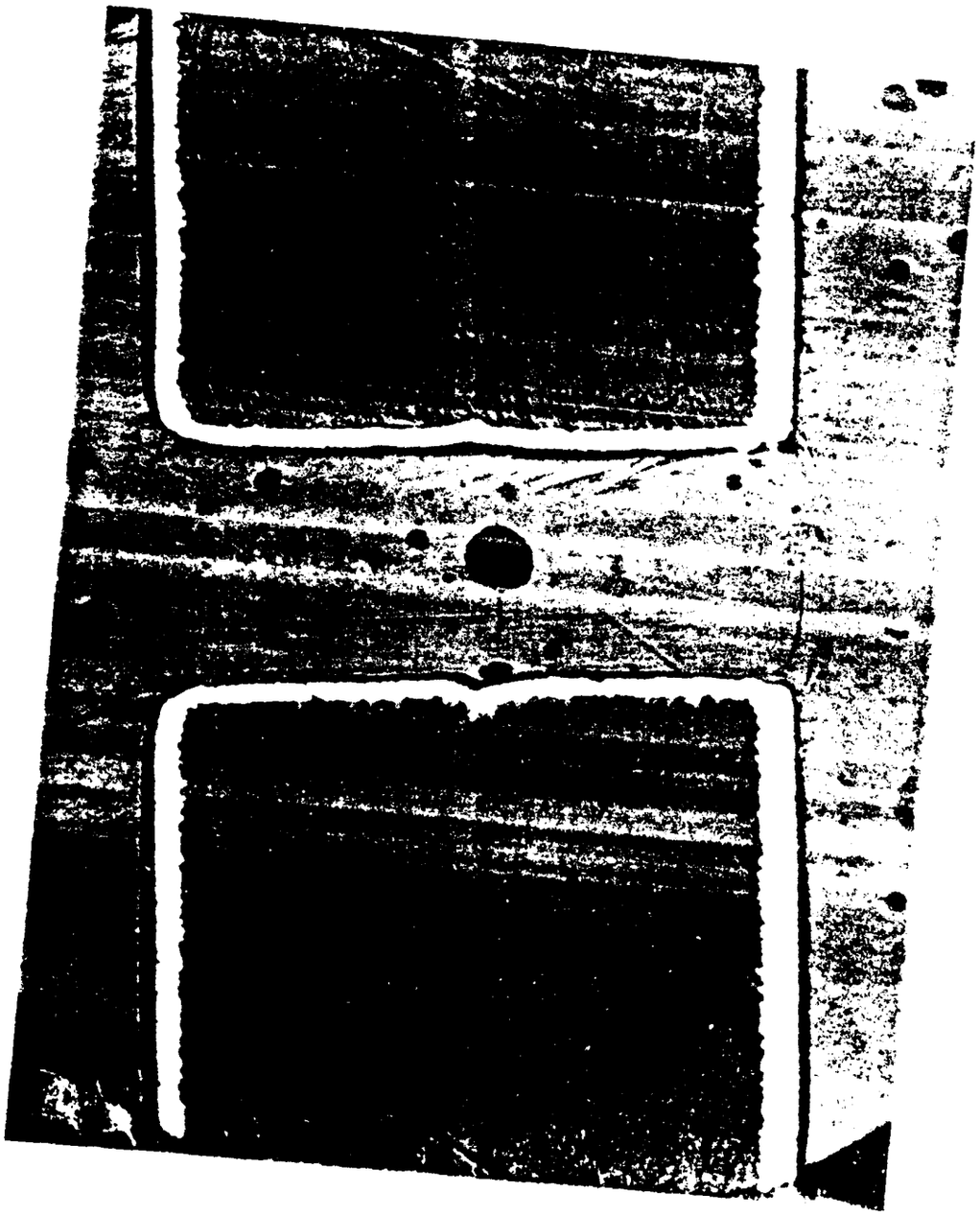

FIGURE 3.4-2. PLATED THROUGH HOLE
AT 88 TIMES MAGNIFICATION

4.0 WAVEGUIDE TO STRIPLINE TRANSITIONS

To ensure the best possible interface between waveguide and stripline, Sanders elected to pursue the development of the probe transition as described on pages 47 and 48 of "THE HANDBOOK OF TRI-PLATE MICROWAVE COMPONENTS" published by Sanders Associates. The X band impedance plot is shown in Figure 4.0-1.

The transition was scaled to 44 GHz and tested. The transition consists of a 50 ohm stripline transmission line which extends part way into the broad wall of the waveguide. The probe is parallel to the electric field for the dominant TE_{10} waveguide mode. The waveguide is terminated in a short circuit approximately one-quarter wavelength from the probe. The configuration is shown in Figure 4.0-2 and the VSWR data in 4.0-3.

5.0 ANTENNA ELEMENTS

Sanders developed the Tee-Fed Stripline Slot between 1972 and 1979 followed by a patent award. During an internally funded project the bandwidth was extended from 13 to 30 percent. The large bandwidth of the stripline Tee-Fed Slot ensured the placement of the operating band within the resonant window. Thus the printed circuit stripline Tee-Fed Slot may be considered essentially insensitive to normal variations in material composition and environmental fluctuations.

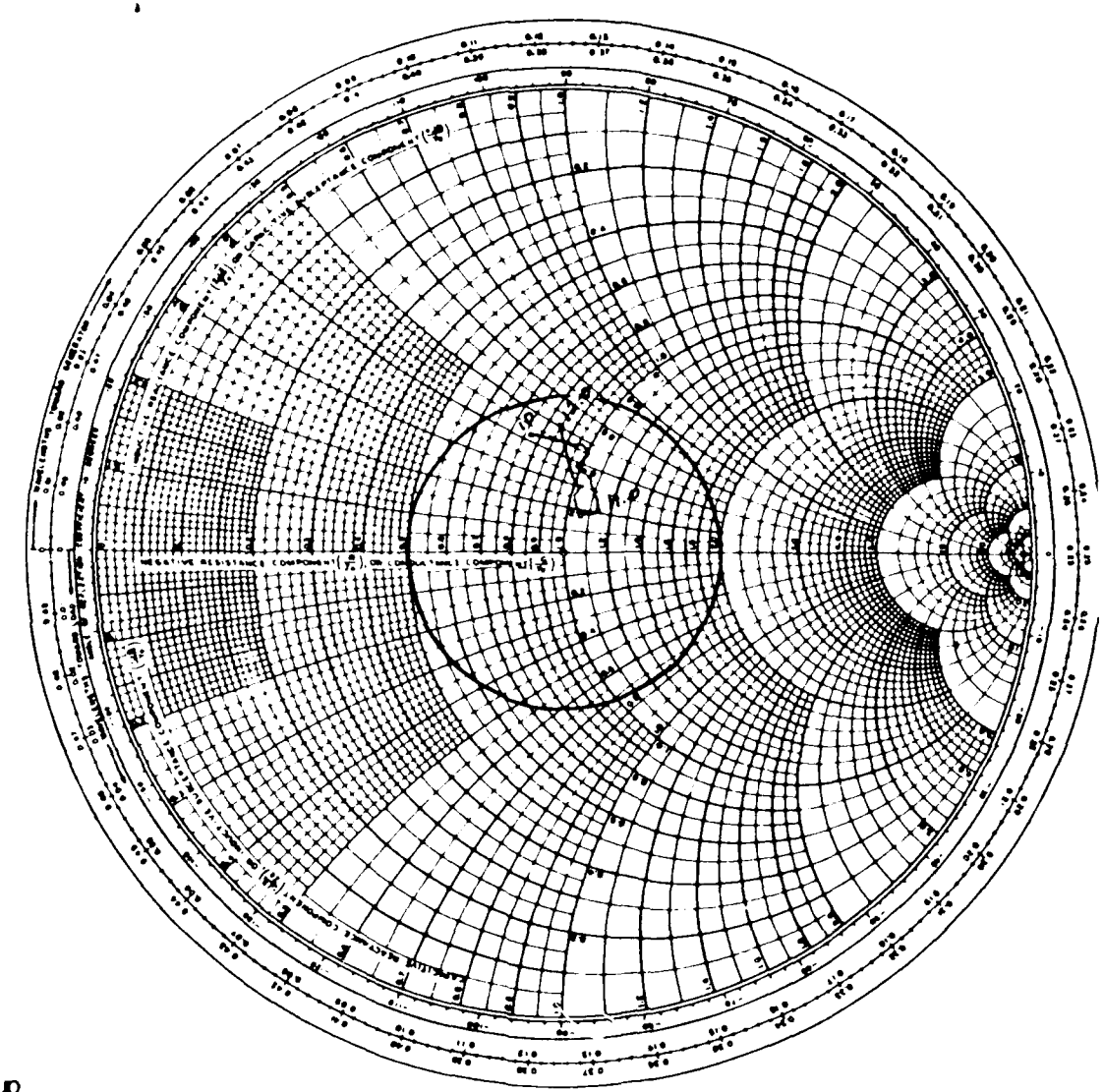

Federal Systems Group
SANDERS

V-83 0173-024

FIGURE 4.0-1. X BAND IMPEDANCE PLOT OF PROBE TRANSITION

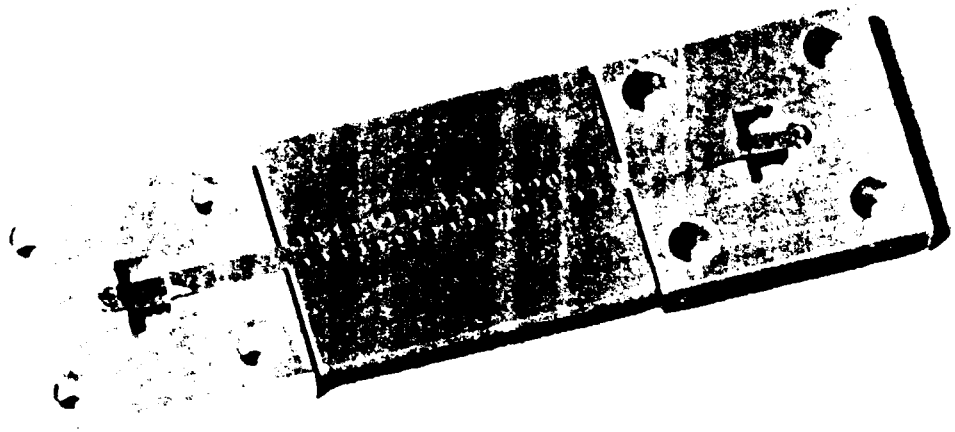

FIGURE 4.0-2. PROBE TRANSITION

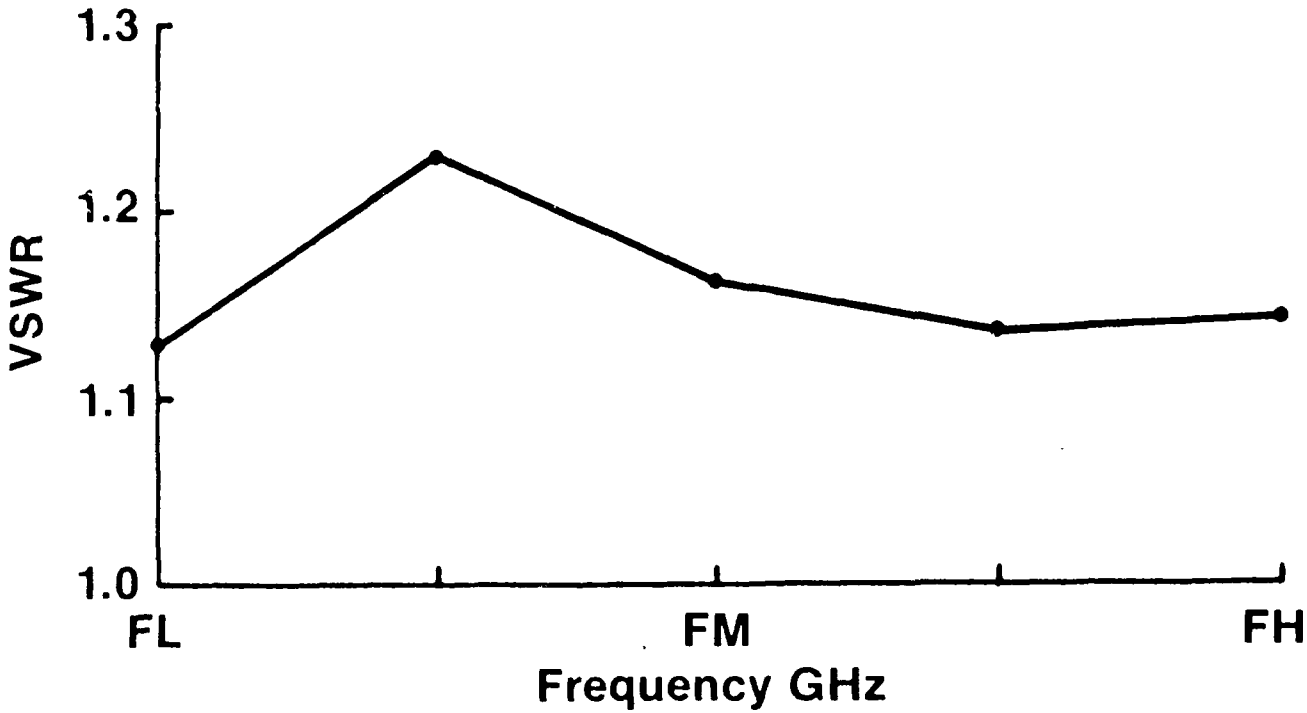

Federal Systems Group
SANDERS

V-83-0173-011

FIGURE 4.0-3. BACK TO BACK PROBE TRANSITIONS

5.1 ANTENNA ELEMENT CHARACTERISTICS

The Sanders Tee-Fed Slot has been successfully designed and scaled at various frequencies from L to K_a bands. Using the same proven design we successfully scaled from X to Q Band with expected results.

The gain of the element was measured at both 11 and 44 GHz to be 6 dBi. The impedance of the individual slot from 43 to 45 GHz is given in Figure 5.1-1 and E and H Plane patterns in Figures 5.1-2 and 5.1-3.

6.0 ANTENNA ARRAYS

Sanders successfully designed and fabricated a 16 element wideband conformal array at 11 GHz and scaled it to 44 GHz with impressive results. The 44 GHz array configuration is shown in Figure 6.0-1.

6.1 WIDEBAND ARRAYS

As a result of certain feed constraints and cavity sizes, spacing for the elements was selected at .745 wavelengths in the E Plane and .672 wavelengths in the H Plane. Element spacing as close a .5125 wavelengths with other feed network designs are [illegible].

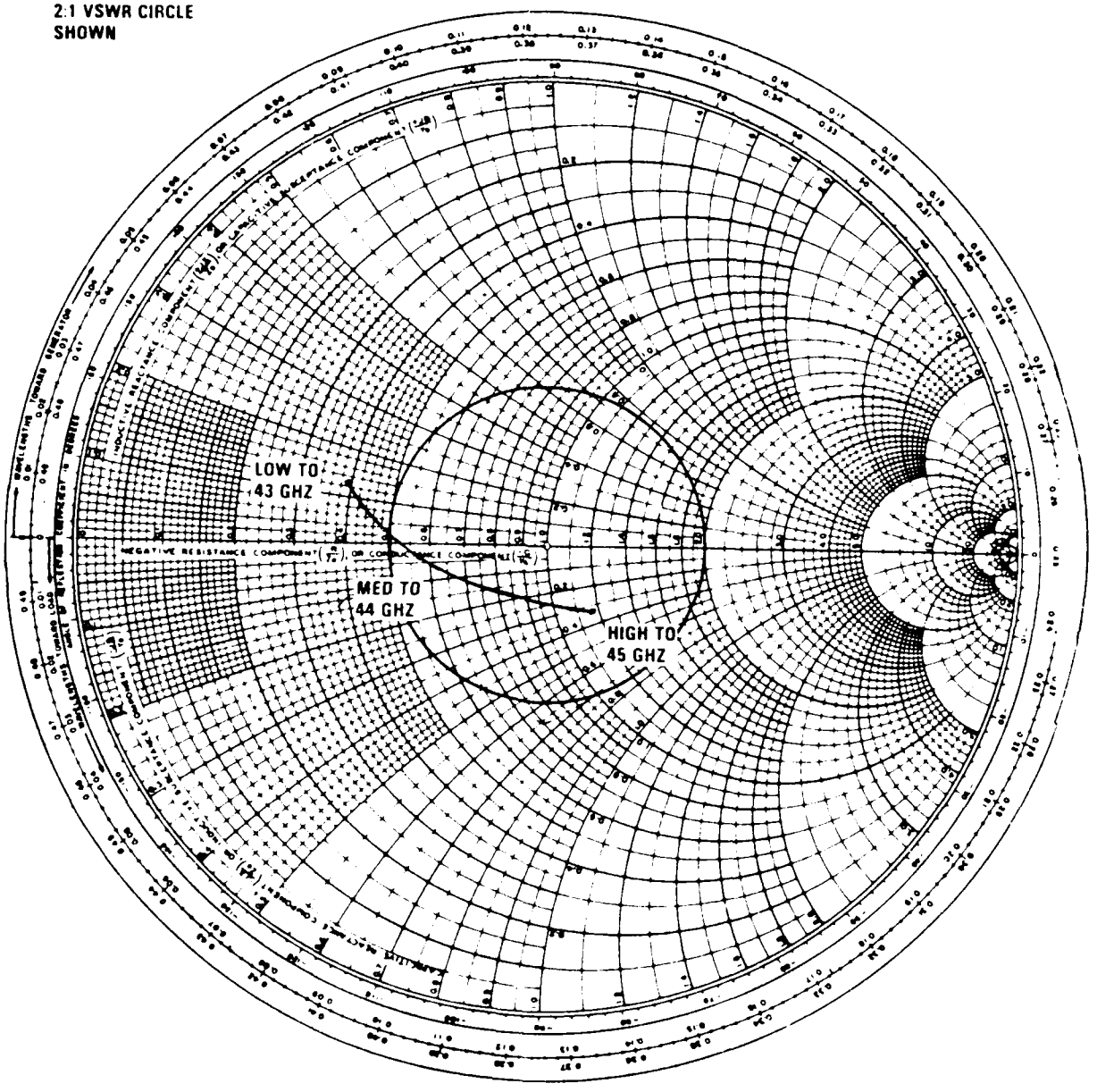

FIGURE 5.1-1. IMPEDANCE OF SLOT ANTENNA

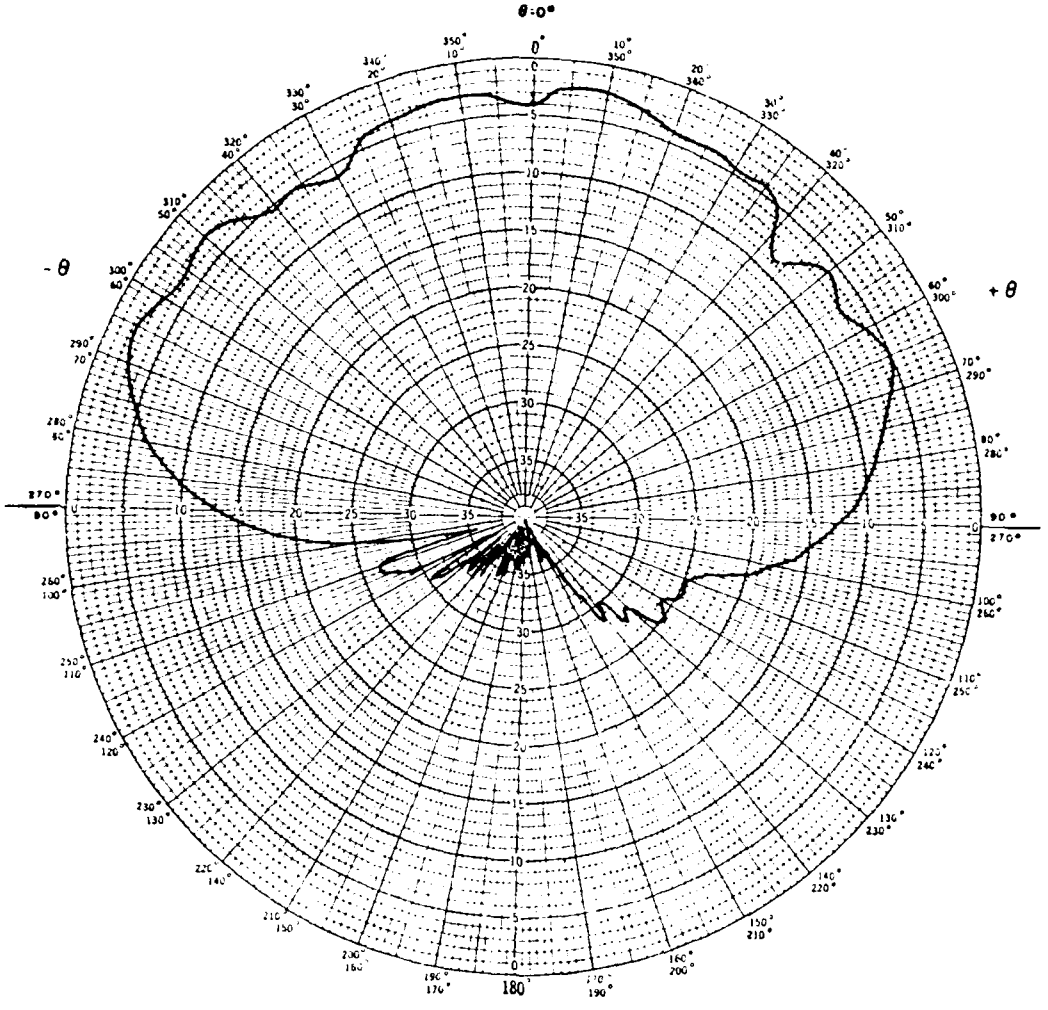

FIGURE 5.1-2. MEASURED PATTERN, 44 GHz, E PLANE

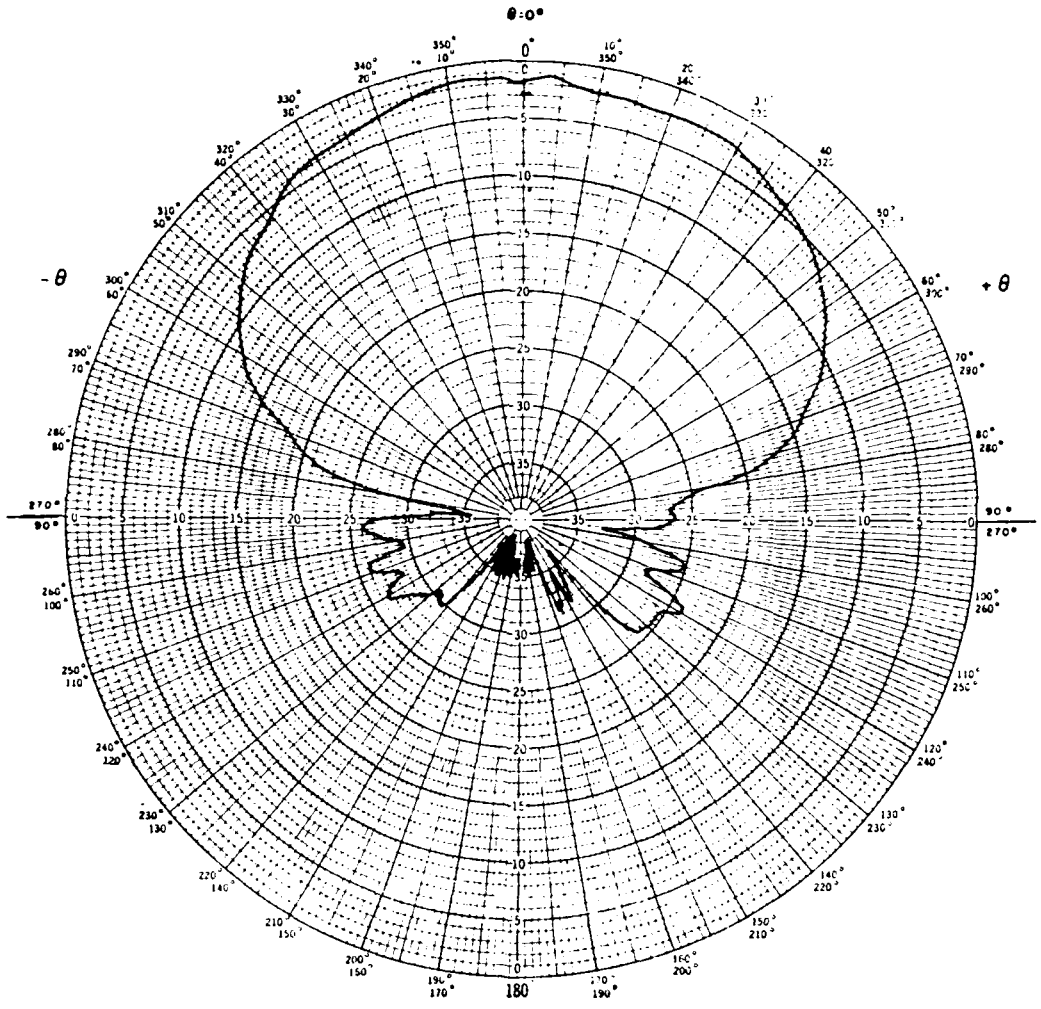

FIGURE 5.1-3. MEASURED PATTERN, 44 GHz SLOT, H PLANE

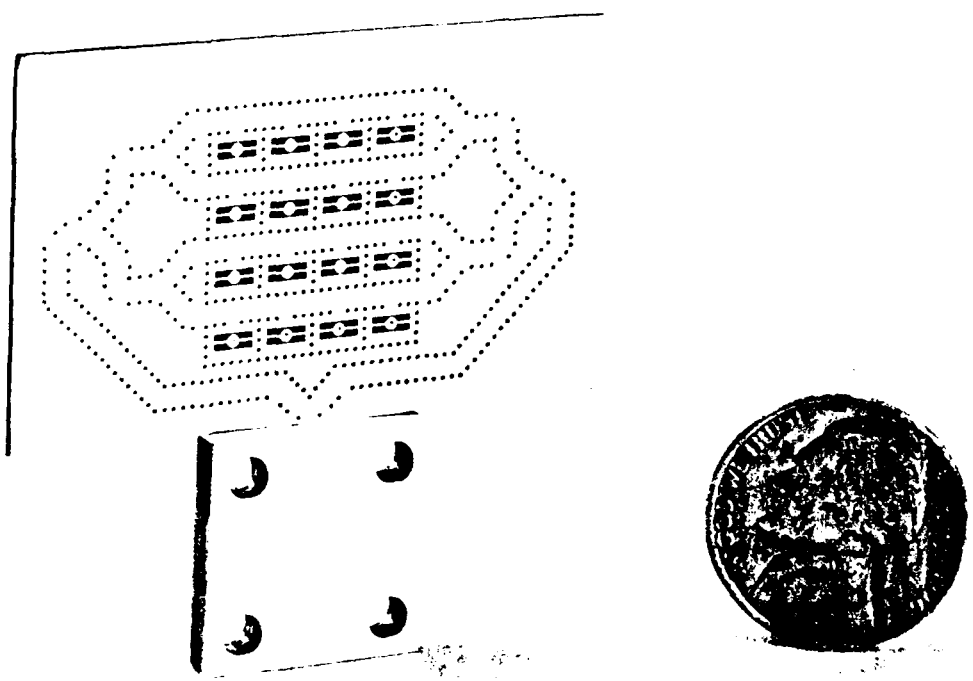

FIGURE 6.0-1. 44 GHz ARRAY

Sanders concluded at the outset that some applitude taper would be required in order to meet the -16 dB sidelobe specification. Allowing for some error in the feed network and in fabrication, we elected to provide a taper which would theoretically exceed that required for -16 dB sidelobes giving a -22 dB first sidelobe level in the E Plane and -18 dB in the H Plane. The taper is presented in Table 6.1-1.

-9 dB	-6 dB	-6 dB	-9 dB
-3 dB	0 dB	0 dB	-3 dB
-3 dB	0 dB	0 dB	-3 dB
-9 dB	-6 dB	-6 dB	-9 dB

RELATIVE POWER DISTRIBUTION OF ARRAY FEED

TABLE 6.1-1

The computed E and H Plane patterns for the above taper and spacing are shown in Figures 6.1-2 and 6.1-3.

Figures 6.1-4 and 6.1-5 shown measured patterns at 11 GHz and Figure 6.1-6 and 6.1-7 show patterns at 44 GHz.

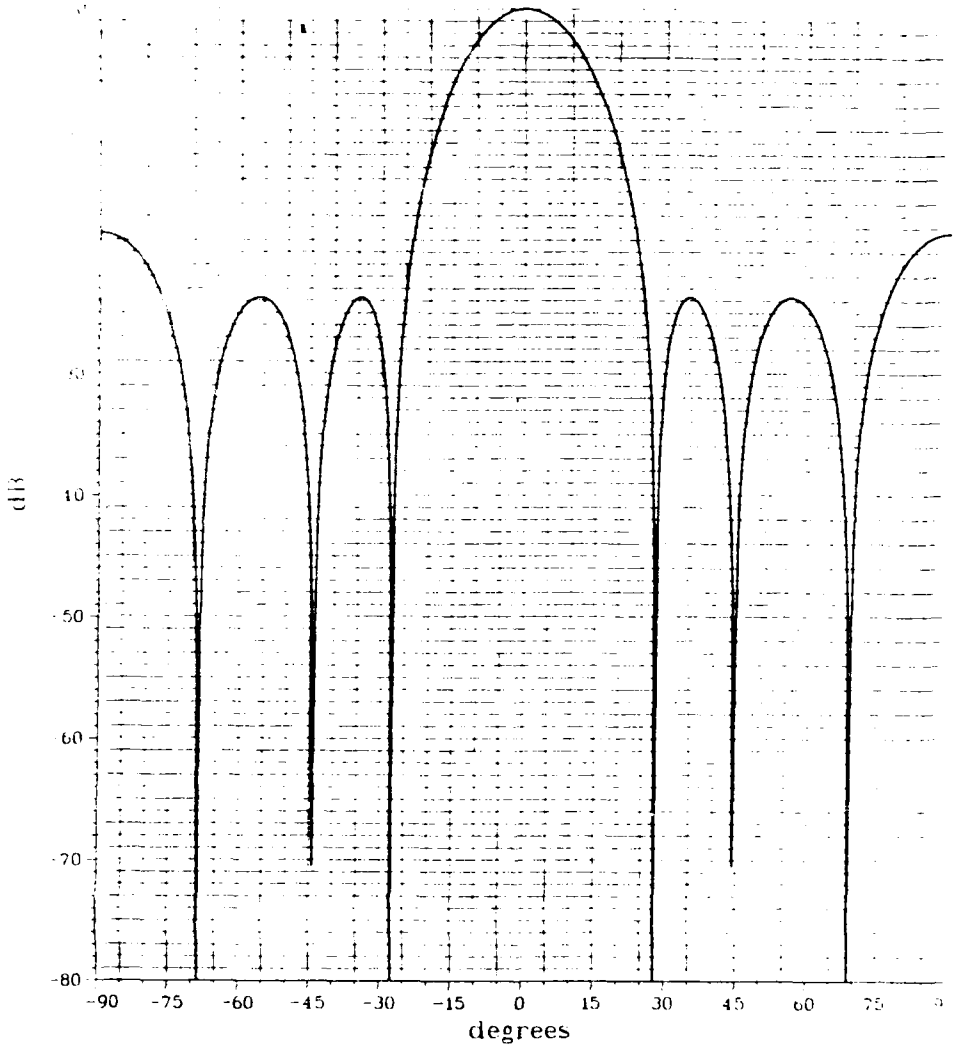

FIGURE 6.1-2. COMPUTED PATTERN; E PLANE

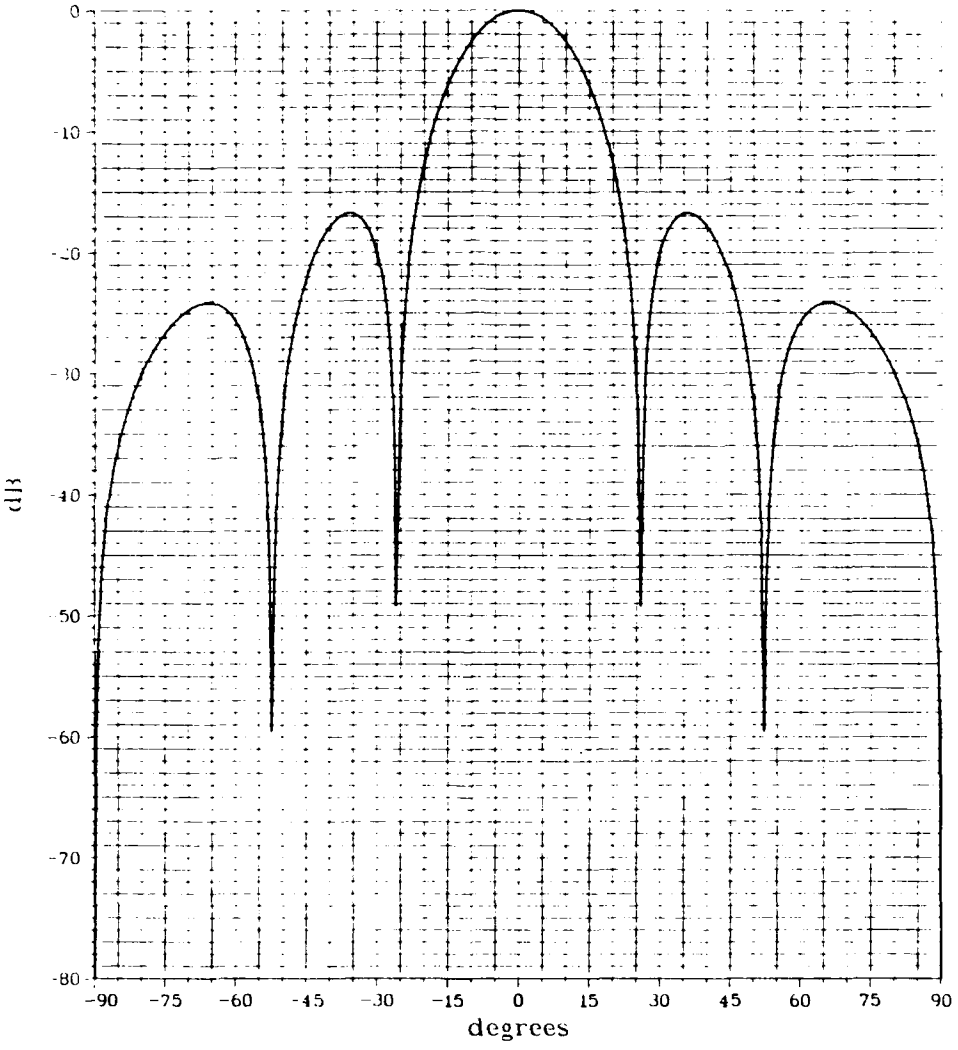

FIGURE 6.1-3. COMPUTED PATTERN; H PLANE

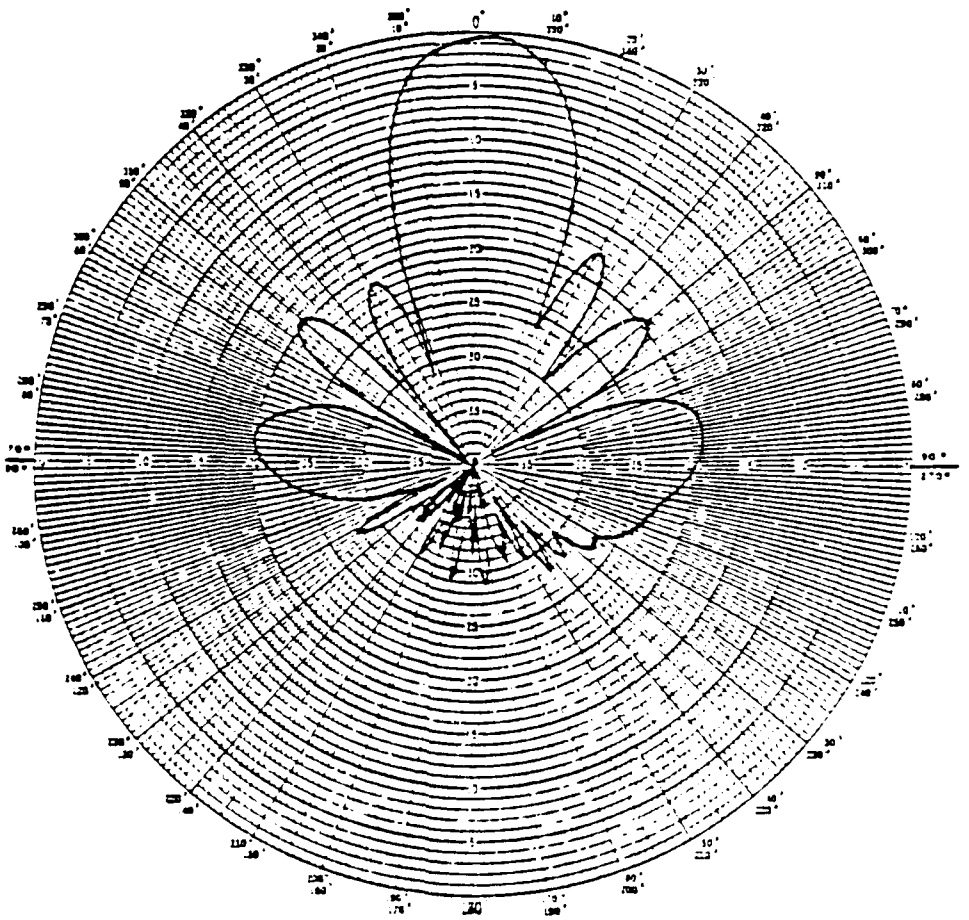

FIGURE 6.1-4. MEASURED ARRAY PATTERN; E PLANE, 11 GHz

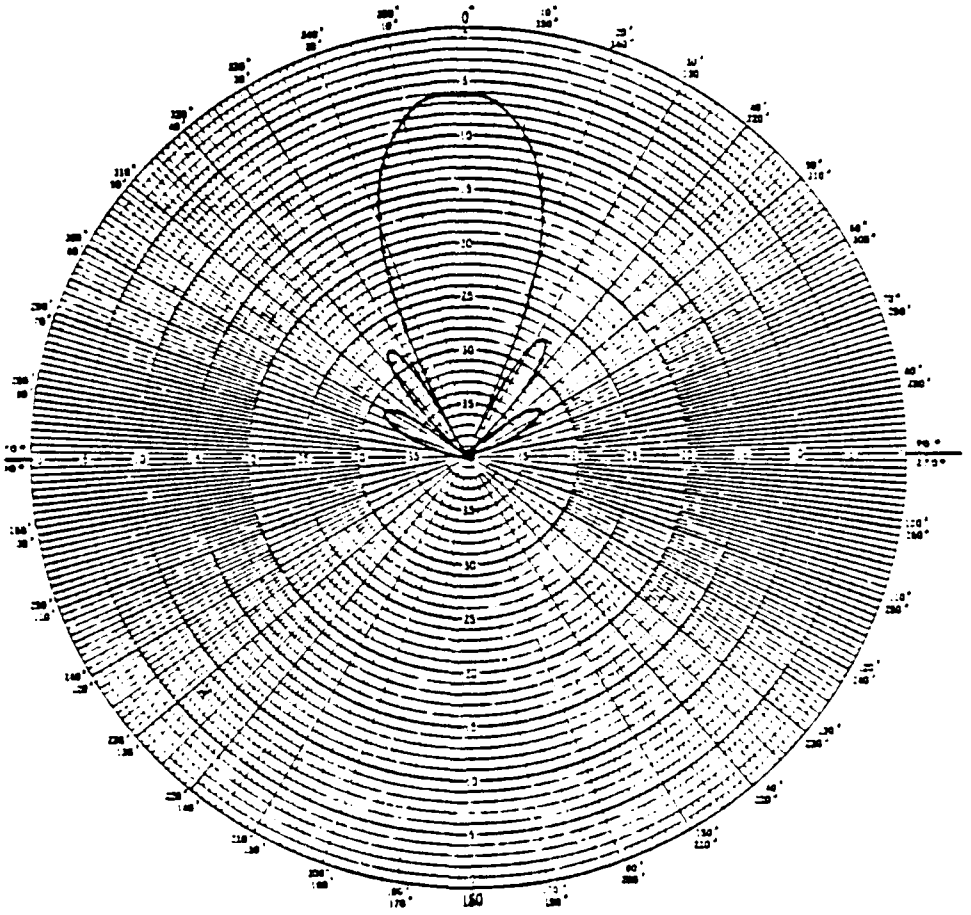

FIGURE 6.1-5. MEASURED ARRAY PATTERN; H PLANE, 11 GHz
(NOT NORMALIZED)

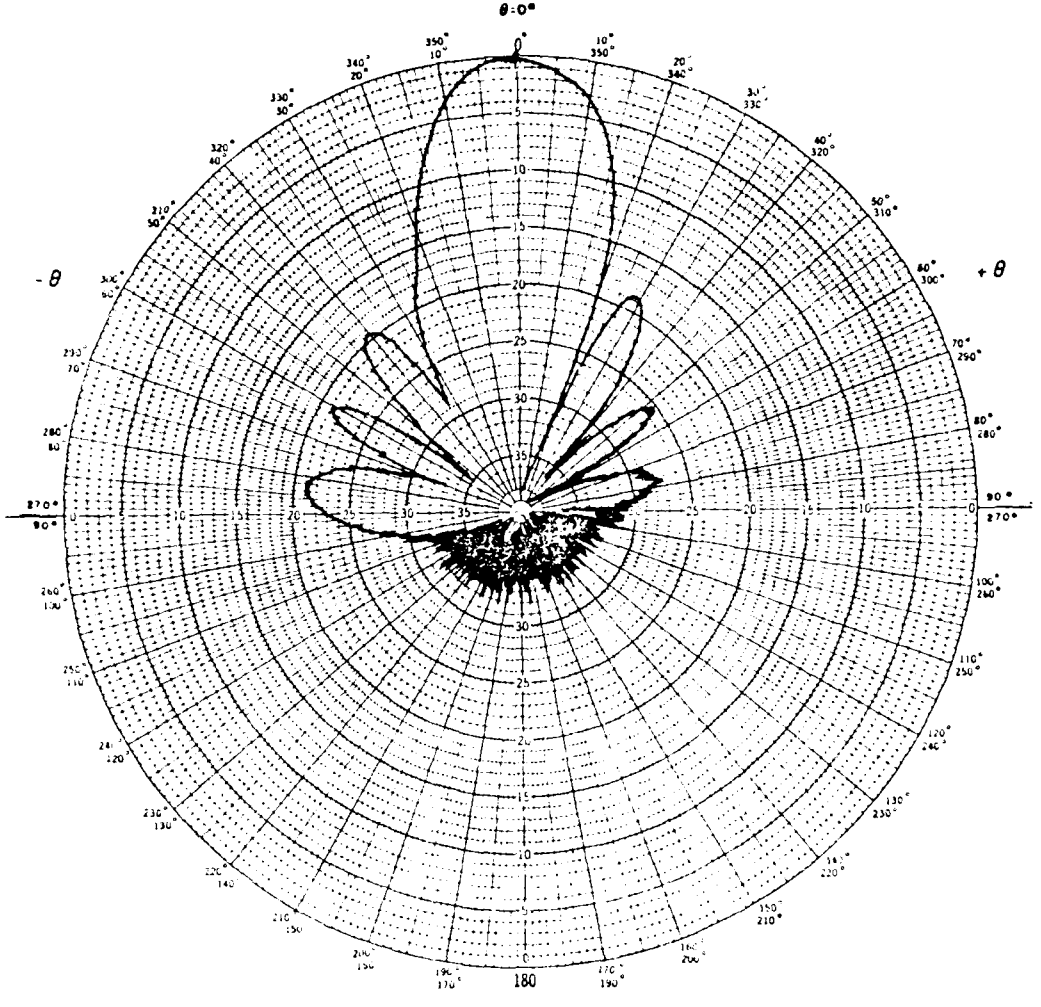

FIGURE 6.1-6. MEASURED ARRAY PATTERN; E PLANE 44 GHz

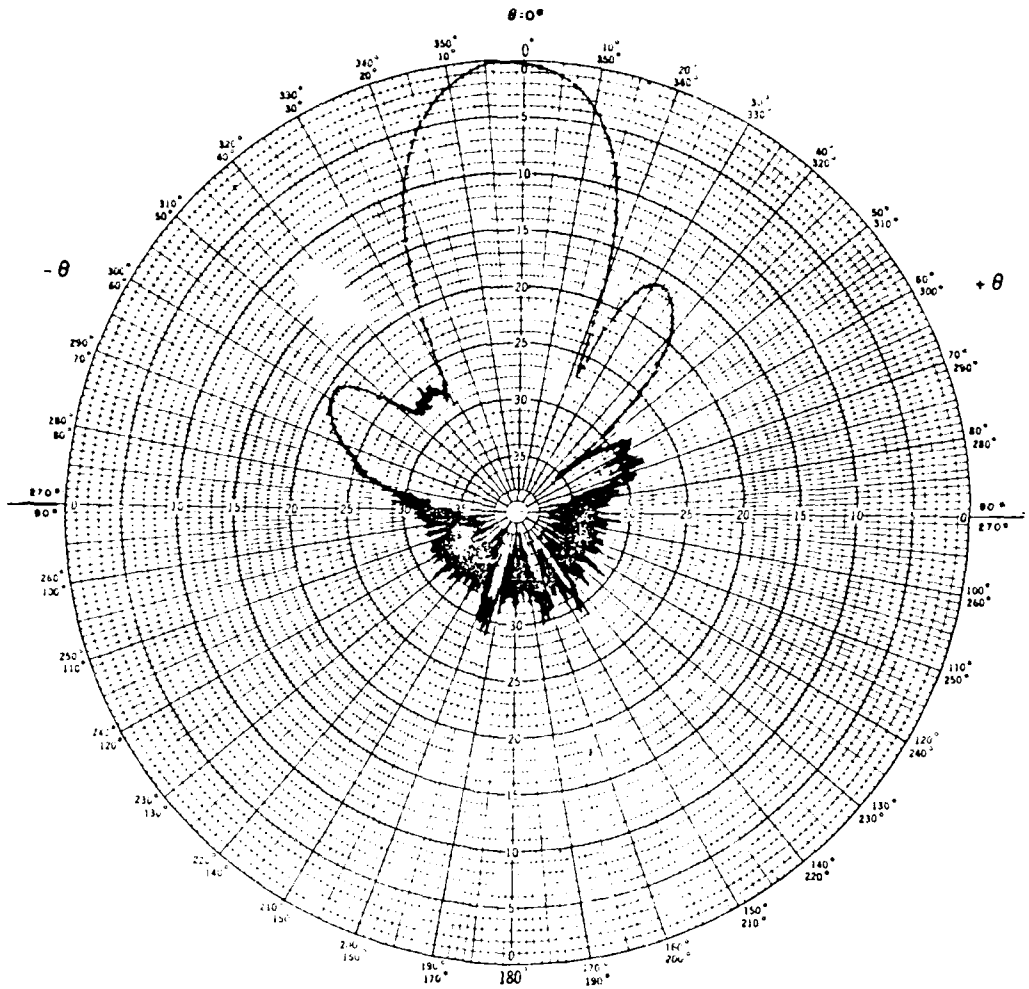

FIGURE 6.1-7. MEASURED ARRAY PATTERN; H PLANE, 44 GHz

Examination will show exceptionally good agreement between computed and measured pattern data in X and Q Band and good symmetry on the main beam between E and H Planes. Gain was measured to be 17 dBi at 44 GHz. Extended bandwidth gain measurements are shown in Figure 6.1-8. VSWR at Q Band is shown in Figure 6.1-9.

6.2 ARRAY GAIN

The directivity of the 16 element array is calculated to be 19 dB. The gain is obtained by substracting the estimated loss budget from the directivity.

LOSS BUDGET

INPUT VSWR (1.55)	=	.2 dB
AMPLITUDE TAPER	=	.6 dB
ELEMENT LOSS	=	1.0 dB
FEED NETWORK LOSS	=	1.0 dB
	LOSS	2.8 dB
	DIRECTIVITY	19.0 dB
	ESTIMATED GAIN	16.2 dBi

7.0 CONCLUSIONS

Scaling from X band to Q band is a viable technique for achieving predictable broad band antenna performance. Taking into account all scaling factors, including loss, the 44 GHz array performed as predicted.

AD-A142 003 PROCEEDINGS OF THE ANTENNA APPLICATIONS SYMPOSIUM HELD AT MONTICELLO ILLI (U) ROME AIR DEVELOPMENT CENTER GRIFFISS AFB NY MAR 84 RADC-TR-84-52-VOL-1 2/3

UNCLASSIFIED F/G 9/5 NL

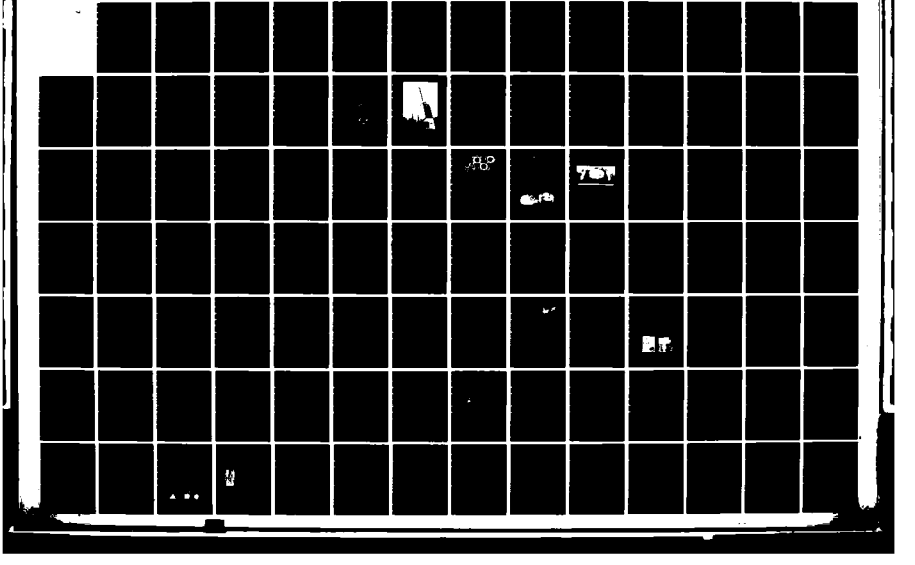

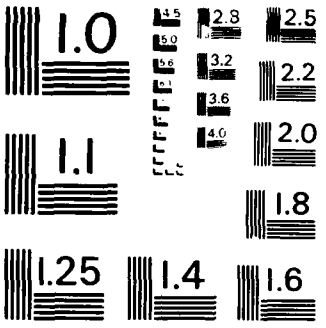

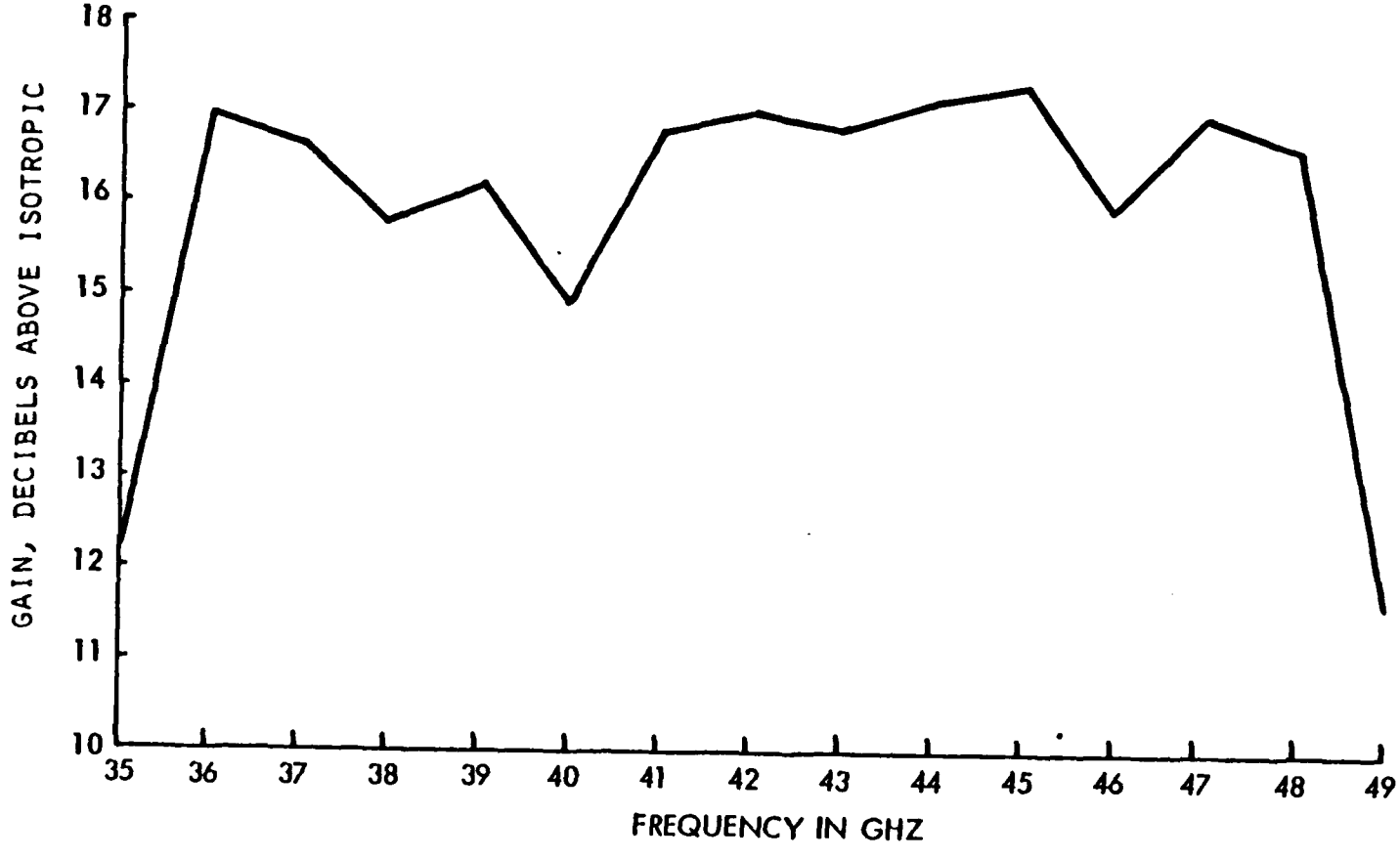

FIGURE 6.1-8. 16 ELEMENT ARRAY

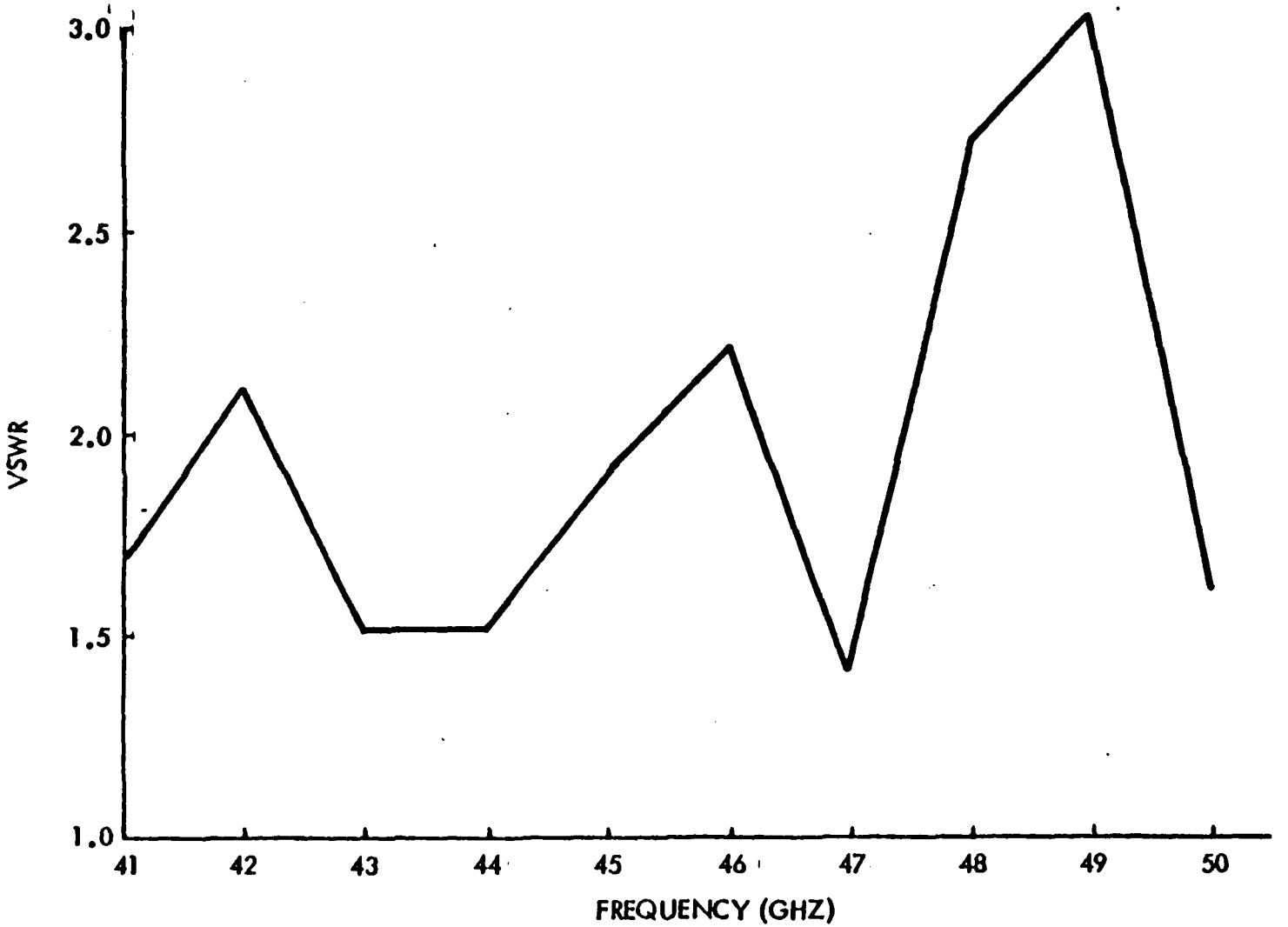

FIGURE 6.1-9. 44 GHz PHASED ARRAY

Extra care must be provided in the fabrication process to produce components and array structures to the tolerances required at Q band.

Array patterns from 35 to 49 GHz clearly showed that increased bandwith may be achievable beyond this range by implementing other types of corporate feed structures.

The measured patterns and data clearly show the feasibility of using stripline feed networks for stripline slot element arrays at 44 GHz. A very cautious and conservative design approach was chosen in order to have a high probability of success in achieving this limited objective within a limited time and cost budget. This approach led to the use of a feed structure that was not entirely within the planar area of the array aperture. By avoiding the additional risks involved in constraining the area used for the feed network, a clear demonstration of excellent quality control in printed circuit and plated-through-hole processes at EHF was achieved.

DEVELOPMENT OF SCANNING DIPOLE ARRAY*

D. Davis, G. E. Evans, V. L. Fisher, A. H. Johnson
Westinghouse Electric Corporation
Baltimore, Maryland

Abstract

A dipole was recently developed for use in a phased array at 420 to 450 MHz. It was designed to scan ±40 degrees in elevation and ±48 degrees in azimuth. The data presented includes analytical simulation, VSWR testing of the dipole both isolated and in simulators, and patterns measured with a finite array. The simulators include single and dual mode devices as well as two 11-element columns. The extensive simulator work was necessary partially because of the small size of the array. The columns were used in conjunction with computer analyses to determine VSWR throughout the scanning coverage. The data from various sources agrees well, and predicts that the VSWR across the frequency band across all scan angles will be less than 1.9:1.

---

*Development performed under contract with Naval Research Laboratory, Washington, D.C.

1.0 Dipole Design

Designing a dipole for use in a phased array environment requires a substantial breadboard development effort. To further complicate the task, a dipole in an array with relatively few radiators cannot be accurately simulated using infinite array reflecting walls. Since a UHF array 10 to 15 wavelengths long is already large, any increase in size to use additional elements is usually resisted; therefore, most of the dipoles are more nearly end elements than an element centered in an infinite array. To properly account for these characteristics a multi-step design sequence is followed.

The sequence includes theoretical analysis with computer modeling, free space element breadboarding, single and dual mode infinite array waveguide simulators, and multi-element E-plane and H-plane simulators.

Selecting a promising dipole configuration is done following a computer modeling analysis which predicts the complex reflection coefficient variation with frequency and scan angle in representative planes. The model is also used to predict trends in addition to the starting dimensions for the breadboard dipole configuration. The model filters out the unworkable configurations and properly focuses the breadboarding effort in promising directions. Figure 1 shows the predicted response of the E-plane and H-plane scan with frequency for the dipole

configuration to be breadboarded. It is computed using a field mapping program that provides a direct solution of Maxwell's Equations. The program essentially uses a computational simulator, with E- and H-plane shorting walls to represent the other radiators in an infinite array.

2.0 Dipole Measurements

The first step is to build and test a dipole with dimensions from the computer model. By matching the dipole over a ground plane in free space an understanding of how slight modifications in dimensions affect the dipole response is obtained. The next step is to build and test the "free space" dipole in an infinite array waveguide simulator to compare with modeling data from similar theoretical analyses. Figure 2 shows schematically two such simulators that were used. The single mode (one dipole) simulator provides reflection coefficient data for the dipole in a scanned configuration. The four conducting walls simulate an infinite array while their spacing determines the simulated scan angle. With the dimensions shown the H-plane scan angle is $\pm$29.5 degrees from broadside. By adding another dipole and suitably placing the conducting walls two scan angle pairs result. Driving both dipoles in phase provides the same information measured in the single mode simulator; driving them out of phase gives nearly $\pm$30 degrees scan in both E-plane and H-plane simultaneously or 44 degrees along the diagonal.

Figure 3 shows the combined single and dual mode simulator results. Although the computer models assume a perfect termination of radiated fields, the breadboard simulators must provide an acceptable one. Two techniques have been developed. In one, a sliding load technique requires that at least three measurements be made with the termination at different distances from the dipole. The center of a circle drawn through the measured data points is the value used for the dipole reflection coefficient. In the other technique, flared conducting walls are attached to the simulators to resemble a waveguide horn that is matched into free space.

After achieving acceptable VSWR response in the previous simulators through several configuration modifications, the next step in the design process will account for the finite array effects. Figure 4 shows the multi-element simulator. By making the mutual coupling measurements from a single element to all others, the complex reflection coefficient can be calculated for any scan angle. Figure 5 shows the match of the central dipole in the 11-element simulator. Comparing data for an H-plane scan angle, that the eleven element simulator has in common with the single mode simulator, shows good agreement and provides confidence in the hardware simulation accuracy. Corresponding E-plane scan data generally agrees with the theoretical predictions of Figure 1. Figure 6 shows close agreement with the dual mode simulator E-plane results at two scan angles.

3.0 Composite Data

A family of frequency and scan angle responses has been compiled in Figure 7. This represents the final dipole configuration which is shown in Figure 8. Note that the best performance is not at broadside. The dipole was designed to average the VSWR extremes to reasonable quantities. Figure 9 shows the same data as Figure 7 but on a coverage diagram including scan limits. The useable coverage does not introduce grating lobes assuming a 15 degree array tilt and a 25 degree maximum roll or tilt. The maximum VSWR is less than a 1.5 to 1 for the most used scan region. Even at the corners of the coverage diagram the VSWR is less than a 1.9 to 1 over the frequency band.

It has been shown by theoretical modeling that the H-plane scan can be extended with the addition of a capacitive top hat supported above the dipole spaced a quarter wavelength away. This additional degree of freedom is needed to effectively control the H-plane match without significant effect on the E-plane VSWR. It should be noted that this additional structure will greatly complicate a radome design; however, if additional scan is needed the increased cost and weight may be justified.

4.0 Pattern Tests

The gain of an infinite array in different scan directions is proportional to the pattern of an element embedded in the array with all others terminated.[1] Consequently such an element pattern is valuable as an economical test of the array before committing the design to production.

The equality is true since the total array current can be taken as a superposition of contributions with each element driven one at a time and coupling to all others. The total gain as a function of angle therefore has that pattern as a factor.

We would like to compare the measured patterns to the ideal case. The gain changes with angle for three reasons. First, the beamwidth, being constant in $\sin\theta$ space, widens in real space as $1/\cos\theta$. For constant radiated power the gain must reduce as $\cos\theta$. Second, if the beam is steered out of real space, it must present a reactive load to the source. Third, the radiator is not perfectly matched for all scan angles. Comparing the total pattern with the first two factors, gives a measure of mismatch loss vs. scan.

The test vehicle is the 11 element simulator. When in the row configuration, with dipoles collinear, it simulates about 30° of elevation scan (frequency dependent) as seen by the driven element. We

anticipate that as we scan in azimuth the beam peak moves out of real space at 60° as in Figure 10a. However, the test antenna is only 11 elements long, and therefore has a wide beam that gradually steers into imaginary space as in Figure 10b.

Obtaining an estimate of the actual finite array pattern is difficult to do exactly but simple approximately. We neglect diffraction around the edge which adds lobes beyond real space. We consider the wide pattern of the 11 element array to be synthesized as the sum of many narrow superimposed sin x/x patterns. Some of these are beyond real space and represent a reactive load and unavoidable loss. Others are in real space but broadened by cos θ and represent absorbed power.

Figure 11 shows the measured pattern for element six (central). At midband the theoretical pattern for an infinite array is drawn and the measured pattern is seen to approximate it, limited by its finite beamwidth. The dashed curve shows the finite approximation described above. Except for diffraction, the difference between that and the measured pattern should be the array mismatch loss. It agrees reasonably with simulator tests.

Figure 12 shows corresponding patterns for dipole two. C. J. Miller has pointed out that when an element is in an array scanned left, the coupling to elements on its left reradiates more or less in a progressive reinforcement, whereas coupling backward

to the right reradiates at wildly differing phases adding up to little. Therefore, if we leave off right hand neighbors it has little effect, while left hand neighbors drastically alter the pattern to that of an isolated dipole. These two conditions are seen in Figure 12 for a dipole second from the left end. For the array steered right the element has the normal nearly squared pattern, except more nearly square due to the larger (effectively 20 dipoles) test array. For the array steered left a rounder pattern corresponding to a few dipoles results.

The element patterns indicate reasonably good efficiency vs. scan, agreeing with simulator tests.

Acknowledgement

Much of the design detail and the computations have been extrapolated from work done by Mr. C. J. Miller, whose assistance we gratefully acknowledge.

References

1. Hansen, R. C. (1966) Microwave Scanning Antennas, Volume II, Array Theory and Practice, Academic Press, New York, pp. 301-304.

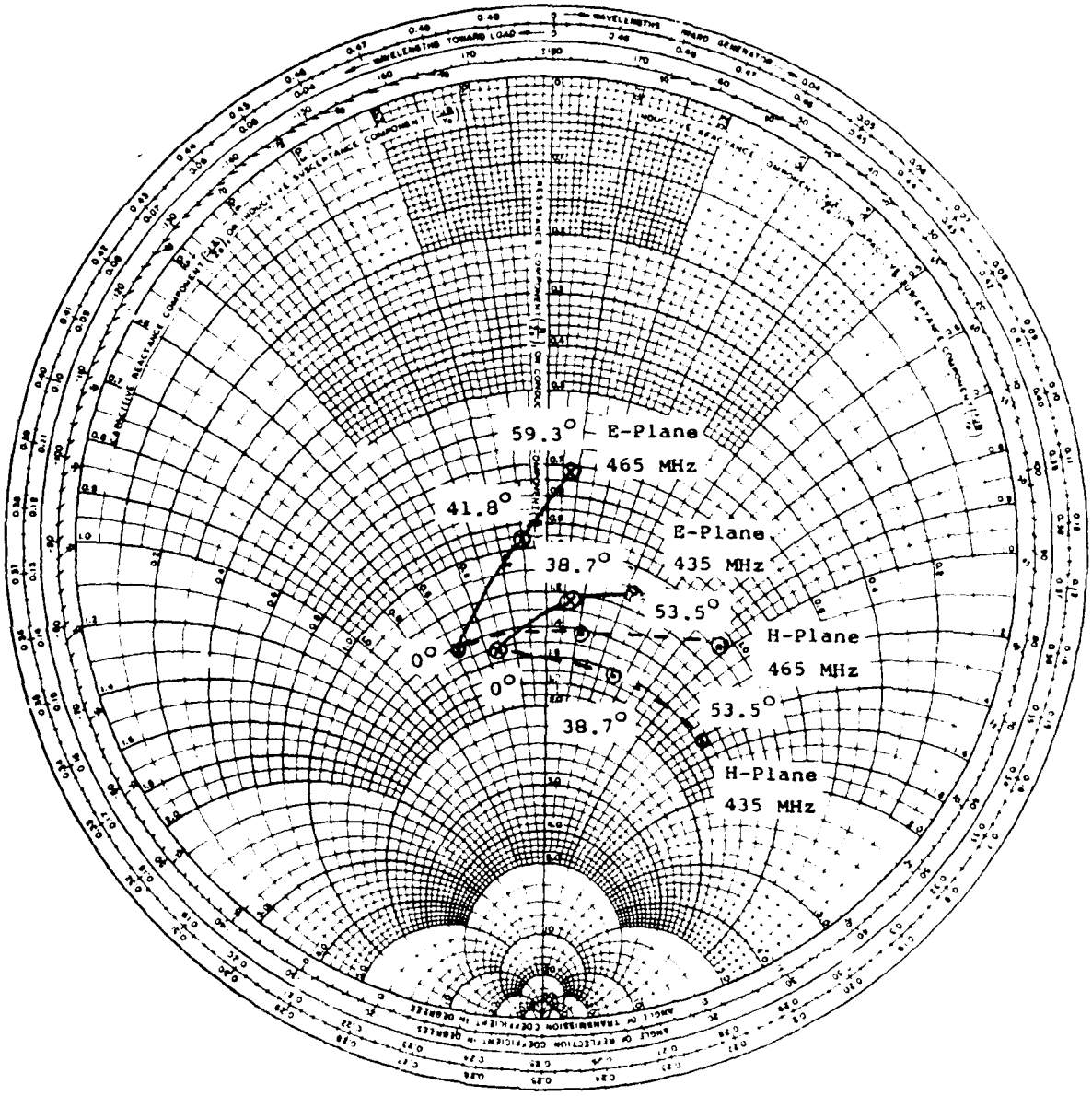

Figure 1. Summary of Computer Model of Scanning Dipole.

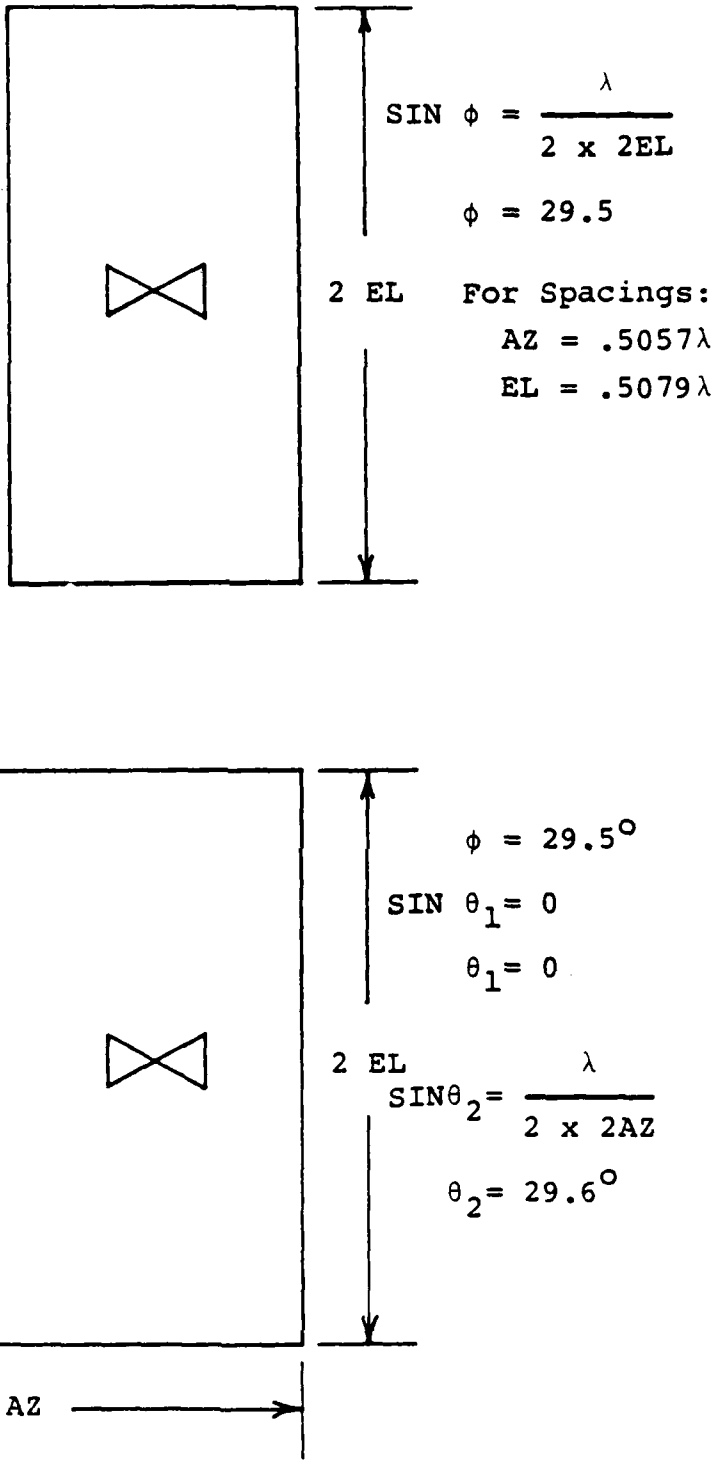

Figure 2. Single and Dual Mode Simulator.

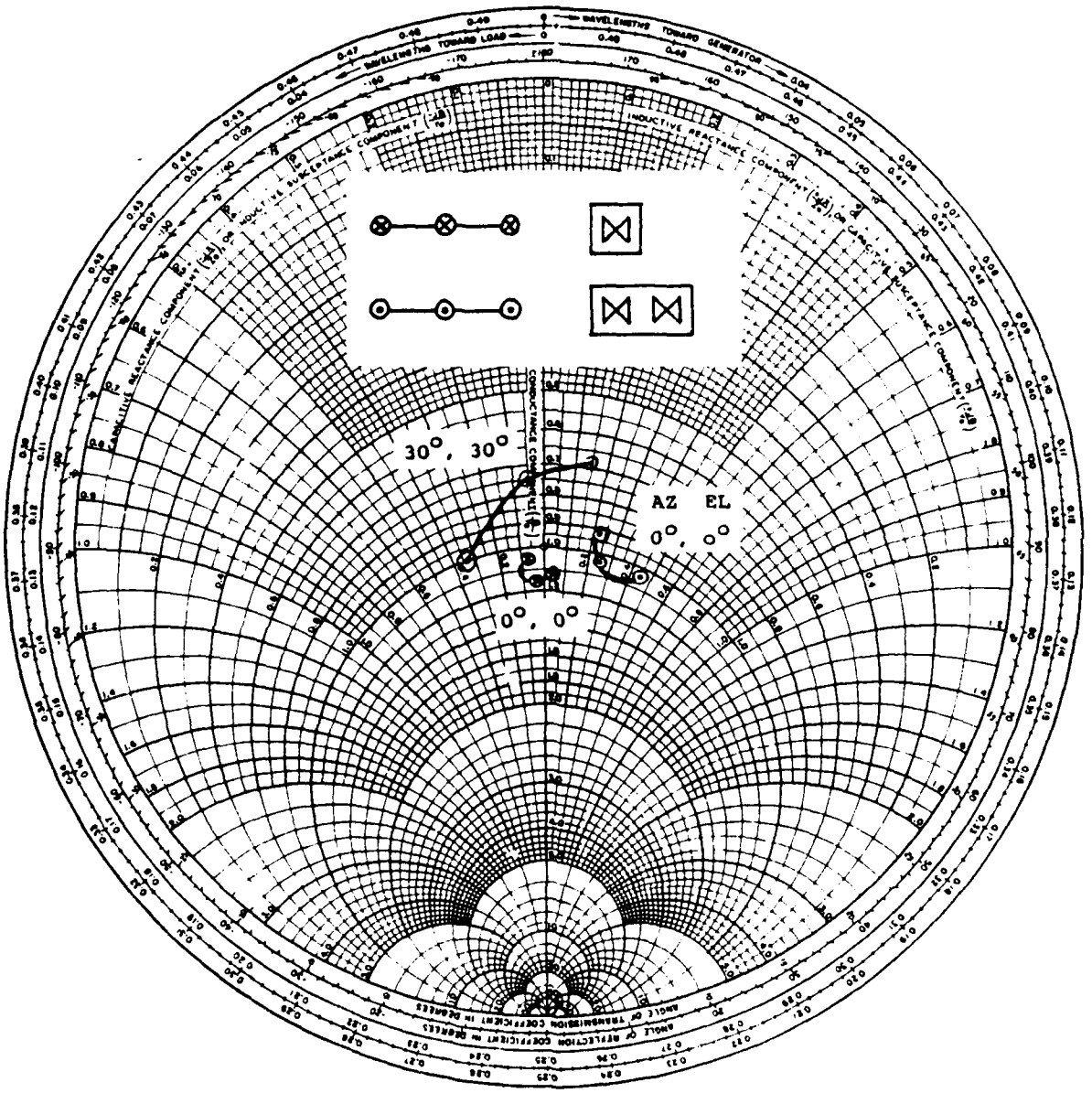

Figure 3. Single and Dual Mode Simulator Results.

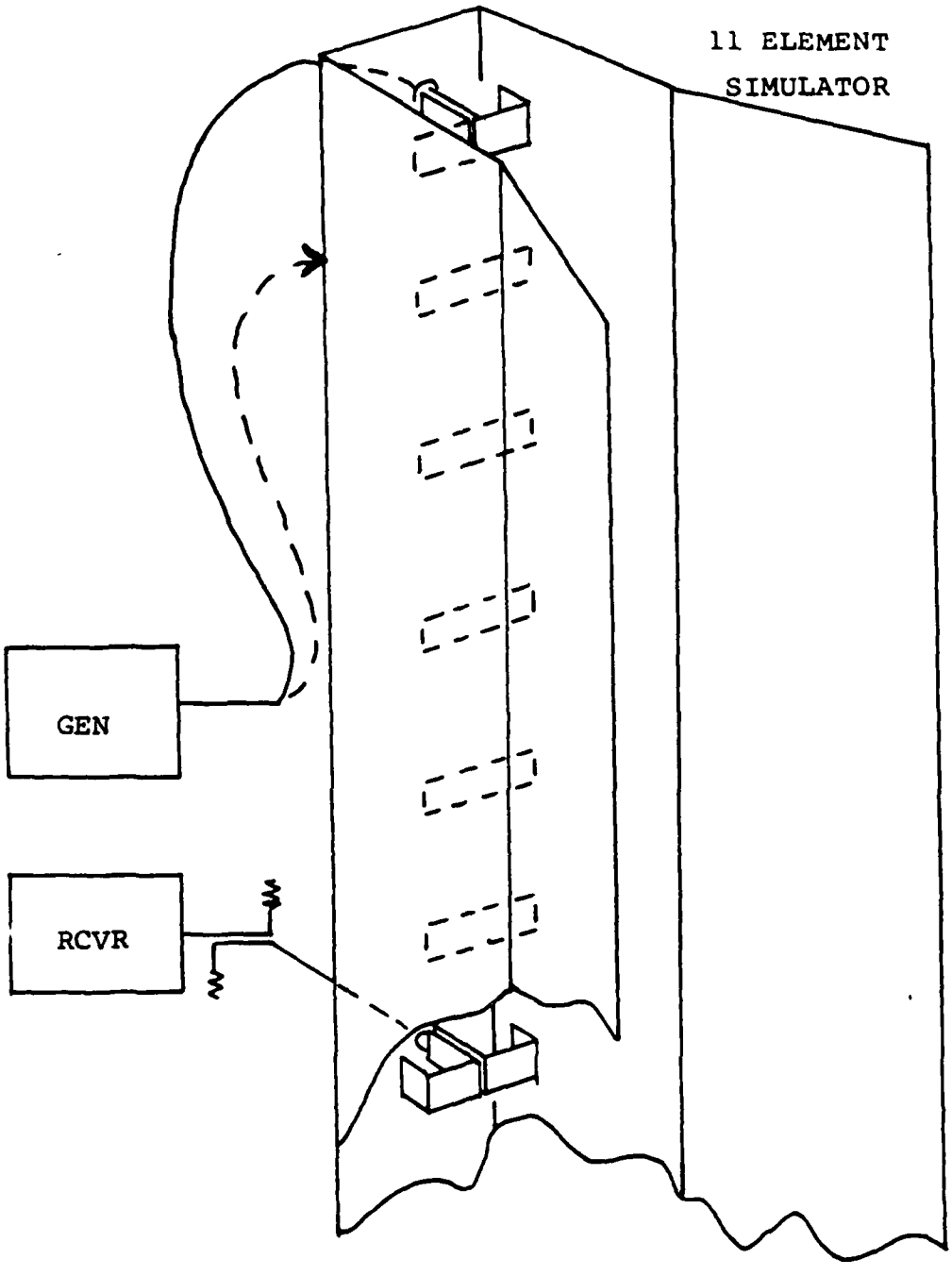

Figure 4. Multi-Element Simulator Measuring Technique.

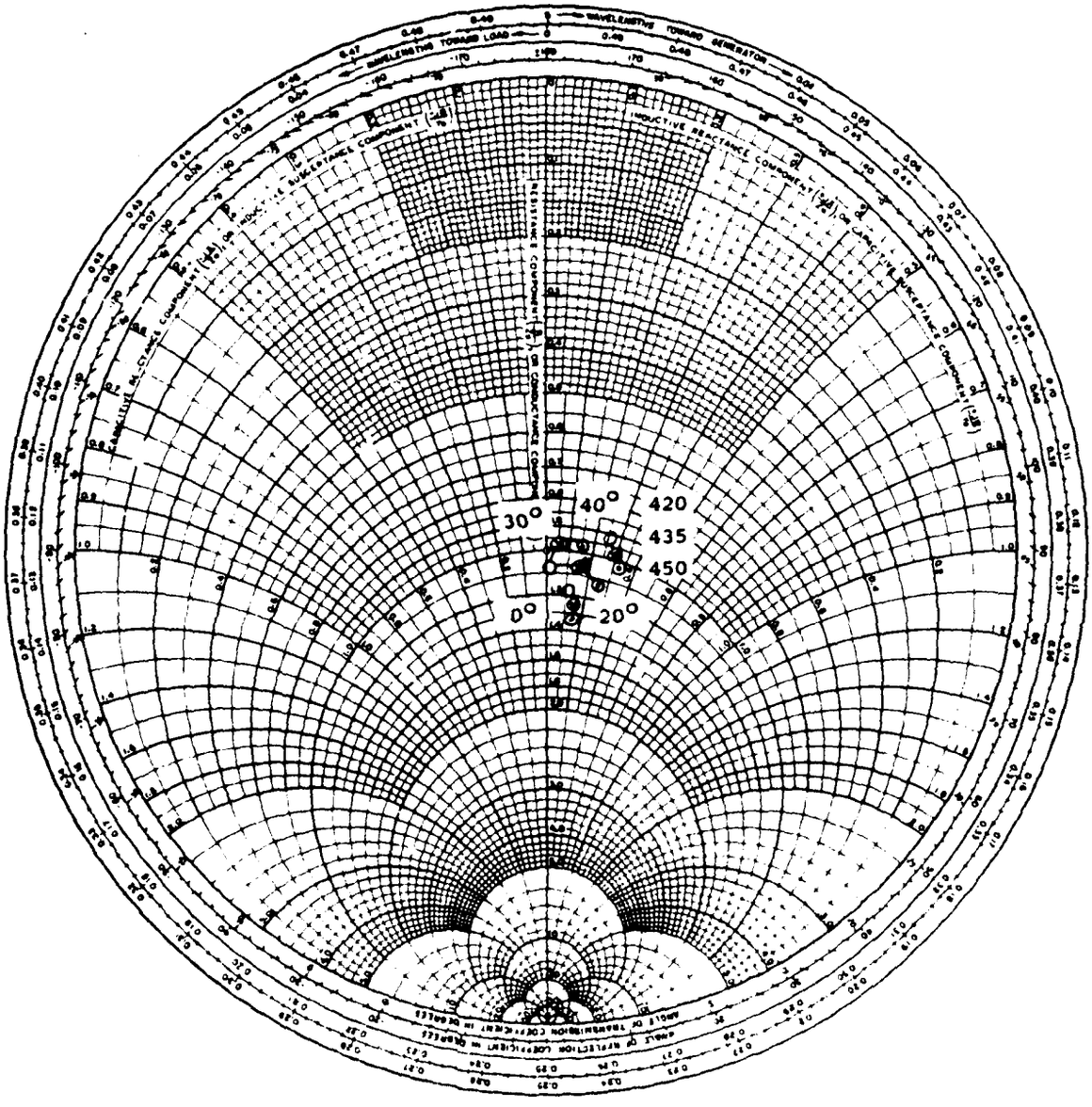

Figure 5. Central Dipole VSWR in H-Plane Scan.

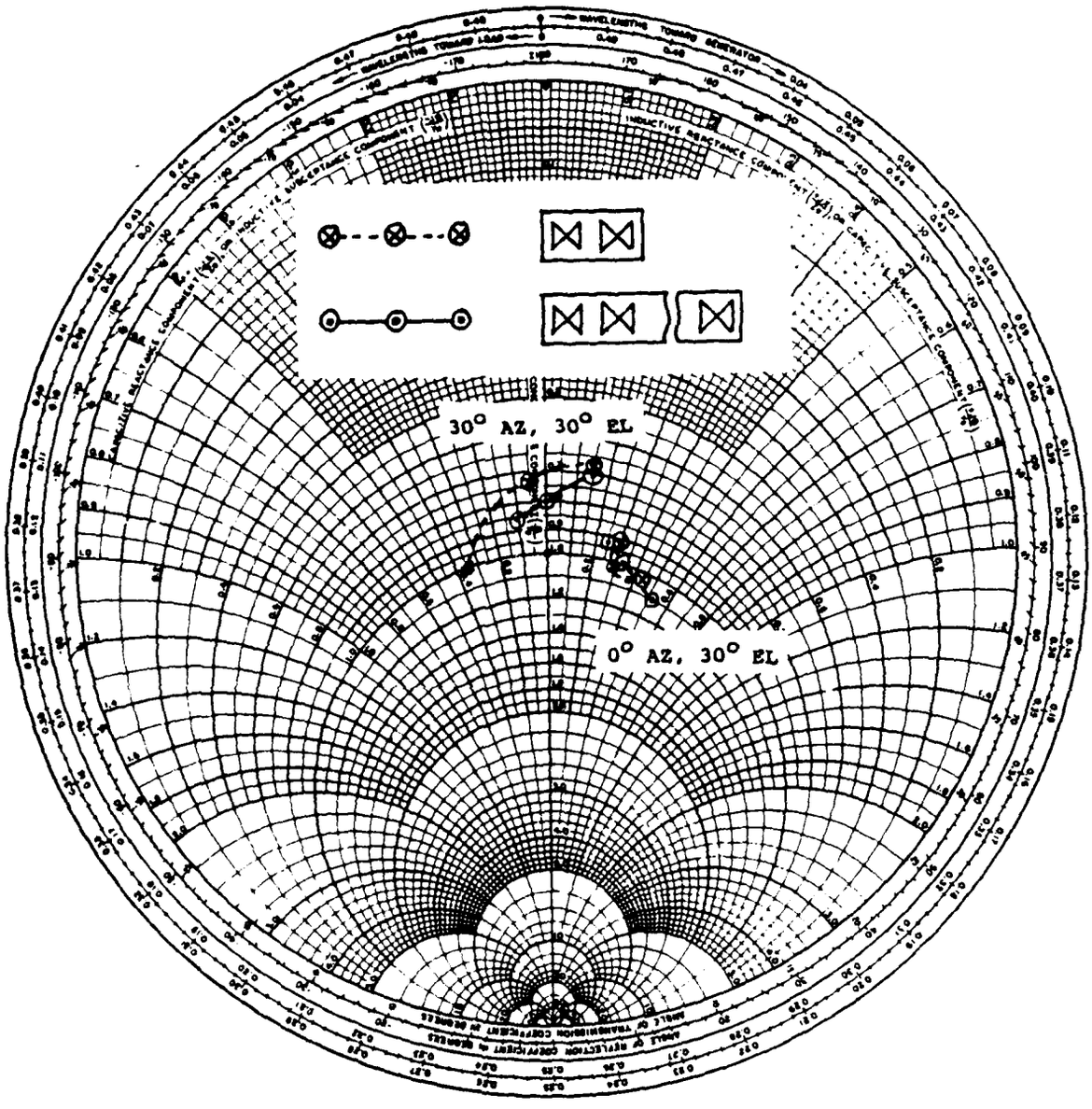

Figure 6. E-Plane Comparison with Dual Mode Simulator.

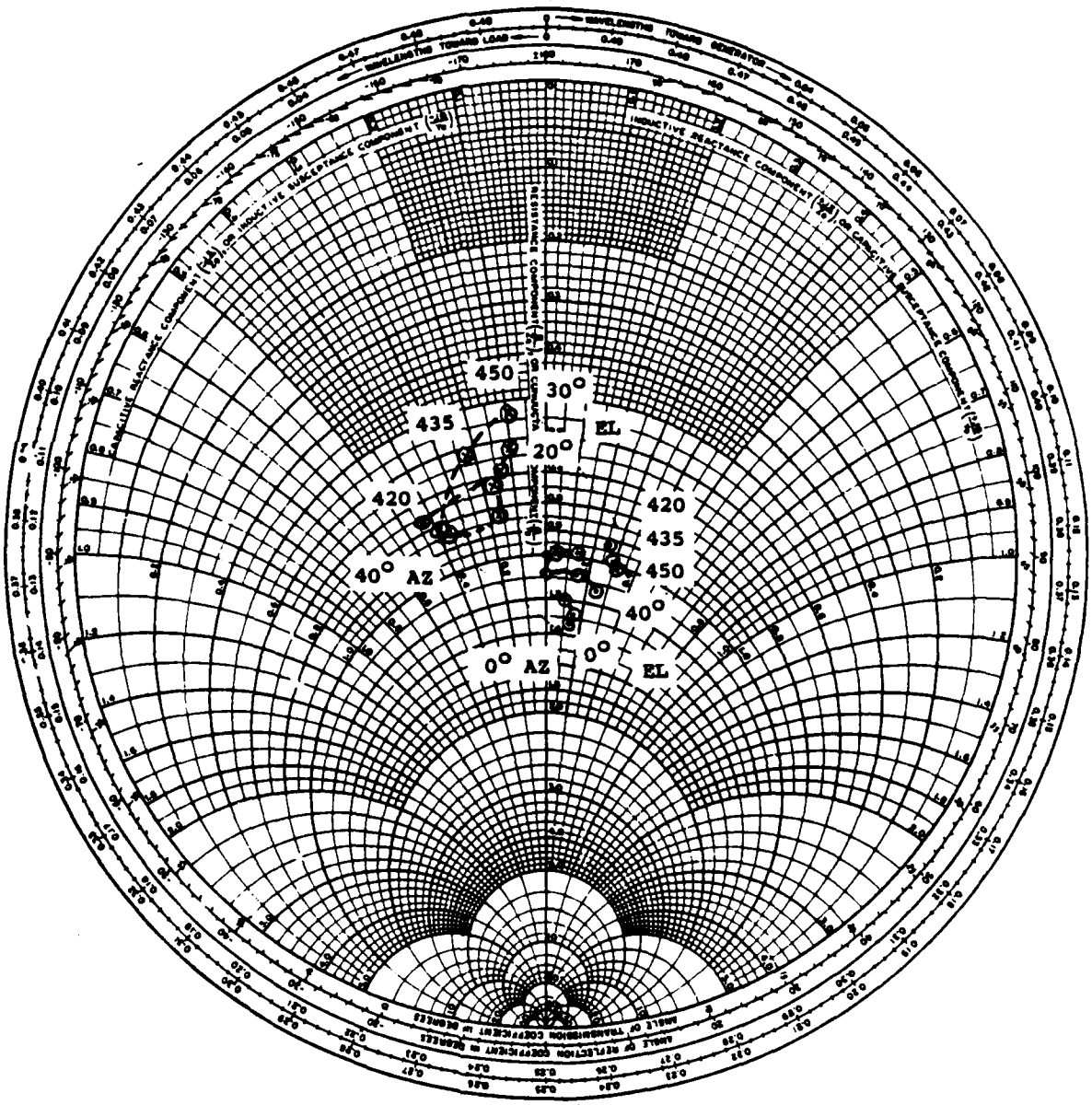

Figure 7. Summary of all 11-Element Simulator Data.

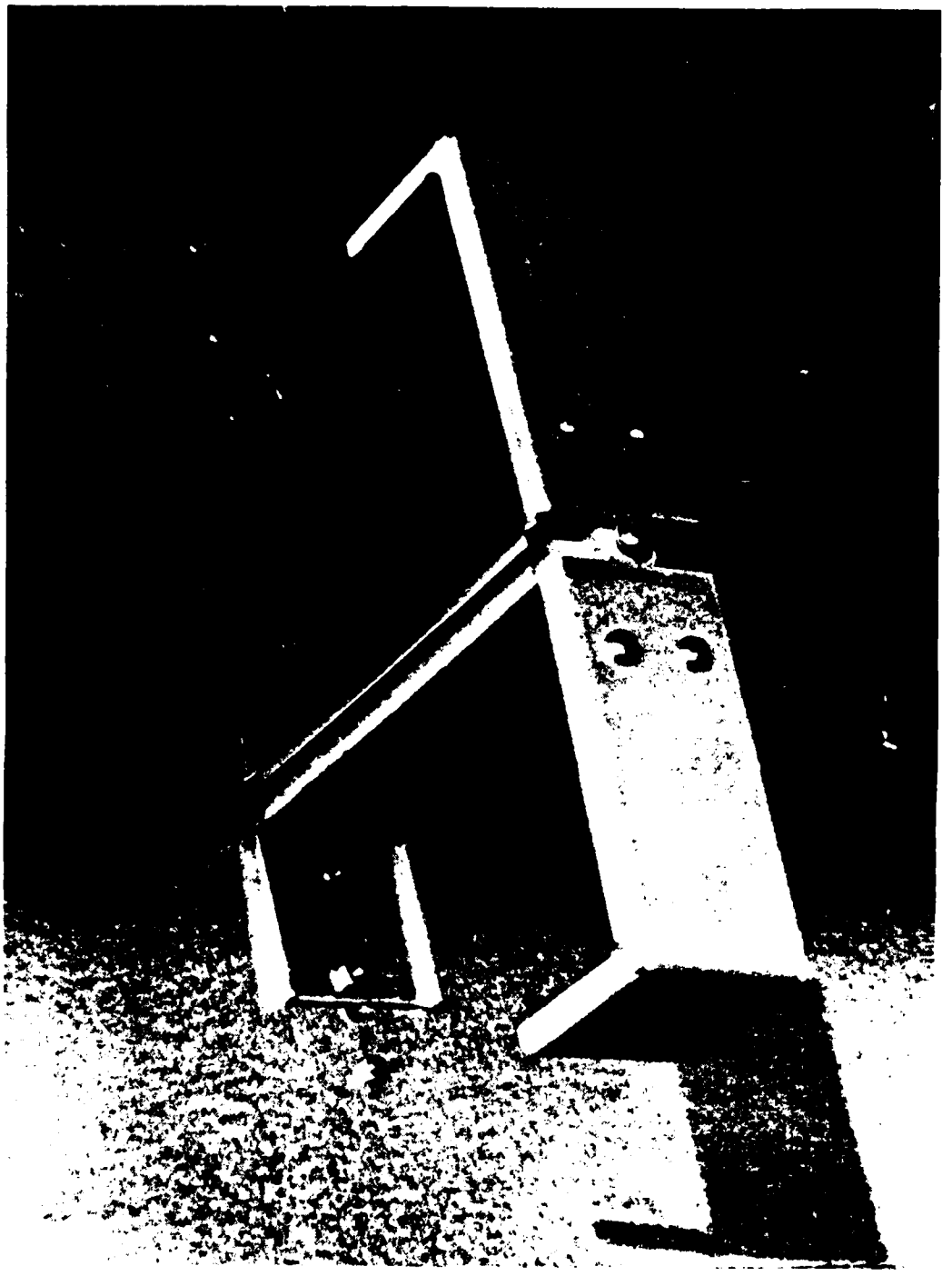

Figure 8. Final Dipole Configuration.

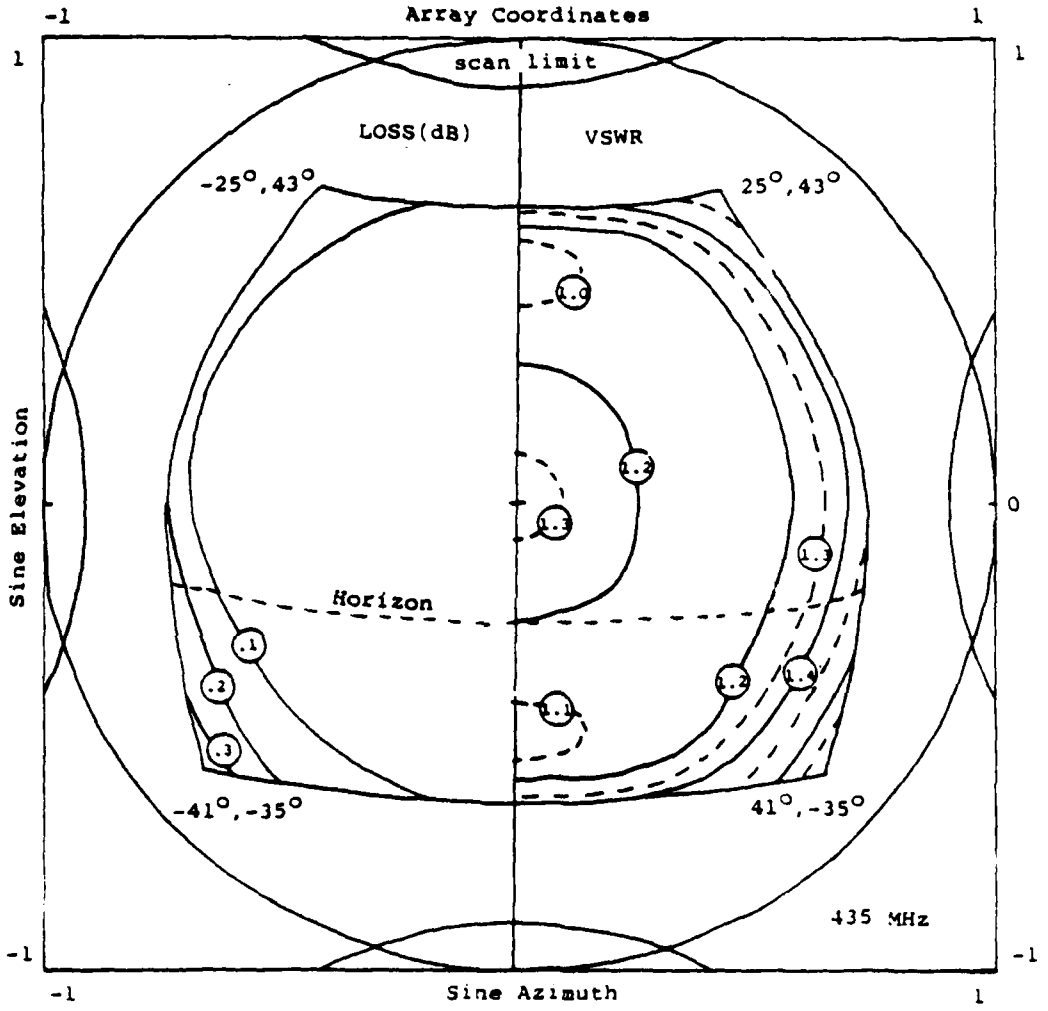

Figure 9. Summary of Simulator Data on Coverage Plot.

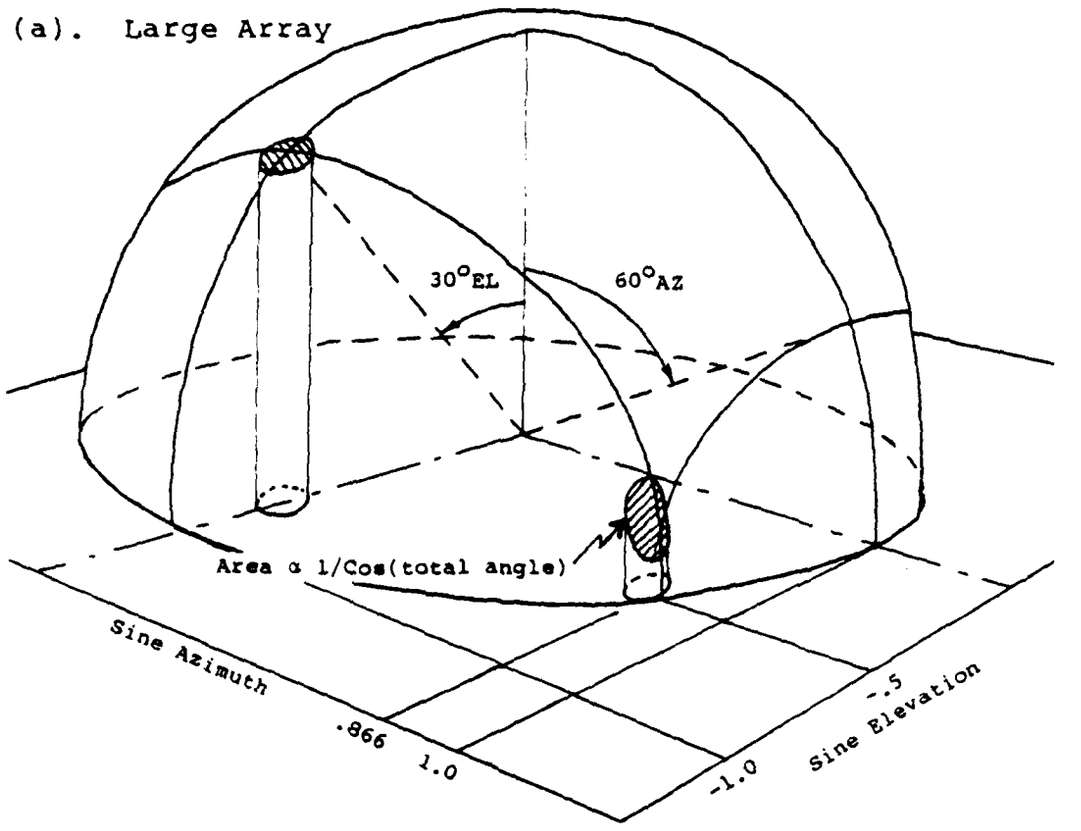

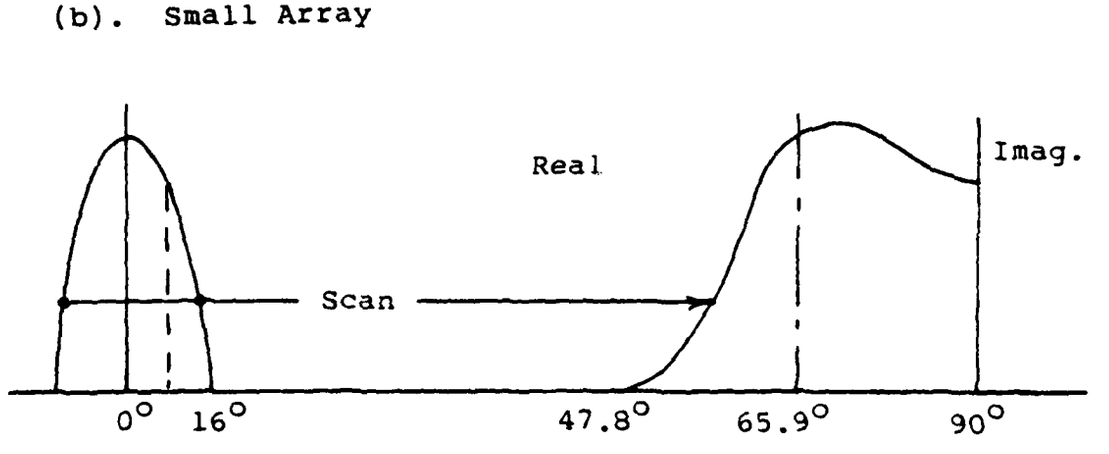

Figure 10. Beam Changes with Scanning.

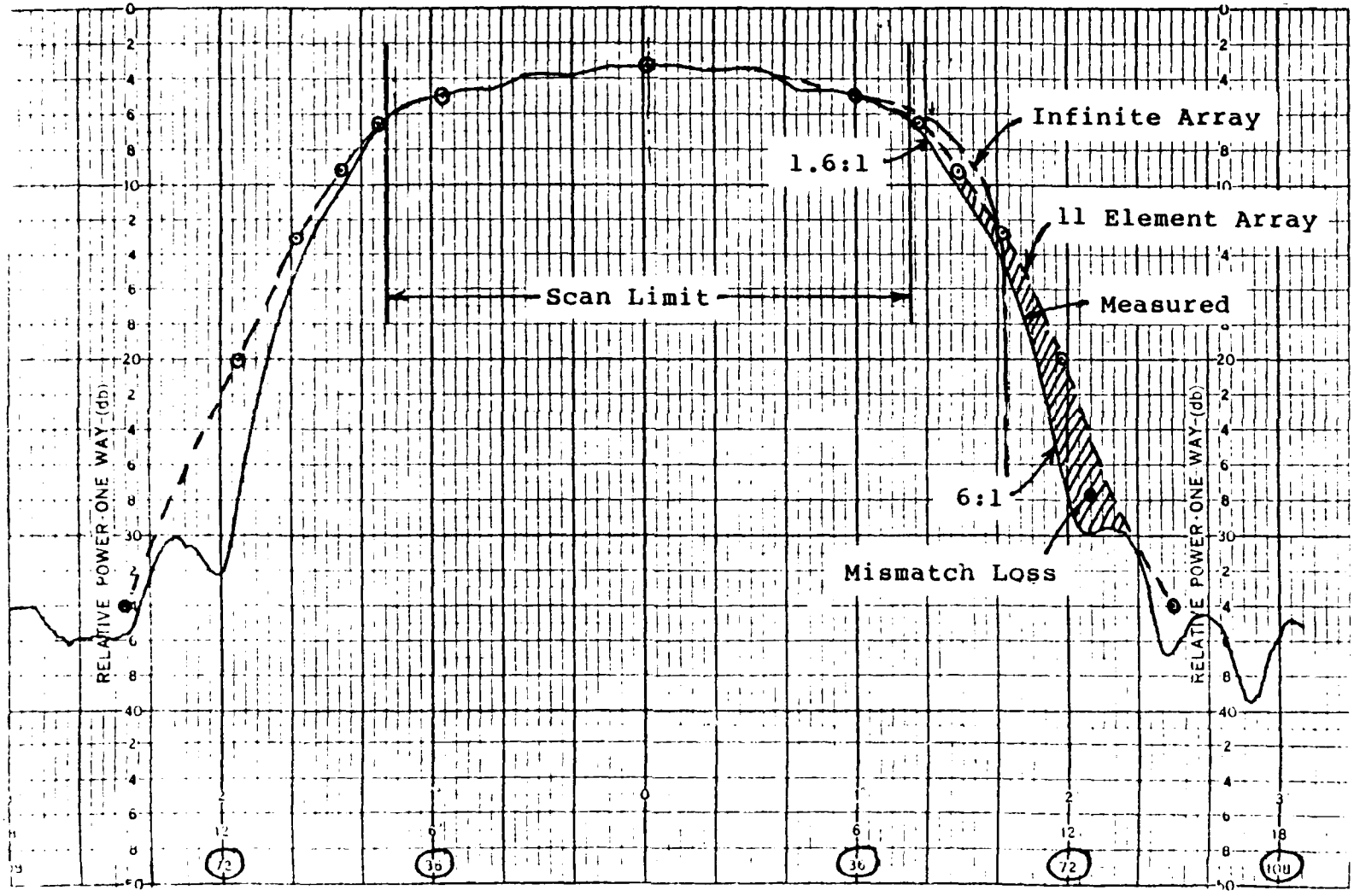

Figure 11. Measured E-Plane Pattern at 435 MHz, 11 Elements at #6.

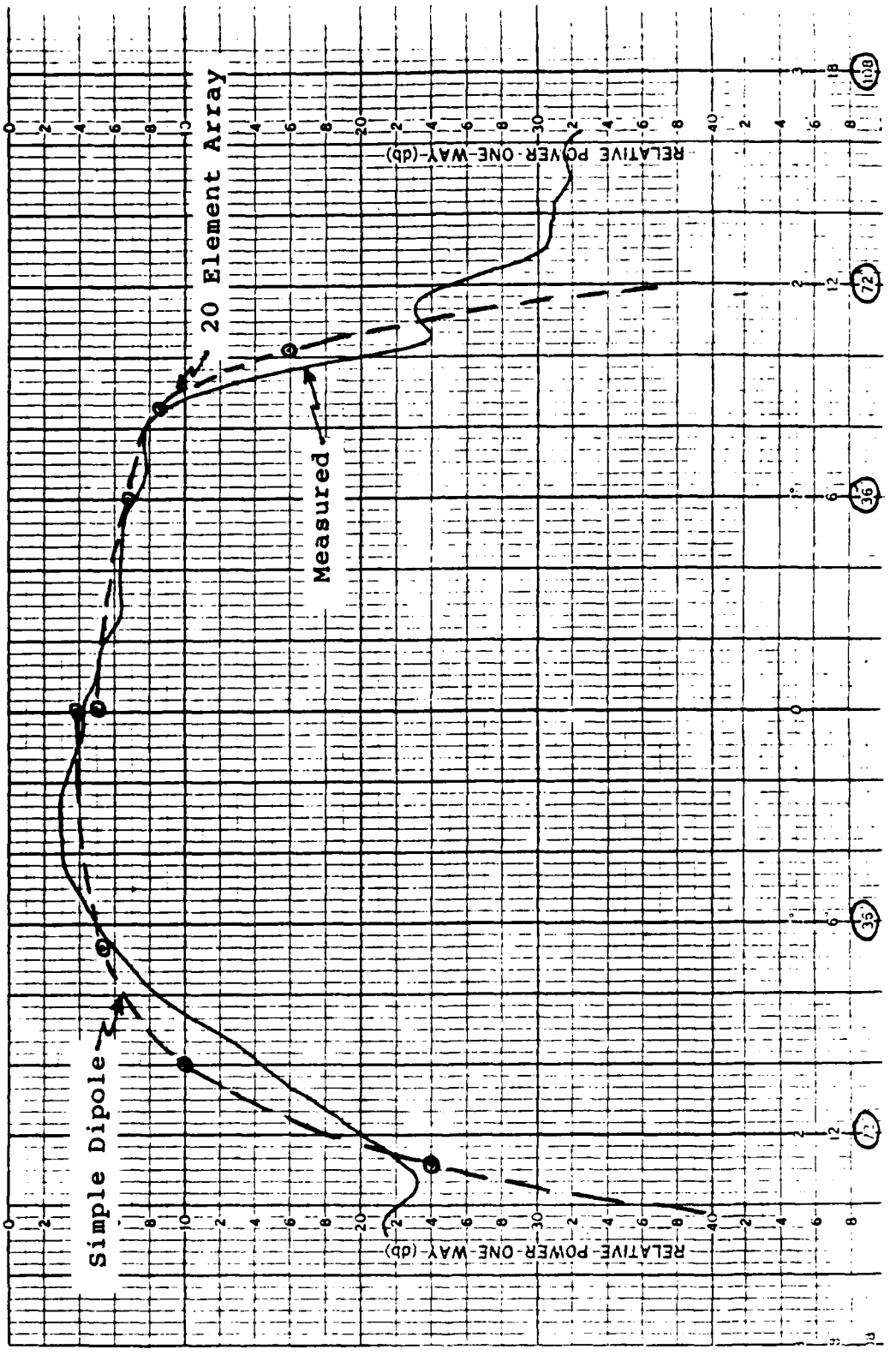

Figure 12. Measured E-Plane Pattern at 435 MHz, 11 Elements at #2.

THE DESIGN OF A LOW LOSS LIGHT-WEIGHT S-BAND PHASE SHIFTER

C. A. Hancik, N. Moldovan, and D. E. Heckaman
Harris Government Data Communications Division
P.O. Box 92000
Melbourne, Florida 32901

1983 Symposium on Antenna Applications
September 21-23, 1983
Allerton Park
Monticello, Illinois

THE DESIGN OF A LOW LOSS LIGHT-WEIGHT S-BAND PHASE SHIFTER*

C. A. Hancik, N. Moldovan, and D. E. Heckaman

Harris Government Data Communications Division

ABSTRACT

This paper discusses the design and fabrication of a low loss, light-weight 4 bit phase shifter for use in airborne phased array antenna applications. The phase shifter operates over the 2.2 to 2.3 GHz frequency band with a maximum average insertion loss of 1.0 dB over the 16 possible states. It dissipates less than 30 mW power. The entire assembly consists of four levels of circuitry packaged into a right circular cylinder weighing 1.2 ounces and measuring 2.80 inches (outer diameter) and .75 inches thick. Novel packaging techniques resulted in the use of a one layer, thin (.002 inch), flexible circuit, folded between ground planes and low loss dielectric spacers. The use of one flexible circuit allowed all circuit metallization and RF interconnecting to be done simultaneously during the printing and etching fabrication process.

---

*The work is sponsored by RADC/EEA, Hanscom AFB, Massachusetts

1.0 INTRODUCTION

Conformal Airborne Phased Array Antenna Systems are gaining popularity in satellite communication applications. Their unique feature of being low profile (either flush mounted or conformal) when integrated with the aircraft fuselage makes them attractive from an aerodynamic standpoint. To achieve the desired gain necessary to receive low power signals from a satellite at scan angles as large as 60 degrees, these arrays must be very large, which in turn makes them both heavy and costly. The key, then, in airborne array design and development is to minimize both array loss and weight by incorporating low loss, light weight RF circuitry designs and packaging techniques. This paper dicusses the development of a low loss, light weight S-band 4-bit phase shifter. Its application is part of the conformal array antenna system shown in Figure 1.0-1.

2.0 SPECIFICATIONS AND CIRCUIT DESIGN APPROACH

Table 1 gives a brief summary of the phase shifter specifications.

From the definition of the problem, it was clear that the insertion loss and weight specifications would be the most difficult to meet. While a ferrite phase shifter would solve the problem of insertion loss, it cannot meet either the weight or power requirements. Thus, it was decided that conventional phase shifter techniques must be improved upon. Three types of

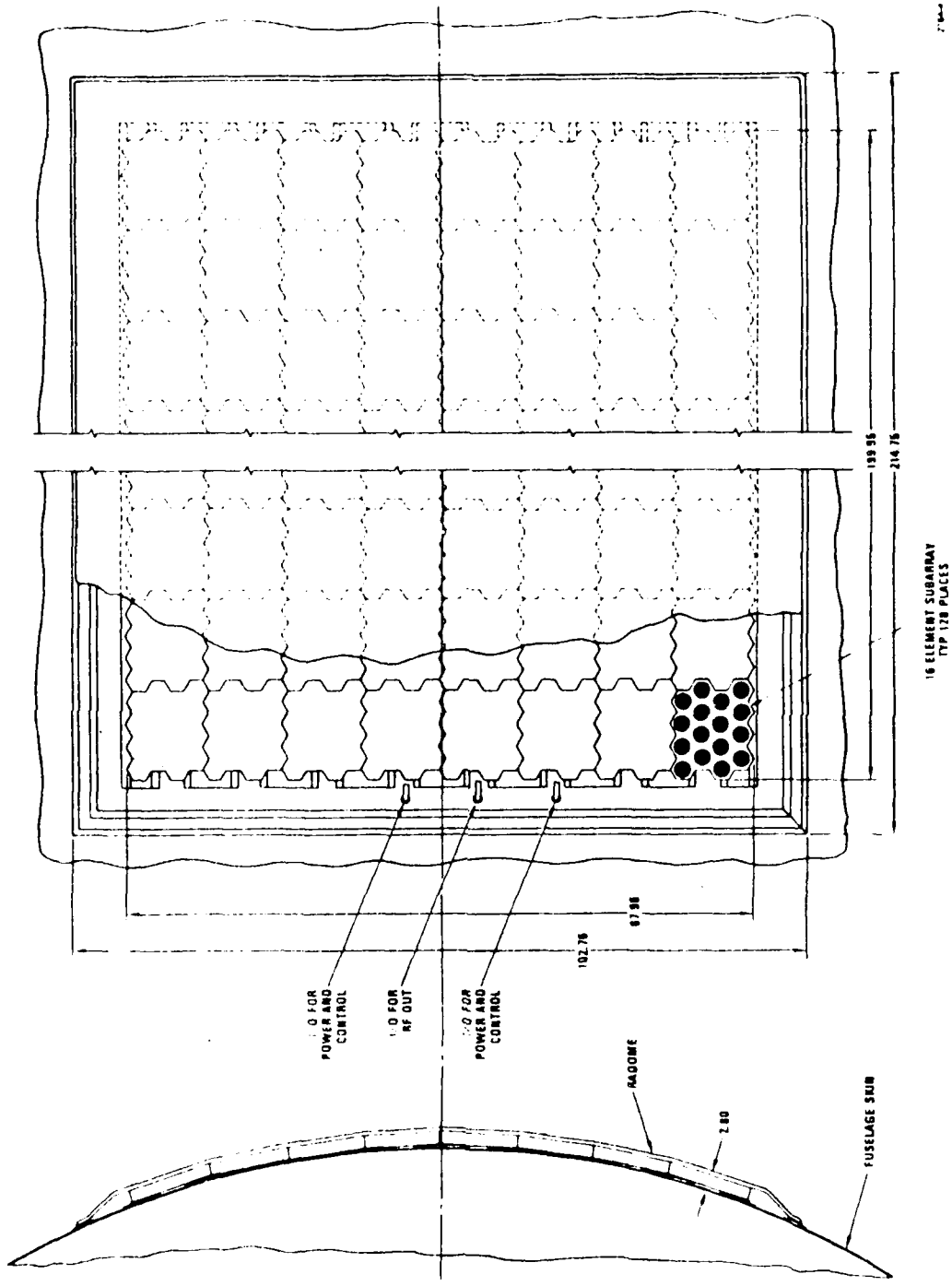

Figure 1.0-1. S-Band Conformal Array
(All dimensions in inches)

Table 1. Phase Shifter Specifications

Type:	4-bit
Frequency of Operation:	2.2 - 2.3 GHz
Return Loss:	$\leq$-19 dB, any combination of bits
Insertion Loss:	$\leq$1.0 dB average
Size:	$\leq$3.0" in diameter
Thickness:	$<$1.0"
Power Dissipation:	$\leq$30 mW, max
Weight:	$\leq$2 oz.
Phase Accuracy:	$\pm$11.25^{o}

circuits have commonly been used for phase shifters: branch-line hybrid, switched line, and loaded line. For minimum insertion loss it was determined that branch-line or hybrid coupled circuits should be utilized for the 180^{o} and 90^{o} bits, while a loaded line configuration should be used for the 45^{o} and 22.5^{o} bits.[1]

2.1 Branch Line Hybrids

For the two larger bits, (180^{o} and 90^{o}), the branch line approach was chosen for several reasons. For a 3.0 dB coupler, the VSWR remains below 1.2 for a bandwidth of approximately 7%.[2] Since the desired bandwidth is 4.4%, a properly tuned branch line coupler contributes less than .04 dB of insertion loss (S_{21}), excluding conductor and dielectric

loss. Furthermore, DC continuity is maintained; this was an important design consideration, as it eliminates the need for lossy DC blocking capacitors. Since the aperture of the phased array is at DC ground potential, a diode current return path was unnecessary.

For this type of phase shifter, both the "through" and "coupled" ports are terminated in PIN diode activated 50 ohm transmission line open stubs. While the PIN diodes switch these lengths "in" (forward biased diodes) and "out" (reversed biased diodes) of the signal path, it is the length of the stubs that determine the amount of phase shift experienced between on and off states. Optimum return loss over the desired band is achieved by ensuring a 90° electrical length in both the series and shunt arms of the hybrid, varying the length of the transmission lines between the coupler and diode, and varying the diode mounting gap.

The 180° and the 90° phase shifter bits were modeled and examined using SUPER COMPACT. This is a CAD tool specifically developed to analyze and optimize RF and microwave circuits. With it, effects due to dispersion, dielectric and conductor loss, conductor material and composition, various discontinuities and diode parasitics were incoporated in the circuit model and analyzed.

2.2 Series Loaded Line (45° and 22.5°)

For the smaller bits, it was determined that a series loaded line configuration was desirable.[4] This design possesses advantages similar to branch line hybrids and provides substantially lower insertion loss. Since these bits occupy less space, they were placed upon the same substrate. The design incorporates two open stub bits separated by a 90° length (at midband) of 50 ohm line. The lengths of both the 50 ohm lines between stubs and the stubs themselves were determined by computer optimization. In a reversed bias state, these bits appear to be short, low loss 50 ohm paths. When forwarded biased, they remain matched to 50 ohms, but incur slightly more forward loss.

2.3 Component/Diode Selection

The second major factor to influence the insertion loss (S_{21}) of the assembly was the diode. Naturally, a low series resistance (Rs) model was sought. In a PIN diode, this means that the intrinsic ("I") region must be small, and therefore, less recombination of holes and electrons occurs. Unfortunately, PIN diode junction capacitance (Cj) is inversely proportional to "I" region width, so that as Rs decreases, Cj increases.

The specifications for the diode chosen are shown in Table 2. For mechanical considerations, this diode was hermetically sealed in a right circular cylindrical (#040) package. This low parasitic structure has a package capacitance

Table 2. Diode Specifications

Parameter	Value	Conditions
Rs	.7	25 mA, 100 MHz
Cj	.25 pF	-50V, 100 MHz
TL	400 ns	IF = 10 mA, IR = 6 mA
Vb	100V	IR = 10 μA

of .09 pF and a package inductance (Lp) of only .40 nH. Gold ribbons (.050" x .001" x .250") were used to attach the diode to the RF conductor. All diodes were mounted flush with the substrate. This method of mounting protects the diode while supporting it to relieve stress on the thin leads. Thermo-compression welds were used to fasten the ribbons to the gold plated copper and Kovar diode case; however, the free ends were soldered to the circuit board. Future circuits will use copper ribbons to further reduce loss.

3.0 SUBSTRATE SELECTION AND PACKAGING TECHNIQUE

To achieve minimum loss, stripline with a wide ground plane spacing was required. Using SUPER COMPACT's transmission line analysis program, various covered microstrip, stripline and suspended substrate configurations were investigated. A matrix of transmission line parameters was generated for conventional substrates in varying thicknesses and packaging configurations.

The candidates included .025" and .050" Alumina, .008" and .031" duroid, .025" fused silica, and a composite polyimide/low loss foam.

The results of this study concluded that an etched stripline conductor on a polyimide film (.002") supported between ground planes by low density foam spacers was the optimum configuration. The foam, which weighs only 3.1 lbs./ft^3, not only provides mechanical support, it is nearly electrically transparent! Because of its low relative dielectric constant (ϵ_r=1.07) dielectric loss is almost eliminated. The polyimide substrate is single-side metallized with 1 oz. (1.35 mils) rolled copper to reduce conductor loss. Thin copper ground planes are bonded to the foam to complete the assembly. The design, aside from meeting the low-loss and light weight goals, proved to be structurally sound as well. This pseudo-suspended substrate stripline configuration is shown in Figure 3.0-1.

4.0 INTEGRATION TECHNOLOGY*

The final development of the phase shifter consisted of 4 circuits: a 180° bit, a 90° bit, a 45°/22.5° bit and a circular polarization bit. The circular polarization circuit, though not truly part of the phase shifter, had to be placed within the assembly and be consistent with the low-loss/

*Patent Applied For

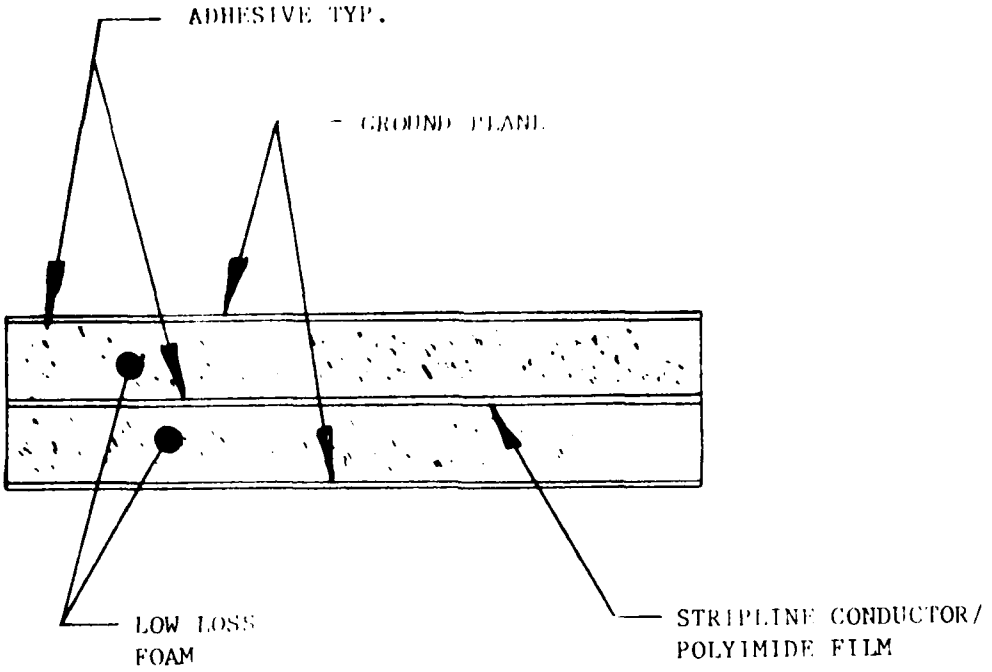

FIGURE 4.0-1. PSEUDO-SUSPENDED SUBSTRATE STRIPLINE CONFIGURATION

lightweight goal. Each of the 4 layers of circuitry were designed for and constructed on circular substrates. This was done to facilitate their being stacked, one atop the other, in a cylinder. Unfortunately, this raises the question of how to interconnect the RF paths between levels. To solve the problem a novel interconnection technique was employed. By design, the input and output RF ports of the 180° and 90° bits were placed at right angles to each other. Next, all of the circuits are fabricated in one plane, including the RF interconnections (See Figure 4.0-1). After the components have been attached, the

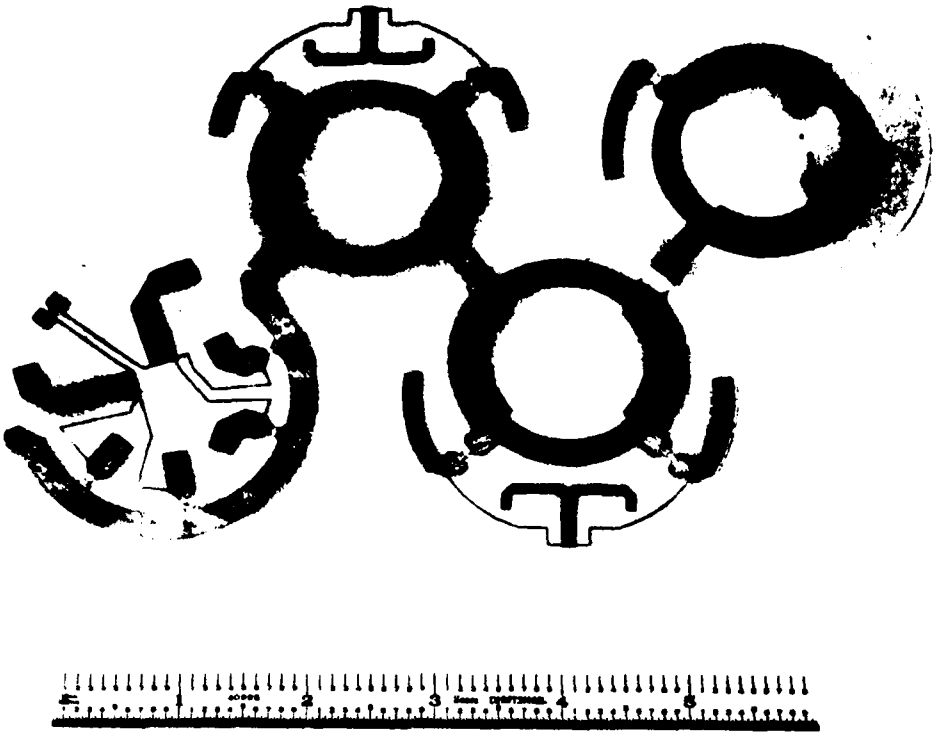

Figure 4.0-1. Four Level Substrate Prior to Folding

circuits are folded into a right circular cylinder. Appropriate discs of foam, adhesive and ground planes are inserted and bonded together. Figure 4.0-2 depicts all the components of the assembly; while Figure 4.0-3 illustrates the folded assembly and housing. The use of one flexible circuit allowed all stripline conductor metallization and RF interconnecting to be done simultaneously during the printing and etching fabrication process. The bonded assembly is housed in a cylindrical can measuring 2.80" in outer diameter, .75" in height. The entire assembly weighs only 1.2 oz. The result is a low loss, light

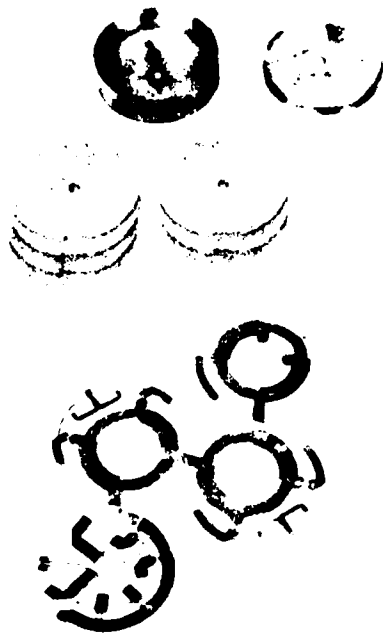

Figure 4.0-2. Phase Snifter Assembly Components

Figure 4.0-3. Folded, Assembly and Housing

weight, cost effective, easy to integrate, 4-bit, digitally controlled phase shifter. This design, due to its simplicity, has the potential to be highly reliable as well. A photograph of the completed phase shifter is shown in Figure 4.0-4.

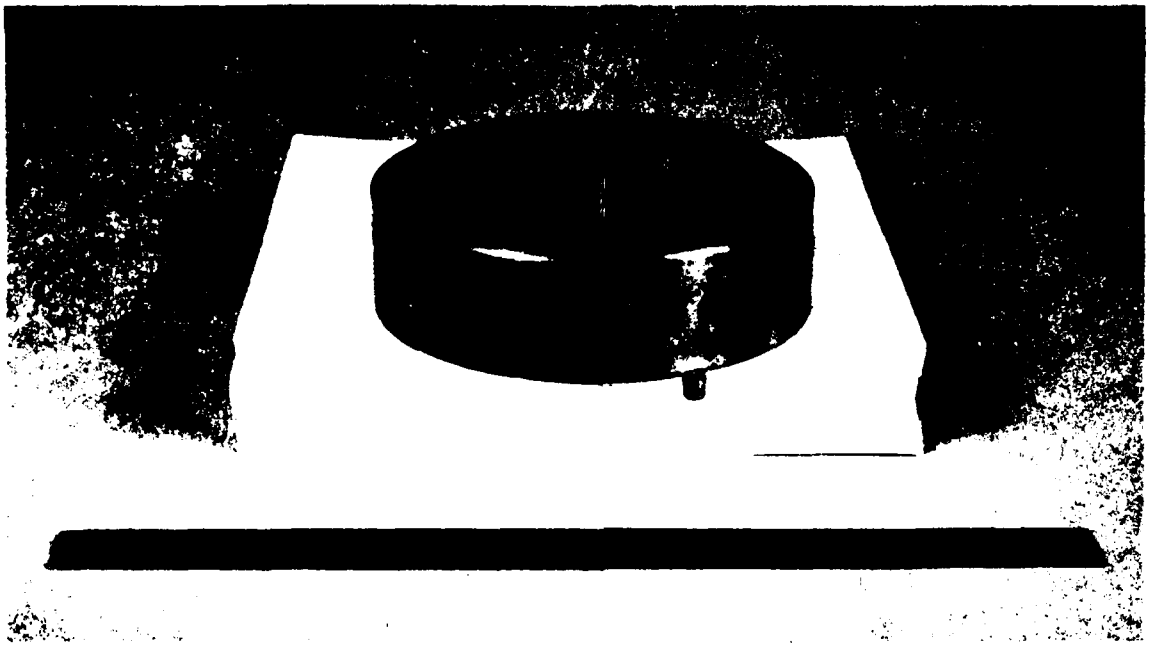

Figure 4.0-4. Integrated Phase Shifter Assembly

Table 3. Phase Shifter Results at F = 2.20 GHz

Bit/Bias	S_{21} (dB)	S_{11} (dB)	Shift
180°/FWD	.46	24.4	180.2°
180°/REV	.25	37.6	
90°/FWD	.35	40.0	91.9°
90°/REV	.27	21.0	
45°/FWD	.30	26.0	41.3°
45°/REV	.05	22.5	
22.5°/FWD	.25	24.9	18.5°
22.5°/REV	.05	22.5	

5.0 RESULTS

The test results shown in Table 3.0 include insertion loss, return loss, and phase shift of individual bits for both bias conditions. All through losses exclude a .1 dB connector loss. A graph of phase shift versus frequency is shown in Figure 5.0-1 for each of the 16 phase states. The insertion loss for each state is also given. With this model, the average insertion loss for all states is .98 dB. Phase accuracy is $\pm$4.5 degrees. Maximum diode bias current is required for 337.5^{o} of shift. Under this condition, the 8 pin diodes draw 20 mA each through a nominal 1Ω series resistance, consuming 25.6 mW.

5.1 Improvements

The foreseeable improvements for the assembly are many. The use of lower series resistance diodes would reduce insertion loss. Two devices are presently under consideration. Integration of the bias connections can also be achieved. By locating all DC input lines either on the same level or on top of each other in their respective levels, a single plug connector can be used. To assure high quality, low loss circuit/component transitions, copper ribbons will be used to attach the copper/Kovar encased diodes to the transmission lines. Instead of soldering, thermo-compression bonding techniques will be used for diode mounting.

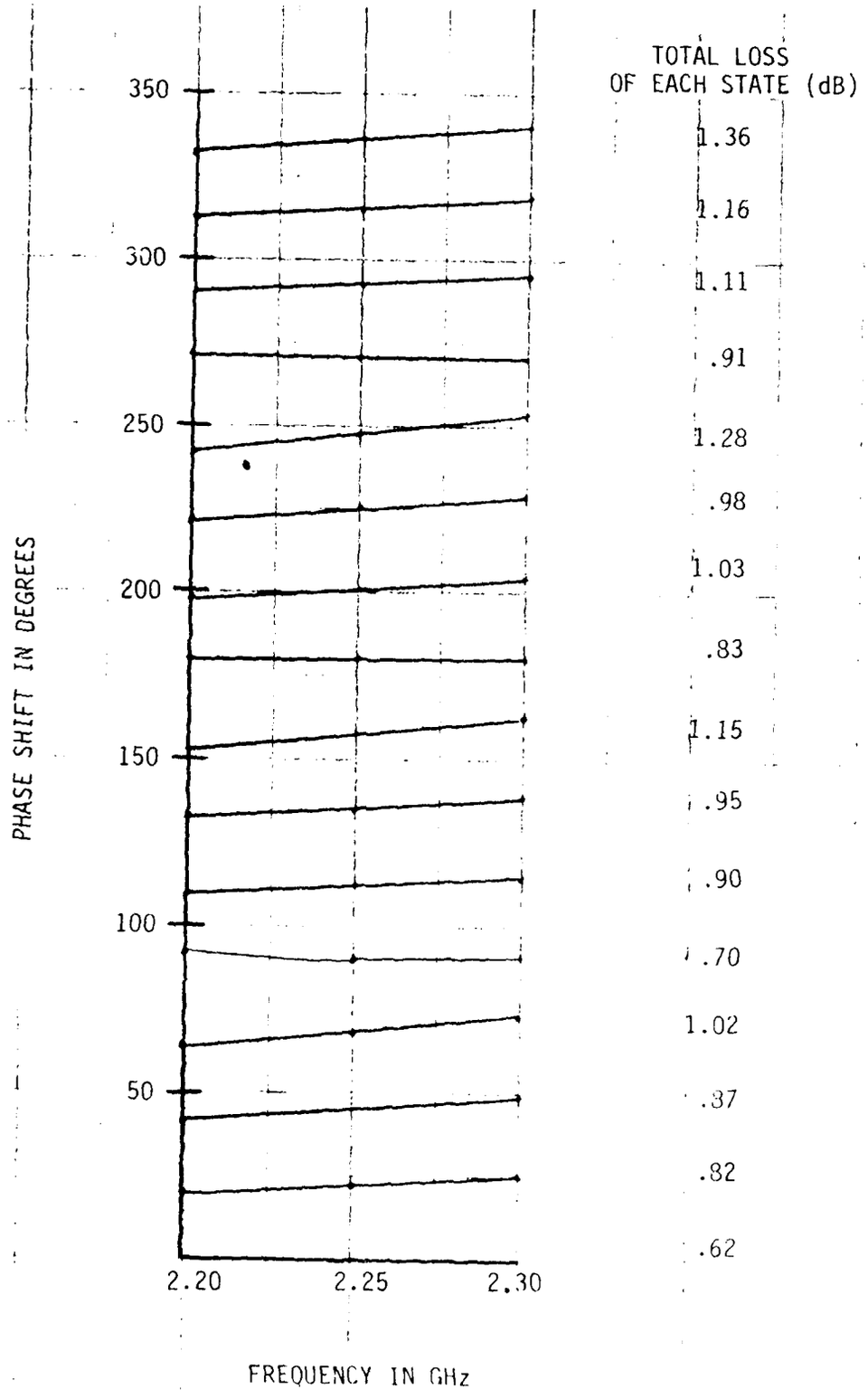

Figure 5.0 I. Phase Shift Versus Frequency

6.0 SUMMARY

The design of a low-loss, lightweight, low cost, 4 bit S-band phase shifter has been presented. The assembly employs a new pseudo-suspended substrate stripline technology which allows fabrication and integration of multilayer circuits from a single, planar substrate. This folding approach eliminates bothersome interlevel RF connections as well as the need for multiple conductor masks. The low density foam which encases the substrates provides excellent mechanical support and is nearly transparent to RF signals. The finished product, due to its size, weight, loss, power, and cost characteristics is ideally suited for use in conformal airborne phased array antennas with large scan angles.

7.0 REFERENCES

[1]Holden, R. L., R. W. Burns "A High Power UHF Microstrip Diode Phase Shifter," 1972 IEEE-GMTT International Microwave Symposium Digest, p. 47.

[2]Howe, H., Stripline Circuit Design, Microwave Associates, Burlington, MA, 1974.

[3]Glance, B., "A Fast Low Loss Microstrip P-I-N Phase Shifter," IEEE-MTT-22 No. 1, January 1979, p. 14

[4]Fisher, M. E., M. R. Barber, "Digital-Refelection-Type Microwave Phase Shifters," Microwave Journal, May 69, p. 63.

A COMPACT FULLY OVERLAPPING SUBARRAY ANTENNA*

by Pat A. Valentino, John J. Stangel
and Salvatore Milazzo
Sperry Defense Electronics
Great Neck, New York

Abstract - This paper describes a new limited scan antenna technique for electronic scanning arrays. The antenna uses a novel coupling network to achieve fully overlapping subarrays with minimal antenna depth. The coupling network is comprised of contraposed input and output ports interconnected through a one wavelength section of radial waveguide.

Antenna and network design principles are discussed in detail. Performance parameters are defined and the major features of the design including very low sidelobe and adaptive nulling capabilities are presented. An experimental demonstration antenna is described, and experimental results for the antenna and coupling network demonstrating the capabilities of the design are presented.

*This work was supported in part by USAF Rome Air Development Center under contract number F19628-81-C-0078.

INTRODUCTION

This paper addresses a new, highly efficient, limited scan antenna technique for electronic scanning arrays. The antenna uses a novel coupling network to achieve a fully overlapped subarray antenna with a minimal size and less complex constrained feed network. Overlapping subarray or transform feed antennas are well documented in the literature. [1-7] They afford benefits for:

- o reducing the number of phase shifters required to scan a limited angular sector
- o reducing the complexity of electronic time delay circuits to obtain wide instantaneous bandwidth
- o economically implementing adaptive nulling and jammer cancellation
- o providing low sidelobe performance by compensating for antenna tolerance errors

Mailloux [1], Fante [2], Tang [3], Rudge [4] and Borgiotti [5] have published analytical and experimental results confirming and quantifying these benefits with lens fed subarraying systems. In these classical implementations, the primary collimating device is a lens or reflector. The subarraying networks are Butler matrices or Rotman lenses, located in the feed package at the focal points of the lens. The result is a physically deep configuration which is characteristic of optically fed array systems and which is not readily adapted to the highly mobile, compact radar applications.

Several constrained alternatives to the lens-fed subarraying systems have also been described by Tang[3], Stangel[6], and Ploussios[7]. These alternatives fall into two general categories.

The first, a conceptually straightforward extension of the lens fed system, simply substitutes a Butler matrix (or a three-dimensional network of Butler matrices) for the primary collimating lens. For large aperture antennas, this is not an attractive approach because of the complexity of the Butler matrices required. Cost, loss and weight would be prohibitive, and furthermore, it is doubtful that the overall package depth of the antenna could be substantially reduced from that of the equivalent lens-fed design.

The second category of constrained subarraying systems uses partially overlapped or interlaced subarrays. A variety of specific design approaches have been suggested which will generally result in significant reductions in antenna depth. Invariably, these designs exhibit poorer sidelobe and loss performance, or reduced scanning capabilities in comparison to that of the fully overlapped subarrays provided inherently in lens-fed systems.

This paper addresses an innovative design for an array feed network which provides the performance and benefits of an overlapped subarray antenna while overcoming the physical drawbacks of the classical transform fed lens and beamforming network designs. This network, called the optically coupled network (OCN)[8], provides fully overlapped subarray excitations to the radiating elements of a high gain array antenna with a total network depth of only a few wave-

lengths. Furthermore, the network is compatible with economical fabrication as a simple, single-layer, printed circuit parallel plate network.

A schematic representation of the network is shown in figure 1. The network generates fully overlapped subarray excitations in a compact constrained feed network through a closely spaced optically coupled parallel plate region. It provides the control savings feature of a transform feed antenna in a compact, easily fabricated, low loss network configuration. The low sidelobe and adaptive nulling capabilities of the network have recently been demonstrated on an experimental model. Measured patterns with better than -40 dB peak sidelobes and -63 dB adaptive nulls were generated demonstrating the capabilities offered by an OCN array feed.

This paper is divided into five sections. The first presents a functional description of the OCN concept along with formulations for its design and operation. Theoretical results are presented in the next section illustrating its overlapped subarray antenna pattern characteristics and the associated far field antenna performance. Antenna configurations are described which provide for wide signal bandwidth, low sidelobe pattern synthesis and adaptive nulling operation. The design, fabrication and test of an OCN experimental model are presented in the third section. Results computed from measured coupling coefficient data are compared to those generated with the analytical model and shown to be in good agreement. The

design of the demonstration antenna is presented in the fourth section along with measured subarray and far field antenna pattern data. The fifth section deals with the synthesis of low sidelobe antenna patterns and adaptive nulling capability. The experimental generation of peak sidelobe levels better than -40 dB are demonstrated using an empirical procedure based on the Low Sidelobe Transverse Feed Technique[10]. Finally, the adaptive generation of pattern nulls 63 dB below the beam peak is discussed. The paper concludes with a summary of the major features of the OCN Overlapped Subarray Antenna design technique confirmed by measured results.

THEORY OF DESIGN

The optically-coupled network (OCN) provides an effective means of covering a limited field-of-view with a high gain array aperture excited by a smaller, more efficient wide angle scan array. This results in an antenna configuration which employs a near minimum number of active controls to achieve the desired coverage. A schematic representation of the OCN was presented in Figure 1. The heart of the network is an optically (or space) coupled parallel plate "pillbox" region coupling two opposed arrays of elements spaced about a wavelength apart to effect efficient energy transfer between the two arrays. There are M input and N output ports, respectively, for the input and output OCN arrays, where N is greater than M. The input array elements are spaced about a half wavelength apart and

the array is scanned generally ± 60 degrees. The output array is a densely packed array of elements where the phase differential between elements due to the input array excitations, is reduced by M/N, for equally sized arrays. These output array elements are interconnected on a one-to-one basis with the array aperture elements which are spaced q times further apart. This results in a 1/q reduction in the phase gradient across the array aperture relative to that of the input array. Conversely, the aperture gain is increased by a factor q. Hence, a reduction in the field-of-view is achieved with a commensurate increase in the antenna gain compared to that of the input array.

A linear array designed for wide scan coverage (± 60 degrees or greater) has a very high scan efficiency compared to one designed for limited scan coverage. The OCN provides a means for utilizing a highly efficient feed array designed for wide angle scan coverage to obtain coverage over a limited scan volume or field-of-view with a near minimum number of active controls. Typically, scan efficiencies in excess of 86% are obtainable compared to 20 - 40% normally realized for limited scan arrays with phase controls behind each array element.

Each input array element port of the OCN is a subarray port predominantly exciting a sector of the array aperture. The resultant subarray excitations are fully overlapped and the performance of the OCN fed antenna is analogous to a transform feed antenna. The field-of-view of the antenna is basically the "window" corresponding to the subarray pattern. A typical subarray pattern is depicted in

Figure 2. Resultant antenna patterns exhibit sharp drop-offs in the field level outside this window as exemplified by the pattern of Figure 3, lending to a design well suited for low sidelobe applications. Also, as with a transform feed, the subarray pattern "window" can be scanned about space by placing phase shifters behind the array aperture elements. Multiple beam generation within this "window" is realized by placing a bemaforming network behind the array input. Thus, the network can be used to efficiently generate a cluster of beams and to scan the beam cluster about a specified scan coverage. Controls can be implemented in either subarray or beam image space by cascading beamforming networks for wide signal bandwidth, pattern synthesis and adaptive nulling capabilities.

Mathematically, very simple formulas describe the relationship between the OCN arrays and the aperture array. A schematic representation of the overlapped subarray antenna concept is shown in Figure 4. Scanning the input array to an angle θ_1 results in a phase differential, $\Delta\phi_2$, between elements of the output array given by

$$\phi_2 = \frac{2\pi}{\lambda} d_2 \sin \theta_1$$

where d_2 = output array interelement spacing. The output ports are connected by equal line lengths to the antenna array elements. The incremental phase shift, $\Delta\phi_2$, imparted to the antenna array elements

causes an antenna beam to form at an angle θa, such that

$$\sin \theta a = \frac{d_2}{d_a} \sin \theta,$$

where d_a = antenna array element spacing.

The value of θa which corresponds to the extreme value of θ, = 90^o defines the field-of-view "window" of the overlapped subarray antenna. This can be expressed as

$$\Delta\theta \text{ window} = 2 \sin^{-1} (d_2/d_a).$$

Thus, for a limited scan design the number of phase controls is reduced by M/N and the field-of-view is set by d_2/d_a.

PERFORMANCE PARAMETERS

The key performance features of the transform feed concept are the ability to generate very low sidelobe excitations, realization of wide signal bandwidths, minimization of the number of active controls for a specified scan coverage and the capability for adaptive pattern synthesis. These features are preserved in the overlapped subarray antenna design by the optically coupled network feed and, in fact, are enhanced by the simplification of the implementation of these features.

The ability to realize low sidelobes was demonstrated by the pattern in figure 3. However, under real conditions it is impractical to build a system to the tolerances required for very low

sidelobes. It becomes practical to devise and incorporate techniques to compensate for tolerance error effects. The transform feed technique, because of its Fourier transform properties, is an apporach for correcting tolerance errors in focal function antennas such as lenses and reflectors.

The OCN space coupled region is analogous in operation to a lens with a similar magnification factor corresponding to the concentration of the array energy within the resultant field-of-view. Therfore, the error effects associated with the feed networks will be manifested only over the spatial region corresponding to the field-of-view and not over all space. The antenna array errors on the other hand will be manifested in the near-in and far-out sidelobe region. Control of the input array excitations will provide compensation for the feed network tolerances and result in low near-in sidelobes. Methods such as the low sidelobe transverse feed technique[10] provide the required error compensation to realize very low sidelobe performance. Results demonstrated better than -40 dB peak sidelobes via simple empirical adjustments.

Because the input array is an image of the antenna aperture and each of its input ports corresponds to a subarray, very wide signal bandwidth performance is readily implemented by placing time delay units behind each of these network ports. Real-time collimation of the wavefront is thereby effected on a subarray basis. To a first order, the controlling factor for the antenna's

signal bandwidth then becomes the bandwith of the subarray which, in general, is very wide. Implementation of these time-delay units in an OCN fed subarray antenna is illustrated in Figure 5.

Patterns computed over a 10% signal bandwidth are illustrated in Figure 6 for a scan angle of 60 degrees. Phase shifters located behind the array elements are used to scan the beam. Time delay units located behind the input array provide the time collimation. Low sidelobe pattern characteristics are maintained over the frequency range, demonstrating the excellent signal bandwidth characteristics of the design.

Another key feature of the overlapped subarray antenna is the ability to incorporate phase and amplitude controls at various network levels to effect control of the antenna pattern characteristics. A typical embodiment illustrating this capability is shown in Figure 7. A series of cascaded beamforming matrix networks are shown to illustrate the various levels at which controls can be incorporated. Typically, controls normally implemented at the subarray level would be placed at either A' or A" while controls implemented in an image of beam space would be placed at B'.

For example, if low-loss, low sidelobe performance is desired, a corporate type distribution network could be used to excite the secondary array with time delay units and phase error compensators located between the distribution network and the input array elements. On the other hand, if multiple beam or phase and amplitude control for pattern synthesis is desired, a multiple beam forming

matrix network would be utilized to excite the input array which, in turn, would be fed through a beam combiner or switching network with active phase and amplitude controls for the beam excitations.

Finally, the overlapped subarray antenna provides an efficient means for implementing pattern controls for adaptive pattern synthesis and null generation. The primary means of countering severe ECM and jammer threats is to design for very low sidelobes and provide it with the ability to adaptively control its pattern characteristics so as to place nulls in jammer directions. In addition to its low sidelobe capabilities, the OCN feed has the capability to provide for cancellation of jammer noise sources.

For jammer sources located within the field-of-view corresponding to the subarray excitations, directional data is obtained by monitoring corresponding beam ports (region B' of Figure 7) of the beam former network exciting the input array. Each of these beam ports corresponds to an orthogonal beam position within this field-of-view. A set of beam weights can be adaptively computed from the signals monitored at the beam ports using orthogonal projection or sample covariance matrix techniques[11] which result in the placement of nulls in the jammer directions for the processed antenna response. An example of this null generating capability is illustrated by the pattern in Figure 8. Four jammers located within the field-of-view are adaptively cancelled by forming pattern nulls in their directions via control of the beam weights from a beam forming network feeding an OCN overlapped subarray antenna.

OCN EXPERIMENTAL MODEL

An experimental model of an OCN feed for a low sidelobe overlapped subarray antenna was built and tested to ascertain its performance capabilities. A parallel plate waveguide "pillbox" type network was used to configure the OCN. A sketch illustrating the dimensional outline of the OCN is shown in Figure 9. A photograph of the network is shown in Figure 10. Coaxial waveguide launcher type probes form the input and output array elements. This facilitates interface with coaxial feed lines. The network was designed with 22 inputs spaced 0.969" apart and 70 outputs spaced 0.323" apart, effecting a 3:1 reduction in the number of controls. The output array was oversized to evaluate edge effects. The network was designed for C-band operation (5.2 to 6.0 GHz).

Numerically controlled machining was used to fabricate the OCN experimental model enabling tight control of tolerances. The objective was an rms phase error of less than 2 degrees through the network. To determine the model's performance parameters, the complex coupling coefficients between the input and output array ports were measured and used to compute far field patterns, assuming the OCN feeds an ideal linear array of dipoles spaced 1.04" apart. This corresponds to a field-of-view "window" of ±18.1 degrees. A 40 dB Taylor illumination function ($\bar{n} = 6$) was used to excite 16 input array elements, and 52 output array elements were used to excite the dipole array. The other OCN ports were terminated.

Resultant far field patterns were computed and compared to an ideal pattern to determine the error levels corresponding to the changes exhibited in sidelobe levels.

The ideal pattern associated with an errorless OCN excited with a 40 dB Taylor function is shown in Figure 11. The same pattern computed using the coupling coefficients measured at band center (5.6 GHz) is shown in Figure 12. The near-in sidelobes increased an average of 5.9 dB and the average far out sidelobes came up to 53.6 dB. This corresponds to a 0.9° rms error associated with the output array elements and a 1.5° rms error associated with the input array elements. The corresponding net effective rms error in the near-in sidelobe (field-of-view) region was computed to be 1.8 degrees. These errors include measurement errors which were estimated to be in the order of 0.5 degrees rms. Thus, the OCN exhibited sidelobe performance and error effects in good agreement with the design objective of a 2.0 degree maximum rms error level.

To demonstrate the error correcting capabilities afforded by the OCN feed, the phase at several of the input array ports was adjusted via computer simulation. The resultant pattern computed using the measured coupling coefficients is shown in Figure 13. Excellent performance is obtained with average peak sidelobe levels improved by 3.4 dB within the field-of-view. This result corresponds to an rms phase error of 0.7 degrees for the input array, a significant reduction over that obtained prior to making the phase corrections. Also note that the far-out sidelobe levels remain

unchanged. This demonstrates that the phase errors associated with the input array and feed network are manifested within the field-of-view.

Subarray patterns corresponding to excitation of the individual input array elements were also generated. Subarray patterns for center and edge input elements computed using measured coupling coefficient data are exhibited in Figure 14 along with the respective ideal patterns. Note the good agreement demonstrating the overlapped subarry characteristics.

DEMONSTRATION ANTENNA MODEL

A demonstration overlapped subarray antenna using the OCN experimental model as its feed, was built and tested. A block diagram illustrating the demonstration antenna configuration is presented in Figure 15. A photograph of the completed antenna mounted at an automatic antenna test facility is shown in Figure 16. The antenna utilizes a Butler matrix beamforming network to excite a linear array of dipole elements through the OCN to provide the capability for generating error compensated low sidelobe patterns and adaptive pattern nulls.

The radiating aperture is formed by a corner reflector fed by a linear array of 32 printed stripline dipole elements supported by a foam dielectric structure. The corner reflector narrows the

elevation beamwidth to 40 degrees and results in a good impedance match with the dipole feed. Semi-rigid coaxial cables interconnect the array with the OCN. In-line coaxial phase trimmers allow for phase adjustment to minimize array phase errors. The 16 x 16 Butler matrix is fed by a stripline corporate distribution network with in-line phase and amplitude controls. Phase matched coaxial cables are used to interconnect the Butler matrix with the OCN input array.

The Butler matrix network was built to the following specifications:

Frequency	5.2 to 6.0 GHz
Insertion Loss	< 3.0 dB
Amplitude Variation Per Beam	0.9 dB rms (Max)
Over Freqeuncy Band	0.35 dB rms (Avg)
Phase Gradient Error	0.79° (Max)
	0.26° rms
Phase Error Per Beam	9.6° (Max) rms
Over Freqeuncy Band	5.0° (Avg) rms
VSWR	< 2.0:1

An initial set of pattern measurements were made exciting the OCN with a -45 dB Taylor function ($\bar{n}$=6). The power divider feed network was directly connected to 16 of the OCN input array elements through the variable phase shifters and attenuators. The Taylor illumination function was generated using the phase shifters and

attenuators to adjust the power divider outputs to the desired values. Prior to installation into the antenna assembly, the phase and amplitude outputs of the OCN due to the input -45 dB Taylor illumination were measured and far field patterns computed assuming an ideal array. The resultant pattern is shown in Figure 17. The pattern exhibits a peak sidelobe level of -35.4 dB with far out sidelobes in the order of -53 dB. This result corresponds to an array rms error of 0.9 degrees and a 1.9 degree rms phase error across the input array. The OCN feed was then connected to the dipole array and far field antenna patterns were recorded over the frequency band from 5.2 to 6.0 GHz.

The recorded pattern at center frequency (5.6 GHz) is presented in Figure 18. The pattern exhibits a peak sidelobe of 32.4 dB within the field-of-view window and average far out sidelobes of -46 dB. These levels correspond to an array error of 2.1 degrees (rms) and a 2.1 degree (rms) phase error for the OCN input array. This increase in sidelobe levels is attributed primarily to the additional array errors associated with the dipole elements and feed cables. Thus, the recorded patterns exhibited sidelobe levels consistent with the parameters of the OCN and dipole array.

Subarray patterns were then recorded for each of the OCN input array ports. Measured subarray patterns at 5.6 GHz for center and edge input elements are presented in Figure 19. These patterns are in good agreement with expected results exhibited

in Figure 14, verifying the overlapped subarray properties of the antenna.

Finally the Butler matrix feed network was connected to the OCN input array and the associated beam patterns recorded. Measured patterns for beams 2,5 and 8 (center beam) are shown in Figure 20. These patterns exhibit performance consistent with the Butler matrix tolerance errors and demonstrate the ability to scan a beam or have multiple simultaneous beams within the Overlapped Subarray Antenna field-of-view. Evaluation of the array patterns for each of the Butler matrix generated beams yielded a ±0.4 degree variation in pointing direction, which agrees with the Butler matrix performance specifications.

ADAPTIVE PATTERN SYNTHESIS

A major feature of an overlapped subarray antenna is the capability to empirically compensate for antenna tolerance errors and to adaptively place nulls in desired spatial directions. Experiments were conducted with the OCN fed Overlapped Subarray Antenna to demonstrate these capabilities. Control of an orthogonal set of beams was effected through the Butler matrix network via the input phase shifters and attenuators. The Low Sidelobe Transverse Feed Technique[10] was used to empirically set the beam-weights to compensate for antenna tolerance errors and realize very low peak sidelobe levels. A general class of low sidelobe

excitations formed by the superposition of weighted orthogonal beams was used to specify the ideal beam weights. Three adjacent beams were employed with relative ideal weights of 0.42:1:0.42 which corresponds to an ideal peak sidelobe level of -40 dB.

Initially the ideal three beam weights were empirically set and the resultant far field pattern recorded. This pattern is presented in Figure 21. Beams orthogonal to the three excited beams should theoretically have a zero response in their beam pointing direction. By forcing this condition empirically, the error effects contributing to sidelobes in those directions are compensated resulting in an antenna pattern which approaches the ideal pattern. This procedure was implemented with the demonstration antenna and the resultant pattern is shown in Figure 22. The pointing direction of adjusted beams are indicated by the vertical arrows. Note that within the field-of-view corresponding to the adjusted beams, peak sidelobe levels of less than -40 dB were realized.

In a similar manner, adaptive nulling capability was demonstrated. Two jammers located on adjacent sides of the main beam were simulated by a far field source and the beam weights for two beams encompassing the jammers were adjusted to form pattern nulls in the jammer directions. The resultant pattern is presented in Figure 23. Null depths of approximately 63 dB were generated, realizing an additional 25 dB of cancellation from the unadapted pattern.

Both the low sidelobe and adaptive nulling patterns were generated at the design center frequency of 5.6 GHz. Patterns were recorded at other frequencies to evaluate the bandwidth characteristics of the adapted patterns. Results showed significant deterioration in performance within ±10 MHz of center frequency. This was attributed to the rapidly varying characteristics with frequency of the Butler matrix and the phase and amplitude controls used to set the beam weights. This demonstrates the need for stable wideband performance from the beamforming and control components in order to maintain the very low sidelobe and adaptive pattern nulls over wide bandwidths.

CONCLUSIONS

A novel Fully Overlapped Subarray Antenna using an optically coupled feed network has been described. The optically coupled network affords the benefits of such antennas with reduced size and complexity as compared to alternate implementation schemes.

The antenna has been demonstrated by an experimental model at C-band. The data has shown an operating bandwidth of 800 MHz, peak sidelobes of -40 dB and adaptive nulling capability to -63 dB.

ACKNOWLEDGEMENT

The authors gratefully acknowledge many individuals at Sperry Defense Electronics and at Rome Air Development Center who contributed to the theory and experimental validation of the antenna

technique described in this paper. We particulary thank John Bongiorno and Peter Sbuttoni, who participated in the design and measurement of the experimental hardware, and Nick Kernweis at RADC/ET, who served as the project monitor for the Air Force program supporting this research.

BIBLIOGRAPHY

- - - - - - - -

(1) R.J. Mailloux, Subarraying Feeds for Low-Sidelobe Scanned Arrays, International Symposium Digest on Antennas and Propagation, vol. 1, pp. 30-33, June 1979.

(2) R.L. Fante, Systems Study of Overlapped Subarrayed Scanning Antennas, IEEE Trans. on Antennas and Propagation, vol. AP-28, pp. 668-679, Sept. 1980.

(3) R. Tang, Survey of Time-Delay Beam Steering Techniques on Phased Array Antennas, Proc. of the 1970 Phased Array Antenna Symposium, Artech House, Inc., Nedham, MA. pp. 254-260.

(4) A.W. Rudge and D.E.N. Davies, Electronically Controllable Primary Feed for Profile-Error Compensation of Large Parabolic Reflectors, Proc. IEEE, vol. 117(2), pp. 351-358, 1970.

(5) G.V. Borgiotti, An Antenna for Limited Scan in One Plane: Design Criteria and Numerical Simulation, IEEE Trans on Antennas and Propagation, vol. AP-25, pp. 232-243, 1977.

(6) J.J. Stangel and J.J. Punturieri, Random Subarray Techniques in Electronic Scan Antenna Design, 1972 G-AP International

Symposium Digest, pp. 17-20, Dec. 1972.

(7) G. Ploussios, Overlapping Subarray Scanning Antenna Study, Rome Air Development Center Griffis AFB, N.Y., Final Tech. Rep. No. RADC-TR-79-101, May 1979.

(8) Patent Pending

(9) USAF Rome Air Development Center, Contract No. F19628-81-C-0078, Constrained Feed Subarray Antenna Program.

(10) J.J. Stangel, et al, Low Sidelobe Transverse Feed Technique, 1979 IEEE/AP-S International Symposium Digest, pp. 274-277, June 1979.

(11) J. Gobert, Adaptive Beam Weighting, IEEE Trans on Antennas and Propagation, vol. AP-24, pp. 774-779, Sept. 1976.

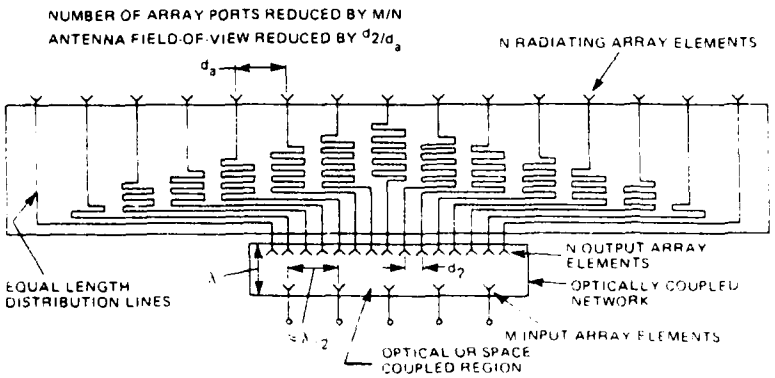

Figure 1. Schematic of Sperry Invented Optically Coupled Network

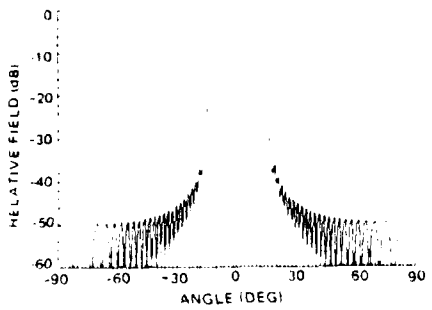

Figure 2. OCN Array Subarray Pattern

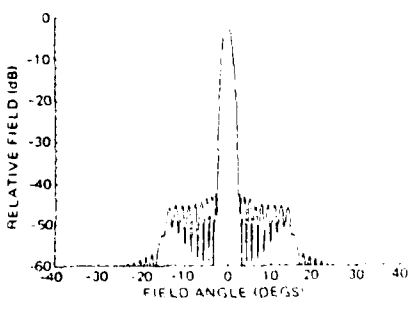

Figure 3. OCN Array Far Field Antenna Pattern

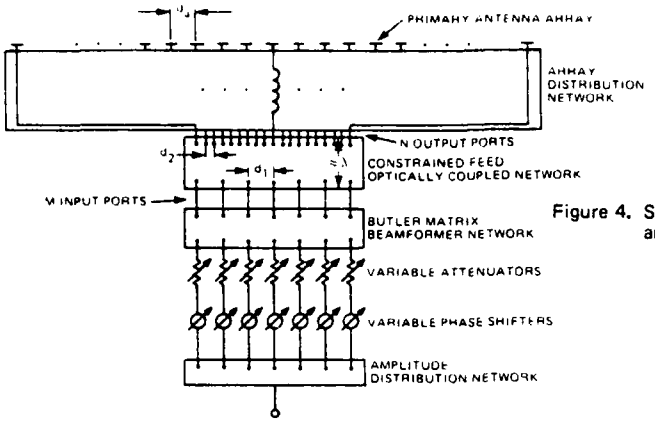

Figure 4. Sperry's Constrained Feed Overlapped Subarray Antenna Concept

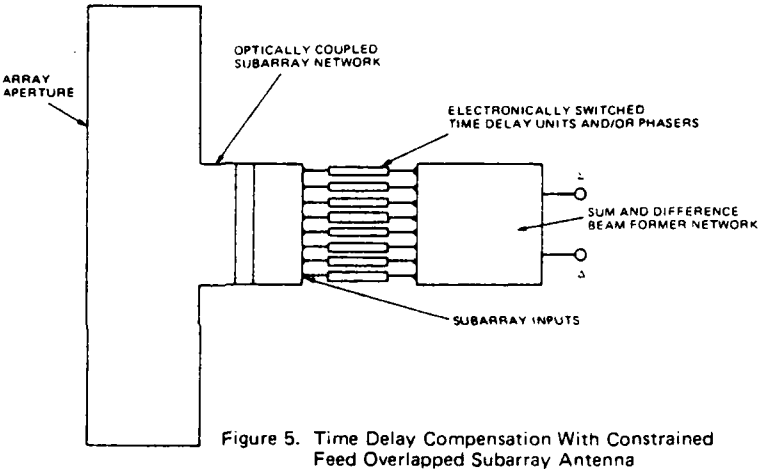

Figure 5. Time Delay Compensation With Constrained Feed Overlapped Subarray Antenna

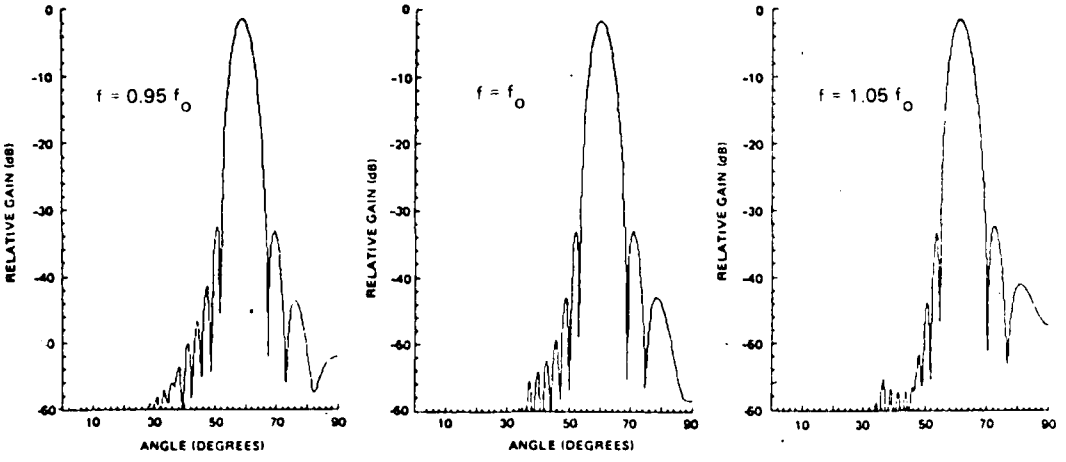

Figure 6. 60° Scan, Time Delay Compensated Antenna Patterns Over 10% Bandwidth

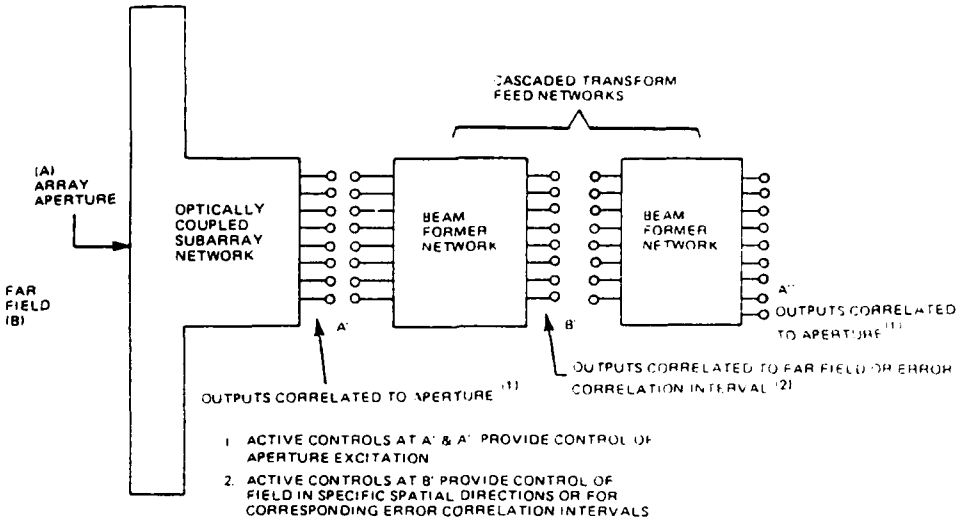

Figure 7. Control of Pattern Function Via Cascaded Beamforming Networks

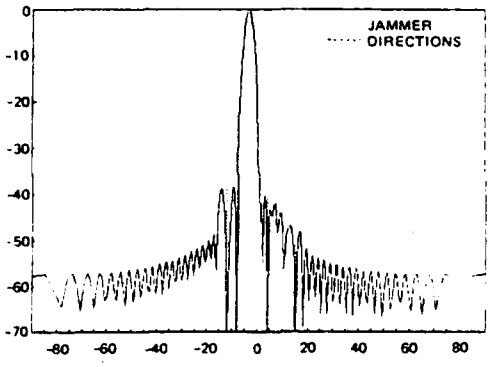

Figure 8. Adaptive Jammer Nulling Via Beam Weight Control of Overlapped Subarray Antenna

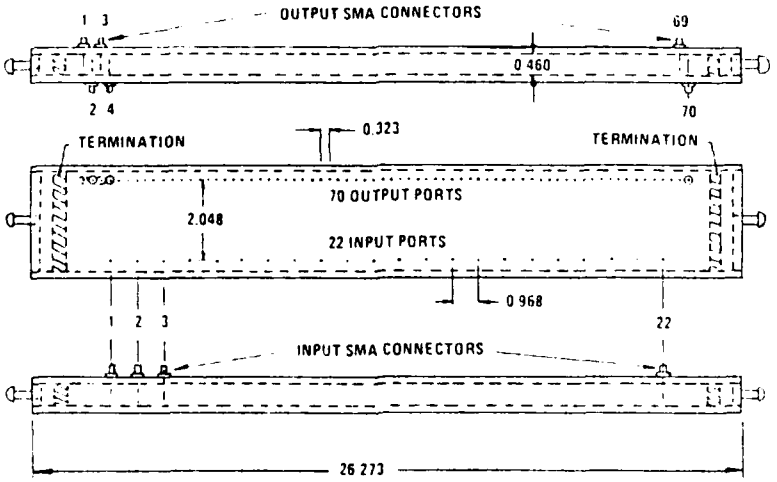

Figure 9. Dimensional Outline of OCN Experimental Model

Figure 10. OCN Experimental Model

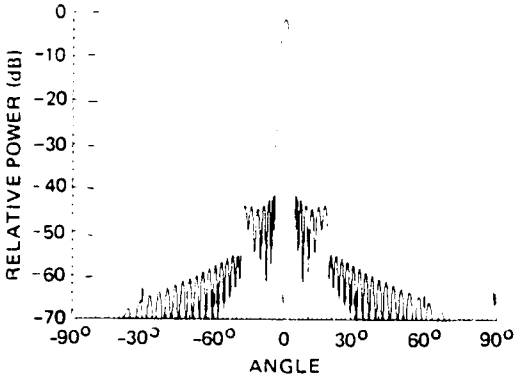

Figure 11. Ideal Far Field Pattern - 40 dB Taylor Excitation

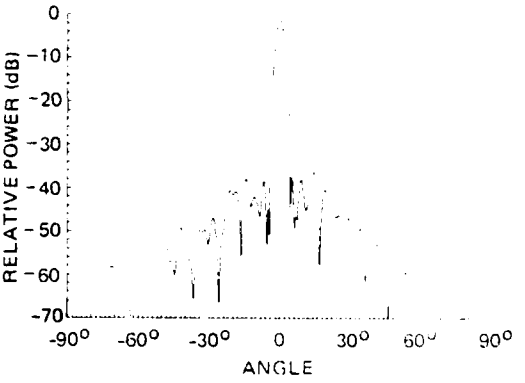

Figure 12. Far Field Pattern Computed From Measured OCN Coupling Coefficients

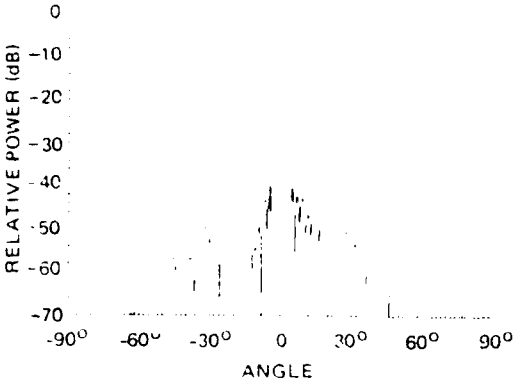

Figure 13. Error Compensated Pattern Computed From Measured Coupling Coefficients

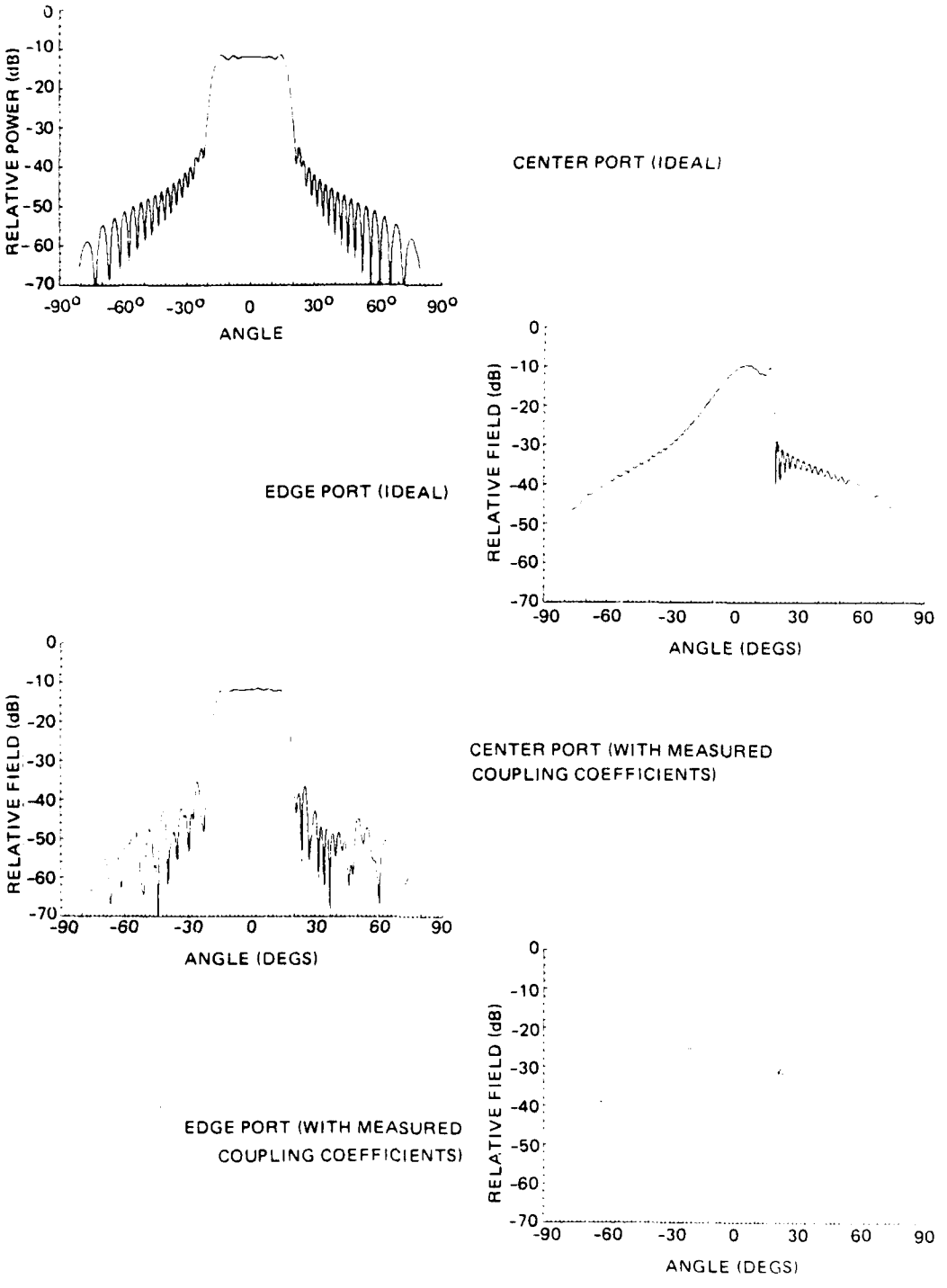

Figure 14. OCN Experiemental Model Subarray Patterns

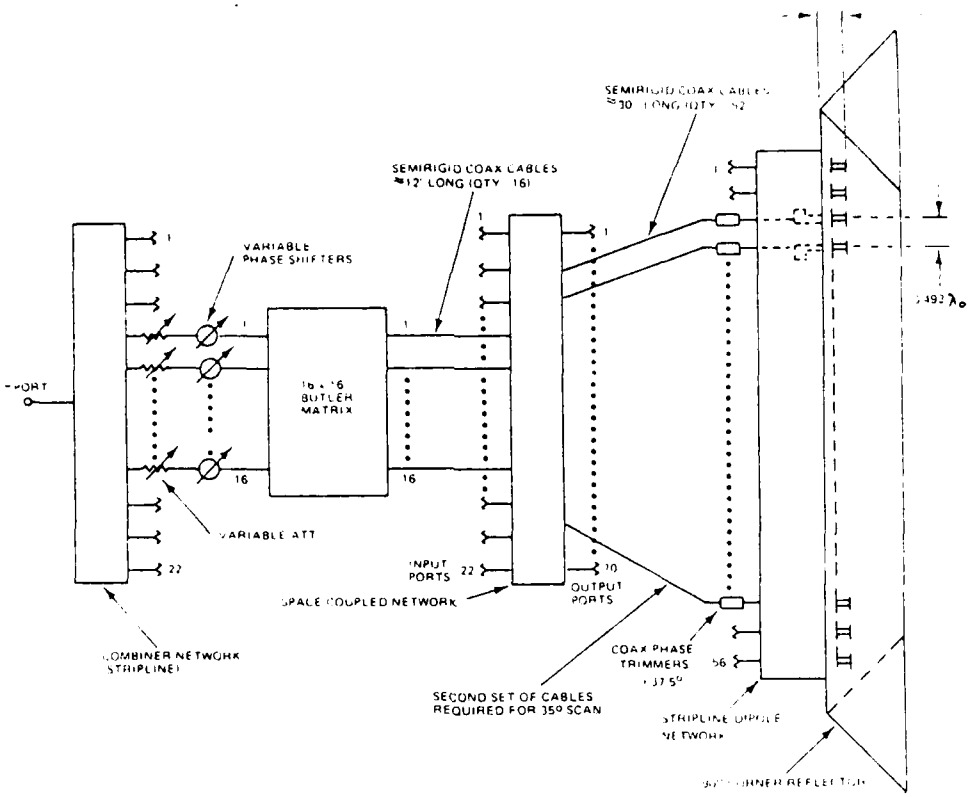

Figure 15. Overlapped Subarray Demonstration Antenna Configuration

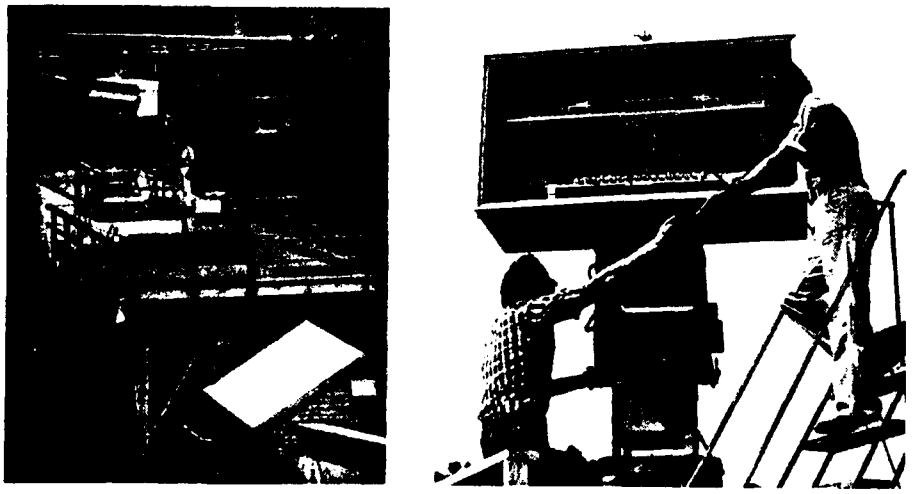

Figure 16. Demonstration Antenna Mounted On Sperry's Automatic Test Site

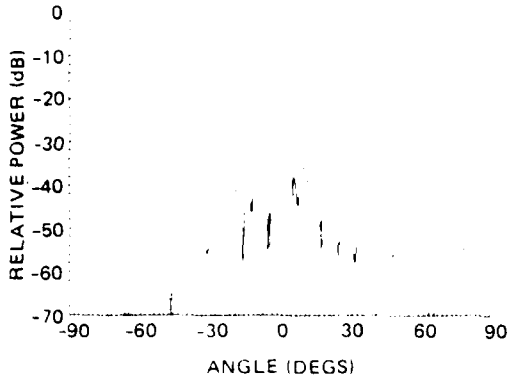

Figure 17. 45 dB Taylor Pattern Computed From Measured OCN Outputs

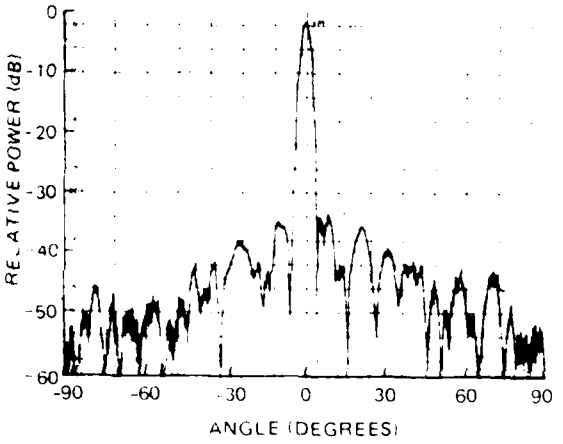

Figure 18. Measured Demonstration Antenna Far Field Pattern

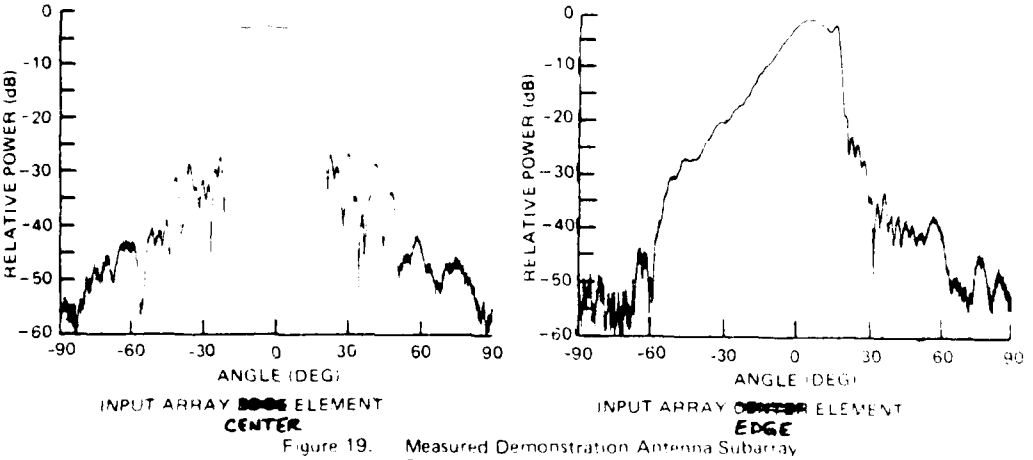

Figure 19. Measured Demonstration Antenna Subarray Patterns

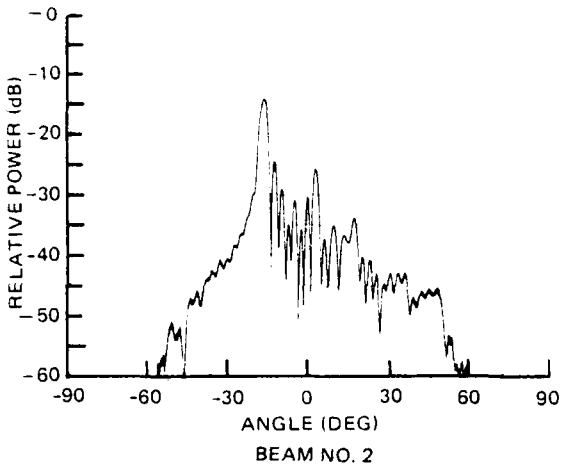

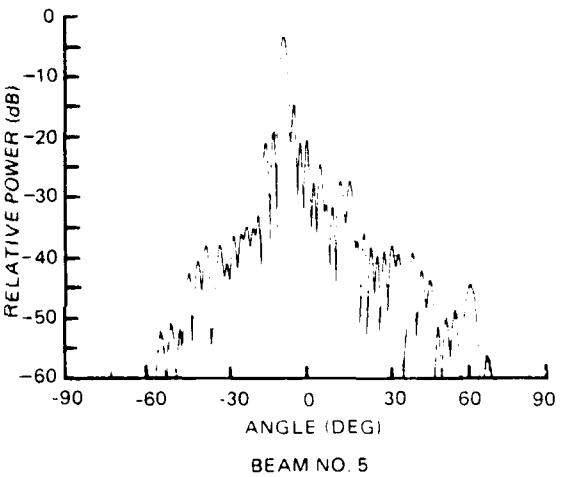

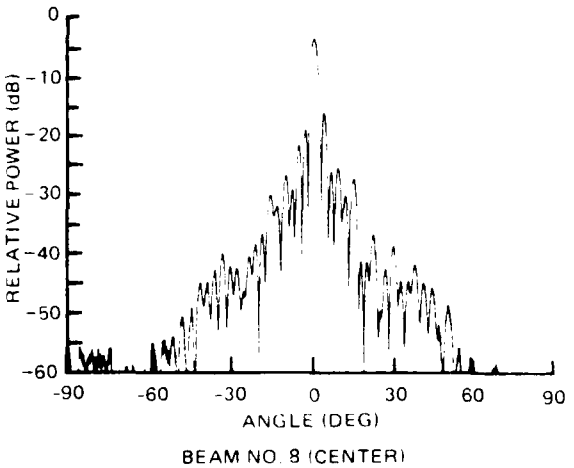

Figure 20. Measured Beam Patterns of Demonstration Antenna With Butler Matrix Feed

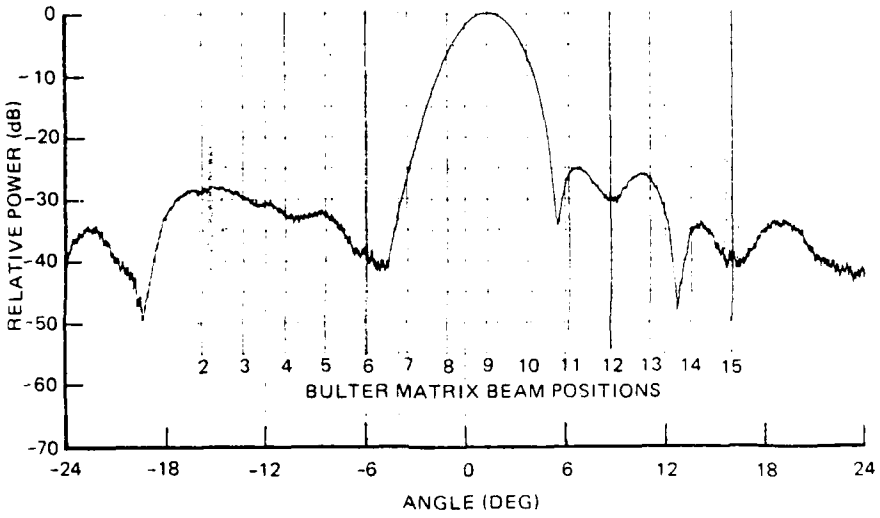

Figure 21. Uncompensated Low Sidelobe Far Field Pattern

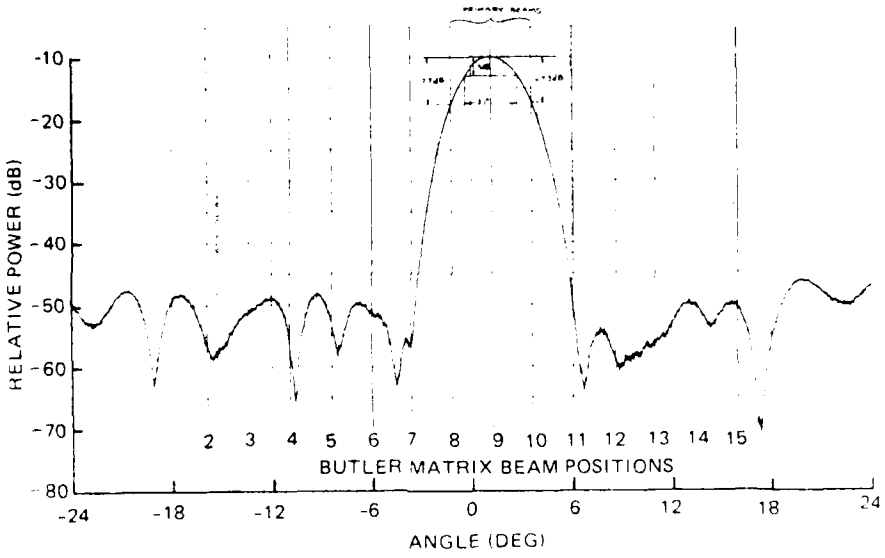

Figure 22. Compensated Low Sidelobe Far Field Pattern

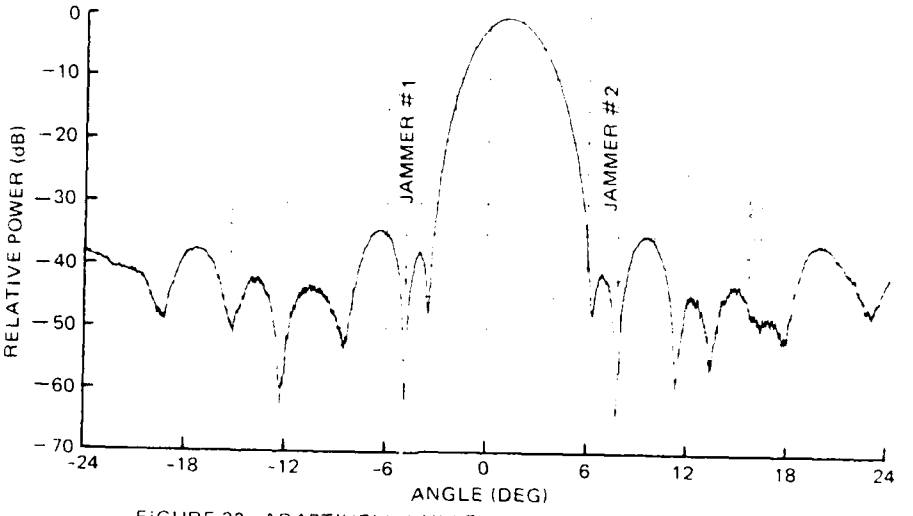

FIGURE 23. ADAPTIVELY NULLED FAR FIELD PATTERN (2 NULLS)

Figure 23. Adaptively Nulled Far Field Pattern (2 Nulls)

GEODESIC CONE ANTENNA

Brian S. Cramer

Lockheed Electronics Company, Inc.
Plainfield, New Jersey

ABSTRACT

The subject of this paper is a novel phased array antenna which is capable of providing 360 degree continuous scanning with low side lobes over a wide band. The antenna consists of a ring of feed elements coupling energy through a coaxial conical waveguide to a circular radiating aperture. Rays from the feed ring are constrained within the conical coaxial waveguide and propagate along geodesic paths in such a way as to be focused in the far field.

A paper presenting a preliminary design of a Geodesic Lens Antenna was presented at this symposium in 1981[1]. Since that time, evaluation has shown performance equivalent to a linear aperture illuminated with a Tchebyshev distribution. Progress achieved in computer aided design and analysis allows tailoring a Geodesic Cone Antenna to the specific needs and constraints of given applications.

[1] J. McFarland, R. Savage; "A Geodesic Lens Antenna for 360 Degree Azimuthal Coverage"; 1981 Antenna Applications Symposium, Sept 1981, Monticello, Illinois

A brief explanation of the function of the Geodesic Cone Waveguide using geometric optics is presented. Design and analysis techniques utilizing geometric optics and modal analysis are described. A half octave demonstration model of a Geodesic Cone Antenna (GCA) has been built and tested and showed good correspondence with predicted performance.

1.0 INTRODUCTION

Many applications require antennas that can point a beam to any direction over 360 degrees of azimuth. These applications often require phased array antennas to achieve fast beam scanning, beam agility, or elimination of mechanical reliability problems.

The subject of the present paper is a novel circular aperture antenna which requires fewer elements, has more precise pattern control, and has lower loss than many alternative approaches.

The key features of the Geodesic Cone Antenna (GCA) are:

- Precise azimuth pattern control via variable amplitude and phase distribution imposed on the circular input array.
- 360 degree beam steering via commutation of the distribution of the input array.
- Low loss focusing via Geodesic Cone Waveguide.
- Vertical beam formation with a number of alternate aperture configurations.

2.0 CONCEPT

The Geodesic Cone Antenna, Figure 1, consists of a Geodesic Cone Waveguide (GCW) with a ring of input elements at the base

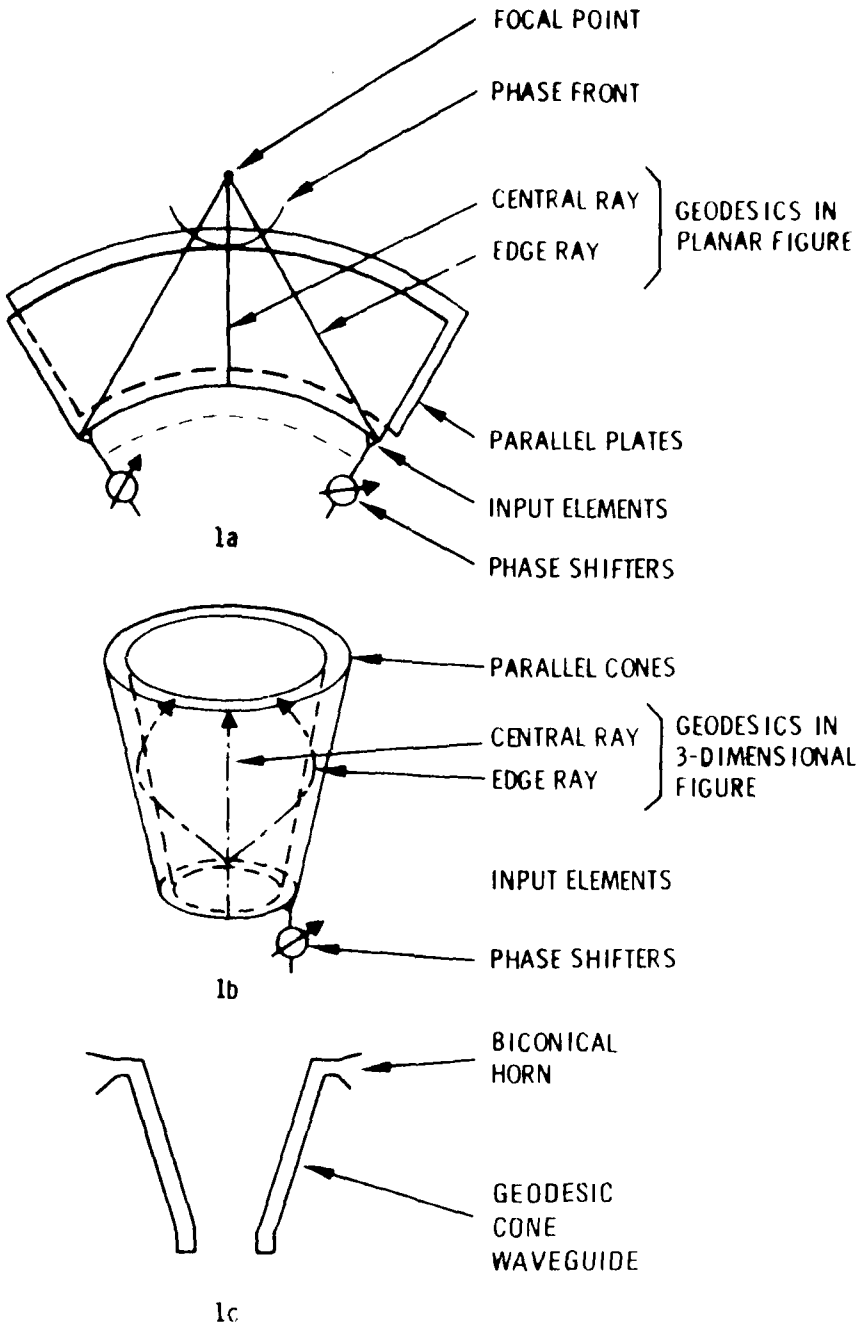

Figure 1. Geodesic Cone Antenna (GCA)

and a radiating aperture at the top. The input elements are fed by a network of phase shifters and power dividers that can provide precise phase and amplitude control to each element.

To form a beam in any direction, energy is applied to all the feed elements simultaneously. The relative amplitude and phase of the signal applied to each element is chosen so that after propagating through the GCW, the energy illuminates a sector (typically 90° to 120°) of the circular radiating aperture. The resulting amplitude and phase distribution provides a low sidelobe pattern focused in the far field.

The operation of the Geodesic Cone Waveguide can be described in terms of a two dimensional model. the conical section (Figure 1b) can be cut along a line from the base of the edge rays to the aperture and unrolled to become a sector of a radial waveguide (Figure 1a). By placing a circular phase distribution on the radiating elements, the energy can be focused to a point in the planar geometry. The ray paths that are linear in the two-dimensional representation follow geodesic paths in the three dimensional Geodesic Cone Waveguide. The ray paths beyond the parallel plate region, that focus to a point in the two-dimensional representation, result in a collimated beam focused in the far field in the fully formed cone (Figure 2).

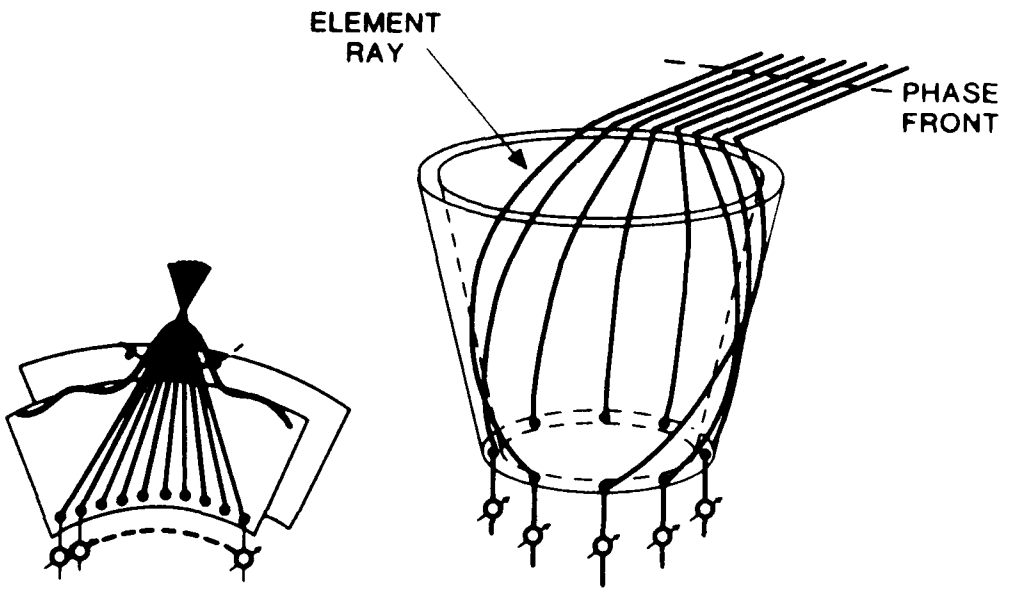

Figure 2. Geodesic Cone Waveguide Concept Development

All of the feed elements are utilized in forming any beam. In order to scan the beam to any azimuth position, the signal distribution to the feed elements is commutated around the base. By modifying the signal distribution at the feed elements of a Geodesic Cone Antenna, many beam shapes can be obtained. Beamwidth is continuously variable from the narrowest beam (design limit) to very broad beams and omni patterns. Also achievable are difference patterns and multiple beam patterns. By dividing the input array into segments with separate feed networks, it is possible to form independently controllable beams.

3.0 DESIGN APPROACH

The design of a Geodesic Cone Antenna involves the following steps:

- Selection of an Equivalent Linear Aperture (ELA) necessary to meet the beamwidth and sidelobe level requirements.
- Selection of the GCA dimensions based on trade-offs of size and degrees of aperture illuminated.
- Synthesis of the optimum input element phase and amplitude values using a modal analysis computer program.
- Synthesis of far field patterns incorporating selected levels of error using a modal analysis computer program.

A GCA has a continuous circular aperture, the performance of which can be exactly related to the performance of an Equivalent Linear Aperture (Figure 3). The length of the Equivalent Linear Aperture is equal to the projection of the illuminated portion of the aperture. In the initial step of the design process the linear aperture required to meet the performance specifications (at broadside) is determined. Figure 4 shows the beamwidth vs. sidelobe trade-off for a linear aperture with a Tchebyshev distribution. For an example application the equivalent linear length is derived from such a figure.

Using design curves generated from a geometric optics analysis, the preliminary dimensions of a GCA are determined. The input diameter of the GCA is related to the ELA by a proportionality factor called the Aperture Utilization Factor (AUF). The AUF is related to the maximum scan angle of the feed elements (α) as follows:

$$AUF = \sin \alpha \tag{1}$$

The required minimum input diameter of the GCA is:

$$D_{IN} = ELA/AUF \tag{2}$$

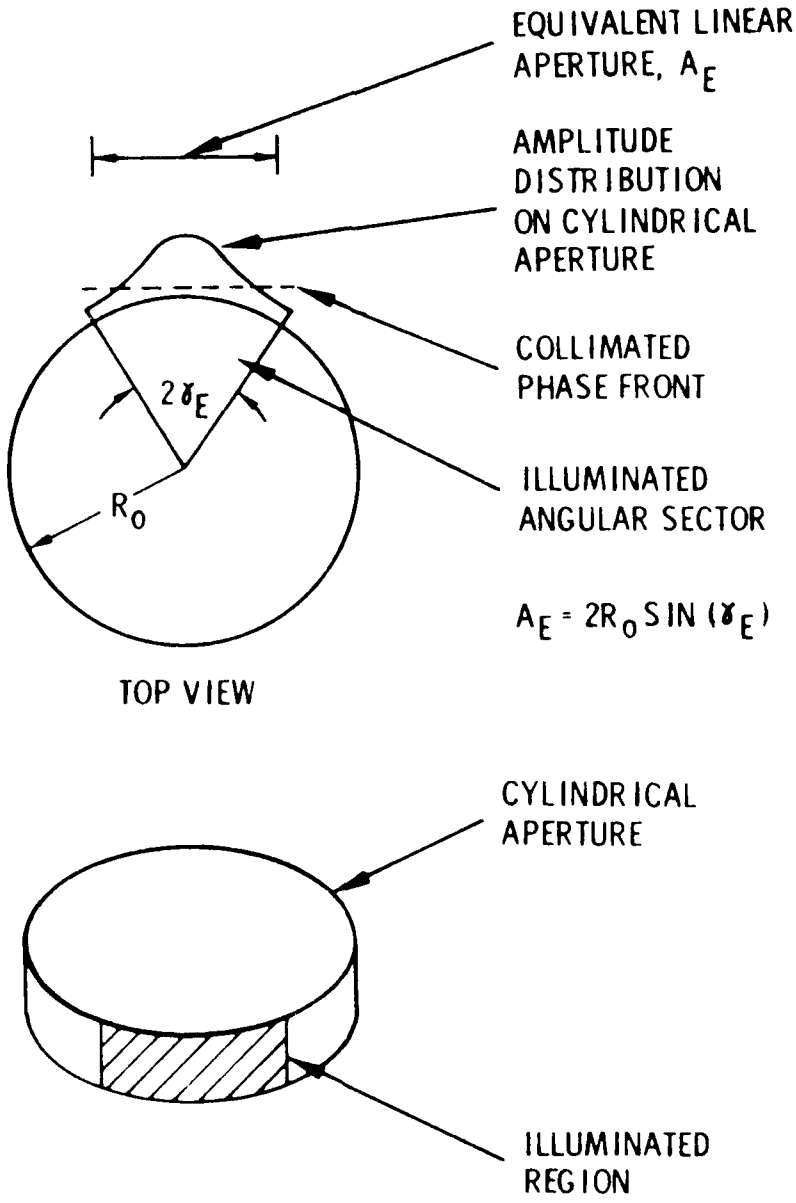

Figure 3. Radiation from a Collimated Illumination of an Angular Sector of a Cylindrical Aperture can be Related to Radiation from an Equivalent Linear Aperture

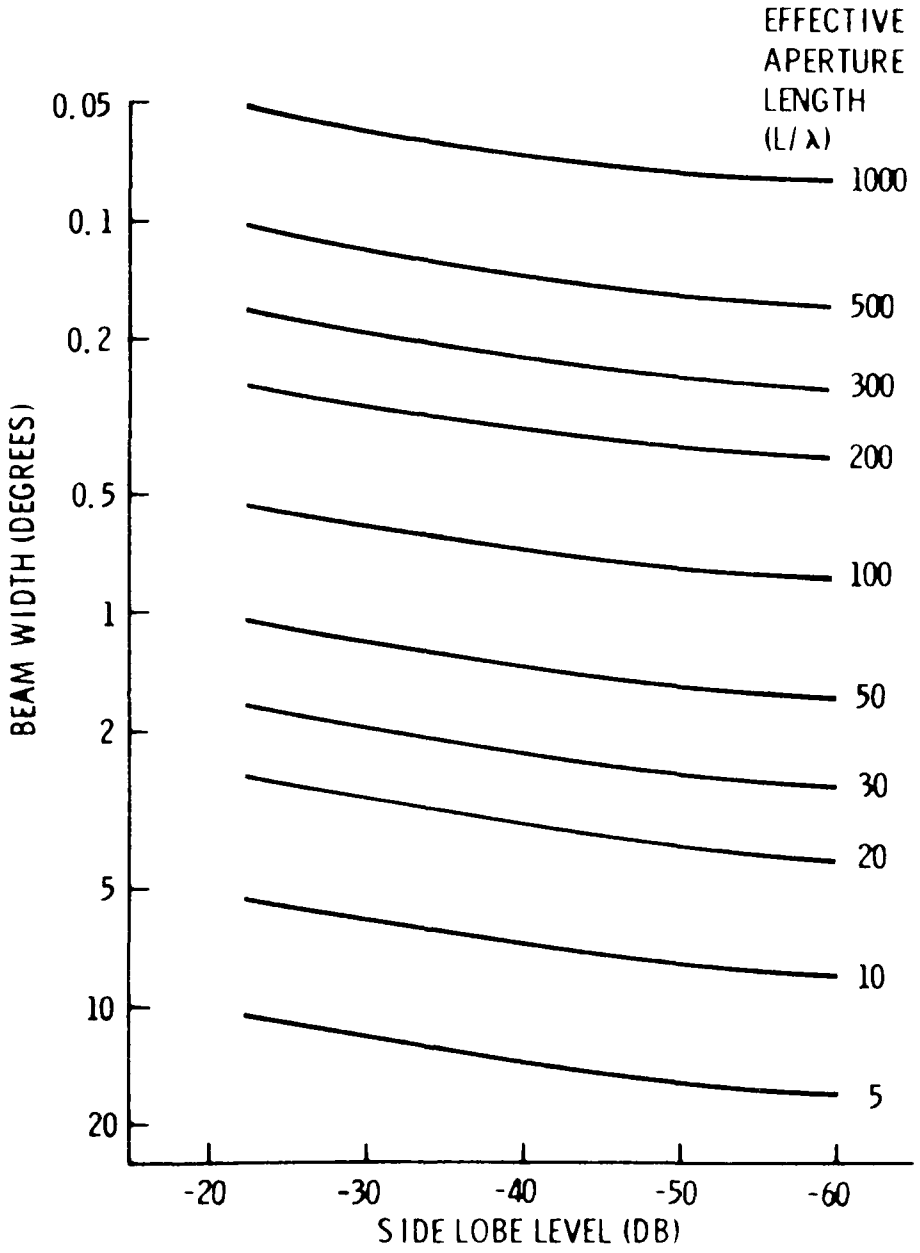

Figure 4. Beamwidth versus Sidelobe Level for a Tchebychev Distribution

Figure 5 is used to determine cone height, output diameter and the illuminated angular sector of the aperture given the input diameter and the maximum element scan angle. For each set of inputs, there is a family of possible solutions defined by the line corresponding to the maximum scan angle. It is at this point that geometric constraints on the size and shape of the Geodesic Cone Antenna are taken into account. Each of the possible solutions will provide the required performance so the most convenient combination of dimensions can be chosen; however, to maintain low-reflection aperture performance, the illuminated sector is normally limited to less than 120°. This limits the angle of existing waves to a maximum of 60 degrees from the normal.

This provides all the basic dimensions of the GCA. Some other considerations are that the spacing between the conical plates must be less than half a wavelength at the highest operating frequency to prevent crossed modes, and that the feed elements should be spaced at or near a half wavelength at the high end of the band. The design of the aperture is not considered in this paper.

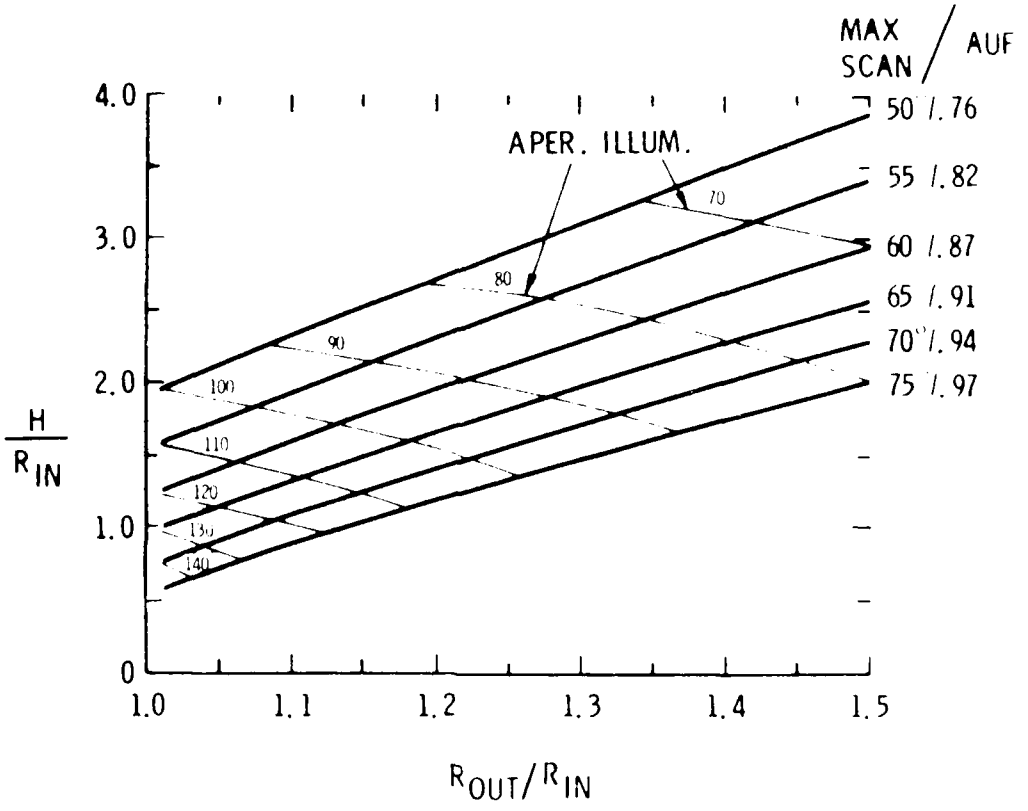

Figure 5. Geometric Optics Relationships in Geodesic Cone Waveguide

Modal Analysis techniques in a computer simulation are used to derive the optimum input feed distribution to form a desired beam shape on a Geodesic Cone Antenna. A computer program has been written that relates the input and output of a GCA in terms of TE_{NO} waveguide modes. This enables synthesis of an input distribution from a desired pattern. The computer program can also derive a far field pattern from an input distribution. A beam pattern based on the optimum input distribution would be an upper bound of performance. The program has the capability to insert selected error levels and quantization parameters at the feed elements prior to the modal derivation of the aperture distribution and the far field patterns.

4.0 EXAMPLE DESIGN PROBLEM

As an illustrative example of the design approach, consider the following requirements:

Maximum operating frequency - 12 GHz

Maximum azimuth beamwidth - 3° (at 12 GHz)

Maximum sidelobe level - 40 dB (at 12 GHz)

The resulting GCA dimensions assuming maximum element scan of

60 degrees and an illuminated aperture of 90 degrees are:

Input radius - 13.2 inches

Output radius - 16.1 inches

Height - 26.4 inches

Number of feed elements - 166

Figure 6 is the calculated far field pattern for this example GCA given RMS amplitude error of 0.5 dB and RMS phase error of 2 degrees. The resulting bandwidth of 3.2 degrees and the peak sidelobe level of -38 dB are consistent with the design goals.

To meet the same performance requirements over 360 degrees using a group of linear arrays would require 35 to 45 percent more active elements then a GCA (Figure 7). The reduced number of active elements in a GCA results in substantial decreases in size and cost.

5.0 DEMONSTRATION MODEL

Figure 8 shows a 64 element Ku-band Geodesic Cone Antenna demonstration model which was designed and evaluated at LEC. The antenna is fed by a network of power dividers with manually adjustable attenuators to provide the amplitude taper and manually adjustable phase shifters to create the required phase distribution. A simple biconical horn was used for the aperture and the Geodesic Cone Waveguide is constructed of aluminum.

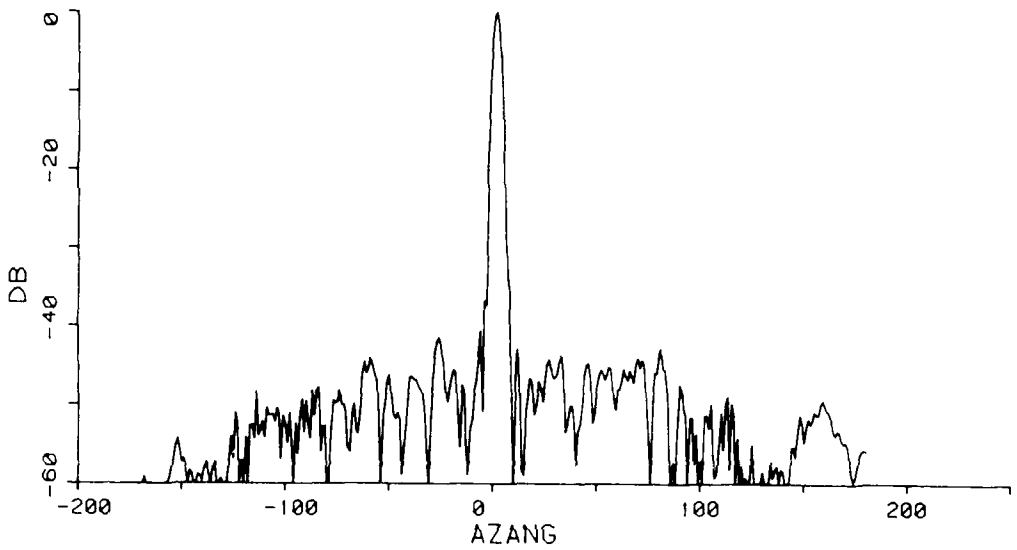

Figure 6. Calculated Farfield Pattern

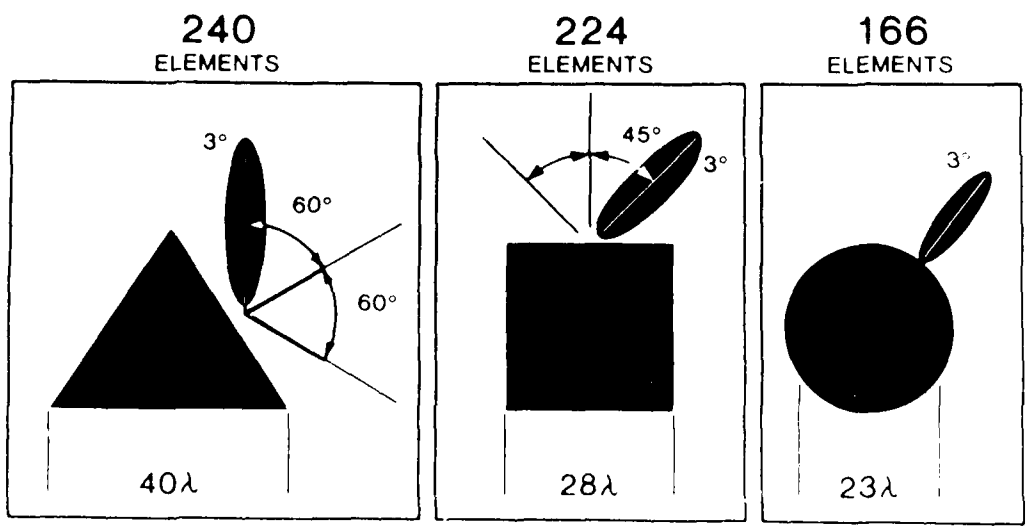

Figure 7. Number of Elements-Comparative Techniques

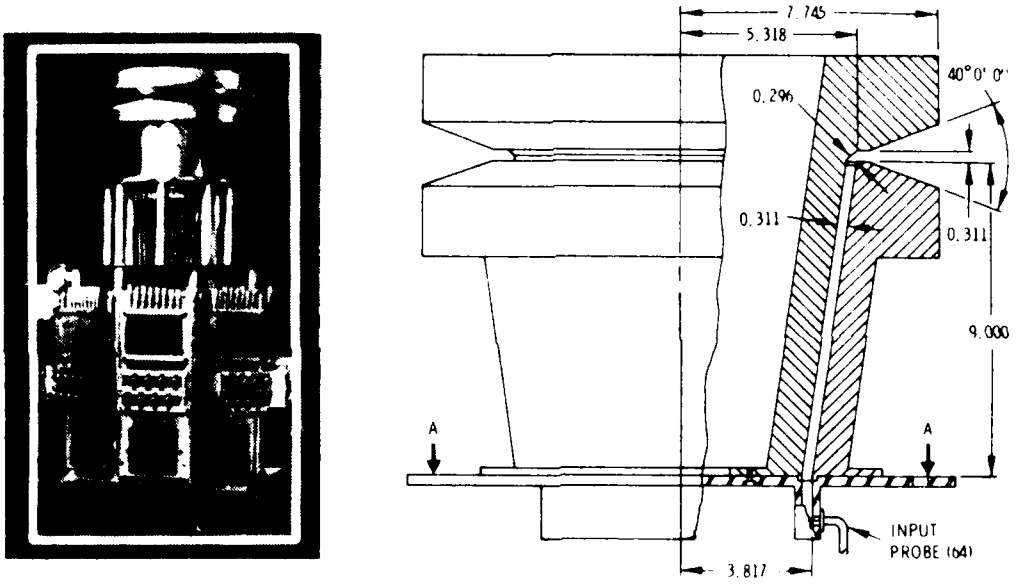

Figure 8. Geodesic Cone Antenna Demonstration Model

The Demonstration Model operates from 12 to 16 GHz. The Geodesic Cone Waveguide and aperture are designed to operate over the full octave from 8 to 16 GHz, but the feed elements currently implemented are only matched over the half octave.

The Demonstration Model was designed to perform as follows (without feed error):

Characteristic	Frequency (GHz)				
	8	12	14	15	16
Beamwidth (degrees)	14	10.4	8.7	7.8	7
Peak Sidelobe Level (dB)	-25	-27.6	-28.8	-29.4	-30

Figures 9, 10 and 11 show the calculated and measured beam patterns at 14, 12, and 15 GHz. The calculated patterns include random errors imposed on the feed element distribution. The magnitude of the error (one dB RMS amplitude error and five degrees RMS phase error) was (1) determined through evaluation of the accuracy, repeatability, and resolution specifications of the mechanical attenuators and phase shifters, and (2) confirmed by laboratory testing of the components. These feed errors increase the sidelobe levels of the patterns. As can be seen from these

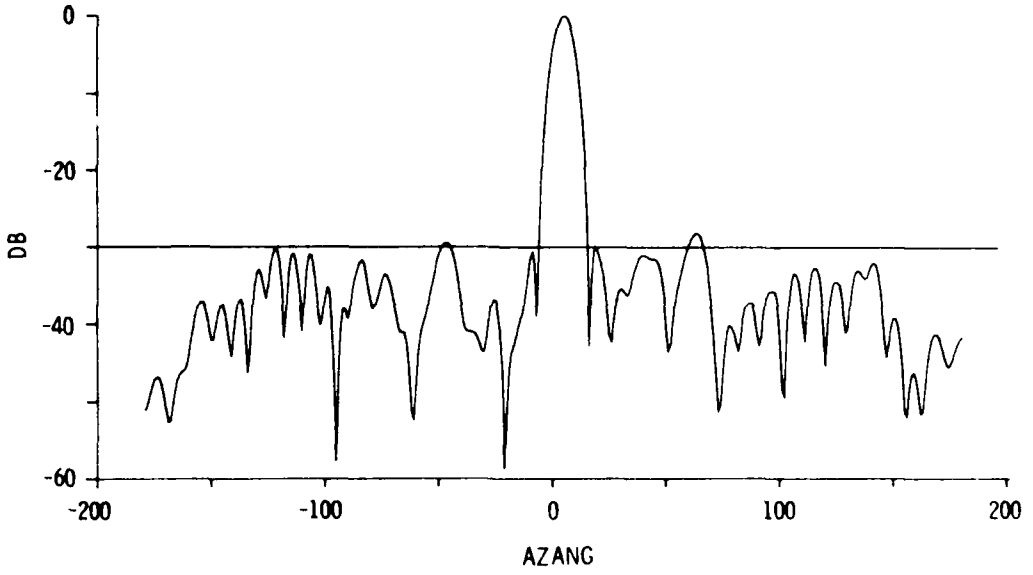

Figure 9a. Calculated 14 GHz Sum Pattern

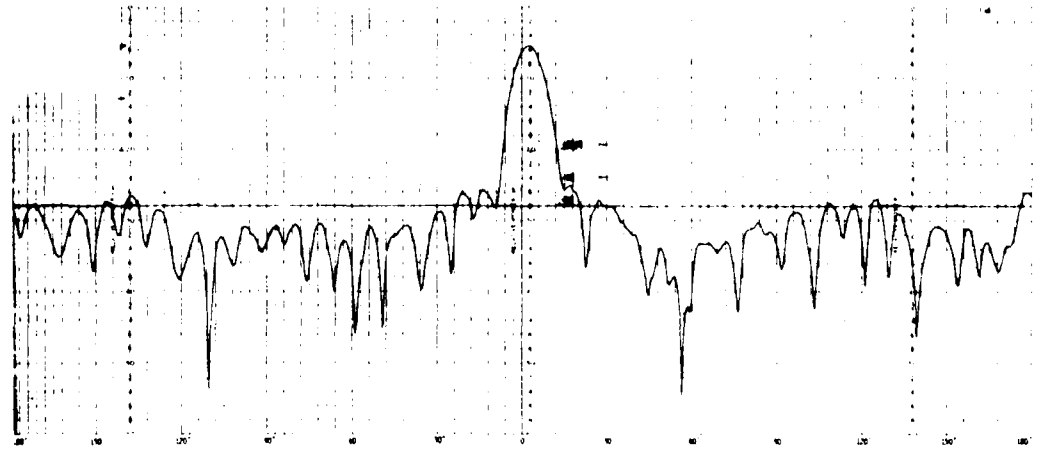

Figure 9b. Measured 14 GHz Sum Pattern

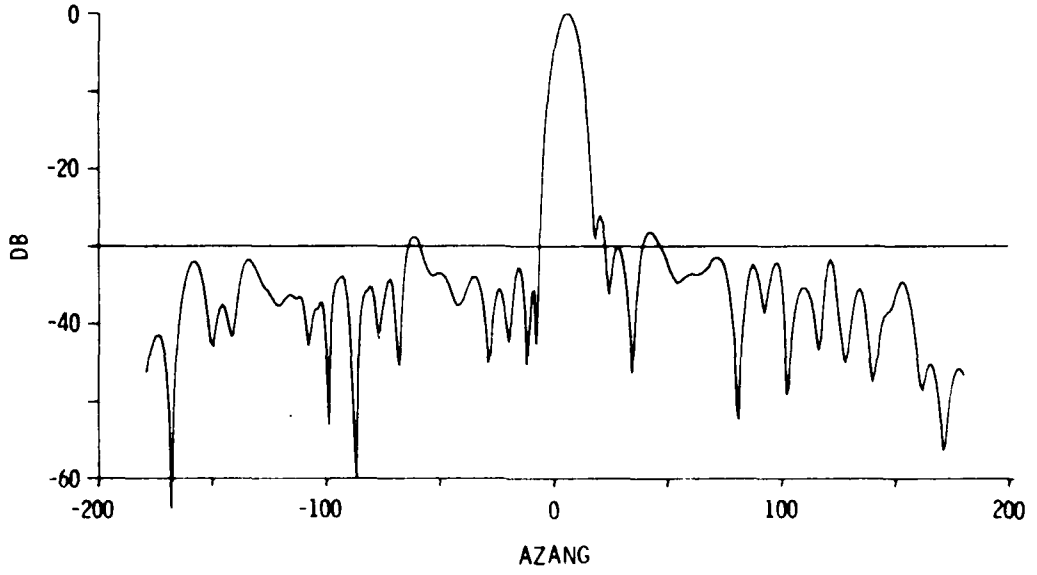

Figure 10a. Calculated 12 GHz Sum Pattern

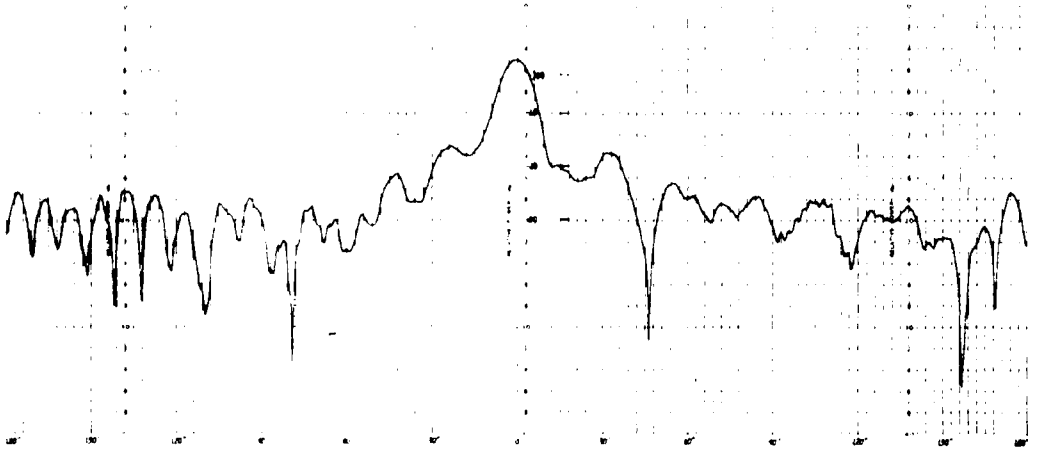

Figure 10b. Measured 12 GHz Sum Pattern

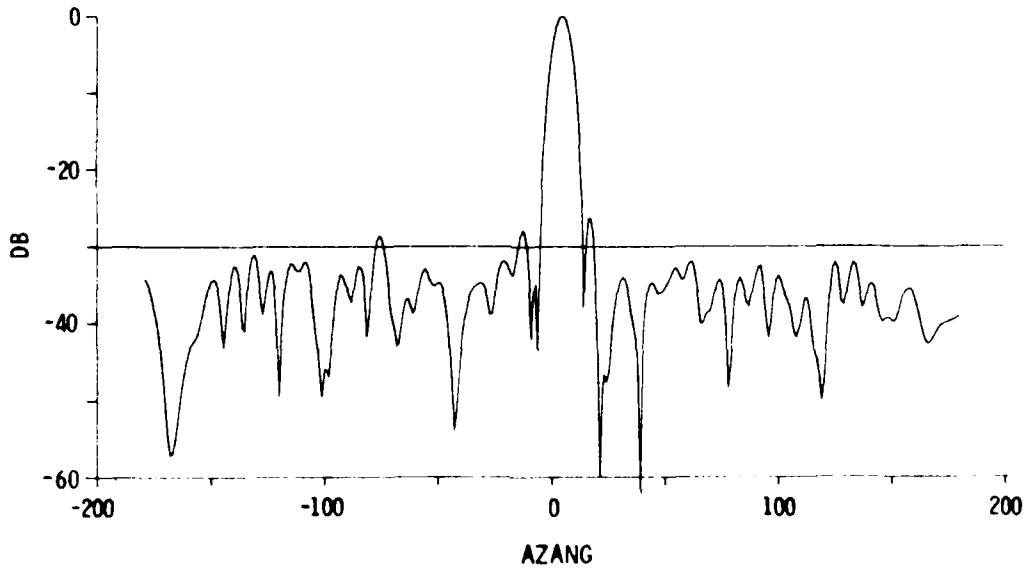

Figure 11a. Calculated 15 GHz Sum Pattern

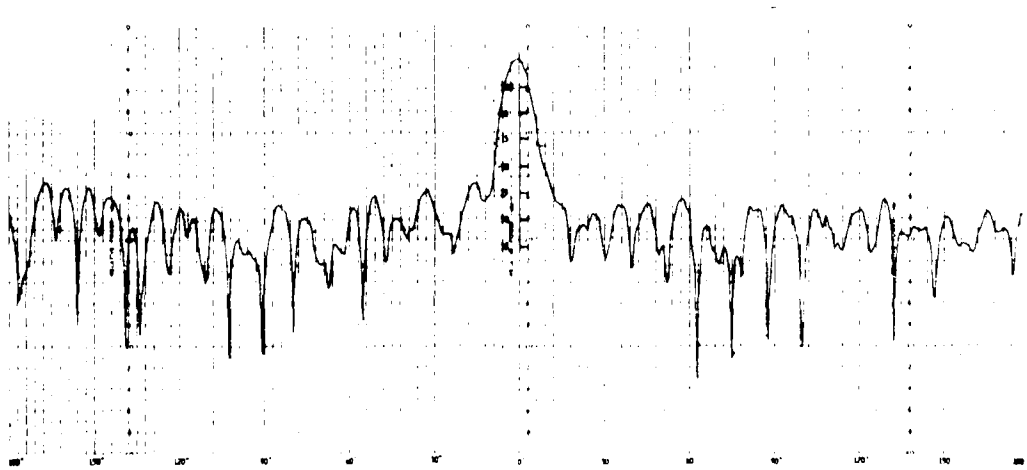

Figure 11b. Measured 15 GHz Sum Pattern

figures, the calculated patterns correlate well with the measured patterns. Figures 12 and 13 show both the calculated and measured omni and difference patterns. These results clearly verify the predicted performance of the 64-element demonstration model.

6.0 CONCLUSIONS

The Geodesic Cone Antenna is an approach which offers size, weight, cost and performance advantages for many 360 degree applications. Analytic methods for design and analysis have been developed and verified empirically. The GCA offers excellent beam control with low sidelobes and multiple independent beam capability. A GCA can be used as an azimuth scanning feed to a vertical beam scanning aperture resulting in a pencil beam scannable in azimuth and elevation. Applications for the GCA range from radar and ECM to communications systems.

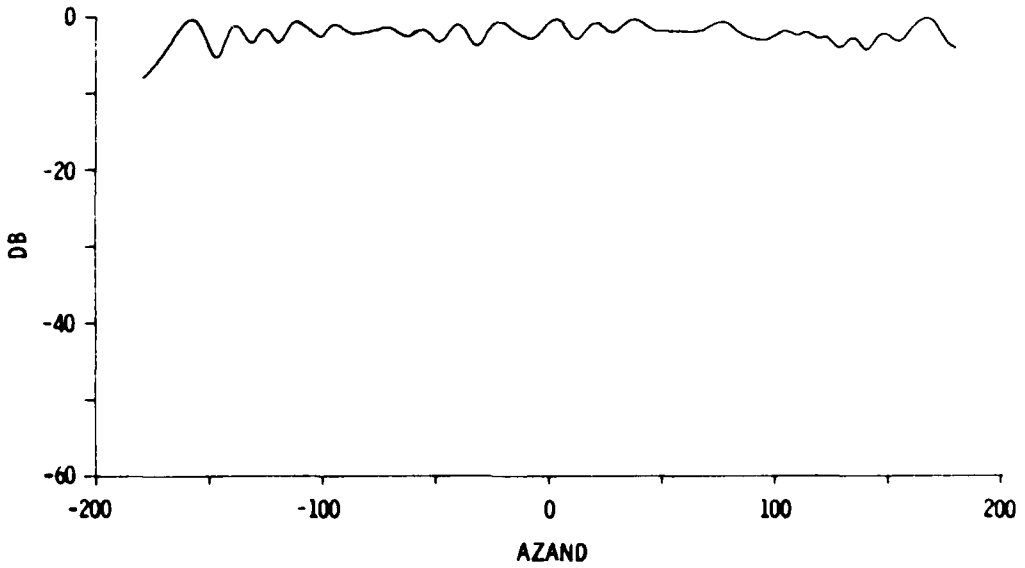

Figure 12a. Calculated 14 GHz Omni Pattern

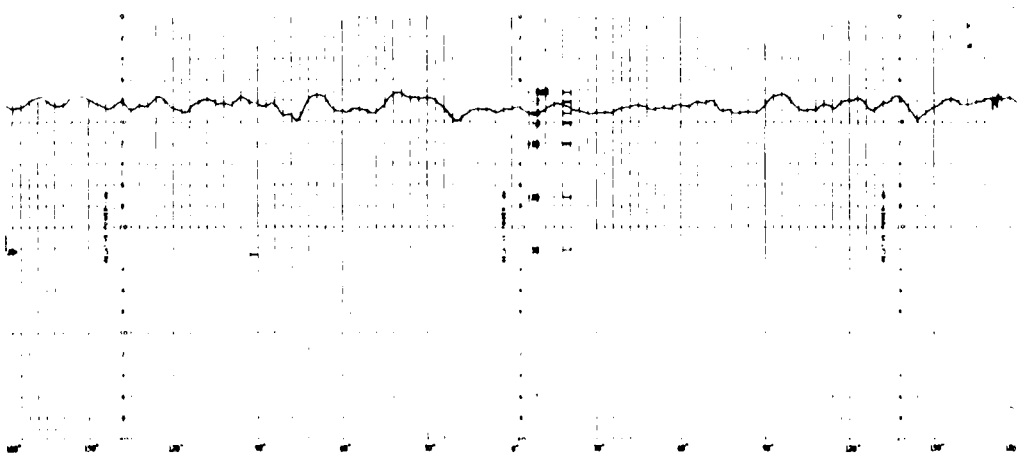

Figure 12b. Measured 14 GHz Omni Pattern

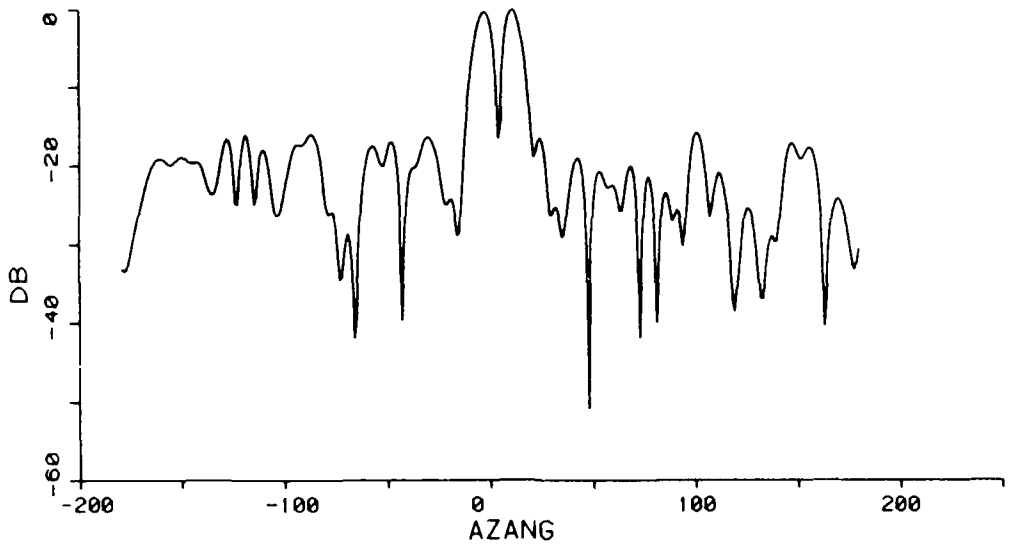

Figure 13a. Calculated 14 GHz Difference Pattern

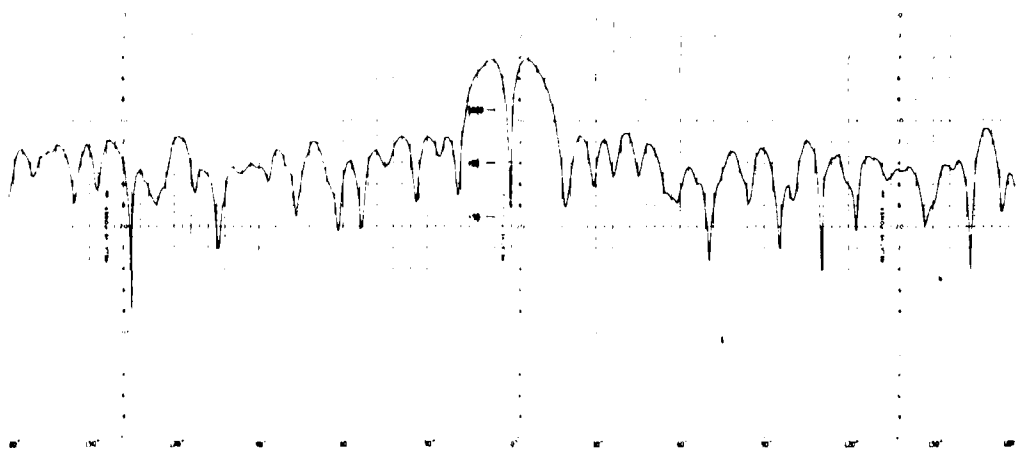

Figure 13b. Measured 14 GHz Difference Pattern

ACKNOWLEDGEMENTS

The author wishes to thank J. Becker, J. Margolin and O. Fahrenfeld for their valuable contributions in this program.

THE MECHANICAL DESIGN OF A HIGH-POWER, DUAL FREQUENCY, MILLIMETER-WAVE ANTENNA FEED SYSTEM

N. Moldovan

Harris Government Communications System Group
P.O Box 92000
Melbourne, Florida 32901

ABSTRACT

This paper describes the mechanical design and fabrication of a high power, dual-frequency, millimeter-wave feed system. The feed system consists of a 35 GHz circularly polarized monopulse subsystem and a 95 GHz circularly polarized feed. The 35 GHz feed is designed to handle 5.0 kW average and 50 kW peak power and the 95 GHz 1.2 kW average and 12 kW peak power. A Frequency Selective Surface (FSS) is incorporated to provide dual frequency capability. Each feed is liquid cooled to provide suitable cooling during high power operation. The two feeds and FSS assembly are mounted in a supporting space frame to provide an optically integral assembly ready to be mounted at the vertex of a reflector.

The paper addresses three main areas: the general feed design, which includes the manufacturing processes, flange considerations and waveguide cooling; the FSS fabrication; and beam alignment for both the primary and secondary field.

1.0 INTRODUCTION

The progression of radar and communications systems into the millimeter wave frequency range has placed added importance on the mechanical design of RF feeds. This is primarily due to component sizes and tolerances, complexity of fabrication, power density, and beam alignment requirements. This paper dicusses the mechanical design and fabrication of a 35 and 95 GHz High Power Feed System. Its application is part of a radar system which includes a 15-foot diameter Cassegrain reflector. A photograph of the complete feed system is shown in Figure 1.0-1.

2.0 FEED SYSTEM DESCRIPTION

The feed system consists of a 95 GHz communications feed, a 35 GHz monopulse tracking feed and an FSS integrated into an assembly illustrated in Figure 2.0-1. The 35 GHz feed uses a common aperture multi-flare horn. Immediately following the horn is a phasing section and a multimode matching section. The phasing section is used to put the various tracking modes in proper phase to achieve circular polarization in the difference channels. The matching section matches the sum and all difference modes from the simple square waveguide to the four square pipes of the quad-flaring/polarizer. The quad-flaring/ polarizer consists of four polarizers which generate circular polarization. Each polarizer is connected to an orthogonal mode

AD-A142 003 PROCEEDINGS OF THE ANTENNA APPLICATIONS SYMPOSIUM HELD AT MONTICELLO ILLI.. (U) ROME AIR DEVELOPMENT CENTER GRIFFISS AFB NY MAR 84 RADC-TR-84-52-VOL-1 3/3

UNCLASSIFIED F/G 9/5 NL

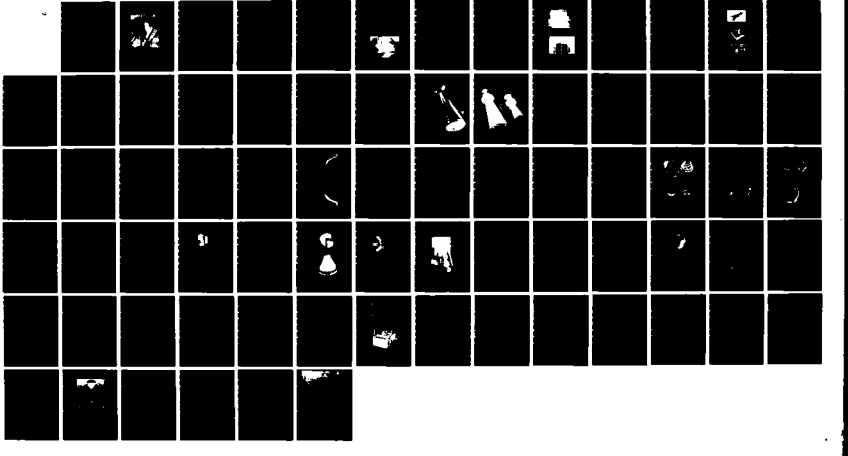

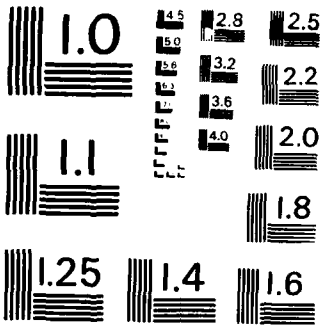

MICROCOPY RESOLUTION TEST CHART
NATIONAL BUREAU OF STANDARDS - 1963 - A

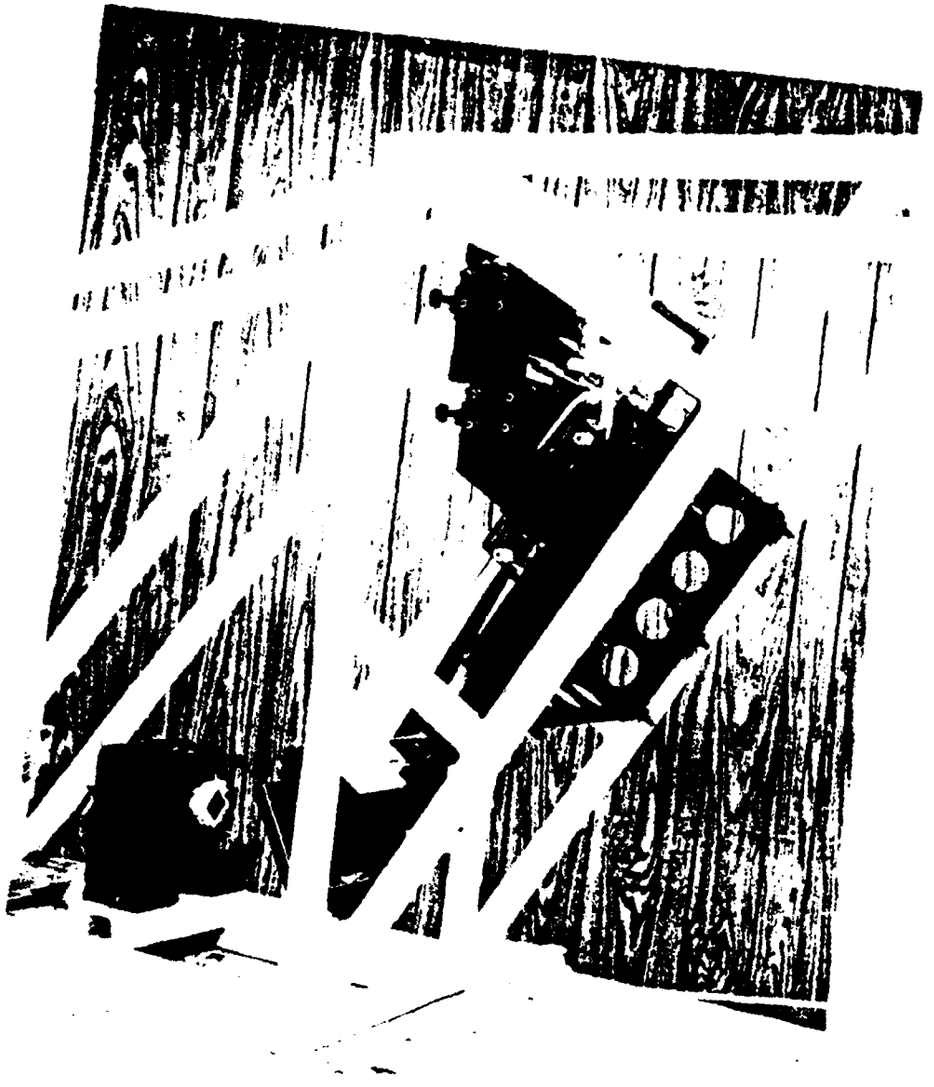

Figure 1.0-1. Photograph of Millimeter Wave Feed

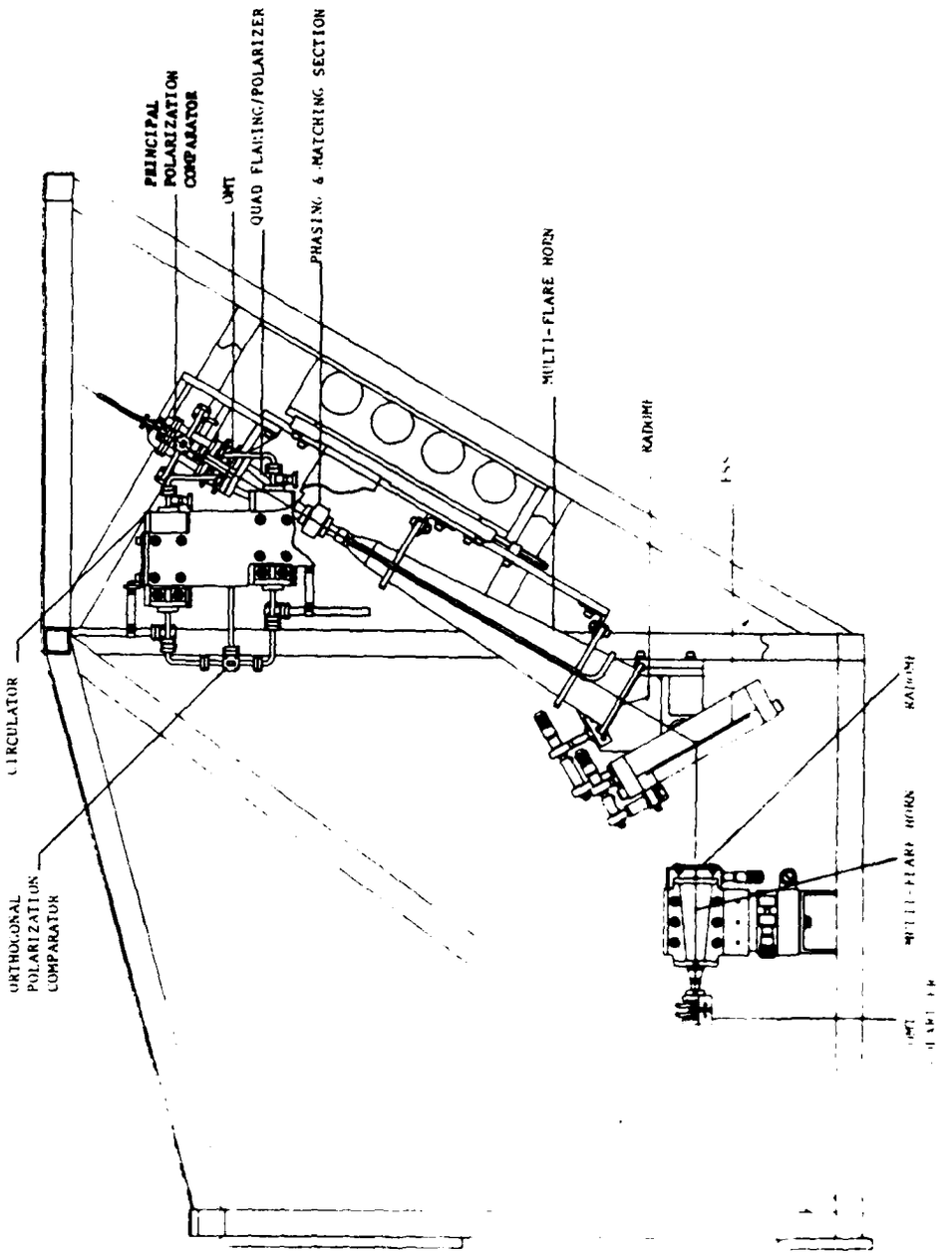

Figure 2.0-1. Feed System Layout

transducer (OMT). The in-line outputs of the OMT's connect to the principal polarization comparator and the side-arm OMT outputs interface with circulators. The orthogonal polarization comparator is connected to the receive ports of the circulators. The 95 GHz feed consists of a multi-flare horn, polarizer and OMT. Each feed contains a horn radome in order to pressurize the feeds with freon/nitrous oxide gas. Between the two feeds is an FSS which allows the 95 GHz signal to pass through, but reflects the 35 GHz signal. The two feeds and FSS are each mounted to separate precision translation assemblies for alignment. A welded tubular space frame integrates the feeds and FSS into an integral assembly ready to be mounted at the vertex of a 45 foot reflector.

3.0 MECHANICAL DESIGN

The key performance parameters which dictated the mechanical design were:

1. Millimeter-wave frequency bands (fabrication, size and tolerance)
2. Power handling
3. Beam alignment

4.0 FEED COMPONENT FABRICATION

Because of the precision involved at millimeter waves, all components in the 35 and 95 GHz feed system were electroformed. Precision mandrels were built to exact dimensions

of the interior waveguide, and copper was deposited on these mandrels to a thickness equivalent to the waveguide wall. The mandrels were then removed and the resulting shell became the final component after flanges were attached and the exterior machined to required tolerances. A Type II copper electrodeposit (additives added to the electrolyte solution) was used to minimize losses and produce a strong, hard, yet ductile deposit. All mandrel surfaces were polished to 10 microinches or better and all dimensional tolerances were held to 0.5 thousandths of an inch at 35 GHz and 0.2 thousandths of an inch at 95 GHz.

5.0 FLANGE DESIGN

The flanged joints were a source of significant concern due to the peak power requirement. In order to ensure a successful joint, sharp edges and cracks had to be eliminated. This was achieved by precise contact pressure and alignment of flanged joints. CPR (through type) brass flanges were used throughout the feeds. To avoid poor metal-to-metal contact, the waveguide flanges were lapped to four light bands (one light band - 11 millionth of an inch) of flatness and then mated with a special soft copper gasket shown in Figure 5.0-1. When the bolts were properly torqued, the gasket's raised lip yields, sealing the joint.

To align the waveguides and gaskets, precision drill jigs were fabricated. Shown in Figure 5.0-2, they contain the following features:

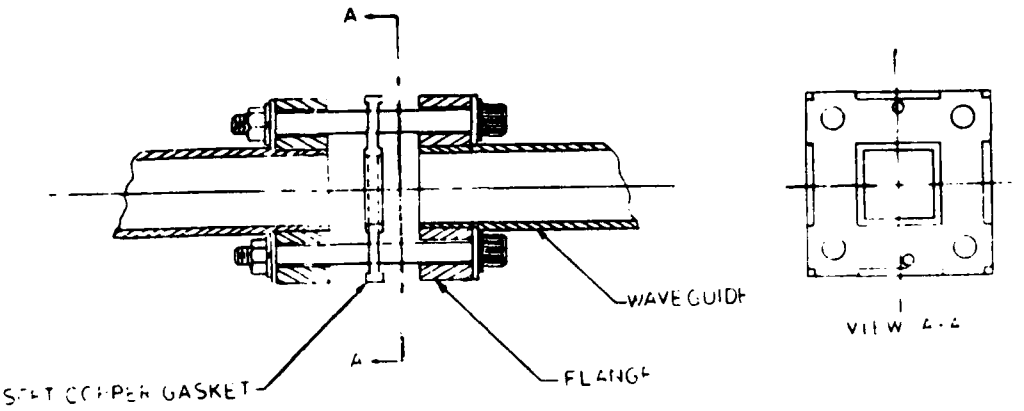

Figure 5.0-1. Gasket Design

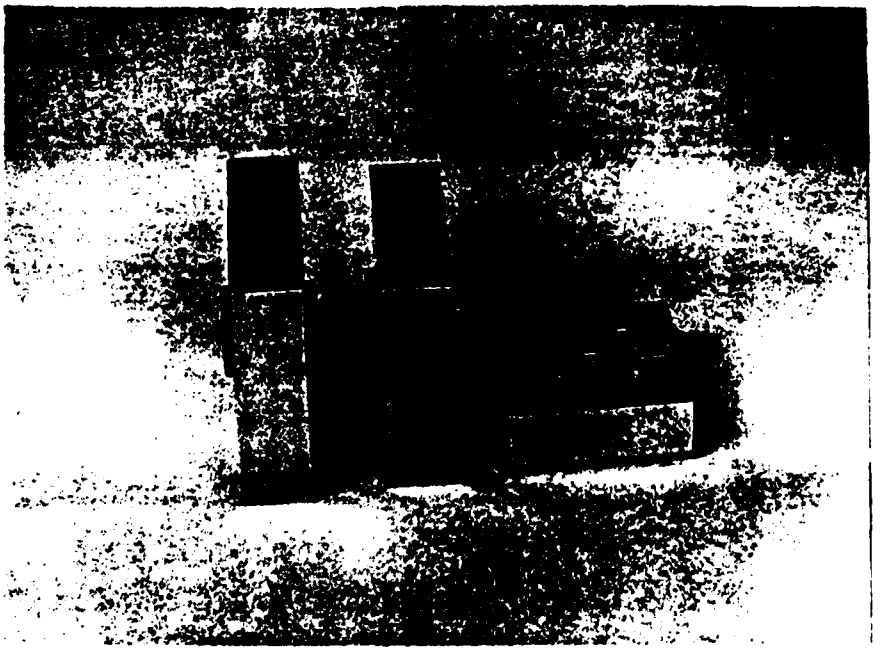

Figure 5.0-2. Precision Alignment Jigs

a. One piece construction fabricated from tool steel, hardened, ground, then lapped to a $\pm$.0002 inch tolerance.

b. The alignment dowel positions in flanges are "matched drilled", therefore reducing tolerance transfer errors.

c. Offset dowel pattern that allows assembly in only one possible way.

These jigs were used quite successfully to form and match drill all flanges. No problems were evident either in the VSWR or the high power tests to indicate that the alignment was not excellent.

6.0 FEED RADOME

Each feed contains a horn radome in order to pressurize the feed system with freon/nitrous oxide gas. The two primary design requirements which influenced the material selection were power handling and a 2 PSI pressure differential. A number of materials were evaluated including a polyimide film (0.002 inches thick), polyethersolfone, polytetrafluoroethylene film (PTFE), and PTFE-quartz. Of these materials, PTFE film was selected because it was the lowest loss and capable of meeting the induced membrane stress during feed pressurization. High power testing of the PTFE Film was conducted to satisfy the electrical design requirement. Mechanically, the Teflon Film was pressure and temperature tested.

7.0 FSS FABRICATION

Fabricating an FSS to operate at 35 and 95 GHz and handle the required power levels proved to be a formidable task in itself. Fabrication requirements of the FSS included a flat plate measuring 7.0 x 4.5 x 0.113 inches in overall size with about 5,000 rectangular holes in it. Each hole measures .0697 x .0684 inches in size with an associated tolerance of $\pm$.0005 inches. Wall thickness between adjacent holes is .007 inch thick. Since these holes are actually short waveguides, the surface finish and corner radii needed to be kept to a minimum.

A number of fabrication methods were evaluated including chemical milling, electroforming, broaching and electromagnetic discharging machining (EDM). Of these fabrication methods, EDM was selected. Figure 7.0-1 shows a photograph of the FSS about 50 percent complete and Figure 7.0-2 shows a photograph of the FSS under a 50:1 optical comparator being inspected after completion. Final mechanical inspection of the finished FSS concluded that the inside surface finish was 21 microinch RMS, hole size RMS error was .00037 in one direction and .00077 orthogonally, and the fillet radii was .006 inch. Plate flatness was .0005 RMS.

8.0 WAVEGUIDE COOLING SYSTEM

A significant amount of heat is generated in the transmission of 5.0 kW of average power in WR-28 and 1.2 kW in WR-10. For example, if the waveguides were cooled only by natural convection and radiation, the temperature rise would be

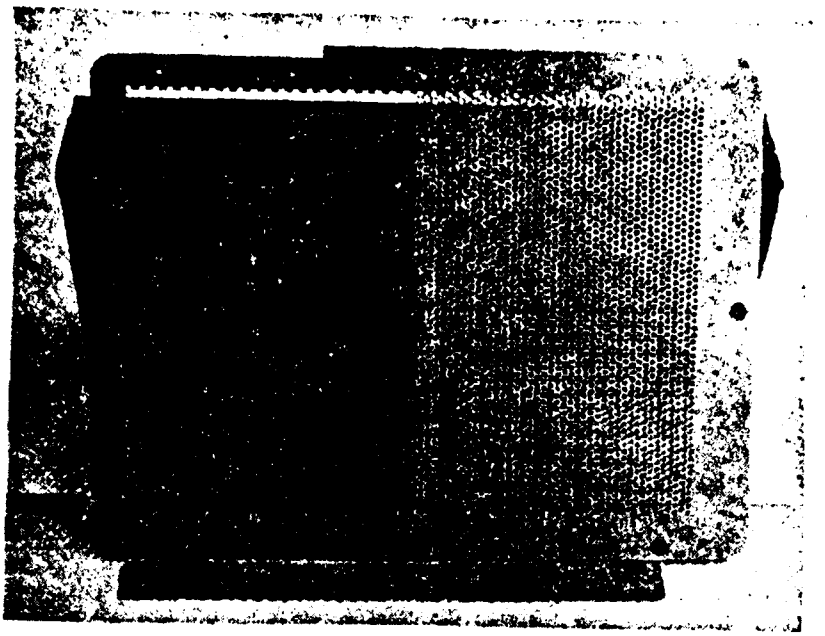

Figure 7.0-1. FSS 50 Percent Complete

Figure 7.0-2. FSS Inspection (50:1 Optical Comparator)

over 480° F for WR-28 and 840° F for WR-10. Since RF performance is altered by the temperature of the components, goals for maximum operating temperatures were established. Therefore, a suitable cooling system was designed around the available liquid coolant and the configuration of the feed system.

Due to the size and complexity of the high power feed components, three liquid cooling methods were incorporated as follows:

a. Copper tubing secured to the side of the waveguide component

b. Cold plate/flange design

c. Water jacket

Attaching copper tubing to the waveguide components is a proven, simple and reliable method of heat transfer between the coolant and the waveguide component. The components that are cooled by this method are: the horns, quad-flaring/polarizer and the high power transmit inputs. Two sizes of tubing were used: 3/16 and 1/4 inch O.D. The tubing were attached to the components with a low temperature (390° F), 95-5 percent tin/silver composition solder. Figure 8.0-1 shows a photograph of the quad-flaring/polarizer and horn with attached cooling tubes.

The OMT's shown in Figure 8.0-2 are cooled by a cold plate/flange design. The cold plate/flange is basically a .600 inch thick through type brass flange with internal coolant

passages. The flange is soldered to the orthogonal port (transmit port) and along the through port (receive port). This design solved two problems. First, the hot spot in the OMT was located at the junction of the orthogonal port and through port. The internal coolant passages allows the coolant to circle this area, efficiently removing the heat. Second, due to their basic design, size, and fabrication technique, an OMT is a fragile component. The cold plate/flange provides added strength to the OMT.

The most critical area of concern was the matching section. This is due to the concentration of transmit energy from the four transit lines converging into a common aperture. Additionally, the matching section, designed to provide good VSWR, has matching elements inside the waveguide. These elements, under high transmit power, required symmetrical cooling to eliminate warping and possible material breakdown. To accomplish this, the matching section was surrounded by a water jacket as shown in Figure 8.0-3. This brought coolant in contact with all four exterior walls, thereby affording symmetrical dissipation of the heat. Component temperature rises measured less than 10° F during high power tests on the 35 GHz feed. Although the 95 GHz feed was not high power tested, predicted temperature rises are similar to the 35 GHz feed.

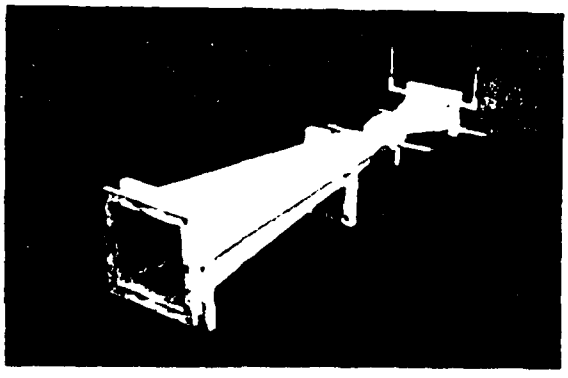

Figure 8.0-1. Copper Tubing Attached to Components

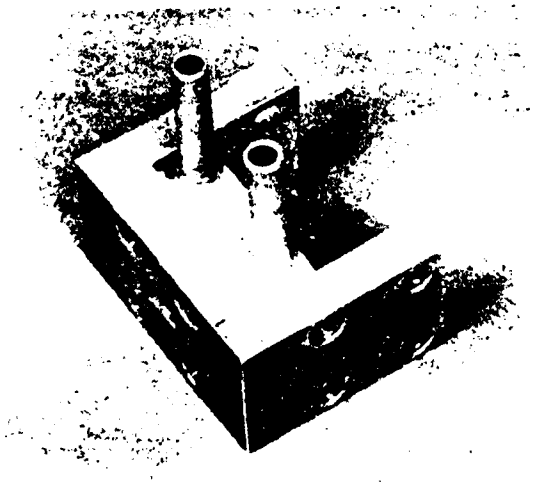

Figure 8.0-2. Cold Plate/Flange, OMT Cooling Technique

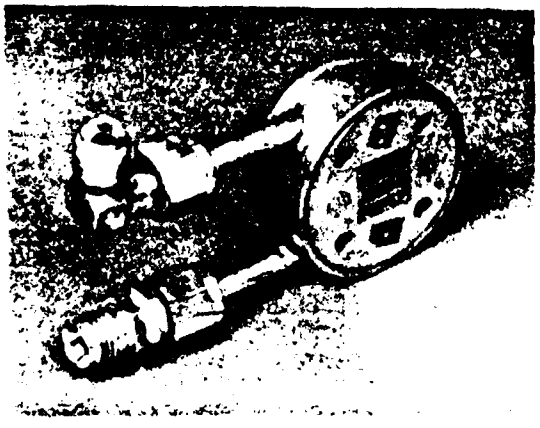

Figure 8.0-3. Water Jacket, Phasing and Matching Section Cooling Technique

8.1 FSS Cooling

The primary cooling system design task was simply to lower the temperature of the FSS to a value that prevents warping caused by thermal expansion. The estimated total heat dissipation in the FSS was 30 watts concentrated in a 3-1/2 diameter centered circle. A suitable method of cooling the FSS was to blow air through the grid. A pressure differential switch was incorporated to detect when the blower was in operation and a fan filter ensured clean air passed through the grid.

9.0 PRIMARY BEAM ALIGNMENT

Initial alignment of the feed system consisted of using optical techniques to set relative distances between the feeds and FSS . Each feed is mounted to separate three axis translation assemblies and the FSS is gimbal mounted in two planes. After initial alignment, primary RF patterns were performed and final ajustments made.

9.1 Secondary Beam Alignment

It was required that the 35 and 95 GHz secondary beams be aligned and maintained through the static and dynamic operating conditions to within 15 μr. To meet this requirement, the mechanical designs for both the FSS gimbal and feed mounting frame were analyzed. A finite element structural model was generated and a dynamic input loading of $2°/sec^2$ angular acceleration simultaneously in both aximuth and elevation (including a 1G load) was analyzed. Figure 9.0-1 shows the RF geometry of the installed

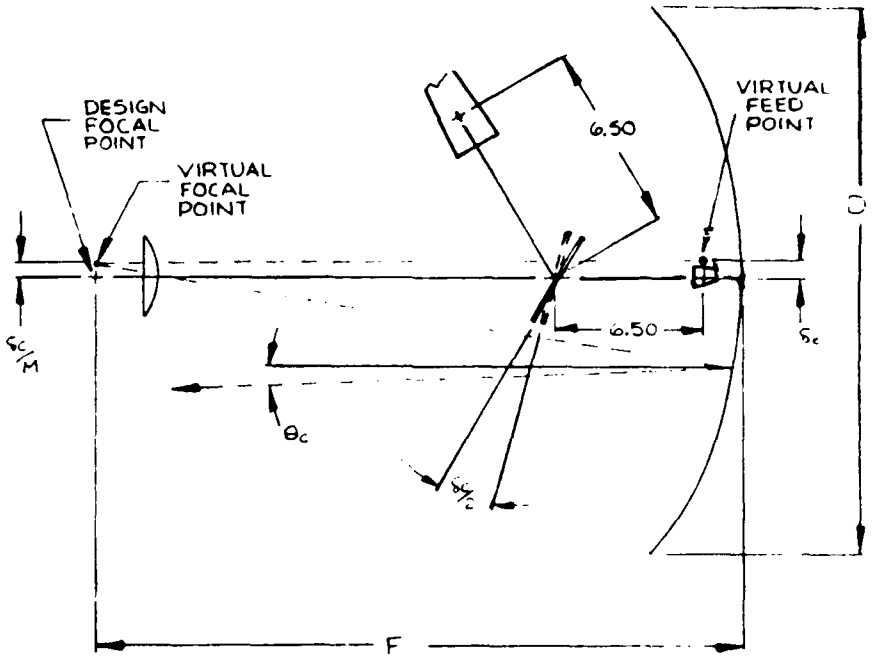

Figure 9.0-1. Radar System Geometry

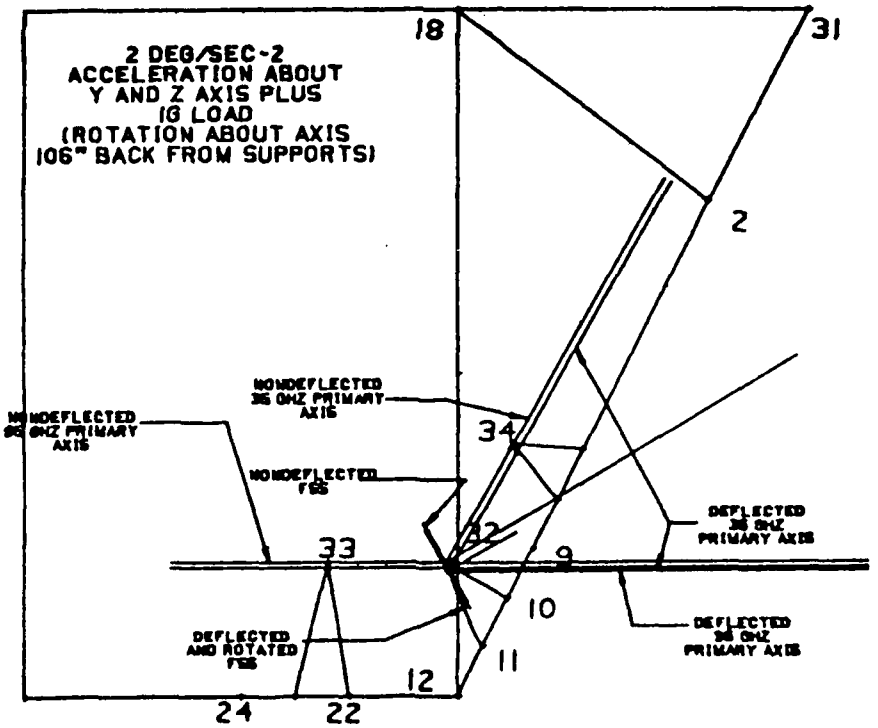

Figure 9.0-2. Displacement of Virture Feed Phase Center From Dynamic Loading Analysis

feed system. Once the displacements normal to the primary axis of each feed (δ_C) is determined, the beam deviation angle, θ_C, can be found. It should be noted that the deflections and rotations of the FSS are necessary to determine δ_C for the 35 GHz feed. Figure 9.0-2 shows a graphic display of the beam deviations due to the dynamic loading. The dynamic analysis concluded that the maximum deviation angle of the 35 GHz feed was 1.9 μr and the beam angle between the 35 and 95 GHz feed was 0.74 μr.

10.0 CONCLUSION

The Harris Corporation has successfully designed and fabricated a high-power, dual frequency (35 & 95 GHz) antenna feed system. The 35 GHz feed is designed to handle 5.0 kW average and 50 kW peak power and the 95 GHz 1.2 kW average and 12 kW peak power. The successful mechanical design and fabrication of the feed system was the result of:

1. A close RF and mechanical design interface which continued through final fabrication and testing stages.
2. The use of Computer Aided Design which allowed structural modeling of static and dynamic load conditions, multiple design iterations in determining final configuration, and high quality detailed drawings for fabrication and assembly.
3. The use of state-of-the-art machine tools and the ability of various craftsmen to fabricate the components to design tolerances.

EARTH COVERAGE CORRUGATED HORNS (44.5 GHz and 20.7 GHz)* †

Dennis C. Weikle

Lincoln Laboratory, Massachusetts Institute of Technology
Lexington, Massachusetts

ABSTRACT

Communications satellites located in geosynchronous orbits will, in addition to more specialized shaped beam or area coverage antennas, generally utilize earth coverage antennas designed to maximize antenna gain over the entire surface of the visible earth. In the microwave and millimeter wave bands, these antennas are usually conical horns which achieve a minimum gain (G_{min}) of 17 - 17.5 dBi at the limb of the earth. This paper describes the design of a single mode (HE_{11}) earth coverage horn that optimizes G_{min}. Measurements performed over a 5% frequency band on experimental models designed to operate at 20.7 GHz and 44.5 GHz demonstrate a G_{min} 17.8 dBi. Other characteristics of the horns are circularly symmetric radiation patterns, low VSWR (1.2), and peak gain of approximately 22.0 dBi.

1.0 INTRODUCTION

The figure of merit for a satellite antenna designed for full earth coverage is the minimum directive gain (G_{min}) that occurs

*This work has been sponsored by the Department of the Air Force.

†"The U.S. Government assumes no responsibility for the material presented."

anywhere within the coverage area. For an antenna with a conventional radiation pattern (non-shaped beam), G_{min} occurs at the edge of earth (EOE) position. This report describes a single mode (HE_{11}) corrugated horn design which optimizes the horn aperture size to produce the maximum EOE gain (as viewed from geosynchronous altitude). The EOE is located approximately 8.6° from the boresight of an antenna pointed directly at the center of the earth. However, to provide for spacecraft attitude instabilities, 9° was used as the EOE angle.

2.0 DESIGN

The aperture size producing the maximum gain at 9° was determined by calculating the gain of various aperture sizes of an HE_{11} mode horn and determining the optimum.[1] The maximum value of EOE gain is obtained with an aperture diameter of 4.99 λ_o (λ_o = free space wavelength). Corrugated horns utilizing this optimum aperture size were then designed for operating frequencies of 20.7 GHz and 44.5 GHz (see Fig. 1).

Circumferential corrugations on the inner walls of the horns are used to generate the HE_{11} mode in order to obtain circularly symmetric radiation patterns. These grooves are spaced approximately 0.38 λ_o apart and are separated by a 0.1 λ_o wall (dimension t in Fig. 1). The depths of the first five corrugations nearest the throat are tapered[2] to provide a good impedance match between the TE_{11} and HE_{11} propagation regions. The groove depth of the remaining corrugations is 0.25 λ.

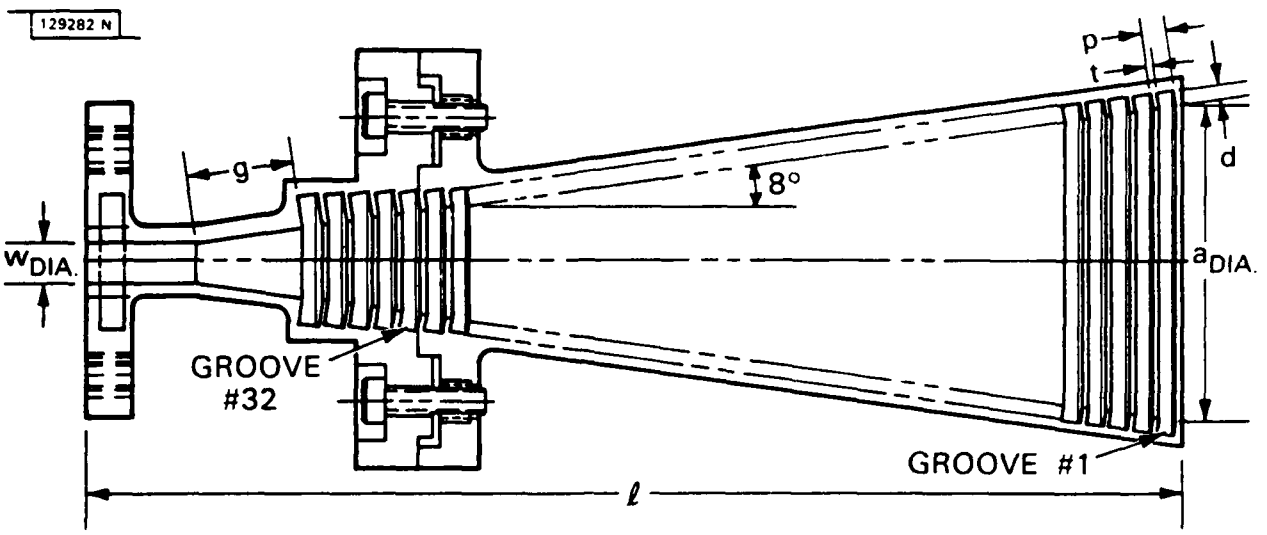

DIMENSION	20.7 GHz	44.5 GHz
a	2.844	1.323
ℓ	9.00	4.50
p	0.217	0.101
t	0.054	0.025
g	0.954	0.442
w	0.404	0.188

DIMENSION d GROOVE NO.	20.7 GHz	44.5 GHz
1 THRU 31	$0.142\ ^{+0.005}_{-0.000}$	$0.066\ ^{+0.005}_{-0.000}$
32	0.163	0.076
33	0.185	0.086
34	0.206	0.096
35	0.228	0.106
36	$0.249\ ^{0.000}_{-0.005}$	$0.116\ ^{+0.005}_{0.000}$

ALL DIMENSIONS IN INCHES
TOLERANCES ±0.005 UNLESS OTHERWISE SPECIFIED

Figure 1. Earth coverage corrugated horn design (20.7 and 44.5 GHz).

With a given aperture size, the phase deviation from a plane in the aperture is determined by the cone angle. Larger cone angles result in higher sidelobe levels and reduced beam efficiency. Smaller cone angles, however, result in increased overall length of the horn and increased difficulty in fabrication. In the present design, a cone angle of 8° with a consequent phase deviation of 0.175 λ was selected. This corresponds to a reduction in aperture efficiency of approximately 3% relative to an aperture with no phase deviation.

Since the deepest corrugations are located near the throat of the horn, they are the most difficult to machine. To ease the fabrication process, a section of the cone in the throat of the horn was not corrugated. The length of this section (g), determined empirically, was chosen carefully. If g is too large, the diameter of the horn at the first corrugation will be large enough to allow the excitation of higher order modes. The value of g also influences the VSWR which depends upon the addition of two dominant reflections: the reflection at the horn throat junction and the reflection at the onset of corrugations.[3] The length of g chosen for the EC horns is 1.67 λ.

3.0 FABRICATION

Initially, the development earth coverage horns were fabricated in a one-piece construction using the electroformed copper

process (see Fig. 2). This process was chosen because the corrugations which are difficult to machine and measure accurately (especially the ones nearest the throat) can be precisely controlled by electroforming. In this way, design modifications could be made in the development models and their effects clearly understood. However, electroforming can be undesirable for two reasons: 1) weight and perhaps more important, 2) electroforming solution sometimes becomes trapped in the corrugation walls. This solution can leak out into the corrugations where it solidifies, affecting the performance of the horn. Therefore, while the electroformed horns served as a useful development tool, the final versions of the horns were fabricated in a two-piece, machined, aluminum construction (Fig. 3). The two-piece construction eased machining by allowing easier access to the throat region of the horn. Three horns were fabricated* for an operating frequency of 20.7 and two for 44.5 GHz at a cost of less than $1000 each. These horns are considered to be flight quality and have weights of 286 grams and 78 grams for the 20.7 GHz and 44.5 GHz versions, respectively.

*The horns were fabricated by P&L Machine, Acton, Mass.

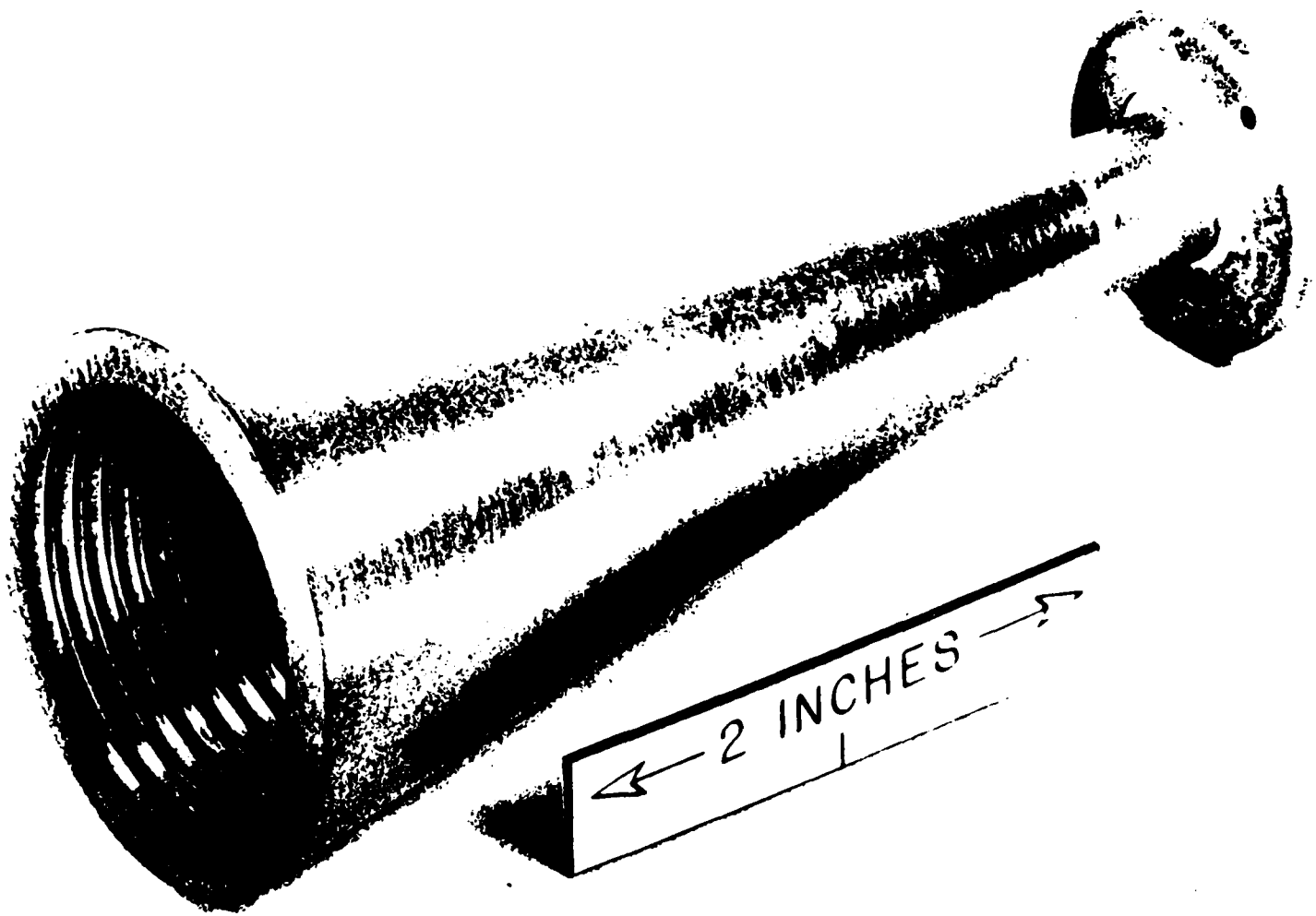

Figure 2. 44.5 GHz electroformed earth coverage horn.

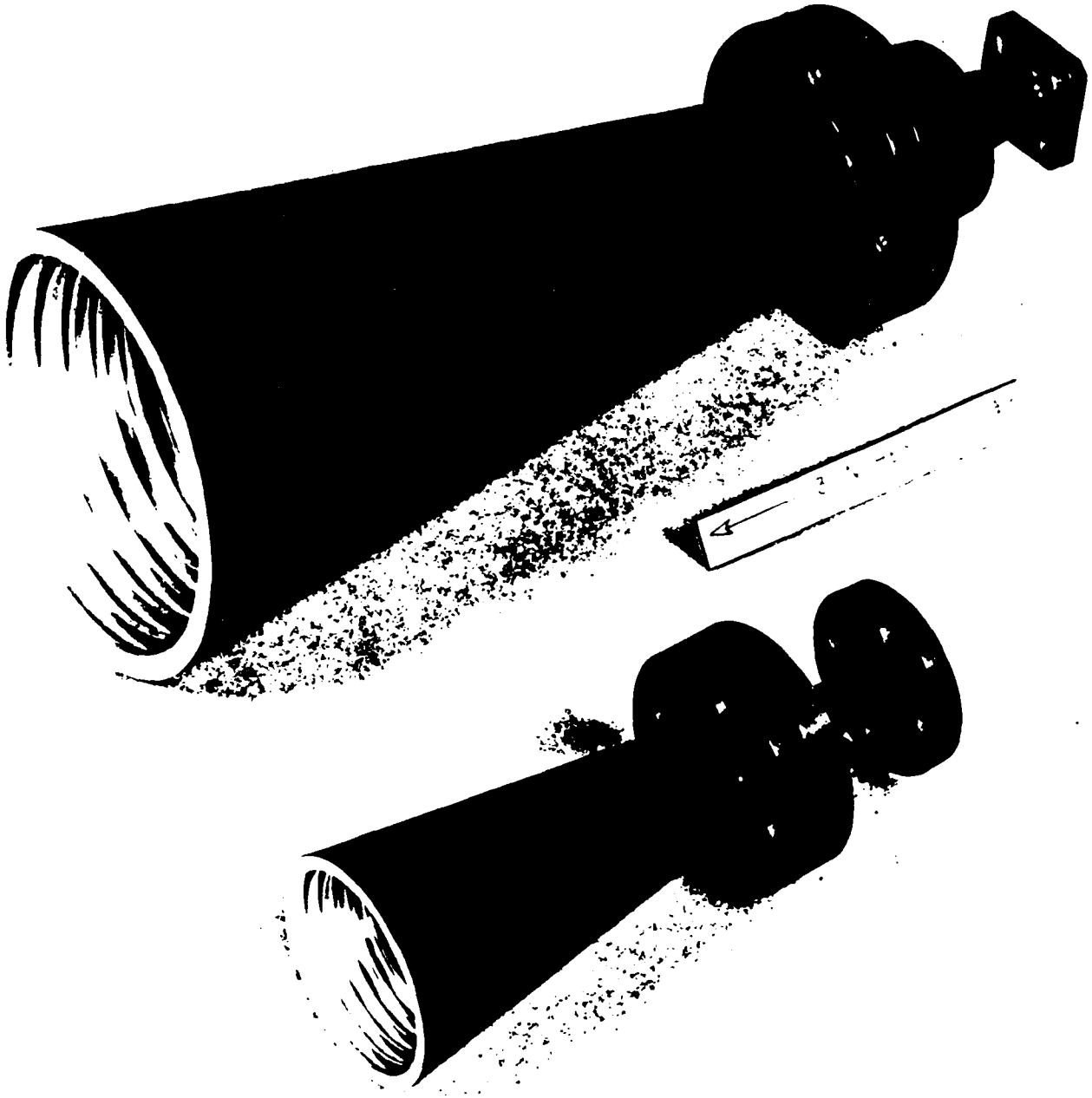

Figure 3. Earth coverage horns - two piece construction.

4.0 MEASUREMENTS

Radiation pattern, gain, and VSWR (return loss) measurements were performed on the earth coverage horns over a 5% frequency band. The gain and radiation pattern measurements were conducted on a 25-ft. range. Radiation patterns were taken at three discrete frequencies covering the respective band of each horn while the gain and VSWR were measured in one continuous frequency sweep. The gains of the horns were determined by comparisons with gain standard horns.

Since the 20.7 GHz and 44.5 GHz horns are scaled versions of one another, their performance is virtually identical. The radiation patterns presented are those performed on a 44.5 GHz horn (two-piece construction), although the patterns are typical of horns designed for either frequency. A measured 44.5 GHz radiation pattern is shown in Fig. 4. (Note - EOE position is -4 dB from peak). To easily observe the axial symmetry, the E- and H-plane radiation patterns are superimposed onto one another. The beamwidth and sidelobe levels agree very well with the theoretical, computer-generated pattern shown in Fig. 5. Measured patterns taken at 43.5 GHz and 45.5 GHz are shown in Figs. 6 and 7, respectively.

The on-boresight swept gain measurement is shown in Fig. 8. At 44.5 GHz, the on-axis gain measured 22.1 dBi which yields an edge of earth gain of approximately 18.1 dB. The EOE gain was

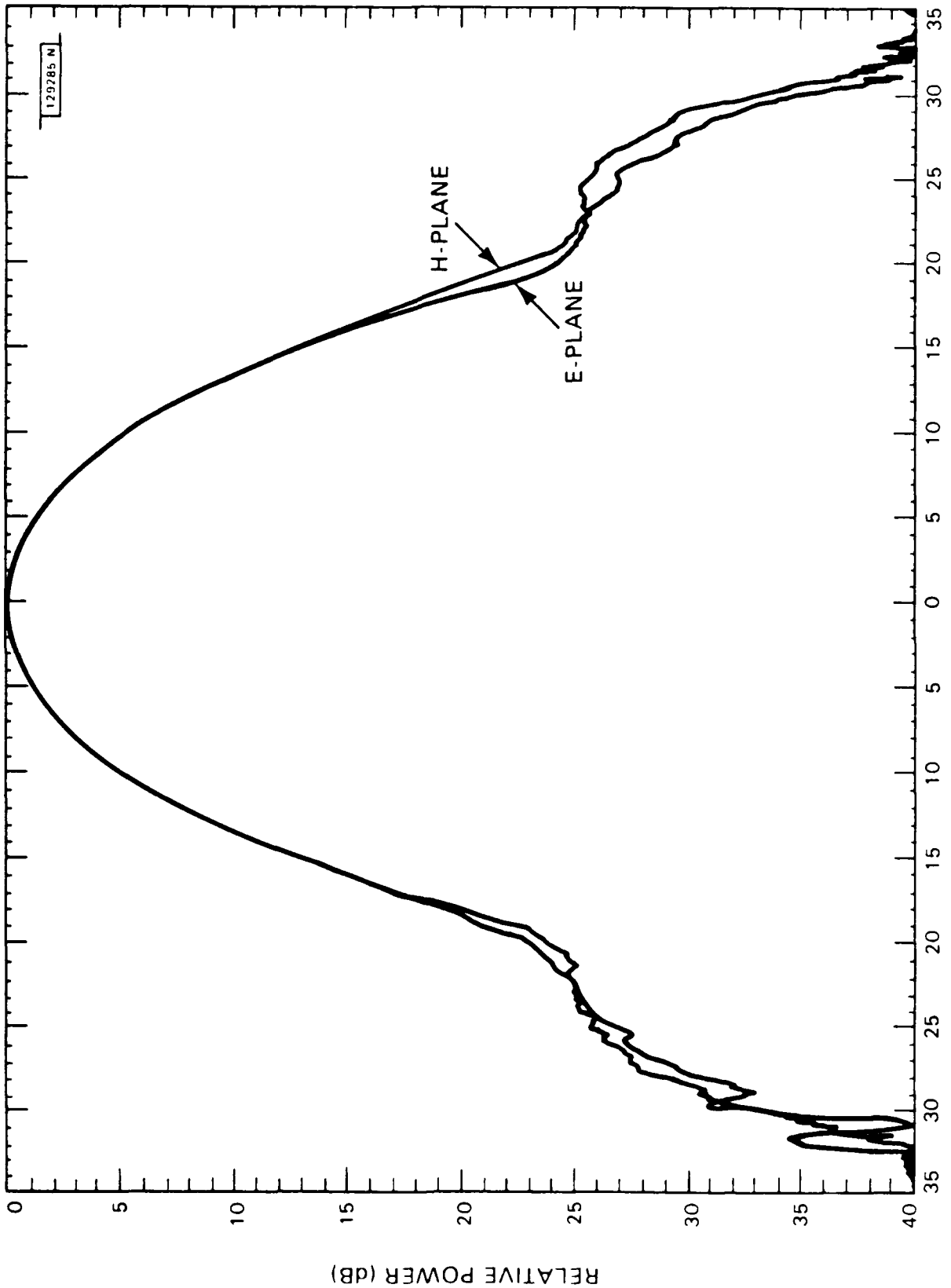

Figure 4. Measured radiation pattern of earth coverage horn - 44.5 GHz.

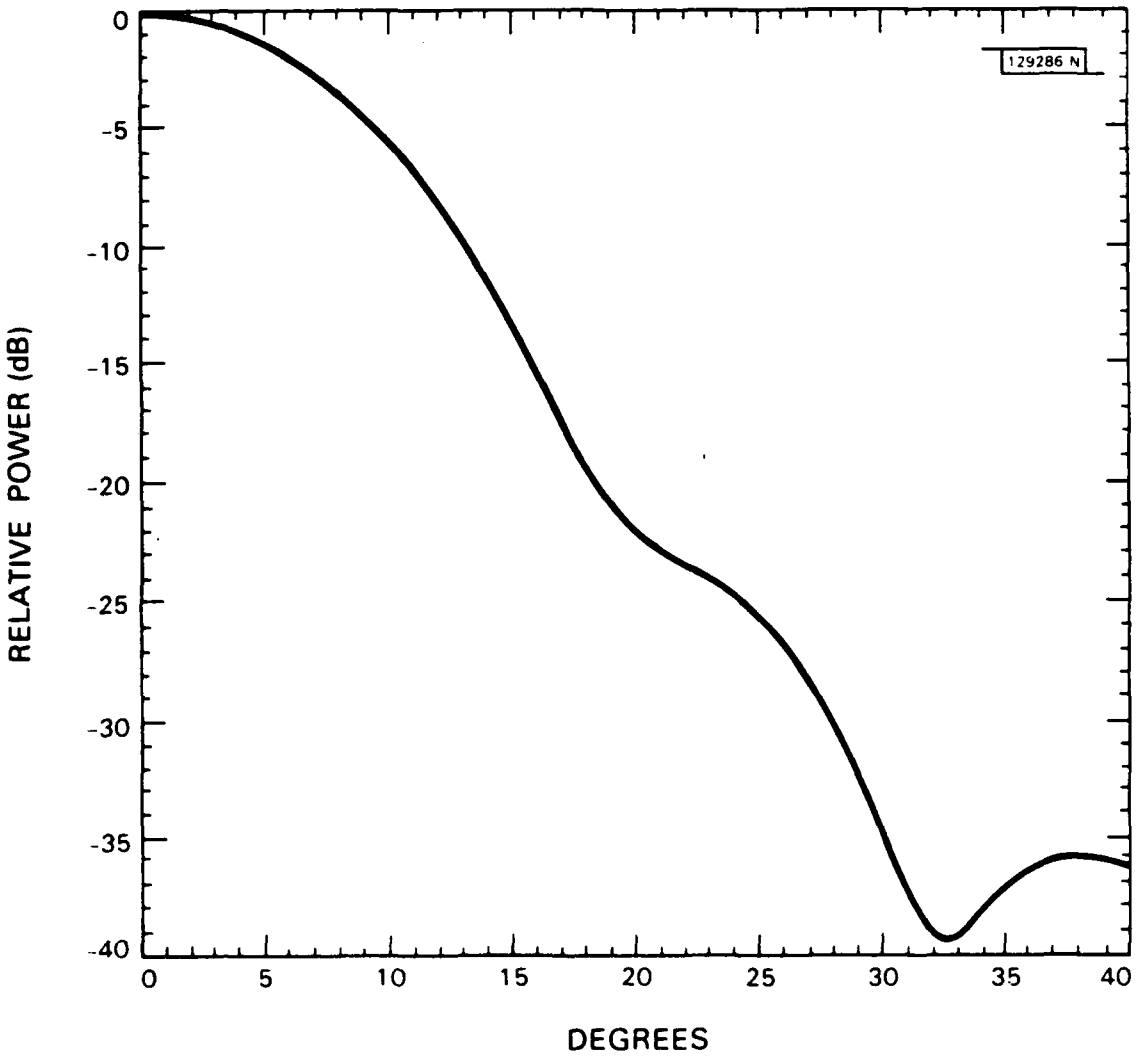

Figure 5. Computer-generated pattern - 44.5 GHz.

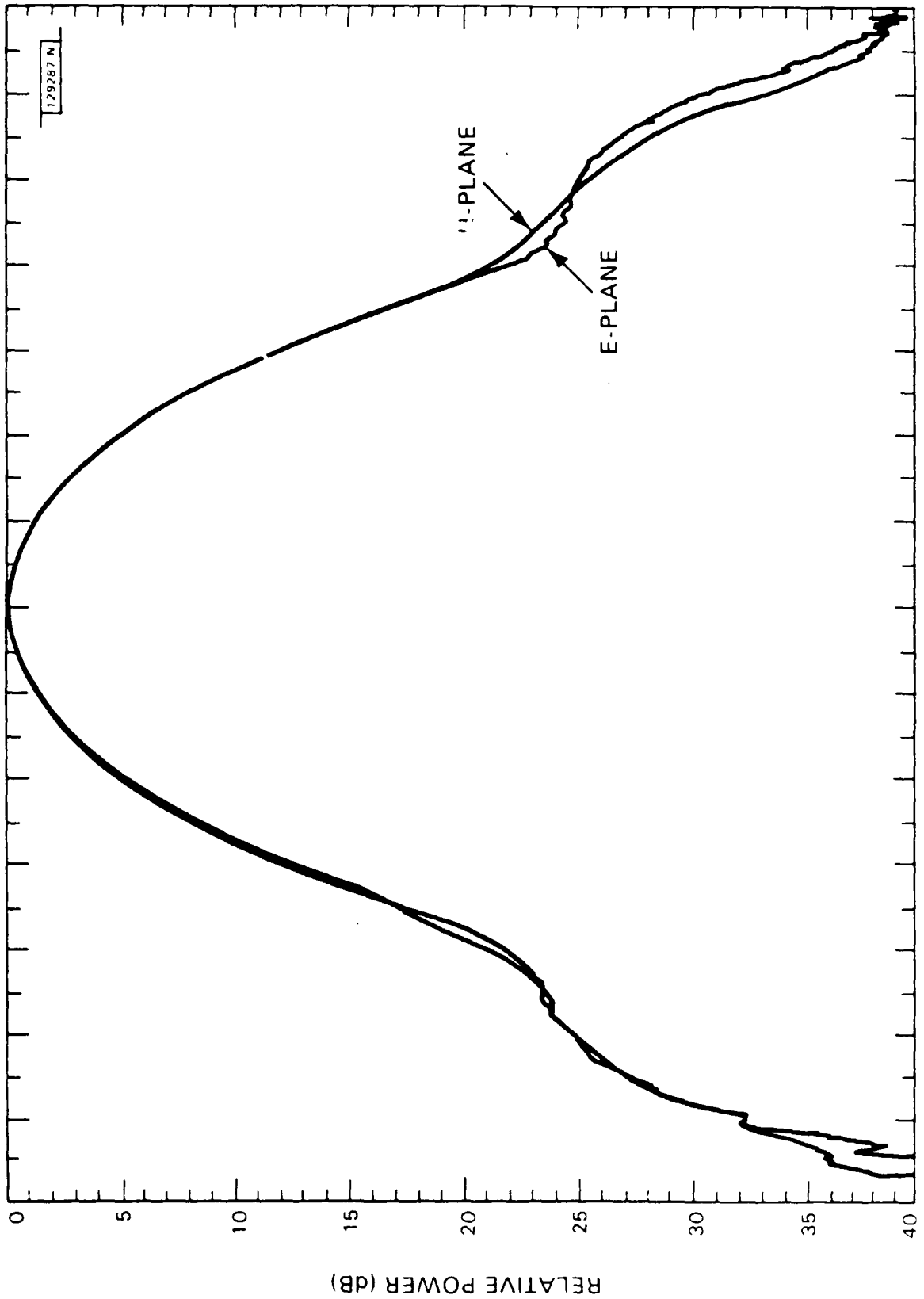

Figure 6. Measured radiation pattern of earth coverage horn - 43.5 GHz.

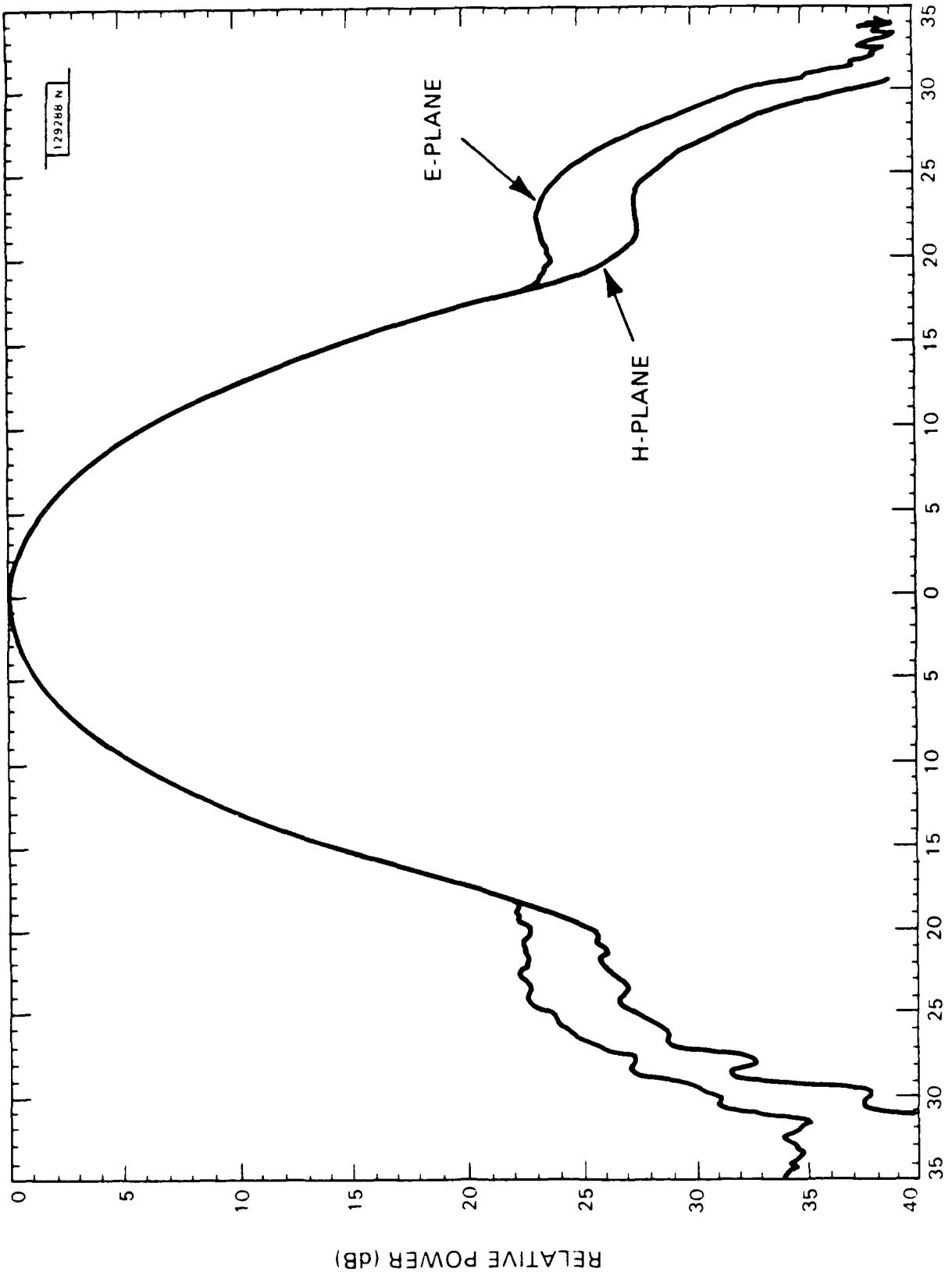

Figure 7. Measured radiation pattern of earth coverage horn - 45.5 GHz.

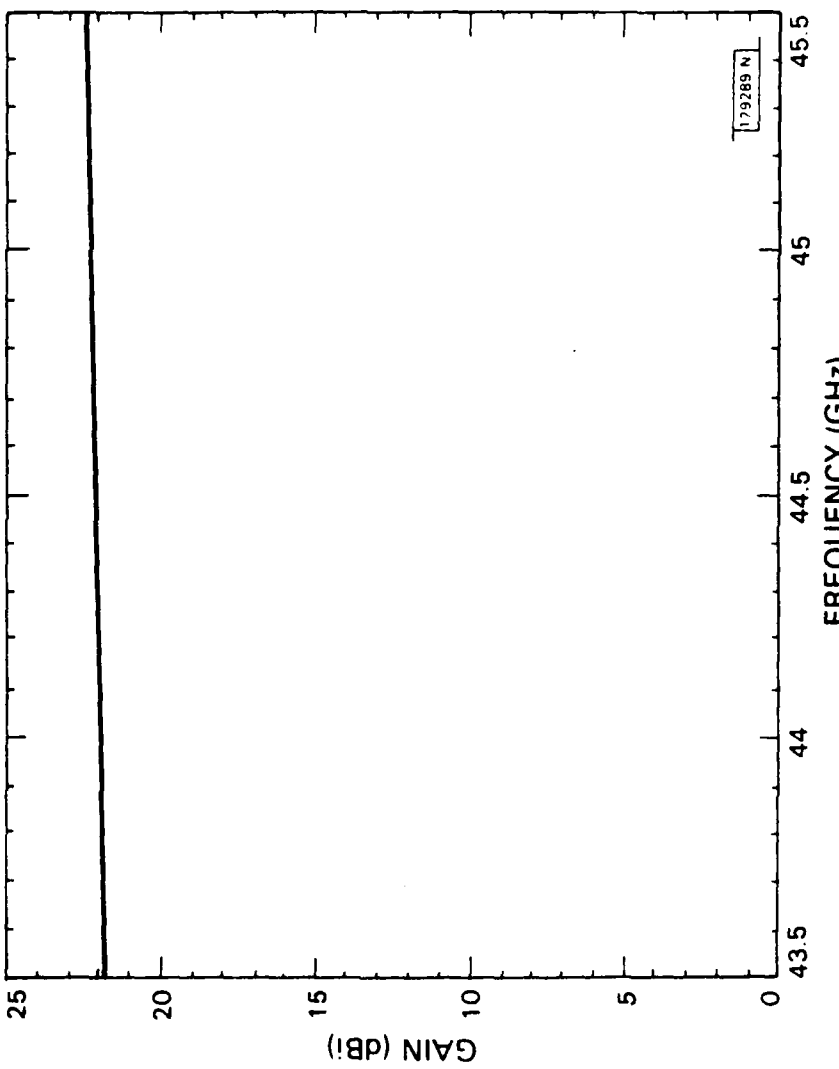

Figure 8. Measured on-boresight swept frequency gain (43.5 - 45.5 GHz).

also measured by scanning the horn 9° off boresight in the H-plane and the amplitude level compared to that of the gain standard (Fig. 9). Here the EOE gain measured 18.0 dBi at 44.5 GHz. The minimum EOE gain occurs at 43.5 GHz and is 17.8 dBi.

A typical swept frequency VSWR measurement is shown in Fig. 10. Of the five horns measured, the VSWR within the frequency band is typically less than 1.2. A listing which summarizes the gain and VSWR measurements on all fivehorns is shown in Table 1. The minimum column in the gain table and the maximum column in the VSWR table indicates the maximum and minimum values that occurred over the frequency band.

Figure 11 shows a spinning linear radiation pattern of a circularly polarized 20.7 GHz earth coverage horn. The horn was circularly polarized by attaching an external sloping septum polarizer* to its circular waveguide port. The axial ratio within the included angle of ±9° from boresight is less than 0.4 dB and is typical of measurements performed at three frequencies over the band.

5.0 CONCLUSIONS

A single mode earth coverage corrugated horn was designed to optimize the minimum gain (G_{min}) within the earth field of view

*Polarizer manufactured by Atlantic Microwave, Bolton, Mass.

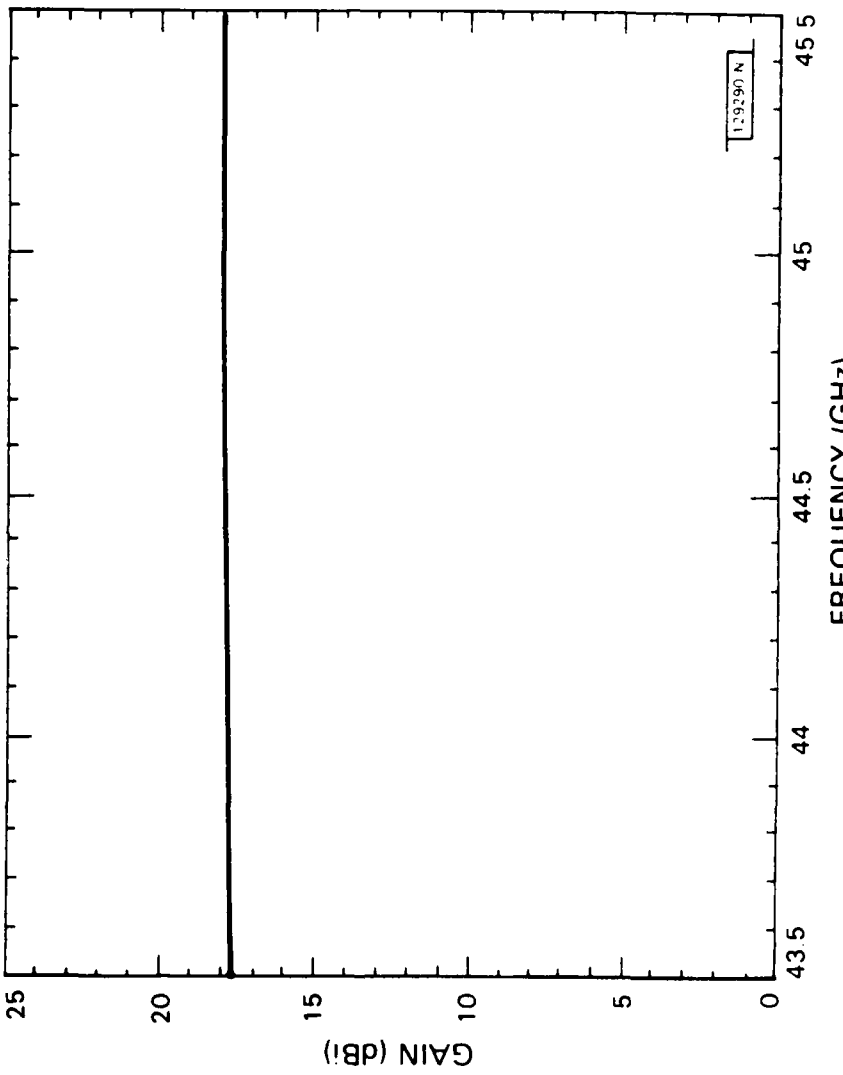

Figure 9. Measured 9° off-boresight swept frequency gain (43.5 - 45.5 GHz).

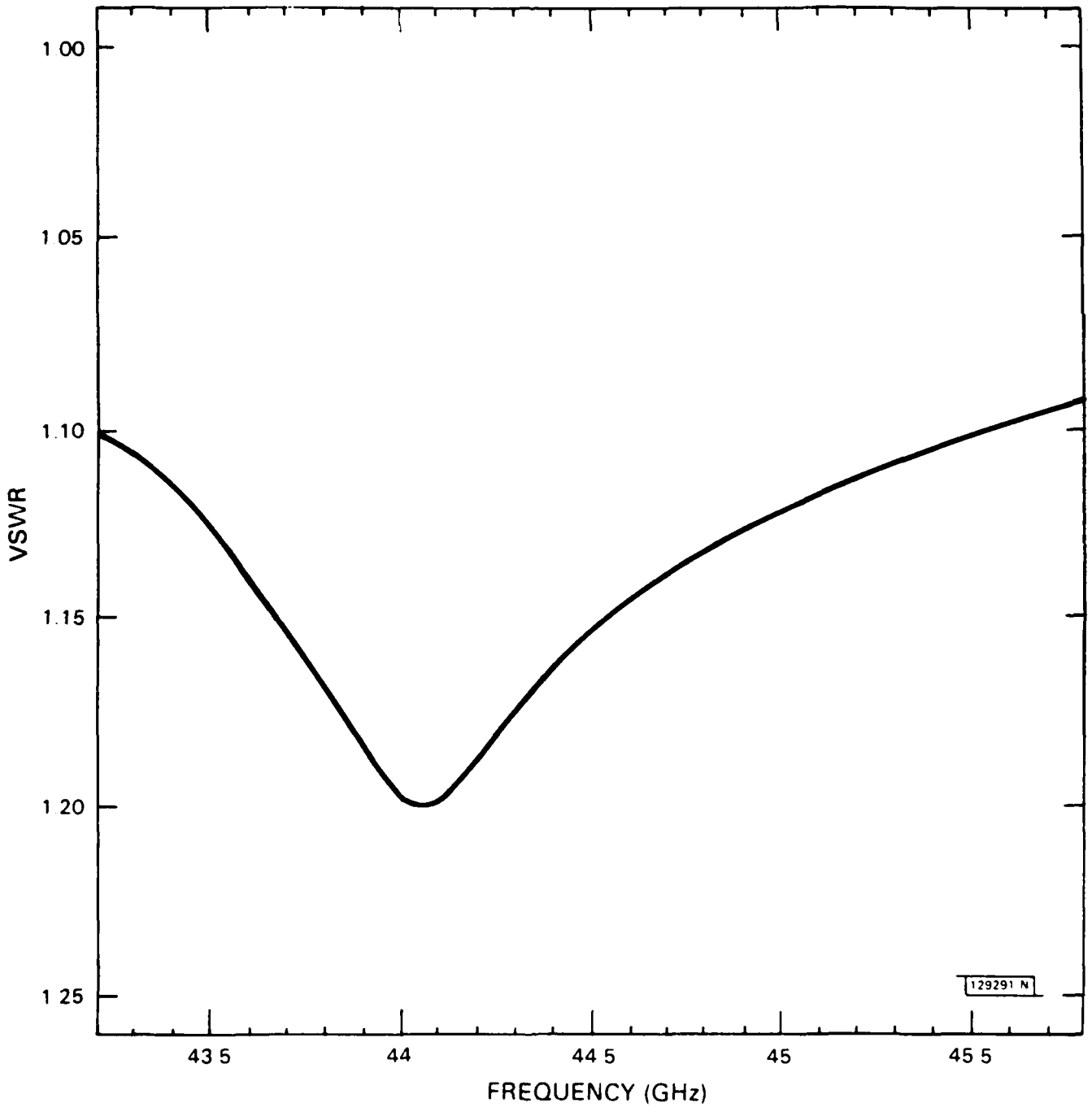

Figure 10. Measured swept frequency VSWR (43.5 - 45.5 GHz).

TABLE 1

EARTH COVERAGE HORN PERFORMANCE SUMMARY

	SER. No.	EOE GAIN (dBi)				PEAK GAIN (dBi)				VSWR			
20.7 GHz EC HORN	////	20.2 GHz	20.7 GHz	21.2 GHz	MIN	20.2 GHz	20.7 GHz	21.2 GHz	MIN	20.2 GHz	20.7 GHz	21.2 GHz	MAX
	1	18.1	17.8	17.8	17.8	22.1	22.2	22.4	22.1	1.21	1.10	1.06	1.21
	2	18.1	17.9	17.8	17.8	22.1	22.2	22.4	22.1	1.20	1.10	1.06	1.20
	3	18.1	17.9	17.8	17.8	22.0	22.1	22.4	21.9	1.20	1.10	1.05	1.20
45.5 GHz EC HORN	////	43.5 GHz	44.5 GHz	45.5 GHz	MIN	43.5 GHz	44.5 GHz	45.5 GHz	MIN	43.5 GHz	44.5 GHz	45.5 GHz	MAX
	1	17.8	18.0	17.9	17.8	21.9	22.1	22.6	21.9	1.15	1.10	1.05	1.21
	2	17.8	17.9	17.9	17.8	21.9	22.1	22.5	21.9	1.15	1.10	1.05	1.19

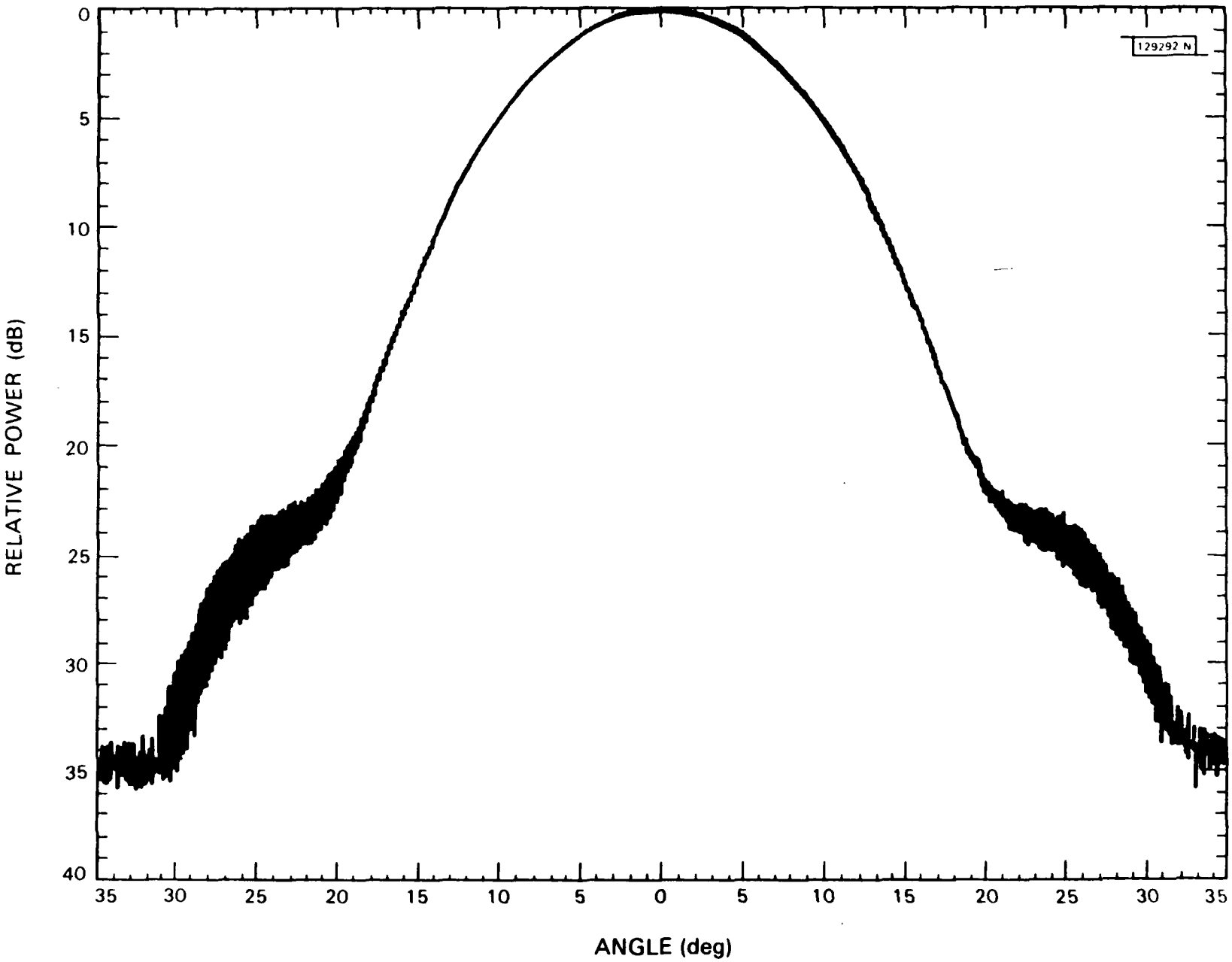

Figure 11. Spinning linear radiation pattern of 20.7 GHz circularly polarized earth coverage corrugated horn.

(as viewed from geosynchronous altitude). Experimental models built at operating frequencies of 20.7 GHz and 44.5 GHz were evaluated over a 5% frequency band for each horn. Measured G_{min}, which occurs at the edge-of-earth position (±9° from boresight), is 17.8 dBi which is very close to the theoretical maximum for a horn with a conventional radiation pattern (non-shaped beam). The horns also produced circularly symmetric radiation patterns and VSWR of approximately 1.2. The aperture diameter is approximately 5 λ, the overall length is 17 λ, and the weight is 286 grams and 78 grams for the 20.7 GHz and 44.5 GHz horns, respectively.

ACKNOWLEDGMENTS

The author is grateful to Robert Piccola for conducting the antenna measurements, to Dr. Andre Dion for providing the theoretical optimization of this antenna, and to Dr. Alan Simmons and Walter Rotman for their assistance in the antenna development.

REFERENCES

1. A Study of a Dual Mode Horn Antenna for Full Earth Coverage From a Geostationary Satellite and a Variable Beamwidth Reflector Antenna. JPL Technical Report 701-198 (6 December 1974) p. 11.

2. Mac A. Thomas, B., (1978) Design of Corrugated Conical Horns. IEEE Trans. on Ant. and Propag. 26:367.

3. Melo, S. F. J., (1979) Improved Primary Radiator for the 11 GHz Band. Electrical Communication 54:125 (1979).

ADVANCES IN SPIRAL ANTENNA TECHNOLOGY

PHILIP B. GREEN
TEXAS INSTRUMENTS

ABSTRACT

Most of the development of the spiral antenna was completed in the fifties and sixties. Efforts in the last decade have concentrated on technology refinement. This paper summarizes some of the more important, but less heralded, advances in spiral antenna technology - concentrating on hybrid spiral structures, utilization of advanced microwave absorbers, upper-frequency extension, and low-cost production techniques.

ADVANCES IN SPIRAL ANTENNA TECHNOLOGY

PHILIP B. GREEN
TEXAS INSTRUMENTS

1.0 INTRODUCTION

Nearly three decades have transpired since Ed Turner at Wright-Patterson AFB reported on the development of a spiral slot antenna.[1] Since that time the state of spiral antenna technology has been advanced considerably. In the late fifties and early sixties efforts of Turner, Kaiser, and many others[2-4] contributed greatly to the understanding and optimization of the Archimedian spiral antenna. During the same time period, Dyson, Mayes, and others[5-7], particularly at the University Of Illinois, applied Rumsey's frequency - independent concepts to spiral structures, giving impetus to the development of the planar and the conical equiangular (logarithmic) spiral antennas. Throughout the period of 1955-1970 contributions from a number of sources greatly enhanced the spiral's theoretical and experimental development.

In the late sixties and seventies, emphasis shifted from spiral antenna development to applications. Because of its unique attributes - broad frequency bandwidth, wide field-of-view, circular polarization, multi-mode capability, and relative simplicity - the spiral antenna found extensive application, particularly in advanced defense electronic systems. As the technology matured and became

more application oriented, the technological advances became less dramatic. In the last decade the advances have been subtle, but none-the-less important in optimizing performance of broadband systems.

This paper describes some of these subtle advances - concentrating on hybrid spiral structures, use of advanced electromagnetic absorbing materials, upper frequency extension, and low-cost production.

2.0 HYBRID SPIRAL STRUCTURES

The lower operating frequency of a spiral antenna is limited by physical size constraints imposed upon the antenna. Considerable effort has been expended to extend the lower operating frequency while maintaining a constrained aperture. Some of these efforts, such as dielectric loading, magnetic loading and modulated arm widths, have been only moderately successful and have not achieved a significant degree of lower-frequency extenstion. Another technique, implemented by Texas Instruments and others, involves the use of hybrid spiral structures.

One such hybrid structure, the planar/conical spiral, is pictured in Figure 1. The planar/conical antenna is a logical merger of planar spiral and conical spiral technology. The antenna shown is a four-element (dual-mode) antenna which draws on the strengths of both planar and conical geometries. The conical spiral

has an advantage that, for a given diameter, it can be designed to operate at a lower frequency than its planar counterpart. This is illustrated in Figure 2 which contrasts the low-frequency patterns of a dual-mode planar spiral and a planar/conical spiral of similar diameter. Note the degraded difference pattern of the planar antenna. The planar spiral, on the other hand, generally has a higher upper frequency limit than does the conical spiral (Figure 3) which is attributed to less feed cable-to-spiral coupling with the planar geometry. The resulting hybrid planar/conical spiral antenna performs well over a 26:1 frequency bandwidth while main-maintaining a 5.5 inch maximum diameter.

Another hybrid geometry commonly used is the planar spiral/ helix antenna. Figure 4 shows a single-mode 2 inch diameter spiral/ helix antenna designed to operate over a 0.7 to 18 GHz frequency band. The helix is 1 inch in length and has 1 1/2 turns. Low-end performance data compared to a conventional 2 inch diameter, cavity-backed planar spiral is shown in Figure 5. The conventional antenna, designed to operate at over a 2 - 18 GHz range, works fairly well to 1.6 GHz. At lower frequencies the polarization ellipticity degrades greatly as shown by the 1.4 GHz pattern. The spiral/helix antenna maintains axial ratios of less than 2 dB to 0.7 GHz.

A slightly different type of hybrid spiral is the dual planar archimedian-logarithmic (Arc-Log) spiral pictured in Figure 6. This hybrid antenna takes advantage of a tigh ly-wound Archimedian

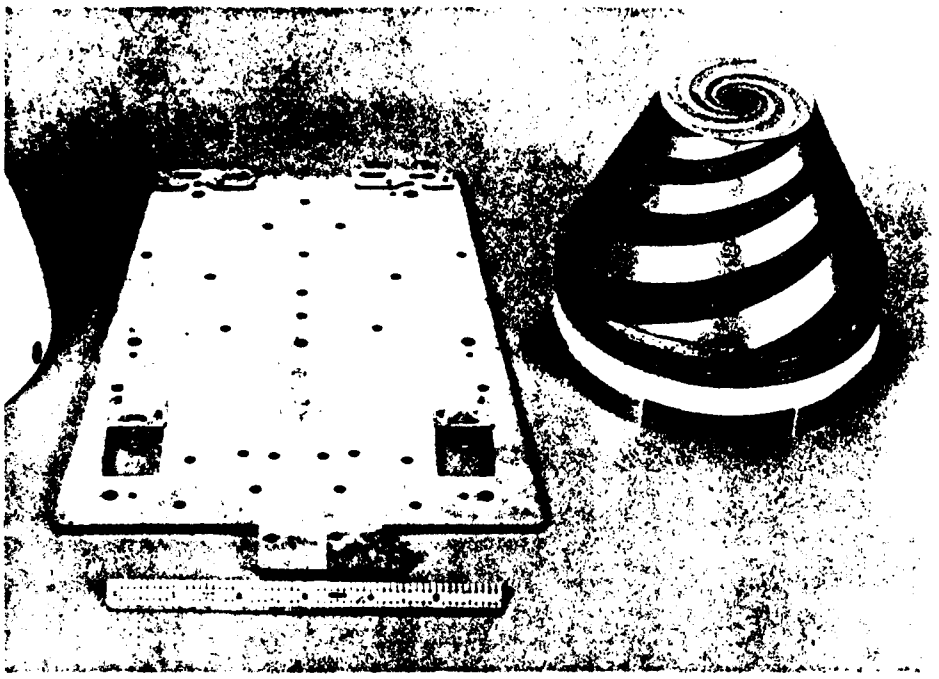

Figure 1. Planar/Conical Spiral Antenna
with RF Processor

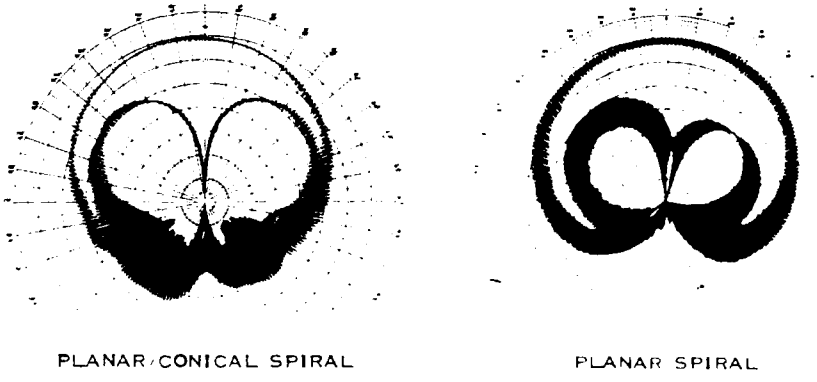

Figure 2. Planar/Conical Spiral vs. Planar Spiral
Pattern Comparison, Dia. = 5.5 Inches
F = 0.9 GHz, Rotating Linear Polarization

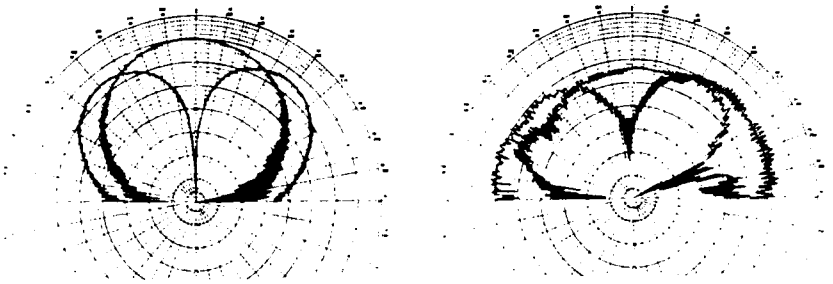

Figure 3. Planar/Conical Spiral vs. Conical Spiral
Pattern Comparison
F = 12 GHz, Rotating Linear Poliarization

Figure 4. Two-inch Diameter Planar Spiral/Helix Antenna

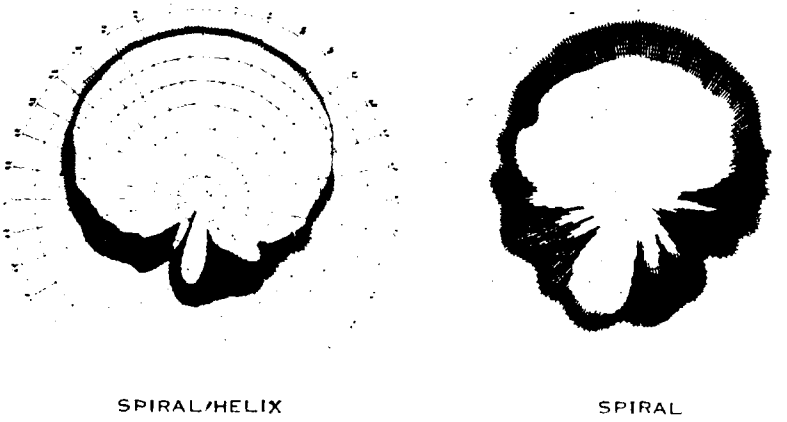

Figure 5. Spiral/Helix vs. Spiral Pattern Comparison
Dia. = 2 Inches, F = 1.8 GHz
Rotating Linear Polarization

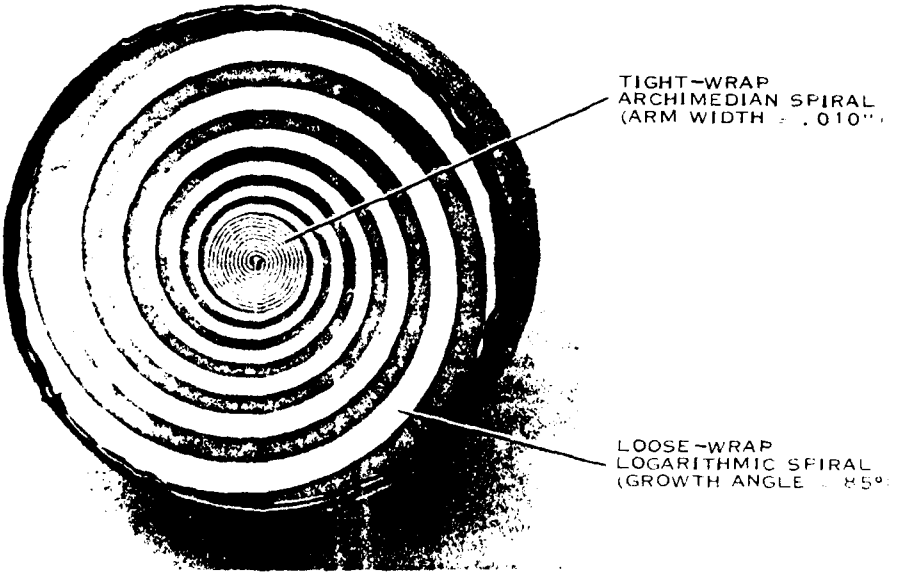

Figure 6. Arc-Log Spiral

spiral which enhances the high-frequency performance and the looser-wrapped log spiral which decreases copper losses and enhances low-frequency gain. These tendencies are exemplified in Figure 7 which shows Ku-band pattern comparison of a log-spiral and the hybrid arc-log antenna and Figure 8 which compares gain for the archimedian spiral and the hybrid structure. In Ku-band the loose-wrapped spirals have slightly more beam skew and off-boresite axial ratio than do the more tightly wound spirals. At the low-end of the operating band, the loose-wrap spirals have several dB higher gain. The Arc-Log configuration combines the advantageous features of both.

3.0 ADVANCED MICROWAVE ABSORBERS

One component of a spiral antenna which has a significant performance impact and yet which is one of the least understood in terms of design techniques is the cavity absorber. Most practical implementations of spiral antenna designs require a cavity or metallic wall backing. Cavities are resonant structures and to achieve broadband performance the resonances must be eliminated or minimized. This can be accomplished by use of microwave absorbing material.

Design procedures for the cavity absorber are varied. Often a "cut and try" experimental procedure is used to obtain optimum performance. Usually a "free-space" absorber is employed in which the impedance at the absorber air interface is matched to free-

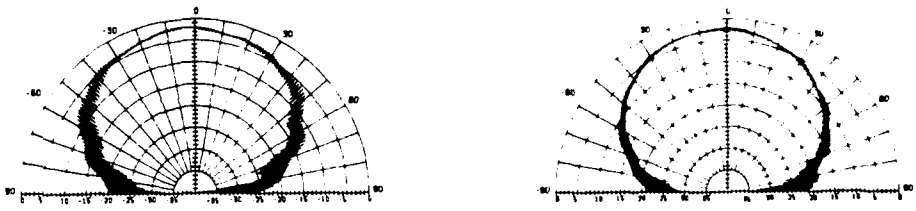

ARC-LOG SPIRAL

LOOSE-WRAP LOG SPIRAL

Figure 7. Arc-Log Spiral vs. Loose-Wrap Spiral
Pattern Comparison
F = 18 GHz, Rotating Linear Polarization

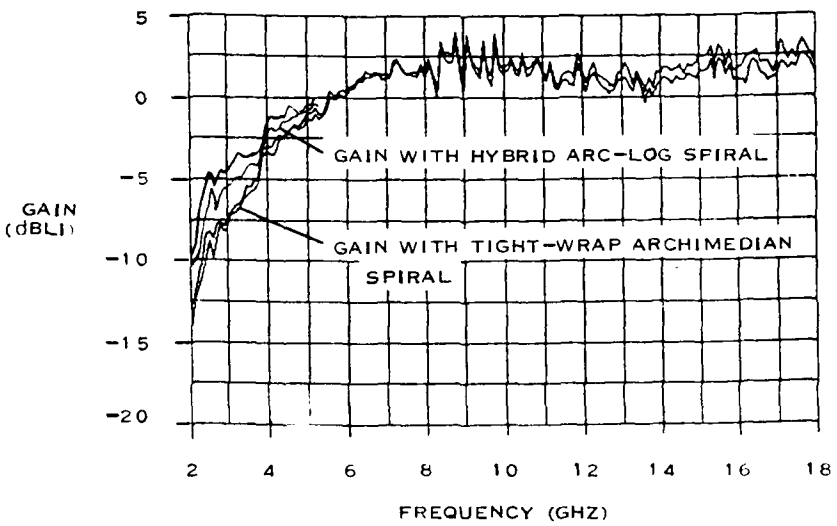

Figure 8. Hybrid Arc-Log Spiral vs. Archimedian Spiral
Gain Comparison
Dia. = 2.5 Inches, Max/Min Polarization

space to minimize reflections. This type of absorber is available from absorber vendors and in some instances "off-the-shelf" absorbers can be successfully implemented in the spiral cavity.

Recent advances in microwave absorber material and processes allow the spiral antenna designer added flexibility in meeting performance. Custom material made from various resins (epoxy, silicon, polybutadiene, etc.) and loaded with various combinations of carbon, microballoons, and ferrite materials have a wide range of electrical properties. An example of how custom absorbers can be applied to a planar spiral antenna is shown in Figure 9. This shows a cut-away view of a 2 inch diameter antenna cavity that is loaded with six disks, each 0.125 inch in thickness. The top layer is of low-dielectric constant foam and the other layers are of carbon and microballoon-loaded silicon. The microwave absorption characteristics of each layer increase from top to bottom. This custom graded configuration gives a "free-space" or low reflection cavity absorber.

A gain versus frequency plot for this custom cavity configuration is shown in Figure 10. The gain over most of the band is flat, indicating cavity reflections have been eliminated. At the low frequencies the gain roll-off is typical of a size-restricted spiral antenna. Superimposed over this c e is the gain from the same antenna with the cavity configuration modified. In this latter case the cavity contains three .25 inch layers - one of foam,

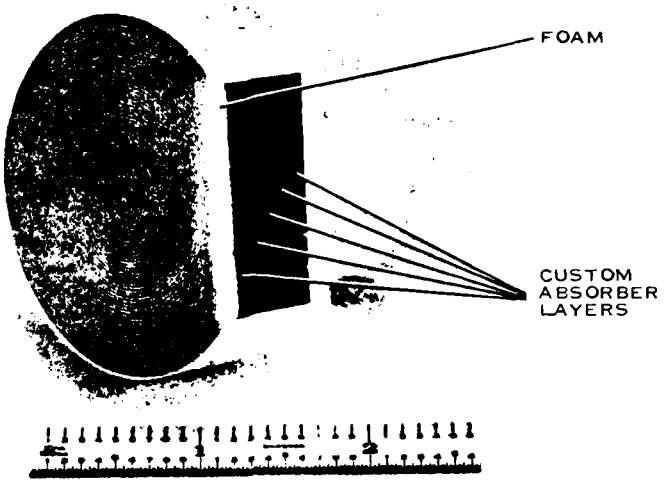

Figure 9. Planar Spiral Antenna Showing Custom Cavity Absorber Configuration

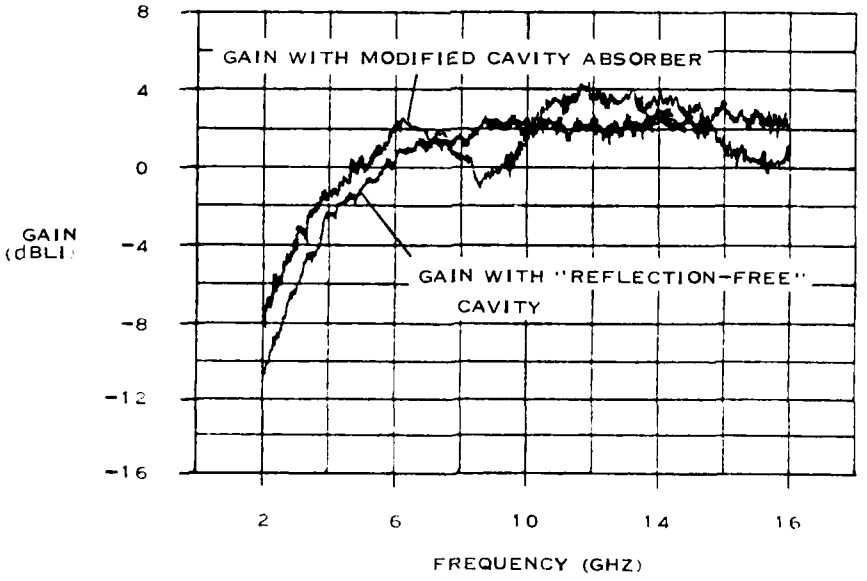

Figure 10. Gain vs. Frequency for Planar Spiral Antenna Showing Impact of Cavity Absorber Configuration

one with a silicon/carbon/iron/microballoon composition, and the bottom with a silicon/carbon/microballoon load. This illustrates the performance dependency of the spiral on the cavity load and how the performance can be optimized over portions of the frequency band.

Other examples of custom absorber use are shown in Figures 11 and 12. Figure 11 shows a concentric ring absorber that is used as a single-piece, free-space absorber for a planar spiral. Figure 12 depicts the custom absorber configuration for the planar/conical spiral antenna. Properly designed absorer loading is of key importance to maintaining uniform broadband electrical performance for both planar and planar/conical antennas.

4.0 UPPER-FREQUENCY EXTENSION

In a previous section it was stated that the spiral antenna lower operating freuqency is limited by size constraints imposed upon the aperture. The upper operating frequency is theoretically unlimited, but is practcally limited by physically realizable feed geometries. The "current band" theory of spiral antenna operation states that mode 1 radiation occurs from an active region centered about a one wavelength circumference band. As frequency increases, the radiating ring shrinks towards the feedtip. When the active region and the excitation region become near-coincident, the performance degrades. Thus, manufacturing tolerances and the capability

Figure 11. Annular Wedge Absorber

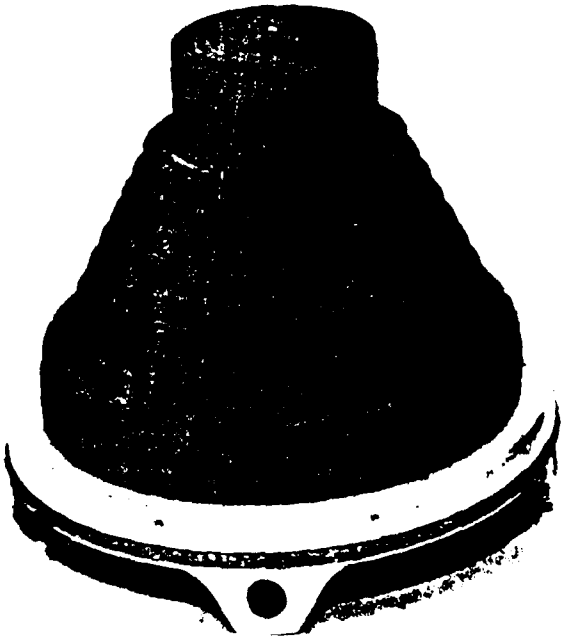

Figure 12. Custom Absorber Configuration for Planar/Conical Spiral

TECHNICAL FEATURES

- PLANAR ARCHIMEDIAN SPIRAL
- 0.5" DIAMETER
- CIRCULARLY POLARIZED
- DOUBLE-RIDGE WAVEGUIDE INPUT
- ABSORBER-LOADED CAVITY
- FREQUENCY: 12-40 GHZ
- GAIN: -5 TO +2 dBLI
- -3 dB BEAMWIDTH: 60° -90°
- AXIAL RATIO: <2 dB @0°

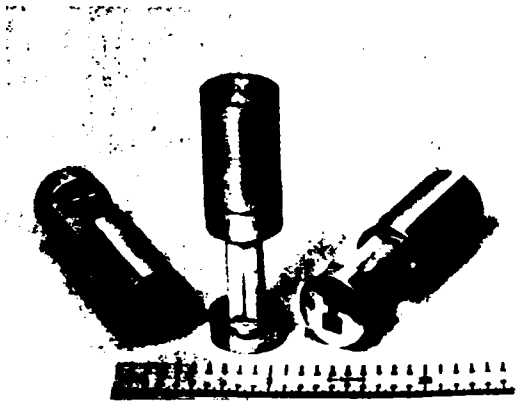

TYPICAL PATTERNS

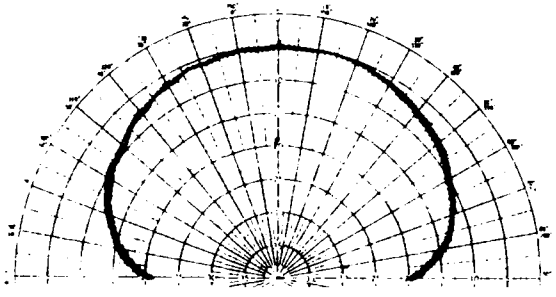

F = 12 GHZ

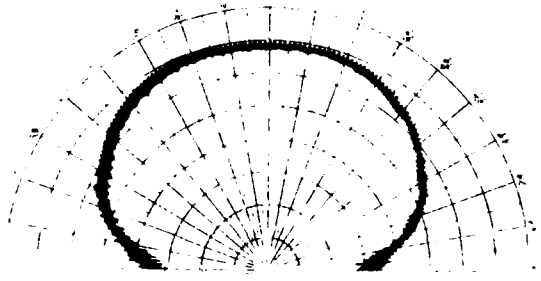

F = 39 GHZ

Figure 13. J-K Band Spiral Antenna

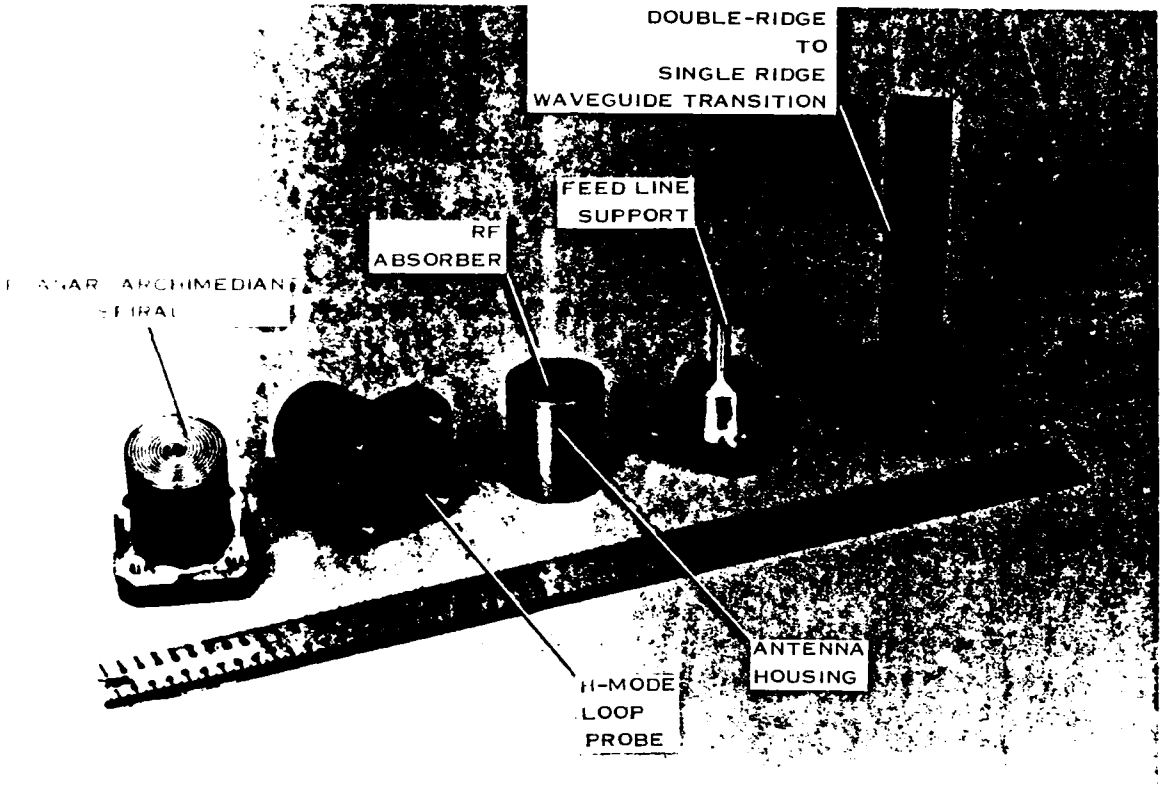

Figure 14. J-K Band Spiral Antenna Construction

to shrink the feedtip are the ultimate high frequency limiting factors.

Another limiting factor is the means of spiral excitation. Conventional methods employ coaxial and stripline baluns and feed networks. These can have very high losses due to material and copper losses and moding problems. This excitation limitation can be overcome by use of waveguide feeds. An example of a waveguide-fed spiral is shown in Figures 13. This shows a photograph and typical patterns of a 0.5 inch diameter, planar archimedian spiral with a dual-ridge waveguide (WRD124C36) input. The antenna operates over a 12 - 40 GHz with performance typified in the figure. Gain and axial ratio are very typical of a spiral antenna. The gain varies from -5 to +2 dB with respect to linear isotropic and the maximum axial ratio is 2 dB. Figure 14 shows the antenna construction. The unique characteristic of this antenna is the loop probe which in employed as a balun. This probe acts as a transition, coupling energy from the ridged waveguide to the balanced spiral feed.

5.0 LOW-COST PRODUCTION TECHNIQUES

One final area for consideration that is having a significant impact on spiral antennas is the advancement of manufacturing and production technology. Advancement of these technologies is primarily motivated by the demand for less expensive systems, particularly in high volume. Table 1 lists several spiral antenna production cost drivers - metallic part fabrication, circuit fabrication,

TABLE 1

SPIRAL ANTENNA PRODUCTION TECHNIQUES

PRODUCTION COST DRIVERS	CURRENT PRODUCTION METHOD	LOW-COST ALTERNATIVE
METALLIC PART FAB	MACHINED OR CAST	INJECTION-MOLDED, PLATED PLASTIC
CIRCUIT FAB	CONVENTIONAL PHOTO-RESIST, ETCH PROCESS	COMPUTER-CONTROLLED LASER ETCH
ABSORBER FAB	MACHINED OR CAST	INJECTION-MOLD
ASSEMBLY	MANUAL	ROBOTICS
TEST	MANUAL	AUTOMATED

absorber/dielectric fabrication, assembly, and test. For each cost driver the current production method and a low-cost, high-volume production alternative is tabulated. These alternatives are under various states of consideration and implementation by Texas Instruments. Robotic assembly as applied to spiral antennas is very much in the conceptual stage. Automated test and evaluation, on the other hand, has been fully implemented by TI and many other companies for several years.

Detailed description of all the low-cost production techniques is beyond the scope of this article. However, the use of injection-molded metallized plastic parts is illustrative of how recent

manufacturing innovations can be applied to the spiral. Plastic and composite materials have found countless applications in recent years, particularly in the consumer market where cost tends to be the significant factor. Application of similar low-cost techniques is inevitable as defense systems become increasingly cost conscious.

A prototype spiral antenna, built to demonstrate the manufacturability and the electrical and environmental feasibility of the low-cost spiral technique is shown in Figure 15. The housing is made of an injection molded plastic (ABS) which has been metallized with a nickle paint. Electrical performance data is shown in Figures 16 and 17. The former shows pattern data from 2 to 18 GHz in 4 GHz steps, while the latter shows a gain vs. frequency curve taken at the antenna peak-of-beam. Performance is typical of that of a conventionally fabricated spiral.

6.0 CONCLUSION

The spiral antenna - a revolution three decades ago - is now in an evolutionary state. Changes and refinements are being made, and until such time that the spiral antenna is completely understood, the performance fully optimized, and the cost greatly reduced, advances and improvements in spiral technology will continue to slowly evolve.

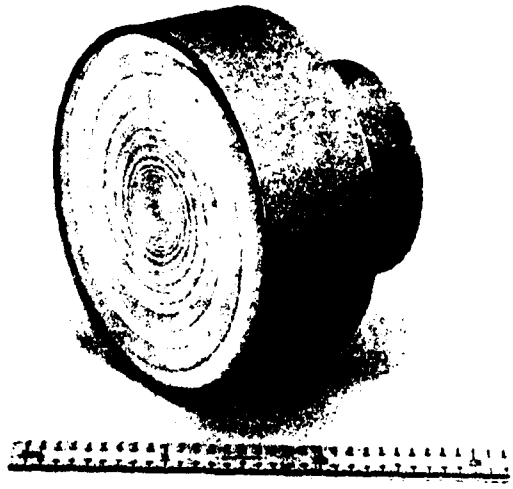

Figure 15. Planar Arc-Log Spiral with Metallized, Non-Metallic Housing

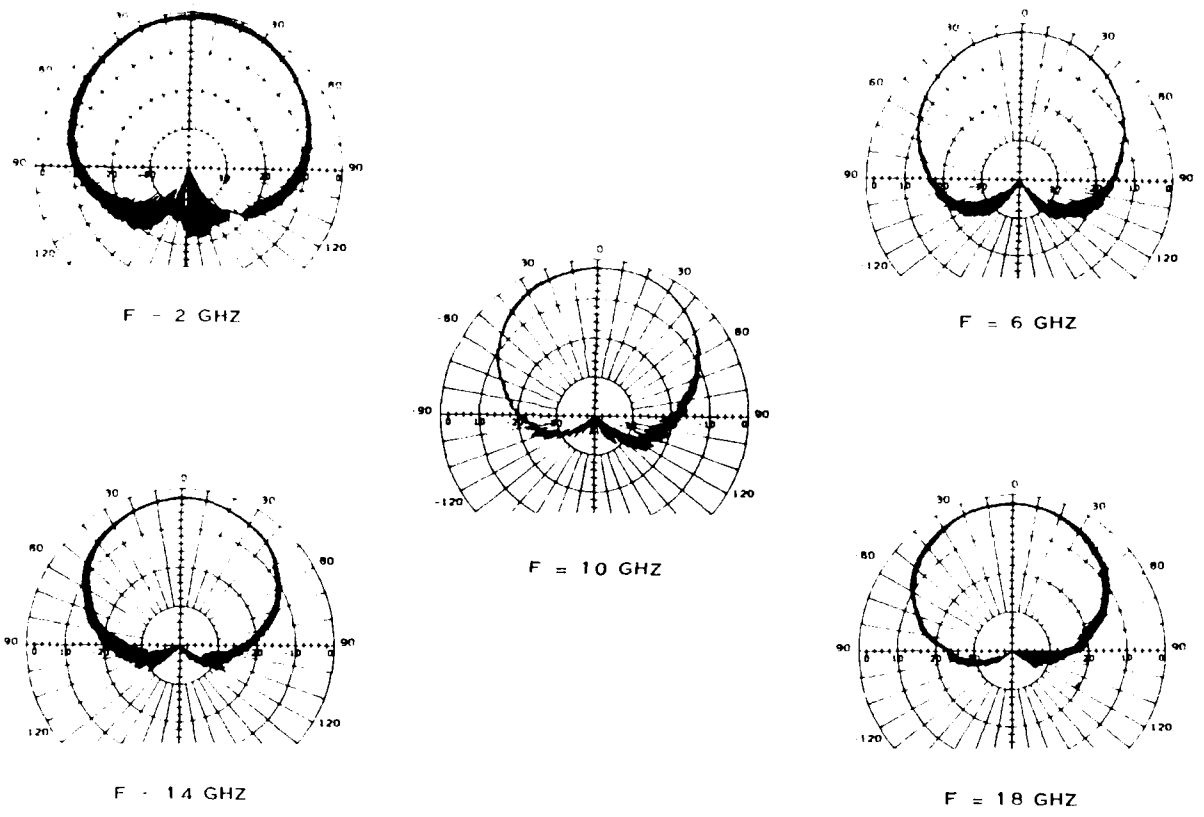

Figure 16. Antenna Patterns for 2.5-inch Spiral Antenna with Metallized Plastic Housing

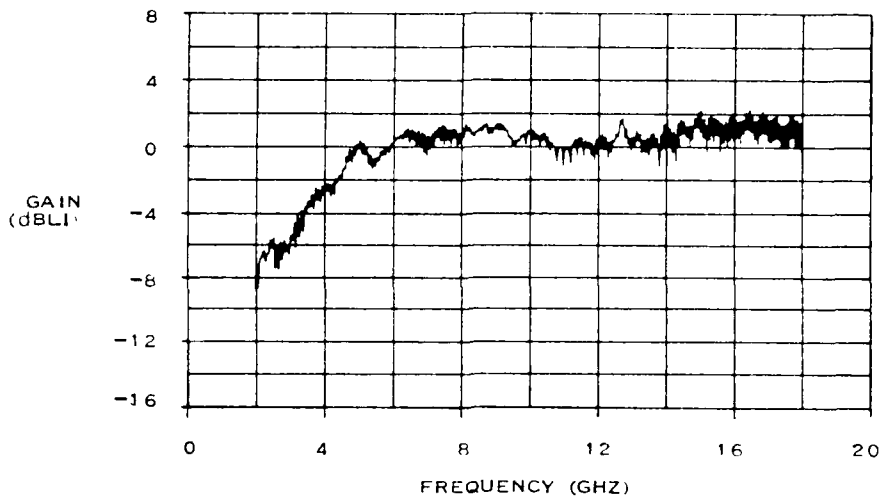

Figure 17. 2.5-inch Non-Metallic Antenna
Gain vs. Frequency
Rotating Linear Polarization

REFERENCES

[1] E.M. Turner, "Spiral Slot Antenna," Wright-Patterson AFB, Ohio, Tech. Note WCLR-55-8 WADC; June, 1955.

[2] B.H. Burdine and R.M. McElvery, "The Spiral Antenna," Massachusetts Inst. of Tech., Cambridge Res. Lab. of Electronics, Rept. Nos. 1 and 2.

[3] J.A. Kaiser, "The Archimedian Two-Wire Spiral Antenna," IRE TRANS. ON ANTENNAS AND PROPAGATION, pp. 312-322; May, 1960.

[4] W.L. Curtis, "Spiral Antennas", IRE TRANS. ON ANTENNAS AND PROPAGATION, pp. 298-306; May, 1960.

[5] J.D. Dyson, "The Equiangular Spiral Antenna", IRE TRANS. ON ANTENNAS AND PROPAGATION, Vol. AP-7, pp. 181-188; April, 1959.

[6] P.E. Mayes and J.D. Dyson, "Multi-Arm Logarithmic Spiral Antennas", Univ. of Illinois, Technical Report No. 46, Contract AF33(616)-6079, June, 1960.

[7] J.D. Dyson, "The Characteristics and Design of the Conical Log-Spiral Antenna", IRE TRANS. ON ANTENNAS AND PROPAGATION, Vol. AP-13, No. 4, pp. 488-499, July, 1965.

DESIGNING ANTENNAS TO PRICE; OR THE ECONOMICS OF ANTENNA DESIGN

Prepared By

George J. Monser
Raytheon Company
Electromagnetic Systems Division

Prepared For

Antenna Applications Symposium
Allerton Park, Illinois

September 21-23, 1983

ABSTRACT

Designing Antennas to Price; Or the Economics of Antenna Design

By George J. Monser

The paper highlights, by example, trade-offs leading to a cost-effective design. Parameters and tolerance for cost versus machined array elements are discussed leading to a projected production cost of under $50.00 per array element.

DESIGNING ANTENNAS TO PRICE; OR

THE ECONOMICS OF ANTENNA DESIGN

By George J. Monser
Raytheon Company
Electromagnetic Systems Division

1.0 INTRODUCTION

Economics holds a dominant position in today's defense market with more and more military contracts emphasizing a design-to-price philosophy.[1] This paper extends the philosophy of design to price as it pertains to antennas.

2.0 CANDIDATE SYSTEM

As a means of describing the significance of design-to-price, it is most effective to consider a candidate system[2] with a fixed system price. The contractor submits a system design and details the design as shown in Figure 1. Each of the major blocks, including the antennas, are assigned bogey cost limits. If all the bogey costs are summed the cost per system will be met. When such cost partitioning is performed, the antenna cost allocation usually falls within 2 to 5 percent of the system cost.

Using the system design in Figure 1 as an example, it was determined from system analysis that about 100 array elements would suffice; 40 for the transmit array and 60 for the receive array. From the system cost and budgeted antenna cost, a projected production unit cost per array element of $[illegible] was derived.

3.0 DETAILED CONSIDERATIONS

Various candidates were considered for the array elements versus the performance requirements. These trade-offs lead to the selection of horn elements arranged in an H-plane array configuration (Figure 2). Horns were preferred since significant gain per element could be readily achieved in an array by forming sectoral horns, thus reducing the number of TWTs in the transmitter and CVRs in the receiver. In addition, horn preference was enhanced since it is adaptable to casting and reduced cost.

With casting in mind, an analytical and empirical parametric study was conducted to evaluate the sensitivity of the design to casting methods. It was known that tolerances of about $\pm$ 0.003 to $\pm$ 0.005 and draft angles of a few degrees (for extraction from the mold) were necessary. From this study effort, it was concluded that the calculated cut-off wavelengths and impedances of original and cast designs would be sufficiently alike (within 4 percent) and that no changes of interior horn dimensions, including the double-ridged launcher section, would be required. These findings were further supported by measuring element gain and VSWR for both design dimensions and modified dimensions. While the 4 per cent change in calculated impedance and the departures in gain

for dimensional changes (on the order of 0.5 dB) appeared significant; the overriding and smoothing effects of the array indicated performance would be maintained.

4.0 COST ANALYSIS

The wrought material machined element cost was estimated for the first small production run at $30.00 per element as compared to the cast element of $10.00 per element plus a one-time tooling cost of $17K. Adding $10.00 per element for "touch labor" in assembly and $25.00 per element for test, the total was within the bogey price of $50.00 each.

5.0 CONCLUDING REMARKS

This paper has emphasized some of the economic aspects of designing antennas to price. It has shown that by using cast methods for the fabrication of horn array elements, significant cost savings can be achieved without compromise in performance.

References:

1. Crecraft, H. E. (March 1982) Shipboard EW Systems, Journal of Electronic Defense, pp 61-72.

2. Archer, D. H. and Black, A. A. (March 1982) Higher ERP with Lens-Fed Multibeam Arrays, Journal of Electronic Defense, pp 51-58.

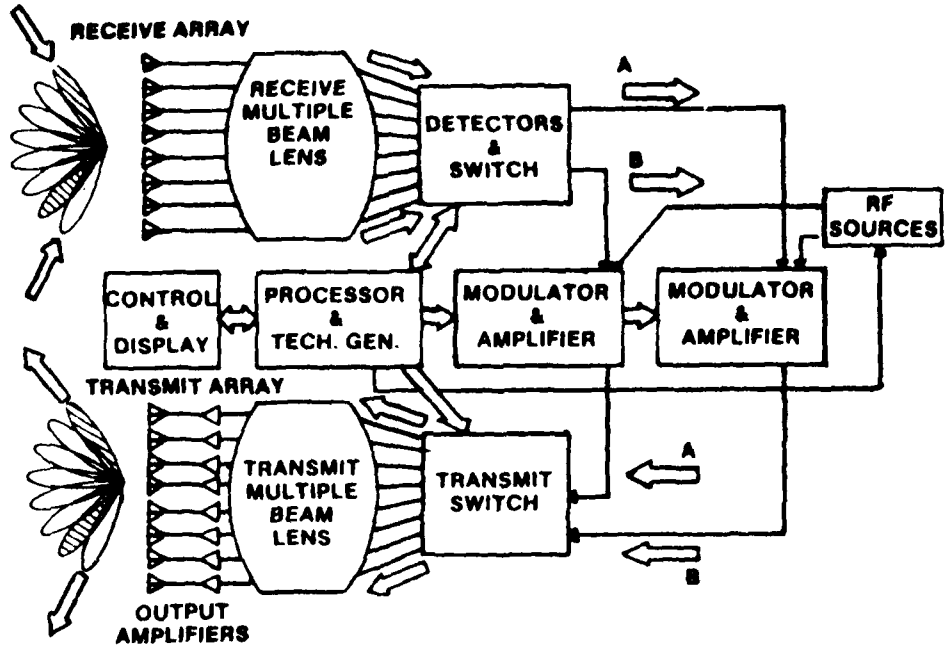

Figure 1. Multibeam Integrated ESM/ECM System (With Switched Interconnection)

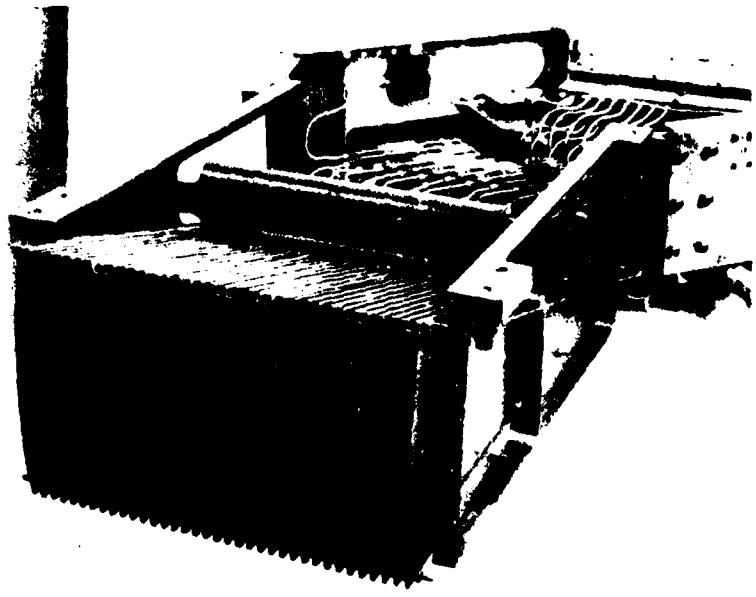

Figure 2. Transmit Array

REBUTTAL TO "FLOATING A SATELLITE ON MICROWAVES"

Presented by :
Harold Shnitkin
Norden Systems, Inc.
Norwalk, CT 06856

Prepared for :
Electromagnetic Sciences Division
Rome Air Development Center
USAF Systems Command
and
Electromagnetics Laboratory
Department of Electrical Engineering
University of Illinois
Urbana, Illinois 61801

AUGUST 1983
X55125

REBUTTAL TO "FLOATING A SATELLITE ON MICROWAVES"

Harold Shnitkin

Norden Systems, Inc.

Norwalk, CT 06856

ABSTRACT

Earlier this year, I came across an interesting article appearing in the Electronic Engineering Times (January 3, 1983) entitled: "Floating a Satellite on Microwaves Advanced by Stanford Research." (Ref. 1) This article discusses a scheme of floating a passive microwave reflector about 100 miles above the surface of the earth by means of microwaves radiated from the ground. The reflector is to bounce microwave signals between two points, 1000 miles apart, for communication purposes. The satellite is claimed to measure about 30 feet in diameter, weigh less than one-tenth of a gram, and operate between 500 KHz and 10 GHz. At this time, a company called Electronics Missiles and Communications Inc. is planning to put $6 million into the project to be carried out at SRI.

This proposed "space mirror", which is hoped to become a low-cost alternative to the complex communications satellites now orbited, has been examined in greater detail, resulting in a number of technical disagreements between the author and the proponents of the "space mirror."

The body of the paper is a rebuttal of the technical claims for the performance of the space mirror made in the referenced article.

Counter arguments are presented in the areas of transmitted power, radiation hazard, structural stability tolerance, and skin depth.

1. Introduction

On January 3, 1983, an article appeared in the Electronic Engineering Times, about a lightweight, passive satellite, held in very low geosynchronous orbit by microwaves radiated from the ground, which is to be used for bouncing communications signals off the satellite to communicate between two ground stations a thousand miles apart. (Ref. 1) The inventor, Dr. Paul Csonka, states that this satellite, which he calls the "space mirror," will weigh less than one tenth of a gram, will be 30 feet in diameter, and will be constructed as a paraboloid shaped mesh made of wires a few hundred angstroms thick. The company holding the patent rights and funding its development, namely, Electronic Missiles and Communications Inc., is planning to put $6 million into the project in the hope that the satellite will become a low cost alternative to the complex communications satellites now orbiting.

Dr. Julius J. Murray, Director of the project at SRI, states that technical feasibility of the space mirror has been demonstrated and that no new technology is needed to build and operate such a device. It is further claimed that the eventual full-sized 30 foot diameter mirror will handle frequencies ranging from the AM band up to 10 GHz and that the wire mesh spacing will be approximately one-fifth of a wavelength. The satellite mirror will be kept in a very low geosynchronous orbit (between 65 and 125 miles) by 600 kw of microwave energy radiated from the ground. Both, Dr. Julius J. Murray and Dr. Paul Csonka, believe that a mirror stability, the radiation

hazard of airplanes flying through the beam and the signal efficiency are adequate for the planned communications link. Figure 1 shows a diagram, reproduced from the subject article, which is to illustrate the concept.

Obviously a device, which without active elements could provide communication between stations 1000 miles apart, would provide an extremely valuable service at a much lower cost than that of active repeaters now in service. But will it work? Let us examine the ideas in detail, using basic antenna theory, in order to refute some of the claims made for the invention.

2. Configuration

The configuration reproduced from the reference article and shown in Figure 1 is misleading. The true contour of a surface of a reflector to communicate between T/R #1 and #2 would not be a paraboloid but an ellipsoid. However, for a station separation of 1000 miles and only a 30 ft. diameter reflector, the surface of this ellipsoid would degenerate into a flat plate. I took the liberty of redrawing Figure 1 to its proper scale to indicate the various dimensions and relative sizes of its components in Figure 2. Now let us examine a number of technical claims made by the inventors using Figure 2 as a reference. It is possible to examine performance by means of the scattering equations for a flat plate with the 79 degree incidence angle for the communications signal, shown in Figure 2.

3. Antenna Size vs. Transmitted Power

At 65 miles altitude a 30 foot diameter disk will subtend an angle of .005 degrees to the microwave transmitter lift antenna, designated by "L" in Figure 2.

If spillover is to be minimized in order to achieve the 100 kw of RF power required at the satellite to maintain its orbit, a 2000 foot diameter antenna would be needed at the upper frequency of 10 GHz. This antenna size appears rather impractical in light of surface tolerances, cost and required beam pointing stability, so that a more practical antenna size of only 100 foot diameter should be assumed. However, the resulting spillover of an antenna only one-twentieth size requires that the radiated power be increased by 400 times the 100 kilowatt value required at the satellite, namely, 40 megawatts. Obviously, a dilemna exists here between choice of antenna size and radiated power requirements.

4. Radiation Hazard

If 100 kilowatts of RF energy impacts upon the 30 foot diameter satellite to keep it at a 65 mile altitude orbit, a surface power density of 150 milliwatts per square centimeter will exist at the satellite. Assuming that power density in the far field of an antenna attenuates as the square of the range, 15,000 milliwatts per square centimeter would exist at 6.5 miles or 34,000 feet altitude.

Since 6.5 miles corresponds to about $.45D^2/\lambda$, the above values are reasonably accurate. I find it difficult to agree with Dr. Csonka's statement, that these radiation levels "will be low enough so as not to be harmful."

5. Structural Stability

Now let me mention an item of which the author does not speak at all, namely, mechanical stability of the reflector. The mirror's reradiation efficiency would degrade rapidly should its flat shape be distorted. Realizing that at 10 GHz, a wavelength equals 1.2 inches, mechanical stability in the neighborhood of $\pm$ 0.8 inch will be required to maintain a $\pm$ 90 phase error limit. (See Appendix 1.) It is difficult to visualize how an earth generated microwave beam traveling 65 miles into space could possibly maintain a 30 foot diameter wire mesh of several hundred angstrom thickness within this flatness tolerance! Whatever happened to consideration of (1) structural strength of extremely thin wires, (2) non-uniform thermal exposure, (3) uniformity and stability of the microwave lifting energy, and (4) perturbation by radiation or particles in space?

6. Skin Depth Considerations

At a frequency of 10 GHz, the proposed reflector wire diameter of "a few hundred angstroms," constitutes about one thirtieth of a skin depth (aluminum and 300 angstroms assumed). To compute the current induced in a thin conductor and to compare this result with an infinitely thick conductor, one must perform an integration of the current density function, as follows:

$$i = i_o \exp(-y/s) \qquad (1)$$

(Reference 2)

Where i_o is the induced current density at the conductor surface

y, the distance into conductor

s, the skin depth

thus,
$$\frac{\int_0^{ks} i\,dy}{\int_0^{a} i\,dy} = \frac{-i_0\, s[\exp(-k)-1]}{-i_0\, s\,(0-1)} \qquad (1)$$

For small values of k, the above function reduces to k, the conductor thickness, expressed in skin depths.

Thus the reflection efficiency (or skin depth loss) of a one-thirtieth skin depth thick conductor is -30 dB in comparison to a thick conductor, by setting K = 1/30. To obtain values of skin depth loss at other frequencies one must recall that skin depth is proportional to $\sqrt{\ }$, and therefore deduce a variation of 3 dB per octave. (Reference 2)

7. Communication Efficiency

In this section, I wish to discuss a computation for the total transmission loss encountered between two earth stations one thousand miles apart. Making reference to Figure 2, as well as to the derivation for the two-way space loss given in Appendix 2, a tabulation of all applicable losses can be prepared. Starting with the 79 degree angle of incidence, a two-way projected area loss of 14 dB must be allowed. Aperture surface tolerances of $\pm$ 0.8 inches result in a phase error loss of 6 dB, (2-ways). Quoting from the authors article, a one-way atmospheric loss of 6 dB or 12 dB two-way must be allowed. In addition, as shown in the Section 6, entitled Skin Depth Considerations, the efficiency of a reflector containing wires several hundred angstroms thick will be -30 dB at 10 GHz. Finally, applying scattering equations to a normally oriented specular flat-plate

scatterer, a total free space attenuation of 86 dB (2-way) has been computed in Appendix 2 for 100 foot T/R antennas. Summing up all contributing signal attenuation factors yields a total of 148 dB.

If one were to assume typical values, such as signal-to-noise ratio of 30 dB, a noise figure of 4 dB and a signal bandwidth of 20 MHz, a required received signal level of -67 dBm would result. This would yield a required transmitter power of +81 dBm or 125 kw at 10 GHz. It thus appears that, unless the antenna size were increased, the power requirements at the 10 GHz frequency are somewhat high. But what about the claim that this "space mirror" can be used at a 1 MHz frequency? According to eq. (8) of Appendix 2 at 1 MHz free space attenuation increases by 280 dB and according to eq. (1), skin depth loss increases by 70 dB. This, of course, would lead to unrealizable values of RF power or antenna size.

8. Conclusion

In light of the technical arguments presented, there appears to be considerable doubt in my mind as to whether this project could result in a successful satellite communication system. One might begin to wonder whether the reporter or those investing $6 million into this project have taken the necessary time to examine its merits in detail.

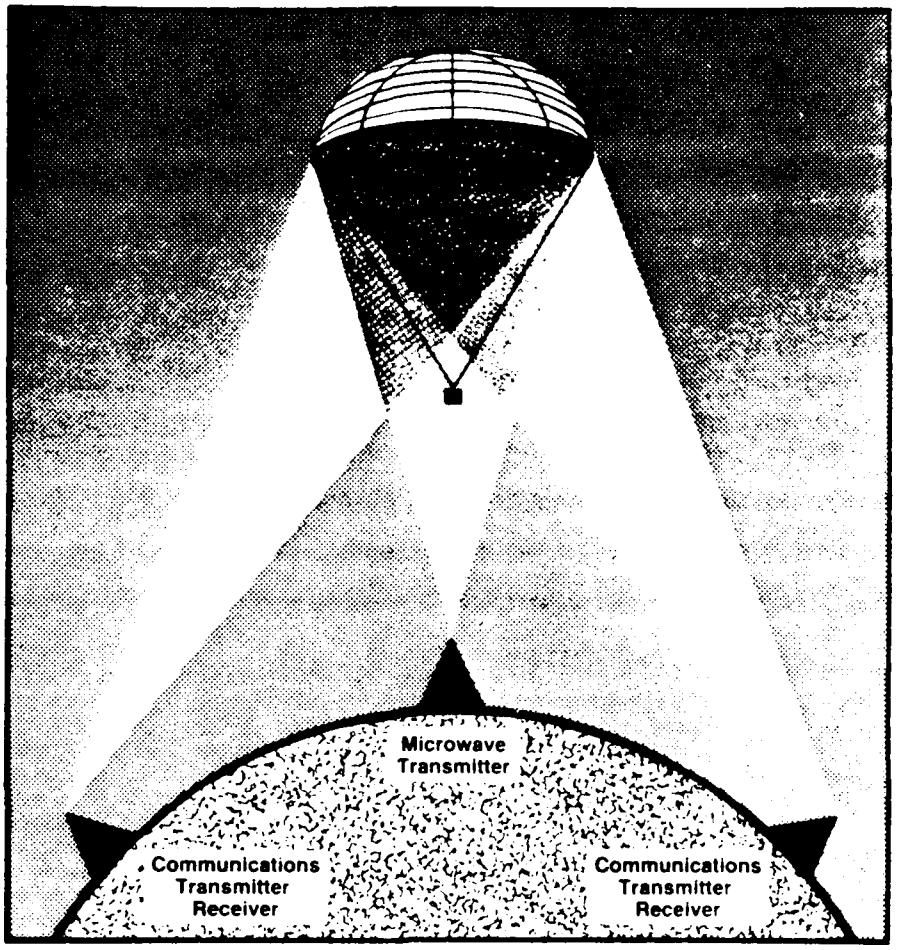

A sub-scale version of a "Space Mirror," a mesh of wires a few hundred angstroms thick with a parabolic shape used to bounce communications, is being developed at Stanford Research Institute. The eventual Mirror will be kept between 65 and 125 miles altitude by microwaves radiated from the ground.

Figure 1. Original Illustration of System Configuration

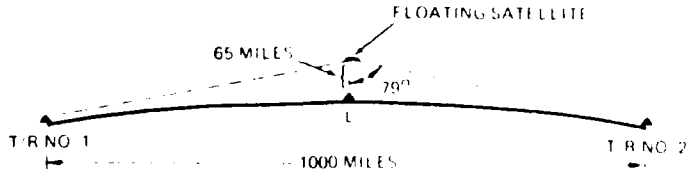

Figure 2. System Configuration Re-Drawn to Scale

APPENDIX 1

PHASE ERROR CAUSED BY DEVIATION FROM FLATNESS

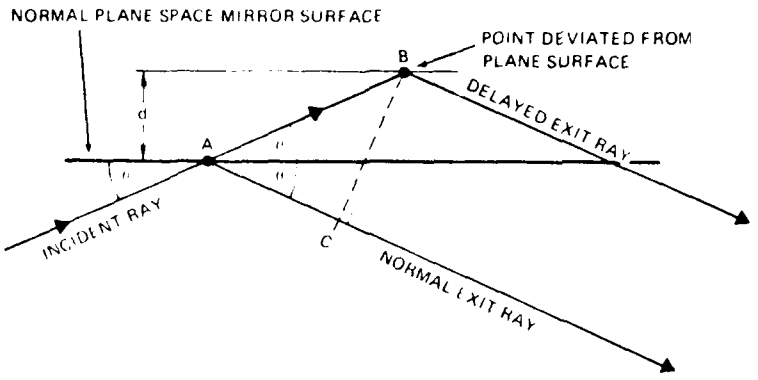

$$\overline{AB} = d/\sin \theta \tag{2}$$

$$\overline{AC} = \overline{AB} \cos 2\theta \tag{3}$$

$$\text{Space delay} = \overline{AB} - \overline{AC} = \frac{d\,(1 - \cos 2\theta)}{\sin \theta} \tag{4}$$

If maximum phase error of 90 degrees is allowed at 10 GHz, then space delay equals 0.3 inches.

Since, from Figure 2, $\theta = 11°$, it follows that d = .79 inches. Consequently, d, the maximum deviation from a flat surface, equals 0.79 inches.

APPENDIX 2

FREE-SPACE ATTENUATION COMPUTATION

$$\text{Two-way, free-space attenuation} = \frac{G_1 \sigma A_2}{(4\pi R^2)} \qquad (5)$$

(Reference 3)

Where G_1 is antenna gain of Station #1 (Figure 2)

A_2 is effective antenna area of Station #2

σ is scatter crossection of mirror, normal incidence

R is distance to mirror (500 miles).

$$\text{But} \quad = 4\pi (A_m)^2/\lambda^2 \quad \text{and} \qquad (6)$$

$$G_1 = 4\pi A_2/\lambda^2, \qquad (7)$$

$$\text{Consequency, 2-way free space attenuation} = \frac{(A_2)^2 (A_m)^2}{\lambda^4 R^4} \qquad (8)$$

Evaluated for a 100 foot diameter, 65% efficient ground antenna, a normal 30 foot diameter mirror, 10 GHz frequency, and 500 miles, yields - 86 dB.

References

1. Roth, H. (1983) Floating a Satellite on Microwaves Advanced by Stanford Research--Article in Electronic Engineering Times, Jan. 3.

2. Jordan, E.C. (1950) Electronic Waves and Radiating Systems, Prentice-Hall, New York, pp. 156-157.

3. Jasik, H. (1961) Antenna Engineering Handbook, McGraw-Hill, New York, pp. 2-15.

MISSION
of
Rome Air Development Center

RADC plans and executes research, development, test and selected acquisition programs in support of Command, Control Communications and Intelligence (C^3I) activities. Technical and engineering support within areas of technical competence is provided to ESD Program Offices (POs) and other ESD elements. The principal technical mission areas are communications, electromagnetic guidance and control, surveillance of ground and aerospace objects, intelligence data collection and handling, information system technology, ionospheric propagation, solid state sciences, microwave physics and electronic reliability, maintainability and compatibility.

Printed by
United States Air Force
Hanscom AFB, Mass. 01731

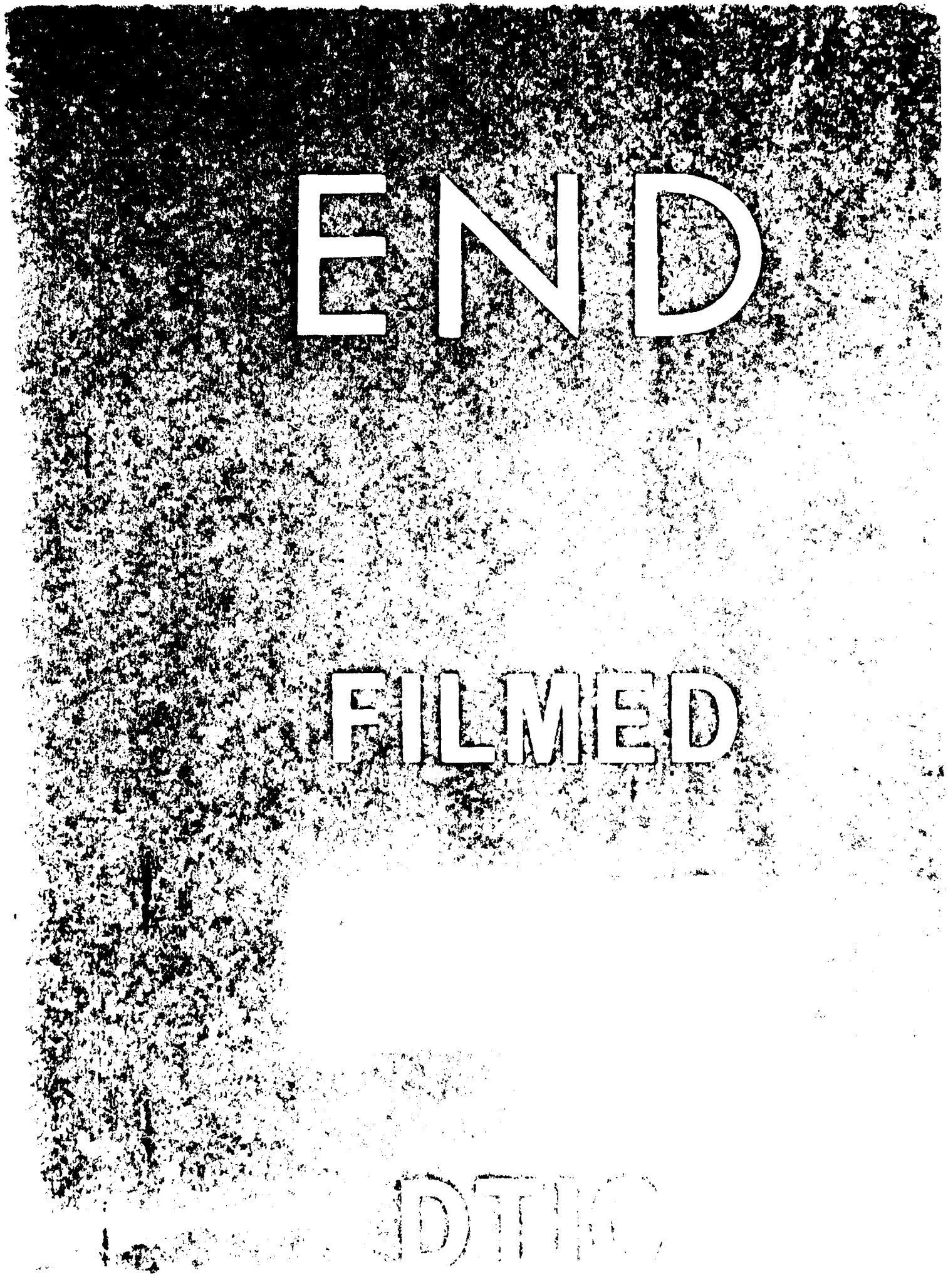
END
FILMED
DTIC